

**OPTIMISING MOISTURE TRANSPORT IN BIO-BASED, EARTH AND NATURAL
HYDRAULIC LIME MORTARS USING HYGROTHERMAL AND CHEMICAL
CHARACTERISTICS**

ABBIE ROSE ROMANO

**A thesis submitted in partial fulfilment of the requirements of Liverpool John Moores
University for the degree of Doctorate in Philosophy (PhD)**

May 2020

Contents Page

Abstract.....	12
Nomenclature List	14
Chapter 1 – Introduction.....	19
1.1. Background / Context of research	19
1.2. Aim and objectives	20
1.3. Thesis Outline	21
1.4. Dissemination.....	22
Chapter 2 – Literature Review.....	24
2.1. Residential dwelling typology in United Kingdom (UK)	24
2.2. Insulating residential properties.....	26
2.2.1. Sick building syndrome (SBS) and Indoor Air Quality (IAQ).....	28
2.2.2. Pathogenic and household nuisances	28
2.3. Bio-based materials	29
2.3.1. Bio-based materials to reduce carbon emissions.....	29
2.3.2. Bio-based materials for improvement of occupant wellbeing	30
2.4. Earth as a bio-based building material	31
2.4.1. Earth affinity with water	33
2.4.2. Hygrothermal ability of earth.....	35
2.4.3. Limitations using earth.....	35
2.5. Moisture transport in bio-based building materials.....	36
2.5.1. Bio-based materials hygrothermal properties	36
2.5.1.1. Moisture buffering	37
2.5.1.2. Water Vapour Permeability.....	40
2.5.1.3. Sorption Isotherms	41
2.5.2. Latent Heat.....	42
2.5.3. Bio-based materials moisture transport mechanisms	43
2.6. Understanding the differences between bio-based materials – the physicochemical impact.....	45
2.6.1. Cellulose based.....	46
2.6.2. Keratin based	47
2.6.3. Thermal methods for analysis for bio-based materials physicochemical characterisation	48
2.7. Limitations of bio-based building materials.....	52

2.7.1. Hysteresis phenomena	52
2.7.2. Legislation and Building Standards	53
2.8. Earth Composites	54
2.8.1. Stabilisers	54
2.8.2. Natural Hydraulic Lime (NHL) Composites	55
2.8.3. Influence of bio-fibres within earth mortar matrix	56
2.8.3.1. Thermal behaviour	56
2.8.3.2. Mechanical properties	56
2.8.4. Fibre to Matrix Adhesion	57
2.8.5. Thermal analysis	58
2.8.6. Alternatives to bio-based earth mortar composites	58
2.9. Conclusion	59
2.9.1 Knowledge gaps in current literature	59
Chapter 3 – Characterisation of bio-fibres	60
3.1. Introduction	60
3.2. Materials	60
3.2.1. Materials Characterisation	60
3.3. Methodology	62
3.3.1. Surface Morphology	62
3.3.2. Density	62
3.3.3. Moisture Buffering Value (MBV)	62
3.3.4. Thermal Conductivity	63
3.3.5. Temperature evolution during transient behaviour	64
3.4. Results and Discussion	65
3.4.1. Density of the materials	65
3.4.2. Moisture Buffering Value (MBV)	67
3.4.3. Thermal Conductivity and SEM micrographs	75
3.4.4. Temperature evolution during transient behaviour	83
3.5. Conclusion	85
Chapter 4 - Physicochemical characterisation of bio-based insulation to explain their hygrothermal behaviour	87
4.1. Introduction	87
4.2. Materials	87
4.3. Methods	87
4.3.1. Preparation and Stabilisation of Samples	87
4.3.2. Thermogravimetry Analysis (TGA) and Derivative Thermogravimetry (DTG)	87

4.3.3. Differential Scanning Calorimetry (DSC).....	88
4.3.4. Fourier Transform Infrared Spectroscopy (FTIR)	89
4.3.5. Scanning Electron Microscopy (SEM)	89
4.4. Results and Discussion.....	90
4.4.1. TGA and DTG	90
4.4.1.1. Cellulose based analysis regarding TGA and DTG	91
4.4.1.2. Keratin based analysis regarding TGA and DTG	95
4.4.2. DSC	97
4.4.2.1. Cellulose Based analysis with DSC	97
4.4.2.2. Keratin Based analysis with DSC.....	100
4.4.3. FTIR.....	102
4.4.3.1. Cellulose Based analysis with FTIR.....	102
4.4.3.2. Keratin Based analysis with FTIR	110
4.4.4. SEM	113
4.5. Conclusion	116
Chapter 5 - Bio-Based Earth Mortar	117
5.1. Introduction	117
5.2. Initial Mix Design Selection	117
5.2.1. Materials.....	117
5.2.1.1. Binders	117
5.2.2. Mix Design	120
5.2.3. Formulation	120
5.2.4. Curing	120
5.2.5. Methodology.....	121
5.2.5.1. Consistence.....	121
5.2.5.2. Compressive and Tensile Strength	121
5.2.5.3. Capillary Action.....	122
5.2.5.4. Moisture Buffering Value (MBV)	122
5.2.6. Results and Discussion	123
5.2.6.1. Consistence.....	123
5.2.6.2. Compressive and Tensile Strength	124
5.2.6.3. Capillary Action.....	125
5.2.6.4. Moisture Buffering Value (MBV)	127
5.2.7. Initial Mix Design Conclusion.....	128
5.3. Further Experimentation of Best Performing Mix Designs	129
5.3.1. Materials.....	129
5.3.1.1. Bio-Fibres	129

5.3.2. Methodology.....	129
5.3.2.1. Surface Morphology and elemental analysis.....	130
5.3.2.2. Dry Bulk Density	130
5.3.2.3. Open Porosity.....	130
5.3.2.4. Thermal Conductivity	130
5.4. Results and Discussion	131
5.4.1. Surface Morphology and elemental analysis	131
5.4.2. Consistence	133
5.4.3. Dry Bulk Density.....	134
5.4.4. Compressive and Tensile Strength.....	135
5.4.5. Open Porosity	137
5.4.6. Capillary Action	140
5.4.7. MBV	142
5.4.8. Thermal Conductivity.....	148
5.5. Conclusion	150
Chapter 6 - Physicochemical characterisation of bio-earth mortar composites to explain their hygrothermal behaviour	151
6.1. Introduction	151
6.2. Materials	151
6.3. Methods.....	152
6.3.1. Thermogravimetry Analysis (TGA) and Derivative Thermogravimetry (DTG).....	152
6.3.2. Differential Scanning Calorimetry (DSC).....	152
6.4. Results and Discussion	153
6.4.1. Thermogravimetry Analysis (TGA) and Derivative Thermogravimetry (DTG).....	153
6.4.2. Differential Scanning Calorimetry (DSC).....	158
6.4.2.1. Specific Heat Capacity.....	162
6.4.3. Fourier Transform Infrared Spectroscopy (FTIR)	166
6.5. Conclusion	170
Chapter 7 – Dynamic moisture movement within bio-earth composites	172
7.1. Introduction	172
7.2. Materials	172
7.3. Methodology	172
7.3.1. Water Vapour Permeability.....	172
7.3.2. Sorption Isotherm	175
7.3.3. Latent heat of sorption.....	175
7.4. Results and Discussion	176

7.4.1. Water Vapour Permeability (WVP)	176
7.4.2. Sorption Isotherms	178
7.4.3. Latent heat of sorption	180
7.5. Conclusion	187
Chapter 8 – Overall Conclusion	188
8.1. Main Findings.....	188
8.2. Further Works	190
8.2.1 Laboratory Work.....	190
8.2.2. Modelling.....	191
References	193

List of figures

Figure 2.1. Dwelling age of properties within the UK 1 (H.M.Government, 2019a).	24
Figure 2.2. Percentage of fuel poor households within the UK ((BEIS, 2018) (Welsh Government, 2018) (Scottish Government, 2019c) (Northern Ireland Housing Executive., 2017)).	25
Figure 2.3a. 1920s Solid masonry wall.	
Figure 2.3b. 1970s Outer facing brick, 50mm clear cavity, lightweight concrete inner	
Figure 2.3c. 2010s Outer facing brick, 50mm clear cavity, 40mm insulation board, medium density inner.	26
Figure 2.4. Risk of condensation analysis in building envelopes due to different insulation techniques with a) no insulation, b) external insulation and c) internal insulation (RIBuild, 2014).	27
Figure 2.5. The optimum zone for RH against different types of house hold nuisances (Simonson et al., 2002).	29
Figure 2.6. Primary energy consumption variation of bio-based and fossil fuel based materials (Jones and Brischke, 2017).	30
Figure 2.7. Embodied carbon quantities for different monolithic wall constructions (Pacheco-Torgal and Jalali, 2012).	32
Figure 2.8. Classification of earth based construction techniques.....	32
Figure 2.9. Moisture and thermal transfer within earth construction (where ϕ = relative humidity, T = temperature and p^{sat}_v = equilibrium vapour pressure) (Soudani et al., 2016)..	33
Figure 2.10. MBV Classification (Rode et al, 2005).	39
Figure 2.11. IUPAC hysteresis loop classification (Thommes et al., 2015).	41
Figure 2.12. Isothermal adsorption curves for building materials (Minke, 2006).....	42
Figure 2.13. Dipole forces within water molecule.....	43
Figure 2.14. Moisture transport within hygroscopic materials (Straube, 2006).	44
Figure 2.15. Parameter and methods of thermal analysis (based on (Feist, 2015)).	49
Figure 2.16. Bio-fibre to matrix adhesion (Ghavami et al 1999).	57
Figure 3.1. Natural bio-based insulation materials and one thermoplastic polymer tested, according to the information presented in Table 3.1.	61
Figure 3.2. Step change in RH within climatic chamber over a singular, 24 h cycle	63
Figure 3.3. Saturated bio fibre thermal conductivity reading.	64
Figure 3.4a. Bio-based samples with thermocouples attached.	64
Figure 3.4b. (L) Run 1' thermocouples arrangement and (R) 'Run 2' thermocouple arrangement.....	64
Figure 3.5a. Bulk density variation of samples in dry and saturated states.	66
Figure 3.5b. Difference between saturated and dry density of examined materials	
Figure 3.6. MBV variation of each sample per cycle.....	67
Figure 3.7a. Change in mass during the 7th cycle of the 10 bio-based materials and 1 recycled plastic during a 24-hour cycle.....	69
Figure 3.7b. Change in mass during a 10th cycle of the 10 bio-based materials and 1 recycled plastic during a 24-hour cycle.....	70
Figure 3.8a. Adsorption and desorption curves to show the categorisation of 6 samples within 'Group 1' (Romano et al, 2018).	71
Figure 3.8b. Adsorption and desorption curves to show the categorisation of 2 samples within 'Group 2'.....	72

Figure 3.8c. Adsorption and desorption curves to show the categorisation of 3 samples within 'Group 3'.....	73
Figure 3.9. MBV of each material and its rating according to NORDTEST protocol, during the 10th cycle within climatic chamber.	74
Figure 3.10a. PET - thermal conductivity of dry, saturated within a climatic chamber during a 24-hour cycle.	76
Figure 3.10b. SEM Image of PET.....	76
Figure 3.10.c. Wool 2 - thermal conductivity of dry, saturated within a climatic chamber during a 24 hour cycle.....	76
Figure 3.10d. SEM Image of Wool 2.....	76
Figure 3.10e. WF - thermal conductivity of dry and saturated within a climatic chamber during a 24 hour cycle.....	76
Figure 3.10f. SEM image of WF.....	76
Figure 3.10g. Wool 3 - thermal conductivity of dry, saturated within a climatic chamber during a 24-hour cycle.	77
Figure 3.10h. SEM image of Wool 3.....	77
Figure 3.10i. Hemp - thermal conductivity of dry, saturated within a climatic chamber during a 24-hour cycle.	77
Figure 3.10j. SEM image of Hemp.....	77
Figure 3.10k. SMR- thermal conductivity of dry, saturated within a climatic chamber during a 24-hour cycle.	77
Figure 3.10l. SEM image of SMR.....	77
Figure 3.10m. Wool 1- thermal conductivity of dry, saturated within a climatic chamber during a 24-hour cycle.	78
Figure 3.10n. SEM image of Wool 1.....	78
Figure 3.10o. Wool 4- thermal conductivity of dry, saturated within a climatic chamber during a 24-hour cycle.	78
Figure 3.10p. SEM image of Wool 4.	78
Figure 3.10q. ICB - thermal conductivity of dry, saturate within a climatic chamber during a 24-hour cycle.	78
Figure 3.10r. SEM Image of ICB.....	78
Figure 3.10s. WWB - thermal conductivity of dry, saturated within a climatic chamber during a 24-hour.	79
Figure 3.10t. SEM Image of WWB.....	79
Figure 3.10u. Straw - thermal conductivity of dry, saturated within a climatic chamber during a 24-hour cycle.	79
Figure 3.10v. SEM Image of Straw.....	79
Figure 3.11a. Thermal conductivity against bulk density.....	80
Figure 3.11b. Thermal conductivity against saturated density.....	81
Figure 3.12. ICB with naturally occurring air pockets and voids on the surface of the sample circled.....	81
Figure 3.13. Temperature change on the surface and within samples throughout 2 experimental campaigns.	84
Figure 3.14. Temperature difference between surface and internal temperature per m ² of bio-based insulation sample.	85
Figure 4.1. TA Instruments, TGA Q50.	88
Figure 4.2. A Perkin Elmer DSC 7.	88
Figure 4.3. Agilent Technologies Cary 630 FTIR.	89
Figure 4.4. FEI Inspect S SEM.	89
Figure 4.5. WWB sample on crucible before entering furnace.	90

Figure 4.6a. TGA (solid line) and DTG (dashed line) for SMR at 53% and 75% RH.	93
Figure 4.6b. TGA (solid line) and DTG (dashed line) for WF at 53% and 75% RH.....	93
Figure 4.6c. TGA (solid line) and DTG (dashed line) for STW at 53% and 75% RH.....	94
Figure 4.6d. TGA (solid line) and DTG (dashed line) for WWB at 53% and 75% RH.....	94
Figure 4.6e. TGA (solid line) and DTG (dashed line) for W1 at 53% and 75% RH.....	96
Figure 4.6f. TGA (solid line) and DTG (dashed line) for W2 at 53% and 75% RH.....	96
Figure 4.7a. SMR DSC thermogram.....	98
Figure 4.7b. WF DSC thermogram.....	99
Figure 4.7c. STW DSC thermogram.....	99
Figure 4.7d. WWB DSC thermogram.....	99
Figure 4.7e. Wool 1 DSC thermogram.....	101
Figure 4.7f. Wool 2 DSC thermogram.....	102
Figure 4.8. Total Crystallinity Index (TCI), Intensity of hydrogen bonding (HBI) and Lateral Order Index (LOI) for cellulose based samples.	106
Figure 4.9a. SMR FTIR spectra.....	107
Figure 4.9b. WF FTIR spectra.....	107
Figure 4.9c. STW FTIR spectra.....	108
Figure 4.9d. WWB FTIR spectra.....	108
Figure 4.9e. W1 FTIR spectra.....	111
Figure 4.9f. W2 FTIR spectra.....	111
Figure 4.10. Regularity of the molecular chain (ROM) for keratin-based samples.	113
Figure 5.1. Dry grain size distribution of earth and sand.....	118
Figure 5.2. XRD Rigaku Miniflex.....	119
Figure 5.3. Diffractogram of earth samples.....	119
Figure 5.4. Casting of (L) prismatic and (R) MBV square samples.	121
Figure 5.5. (L) Compressive and (R) tensile strength equipment.....	122
Figure 5.6 Step change in RH within climatic chamber over a singular, 24 h cycle.....	122
Figure 5.7. Flow test of plain earth mortar.	124
Figure 5.8. Compressive and Tensile Strength of initial 7 mix designs.	125
Figure 5.9. Capillary action of mix designs.	126
Figure 5.10. Earth mortar samples within climatic chamber.....	127
Figure 5.11. (L) SMR (Centre) W1 (R) W2	129
Figure 5.12. Thermal conductivity equipment for samples.....	131
Figure 5.13. Dry Bulk Density of earth mortar samples.....	135
Figure 5.14. Compressive and tensile strength of all mix designs.....	136
Figure 5.15. Samples after tensile strength testing, hair line fractures circled.....	137
Figure 5.16. Open porosity for samples.....	138
Figure 5.17. Relationship between open porosity and dry bulk density for samples.....	139
Figure 5.18. Relationship between porosity and compressive strength of samples.	140
Figure 5.19. Capillary action curve for earth mortar samples.....	141
Figure 5.20. Samples within climatic chamber.....	142
Figure 5.21. Average MBV per cycle for each mix design.....	143
Figure 5.22. MBV classification of samples according to (Rode et al., 2005).....	144
Figure 5.23. Adsorption/Desorption graph for all earth mortar samples after 1, 24 hour cycle.	145
Figure 5.24. Adsorption/Desorption graph for all earth mortar samples after 14, 24 hour cycles.....	145
Figure 5.25. Adsorption/Desorption graph for all earth mortar samples after 15, 24 hour cycles.....	146

Figure 5.26. Adsorption/Desorption graph for all earth mortar samples after 22, 24 hour cycles.....	147
Figure 5.27. Relationship between dry bulk density and thermal conductivity of samples.	149
Figure 6.1. Image of bio-earth mortar composite entering furnace.....	153
Figure 6.2a. TGA (solid line) and DTG (dashed line) for Mix 1 PL at 53% and 75% RH. ..	156
Figure 6.2b. TGA (solid line) and DTG (dashed line) for Mix 1 WL1 at 53% and 75% RH.	
Figure 6.2c. TGA (solid line) and DTG (dashed line) for Mix 1 SMR at 53% and 75% RH	
Figure 6.2d. TGA (solid line) and DTG (dashed line) for Mix 1 W2 at 53% and 75% RH	
Figure 6.3a. Mix 1 PL DSC thermogram.....	160
Figure 6.3b. Mix 1 W1 DSC thermogram.....	161
Figure 6.3c. M1 SMR DSC thermogram.....	161
Figure 6.3d. M1 W2 DSC thermogram.....	162
Figure 6.4a. Specific heat capacity for Mix design 1 from 5-50°C at 53% RH.	163
Figure 6.4b. Specific heat capacity for Mix design 1 from 5-50°C at 75% RH.....	163
Figure 6.5. Average specific heat capacity, Cp of samples at 53% and 75% RH at 20°C.	164
Figure 6.6. FTIR equipment analysing a bio-earth mortar composite sample.	166
Figure 6.7a. M1 PL FTIR spectra.	169
Figure 6.7b. M1 W1 FTIR spectra.....	169
Figure 6.7c. M1 SMR FTIR spectra.....	170
Figure 6.7d. M1 W2 FTIR spectra.....	170
Figure 7.1. WVP experimental set up.	173
Figure 7.2. Experimental set up of thermocouples within earth mortar composite.	175
Figure 7.3. (L) Thermocouple cast on the surface (R) Thermocouple cast 15mm from surface of earth mortar composite.....	176
Figure 7.4. Adsorption curves for bio-earth mortar composites.....	178
Figure 7.5. Dynamic temperature variation of M1 PL for cycle 1.....	181
Figure 7.6. Dynamic temperature variation of M1 W1 for cycle 1.....	181
Figure 7.7. Dynamic temperature variation of M1 SMR for cycle 1.	182
Figure 7.8. Dynamic temperature variation of M1 W2 for cycle 1.....	182
Figure 7.9. Dynamic temperature variation of M1 PL for cycle 21.....	183
Figure 7.10. Dynamic temperature variation of M1 W1 for cycle 21.....	183
Figure 7.11. Dynamic temperature variation of M1 SMR for cycle 21.	184
Figure 7.12. Dynamic temperature variation of M1 W2 for cycle 21.....	184
Figure 7.13. Difference between average surface and 15mm depth temperature over 21 cycles.....	184

List of tables

Table 2.1. Issues affecting degradation of earthen construction.	36
Table 2.2. Moisture buffering parameters.	38
Table 3.1. Raw bio-fibre material characteristics.....	61
Table 3.2. Categorisation of materials 7th Cycle and 10th Cycle through the adsorption/ desorption curve.	73
Table 3.3. Mortar composites moisture buffering properties.....	74
Table 3.4. Bio-fibres and dry thermal conductivity values in a dry state.	82
Table 4.1. Weight loss of all samples at 100°C and 300°C.....	91
Table 4.2. DSC phase transition temperatures for cellulose based samples.	97
Table 4.3. DSC phase transition temperatures for keratin based samples.	100
Table 4.4. Total Crystallinity Index (TCI), Hydrogen Bonding Index (HBI) and Lateral Order Index (LOI) for 4 cellulose based samples.	105
Table 4.5. FTIR analysis of cellulose based samples and associated assignment of bonds at 53% and 75% RH.	109
Table 4.6. FTIR analysis of keratin-based samples and associated assignment of bonds at 53% and 75% RH.	112
Table 4.7. ROM of keratin based molecules at 53% and 75%.	112
Table 4.8. SEM Images of samples stabilised at 53% and 75% taken at 1000 and magnification.....	113
Table 5.1. Dry Bulk Density of mix design components.	120
Table 5.2. Mix design proportions (by mass).....	120
Table 5.3. Quantity of water added to mix designs.	123
Table 5.4. MBV values for initial mix design samples.....	128
Table 5.5. Renumbered Mix Design Proportions.....	128
Table 5.6. Material properties of bio-fibres.....	129
Table 5.7. SEM Images for mixes 1 and 2.	131
Table 5.8. Elemental composition of the composites.	133
Table 5.9. Consistence values of mix designs.	133
Table 5.10. Mix design quantities (by weight).	134
Table 5.11. Capillary coefficient for mix designs.	142
Table 5.12. Stabilised Average MBV for samples.	143
Table 5.13. Thermal Conductivity values for samples.	148
Table 5.14. Calculated r for samples.	150
Table 6.1. Overall weight loss percentages for earth based mortar composites.	155
Table 6.2. DSC phase transitions temperatures for bio-earth mortar composites.....	159
Table 6.3. Specific heat capacity Cp values for samples at 20°C.....	164
Table 6.4. Difference in Cp values for 53% and 75% stabilised samples at 20°C.....	165
Table 6.5. FTIR analysis of earth mortar composites and associated assignment of bonds at 53% and 75% RH.	167
Table 7.1. Mix design proportions (by mass).....	172
Table 7.2. WVP values for bio-earth mortar composites.	176

Abstract

The utilisation of bio-based materials as a construction material presents diverse and under researched challenges that can reduce carbon emissions and improve the hygrothermal performance of buildings. Within the United Kingdom (UK), the residential construction typology of housing is vast. Just within pre-1919 dwellings, energy costs are over 70% higher by comparison to the post-1990 equivalents. This thesis intends to provide tools to effectively optimise bio-based composites for hygrothermal conditions improvement in housing and whilst the composite has been optimised for UK conditions, the impacts of this thesis is versatile and can be applied across the world for example with other construction typologies, building materials and use. This research work can provide relevant information on tailoring bio-based materials whenever indoor hygrothermal conditions are crucial for energy efficiency and comfort of building users, either in the UK, Europe or across the world.

Within the scope of this work, this thesis will aim to optimise the transport of water through bio-based earth mortar composites to be used in residential properties for relative humidity moisture management. Initially, the hygrothermal performance of 11 different bio-based and recycled raw materials was analysed (four different types of (Sheep and recycled) Wool insulation, Hemp, Wood Wool Board (WWB), Saw Mill Residue (SMR), Wood Fibre (WF), Straw, Insulated Cork Board (ICB) and Polyethylene terephthalate (PET). with particular focus on Moisture Buffering Value (MBV). The best 6 performing materials were retested and analysed. It was found that the differences in MBV were negligible and this value alone was not enough to be able to ascertain which material should be selected.

A new methodology of understanding the shape of the adsorption and desorption curves and then grouping this would give a better assessment of the material performance. Earth-lime mortar panels were created using locally sourced material from Liverpool (NW England) and the previous bio-based fibres. Performance analysis of the bio-based composites was done at steady and transient states for hygrothermal optimisation of the panels. Prismatic, $0.1\text{m}^2 \times 0.1\text{m}^2$ squares and disc shaped samples were cast and samples were exposed to cyclical step changes in relative humidity at 75% for 8 hours and 53% for 16 hours at 23°C , in order to mimic a UK household occupancy. Results demonstrate that an optimised mix improved thermal properties if Saw Mill Residue (SMR) is added.

Further to this, traditional, thermal method of analysis (using Thermogravimetry Analysis (TGA), Differential Thermogravimetry (DTG) and Differential Scanning Calorimetry (DSC)) has been for heritage and forensic investigation of the constituent elements of the material rather than a comparison with regards to their hygrothermal performance. The best performing bio-

based composite was Mix 1 SMR with an MBV of 1.26 (g/(m² %RH)) and Water Vapour Permeability (WVP) of 2.5 (x10⁻¹¹) (kg.m⁻¹.s⁻¹.Pa⁻¹).

Latent heat generated in the bio-based composites was explored and analysed to consider the effects within a dynamic hygrothermal environment. Heat energy is released due to the change in state of water molecule from liquid to vapour (and vice versa) due to the latent heat of vapourisation and condensation. The latent heat of both raw bio-based fibres and when combined into an earth mortar matrix was identified, analysed and is consistently demonstrated even after 21 cycles of 24 hours. After these cycles, the mix design with Wool 2 produced the greatest sustained quantity of heat generated with samples temperature increase of 1.59°C during adsorption and 0.97 °C during desorption phase.

The movement of water molecules in and out of samples was researched on a physicochemical basis and organic chemistry analytical techniques were utilised to gain a better understanding of the function and important on the hydroxyl group for hygrothermal performance. Utilising analytical chemistry and thermal methods of analysis for samples conditioned at different RH, can give a greater understanding of a building materials hygrothermal properties.

Nomenclature List

BET – Brunauer-Emmett-Teller theory
CC – Capillary Coefficient ($\text{m/s}^{0.5}$)
Cp – Specific Heat Capacity (kJ/kg.K)
DIN – Deutsches Institut für Normung
DSC – Differential Scanning Calorimetry
DTG – Derivative thermogravimetry
EDP – European product deceleration
EDX – Energy Dispersive Spectrometry
EM – Earth Mortar
EU – European Union
FTIR – Fourier Transform Infrared Spectroscopy
HBI - Intensity of Hydrogen Bonding
HQE – Haute Qualité Environnementale
IAQ – Indoor air quality
ICB – Insulated Cork Board
ISO – International Organization for Standardization
IUPAC – International Union of Pure and Applied Chemistry
JIS – Japanese Industrial Standards
LEED – Leadership in Energy and Environmental Design
LOI – Lateral Order Index
MBC – Moisture Buffering Capacity
MBV – Moisture Buffering Value ($\text{g}/(\text{m}^2 \cdot \%RH)$)
MtCO₂e – Metric tons of carbon dioxide equivalent
NHL – Natural Hydraulic Lime
NHS – National Health Service
PCC – Pearson Correlation Coefficient
PCM – Phase Changing Material
PET – Polyethylene terephthalate
PL – Plain mortar sample
RH – Relative Humidity (%)

RILEM – International Union of Laboratories and Experts in Construction Materials, Systems and Structures

ROM – Regularity of molecular chain

SBS – Sick Building Syndrome

SEM – Scanning Electron Microscopy

SMR – Saw Mill Residue

STW – Straw

T – Temperature (°C)

TCI – Total Crystallinity Index

T_d – Denaturation Temperature (°C)

T_{eva} – Evaporation Temperature (°C)

TGA – Thermogravimetical Analysis

T_t – Transition Temperature (°C)

UK – United Kingdom

UN – United Nations

VOCs – Volatile Organic Compounds

W1 – Wool 1

W2 – Wool 2

W3 – Wool 3

W4 – Wool 4

WF – Wood Fibre

W_L – Water content at liquid limit

W_m – Water content of manufacturing stage

W_{OPT} – Optimum water content

W_P – Water content at plastic limit

WVP – Water Vapour Permeability (mg/m.hr.Pa)

WWB – Wood Wool Board

Supervisory Team

Dr Ana Bras, Department of the Built Environment, Liverpool John Moores University, UK

Dr Sotirios Grammatikos, Department of Manufacturing and Civil Engineering, Norwegian University of Science and Technology, Norway

Dr Stephen Wiley, Civil Engineering Department, Liverpool John Moores University, UK

Declaration

No portion of the work referred to in the thesis has been submitted in support of an application for another degree or qualification of this or any other university or other institute of learning.

A.Romano

A handwritten signature in black ink, appearing to read 'A. Romano', with a stylized, cursive script.

21/05/20

Acknowledgements

I would like to thank all my supervisors for their help and support throughout this PhD journey. Thank you to Sotirios and Steve for the many Skype calls, guidance, confidence boosts and for everything over the last 3 years. Ana, you have opened so many doors for me and given me many opportunities I am truly grateful for you taking a chance on me in the beginning – you have shaped me into the researcher I am today. In an industry where we are a minority, it has been inspiring to work in a research group with a strong, female civil engineer at the helm.

A huge thank you to the technical staff in the Department of Built Environment (particularly Mal and Alan) for key support through both the manufacture of equipment and materials but also for always having an open door for a chat to cheer me up through the hard times or answering my ten thousands of questions. Thank you to Rob and Nicola in the department of Pharmacy and Biomolecular sciences for all of your help and flexibility it is greatly appreciated.

To Vero and John - the European dream team. Your conversations, knowledge and experience have helped me so much over the years. Thank you to my friends, family and LJMU WRU who have picked me up and helped me whenever I needed them throughout this experience.

Thank you to my mom and Paul – you have been the best support system I could ever have wished for. It never goes unnoticed and although you are hundreds of miles away, your love and photos of the cats and kittens never fail to cheer me up.

Finally, Matt. Where do I even start? You bring a tranquillity to my life that I never knew I needed. Your consistency for being so caring, understanding and loving has been invaluable and indescribable. You have been my biggest cheerleader and helped me through this journey since day 1 – thank you doesn't come close.

“For a research worker, the unforgotten moments of [their] life are those rare ones which come after years of plodding work, when the veil over nature's secret seems suddenly to lift and when what was dark and chaotic appears in a clear and beautiful pattern”

Gerty Cori, Nobel Prize winner for Physiology/Medicine in 1947

Chapter 1 – Introduction

1.1. Background / Context of research

The planet is in a climate crisis. As a direct response to the Kyoto Protocol coming into force in 1997 (and the first of its kind as a legally binding commitment to combat climate change between 2008-2012) (U.N., 2008), The Climate Change Act 2008 (H.M. Government, 2008) set a benchmark for the United Kingdom's (UK) government to reduce carbon emissions. The act outlines an 80% reduction of emissions from baseline levels set in 1990 and provides a catalogue of 5 year budgets till 2022 - with a guaranteed reduction in emissions by at least 26% before 2020.

As highlighted by Gieseckam, Tingley and Cotton (2018), within 2014 the construction industry and built environment sector as a whole emitted around 183.5 MtCO_{2e} (Gieseckam and Pomponi, 2017) – where around 25% can be linked to embodied emissions in construction. There is a clear conundrum facing the UK construction industry in terms of balancing an obligation to climate change in addition to meeting the requirements and demands of the building industry (Atkins, ICE and ITRC, 2016; Krausmann et al., 2017). In spite of the rise in emissions, the UK government is shows some commitment to combatting them via mechanisms such as Construction 2025 (H.M. Government, 2013a), Construction Strategy 2016-2020 (H.M. Government, 2016) and industry initiatives via the launch of Environmental Product Decelerations (Passer et al., 2015) and Infrastructure Carbon Review (H.M. Government, 2013b). Further European commitment to reducing carbon emissions and utilising bio waste are demonstrated by schemes such as European Union (EU) commissions bio-economy strategy of 2012 (European Commission, 2017) and where all member states of the EU aim to cut their emissions by 90% by 2050 (European Commission, 2011).

Despite this, between 2014 and 2015 the UK's carbon footprint actually rose by approximately 2% (H.M.Government, 2018). Particularly, the construction industry uses around 55% of the entire nations energy and over 55% of all the countries carbon dioxide emissions (Parsa and Farshchi, 1996).

The EU outlined within the Energy Performance Directive in 2018 to aim to renovate current building stocks to nearly or zero energy buildings (Housing Europe, 2018). Whilst energy efficiency in buildings not only reduces the emissions to the environment on a European scale, it also aligns with the United Nations (U.N.) Sustainable Development Goals 11 and 13 (Di Foggia, 2018).

The buildings energy efficiency is not a standalone problem. Indoor air quality plays an important role in buildings performance and people's health. Affecting particularly low and middle income families in developed countries, especially more time than ever is being spent within buildings (World Health, 2009). Making homes energy efficient by using bio-based solutions is the most effective way to combat the problem of fuel poverty and reduce energy bills. It is also important to understand that any solutions where a 'one size fits all' approach is not suitable nationally let alone internationally (Brás, Gonçalves and Faustino, 2014; CAT, 2018). A realistic and performance driven retrofitting tool that enable tailoring green materials for decarbonisation is essential to meet these targets (Kelly, 2009).

This highlights the urgent need for more environmentally considerate construction techniques and materials as the imminent threat of the depletion of natural resources has never been greater and requires urgent attention (Amziane and Sonebi, 2016). Addressing these is a key objective which has never been more imperative; the built environment must search for a more sustainable construction substance: giving rise to the use of bio-based building materials. A key benefit of these materials is their availability on a local and global scale which can provide a lower embodied energy solution.

As a fundamentally hygroscopic material, bio-based building materials have the ability to passively regulate relative humidity (RH) (Jones and Brischke, 2017). The built environment will continue to look to reduce heat and cooling loads as a form of energy consumption is a key driver for the requirement of a passively operating RH regulator. By controlling the RH, within a residential property thermal comfort is maintained. The hygrothermal behaviour is crucial for these materials performance. As energy savings rely on building solutions rather than occupant awareness/engagement the utilisation of bio-based materials is inherently desired. These materials have other benefits such as improving indoor air quality (IAQ), where within the UK the NHS spends around £1.36billion per year due to indoor air polluted related diseases (P.H.E., 2014). A key issue associated to bio-based and recycled materials is their limited understanding therefore an inability to be optimised. By being able to optimise these bio-based and recycled materials "smart behaviour" will enable a characterisation which aims to contribute to their utilisation within the construction industry.

1.2. Aim and objectives

Aim

The previous research gaps justify the study for the characterisation and optimisation of bio-based earth mortars composites to increase buildings indoor comfort. This thesis will aim to

optimise the transport of water through bio-based earth mortar composites to be used in residential properties for relative humidity moisture management.

Objectives

- Utilise bio-based insulation materials currently available on the market in the United Kingdom to characterise and optimise the performance with the hygrothermal conditions of a residential property
- How hysteresis implicitly affects the movement of water mechanisms within raw bio-fibres, earth mortars and how this can be optimised
- Use literature to develop a novel approach to understanding the fundamental biological and chemical reactions of bio-based materials at different relative humidity's.
- Consequentially, how use this novel approach to understand how this affects the microstructure, biological and chemical reactions within bio-fibre composites

1.3. Thesis Outline

Chapter 1 – Demonstrates the requirement for a moisture buffering technology within residential properties within the UK. This chapter also demonstrates the aims and objectives of this research project.

Chapter 2 – A literature review of the current knowledge on issues with current residential dwellings and how hygroscopic materials can be utilised most effectively to resolve them. Further to this, it also explores the types of hygrothermal and thermal methods for the analysis of these materials.

Chapter 3 – This chapter examines the physical and hygrothermal characteristics 10 bio-based and 1 recycled thermoplastic polymer insulation samples, currently available on the market in the U.K.

Chapter 4 - This chapter will explore the physicochemical differences between the best performing bio-based materials from Chapter 3 at differing relative humidity's. By understanding the influence of temperature via the thermal analysis on the material properties using DSC, TGA, DTG, FTIR and SEM.

Chapter 5 - Initial preliminary experimentation was completed with different mortar compositions. Upon initial selection, bio-fibres were incorporated into the mortars and were physically and hygrothermally tested to optimise mix design selection.

Chapter 6 – The best performing mix design from Chapter 5 were selected and the physicochemical difference when stabilised at different RH was analysed using DSC, TGA, DTG, FTIR and SEM. In addition, the temperature-dependent behaviour of these earth mortar composites specific heat capacity over differing service life temperatures and beyond was analysed.

Chapter 7 – This chapter explores the moisture transfer mechanisms of the mortars to understand which hygrothermal conditions it will perform the most efficiently. Latent heat is explored by incorporating thermocouples into the mortar within a dynamic hygrothermal environment.

Chapter 8 – a conclusion of the research, demonstrating the key findings of this thesis as well as future works.

1.4. Dissemination

Throughout this research project, this PhD thesis has disseminated 3 journal articles, 5 conference proceedings and 5 poster presentations as follows:

Publications in peer reviewed, international journals

A. Romano, A. Brás, S. Grammatikos, A. Shaw and M. Riley, Dynamic behaviour of bio-based and recycled materials for indoor environmental comfort, June 2019, *Construction and Building Materials*, 211, 730-743.

A. Romano, H. Mohammed, V. Torres de Sande and A. Bras, Sustainable bio-based earth mortar with self-healing capacity. *Proceedings of the Institution of Civil Engineers – Construction Materials*, September 2020

A. Romano, S. Grammatikos, M. Riley and A. Brás, Physicochemical characterisation of bio-based insulation to explain their hygrothermal behaviour, October 2020, *Construction and Building Materials*, 258, 120163-120173

International Conferences

A. Romano, A. Brás, S. Grammatikos, S. Wylie, P. Kot and A. Shaw (2018) On the development of self-controlled bio-based panels for building's thermal management. *European Conference on Composite Materials, June 2018, Athens, Greece.*

A. Romano, A. Brás, S. Grammatikos A. Shaw and M. Riley (2019) Bio-based and recycled materials: characterisation and hygrothermal assessment for passive relative

humidity management. International Conference of Bio-Based Building Materials, June 2019
Belfast, UK

A. Romano, A., Brás, S. Grammatikos, A. Shaw and M. Riley (2019) Bio-fibre earth composite mortar: a structural and hygrothermal assessment. *Sustainable Construction Materials and Technologies*, July 2019 Kingston Upon Thames, UK

A. Romano, H. Mohammed, V. Torres and A. Brás (2019) Sustainable bio-based earth mortar with self-healing capacity. *Sustainable Construction Materials and Technologies Conference*, July 2019 Kingston Upon Thames, UK.

A. Romano and A. Bras (2020) Prescriptive bio-based earth mortar composites as a buffer for internal thermal comfort, *Annual Associated Schools of Construction International Conference*, April 2020, Liverpool, UK.

Poster Presentations

European Conference on Composite Materials, June 2018, Athens, Greece.

LJMU Faculty of Engineering and Technology Postgraduate Research Week 2018

LJMU Doctoral Academy Conference 2018

LJMU Research and Innovation Day 2018

1st International Symposium on the infrastructure development - shaping the future using bio-based solutions for structures and buildings, organised by Liverpool John Moores University, Liverpool (Oct 2019)

Chapter 2 – Literature Review

This research project addresses two key problem areas presented to the construction and built environment sector: production of global greenhouse gases from construction materials and moisture regulation within residential dwellings. To understand how this research project can be most effective, a review of the current literature has been completed. This includes issues with current residential dwellings and how hygroscopic materials can be utilised most effectively to resolve them. Further information on specific bio-based materials are within Chapter 3 and bio-based earth composites within Chapter 5.

2.1. Residential dwelling typology in United Kingdom (UK)

The age range of residential dwelling typology within the UK is vast, with only around 17% of home built in the last 30 years and demonstrated within Figure 2.1 (H.M.Government, 2019a). With variation in age comes a variation in building standards and techniques from those that we have today. A consequence of this is that the homes will have different heating requirements not only due to the nature of the construction methodology but also the materials used. For example, within pre-1919 dwellings, energy costs are over 70% higher by comparison to the post-1990 equivalents (H.M.Government, 2019). Considering Figure 2.1, over 20% of the UK residential dwellings are within this category, which consequentially produce around double the carbon emissions.



Figure 2.1. Dwelling age of properties within the UK 1 (H.M.Government, 2019a).

Heating and hot water for UK homes make up 25% of total energy use therefore a requirement of more energy to heat these older homes has a subsequent higher fuel cost. The inability to afford adequately heating energy a home is defined as fuel poverty (B. Boardman, 1991). Particularly in pre-1919 homes the likelihood of fuel poverty is double the national average, however fuel poverty is still a problem for many homes throughout England, Wales, Scotland and Northern Ireland (see Figure 2.2).

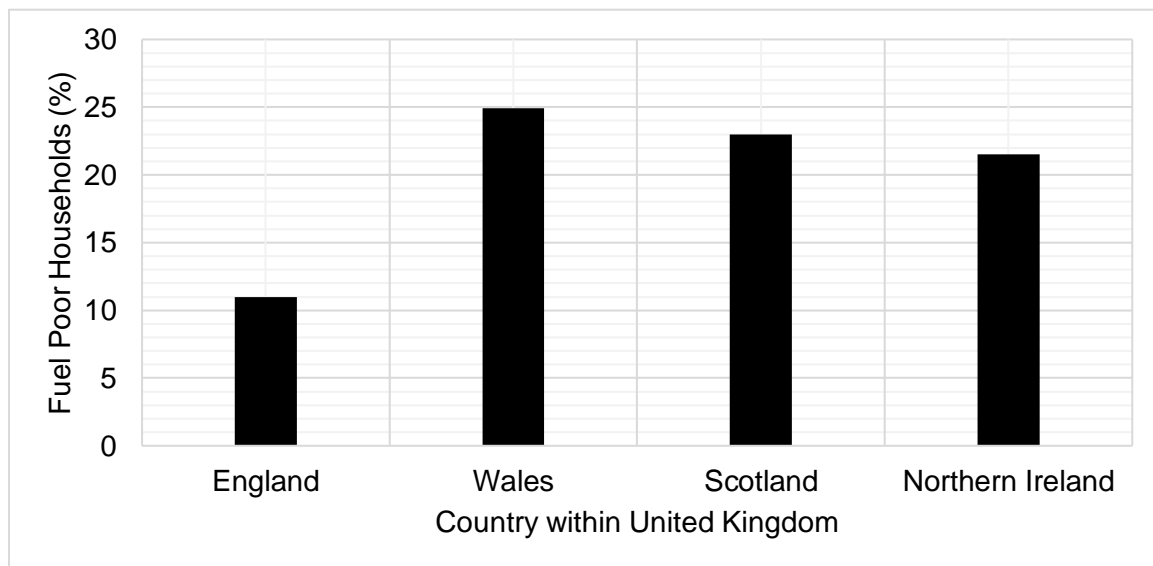


Figure 2.2. Percentage of fuel poor households within the UK ((BEIS, 2018) (Welsh Government, 2018) (Scottish Government, 2019c) (Northern Ireland Housing Executive., 2017)).

Typical building fabrics will have different construction materials and therefore differing thermal affects. To illustrate this, a cross section of a building envelope for residential dwellings from 1920, 70s and 90s can be found in Figures 2.3 a, b and c. From these typologies, the insulation within these homes varies in quantity, performance and location in the envelope and will affect the thermal performance within the internal environment. These figures demonstrate that there is a need for insulation focused retrofitting tools of not only pre-1919 but also post 1919 to pre 2010s homes.

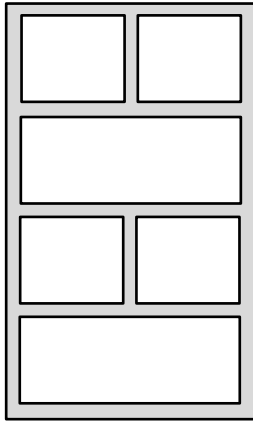


Figure 2.3a. 1920s
Solid masonry wall.

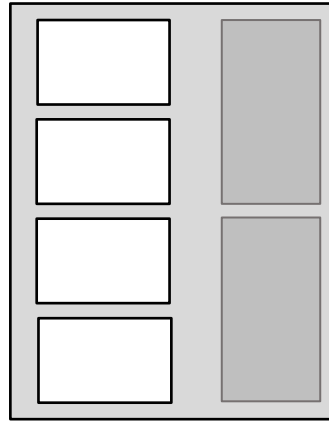


Figure 2.3b. 1970s
Outer facing brick,
50mm clear cavity,
lightweight concrete
inner.

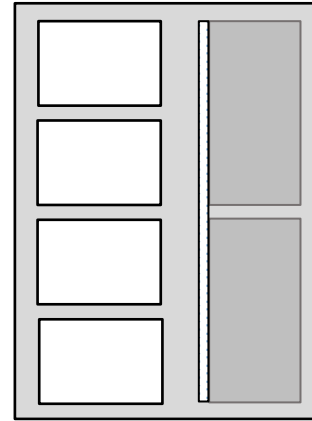


Figure 2.3c. 2010s
Outer facing brick, 50mm clear
cavity, 40mm insulation
board, medium density
inner.

2.2. Insulating residential properties

Thermal insulation aids the reduction of heat losses throughout the building envelope, by reducing the energy demand (Hens, 2017). A moisture buffering panel with hygrothermal characteristics will essentially change the hygrothermal conditions of the building.

Figure 2.4 represents the different insulation techniques for internally insulating buildings envelopes and associated changes to temperature, where the black line is the dew point and blue lines are the temperature gradient where the left hand side is the indoor temperature and right hand side, outdoor. The risk of condensation can be predicted by knowing the different type of materials that compose the envelope, the U-value, their specific water vapour permeability and hygrothermal properties of indoor and outdoor environments. When considering situation c) it is evident that a blue region is between the insulation and main building envelope. Due to the instant reduction of temperature at the interface between insulation and envelope, when cooled below dew temperature could lead to interstitial condensation. For more modern building construction (as seen in Figure 2.3c) a vapour barrier next to the indoor surface has been implemented.

The benefits of a vapour barrier is that it acts as a physical barrier zone for the cold envelope and warmer, more humid air and reduces the likelihood of the formation of condensation. This is particularly important for the colder, winter months as the temperature gradient between the

outside climate by comparison to indoors would be much greater and likely to accelerate condensation production. Over a sustained period of time, this could potentially reduce the service life of these building components (Huijbregts et al., 2015) and energy efficiency of the building.

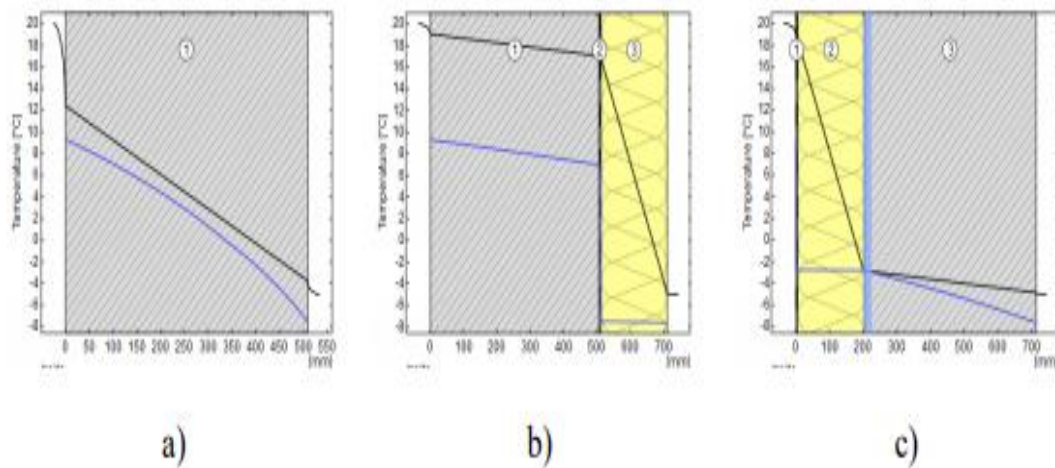


Figure 2.4. Risk of condensation analysis in building envelopes due to different insulation techniques with a) no insulation, b) external insulation and c) internal insulation (RIBuild, 2014).

Issues associated to current retrofitting measures are uniquely attributed to the year of construction. For example dwelling types that have been found to be more prone to overheating include 1960s-1970s and post 1990s mid and 2010 lack sufficient ventilation and protection from heating by the sun ((CCC), 2017). This was investigated by Hall et al., (2013) modelling how the utilisation of hygroscopic building materials can affect mould growth, indoor RH and energy demand for a UK semidetached home over the period of a year. These models demonstrated that over the year the energy demand of the home differed due to seasonal adjustments. An increase in airtightness also increased internal RH accountable to the increase in moisture loading from occupant behaviour.

Further issues surrounding the housing crisis within the UK are multifaceted such as to people living longer hence an increasing need for more housing, technological advancements affecting how much time is being spent indoors such as those who are 'homeworkers' (CCC, 2019) this is particularly highlighted within the current COVID-19 pandemic. Other major problems within the UK housing system highlighted by the Hackitt Review (Hackitt, 2018). It outlines that there are key issues associated to the building regulations and compliance to them is weak so there is an indifference around the build quality.

Even for new build homes, in 2018 less than 1% of new build home met 'band A' requirements for Energy Performance Certification (H.M.Government, 2019b) – addressing the true scope of residents this project could benefit. The consequential effects of these energy inefficient homes create unnecessarily high utility bills, an increase in indoor air polluted related diseases. This demonstrates that there are limited alternatives for minor intervention refurbishment and retrofitting techniques – such as a moisture buffering panel.

2.2.1. Sick building syndrome (SBS) and Indoor Air Quality (IAQ)

An uncomfortable relative humidity and/or temperature are some of the fundamental causes of sick building syndrome (SBS), attributing to several long term occupant hazards such as upper respiratory illnesses (Chao et al., 2003). Aside from long term health issues, thermal comfort affects all occupants and has direct consequences in relation to health and productivity (Balaras et al., 2005) which is further exaggerated when succumbed to SBS (Wargocki et al., 2000).

SBS was explored by Yu and Crump (1998) and Barreca et al. (2018) which demonstrated that the selection of appropriate construction materials is imperative for occupant well being. By considering the thermal comfort of the indoor environment, this can severely reduce the energy demand for residential properties. In developed and industrialised countries, approximately 80-90% of human behaviour is spent indoors where the indoor air quality (IAQ) is integral to the occupants (Al-Horr et al., 2016; Maskell et al., 2017).

2.2.2. Pathogenic and household nuisances

As previously mentioned, consistently RH can be a leading cause of respiratory illnesses but another effect this has is an increase in the release of Volatile Organic Compounds (VOCs) (WHO, 2009). There are many different bacterium and health effects that thrive in different RH (see Figure 2.5), so maintaining the optimum zone for RH to minimise those problems is a key parameter for the performance of a relative humidity buffering panel.

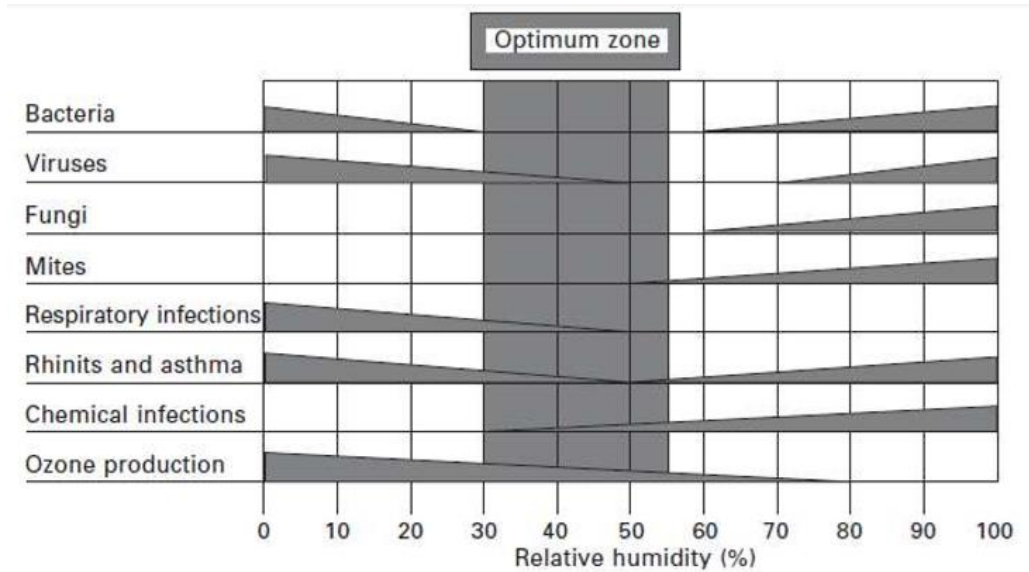


Figure 2.5. The optimum zone for RH against different types of house hold nuisances (Simonson et al., 2002).

2.3. Bio-based materials

Bio-based materials have good humidity buffering properties that reduce buildings energy use through both direct and indirect effects on heating load. The use of bio-based materials represent a renewable source that can be found all over world (Amziane and Sonebi, 2016). Their wide availability and low environmental impact enhances their applicability within research in the built environment (Korjenic et al., 2011). Their fundamental characteristics and properties will be reviewed. Bio-based materials are derived from naturally occurring sources and are defined within Vert et al. (2012).

2.3.1. Bio-based materials to reduce carbon emissions

The imminent threat of the depletion of natural resources has never been greater and requires urgent attention (Amziane and Sonebi, 2016). Addressing these is a key objective has never been more imperative and therefore the built environment must search for a more sustainable construction substance.

The mandate to reduce carbon emissions has given rise to the use of bio-based materials as structural and non-structural components in construction. Bio-based materials are superior to conventional construction materials (such as concrete or brick) due to their relative simplicity,

abundance and ability to mimic and if not better the equivalent fossil fuel based materials. This is highlighted within Figure 2.6 where bio-based materials (green) and recycled naturally sourced materials (red) have a much lower primary energy consumption than their fossil fuel based materials (blue) counterparts therefore lowering any materials generates from biobased materials to have a lower embodied energy (Jones and Brischke, 2017).

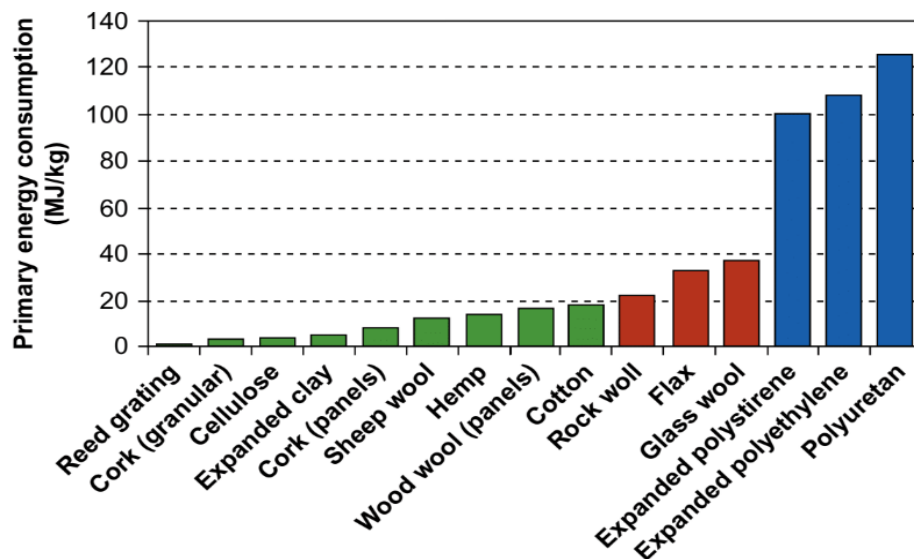


Figure 2.6. Primary energy consumption variation of bio-based and fossil fuel based materials (Jones and Brischke, 2017).

Further fundamental benefits of bio-based building materials include their whole life considerations as they can be recycled (due to their biodegradability) and comparatively lower embodied energy to fossil fuel derived insulation products (such as polystyrene or polyurethane) (Joshi et al., 2004) , which furthers the contribution of these construction materials for a ‘closed production cycle’ where waste is eradicated (McDonough, 2002).

Bio-based materials have also been investigated to reduce a buildings industrial footprint by sequestering atmospheric and embodied carbon dioxide (CO₂) ((Lawrence et al., 2013; Cetiner and Shea, 2018). Due to their hygroscopic nature bio-based materials react passively yet dynamically to vary hygrothermal environmental ensuing a ‘hygric buffer’ (Palumbo et al., 2018) and a boost for indoor thermal comfort.

2.3.2. Bio-based materials for improvement of occupant wellbeing

Continued urbanisation and the utilisation of fossil fuels has not only contributed to global warming but also reduced overall air quality (Pérez-Lombard, Ortiz and Pout, 2008). Bio-based

building materials can contribute to the Energy/unrealised energy efficiency potential and has clear environmental and economic benefits (Jones and Brischke, 2017).

The use of bio-based materials in buildings relies on their ability to influence the indoor air quality (IAQ) by controlling the RH of a room by adsorbing and desorbing water vapour (Darling et al., 2012). When exposed to interior surfaces bio-based products, (most noticeably insulation materials) contribute positively towards improving IAQ. Due to the hygroscopic nature of bio-based products, allows for the adsorption/ desorption of water vapour into their porous structure, in dynamic equilibrium with their surrounding environment, by doing so creating a hygric buffer. This enabled the fluctuations in the hygrothermal environment to be kept to a minimum thus, aiding towards improving IAQ and also reducing the energy requirements of air conditioning (Lawrence et al., 2013; Palumbo et al., 2018). In addition to bio-based products, other naturally occurring materials such as earth can also be attributed to these unique hygrothermal management characteristics. The quantity of moisture accumulated is material specific and dependent on the RH and the temperature of the environment (Palumbo et al., 2016) and by controlling these values it is possible to accurately track the adsorption/ desorption characteristics of bio-based materials.

2.4. Earth as a bio-based building material

Over 2.2 billion people (approximately 30% of the world's population) live in earth based buildings (Costa, Rocha and Velosa, 2016). Using earth as a construction material has many environmental, sustainable and economic benefits (Fratini et al., 2011). As a construction material, earth has the ability to regulate relative humidity within an indoor environment and when incorporated into a building envelope improves the whole properties hygrothermal performance (Janssen and Roels, 2009). Existing for thousands of years, using earth as a construction material is not uncommon and has been fundamental for buildings around the world (Minke, 2006; Emiroğlu, Yalama and Erdoğdu, 2015) .These techniques have been left in the past in favour for more 'fashionable' and fossil fuel intensive materials such as steel and concrete. Pacheco et al (2012) identified (in Figure 2.7) the clear embodied carbon savings for monolithic walls when using earth as a construction material compared to carbon intensive cement.

Wall type	kg CO ₂ eqv
Generic rammed earth	26
Cement stabilized rammed earth 8%	65
Cement stabilized rammed earth 9%	70
Brick or stone and blockwork cavity	71

Figure 2.7. Embodied carbon quantities for different monolithic wall constructions (Pacheco-Torgal and Jalali, 2012)

However, these materials are being rescinded due to environmental pressures and more sustainable construction techniques are regaining importance (Aubert et al., 2015). Using earth as a building material is beneficial due to its low environmental impact (Chabriac et al., 2013) and as it is such an abundant material, it provides locally sourced material reducing carbon emissions associated with the transportation of materials (Cagnon et al., 2014; Asdrubali, D'Alessandro and Schiavoni, 2015). In terms of material properties earth presents a high hygroscopicity in addition to a low thermal conductivity, enabling it to locally regulate RH (Minke, 2006; Lima, Faria and Santos Silva, 2016). The ability to use earth as a part of an earth mortar contributes to its use as an extremely eco efficient and sustainable building material (Melià et al., 2014). Earth construction can take many different forms for different applications which has been summarised within the literature within in Figure 2.8. (Where W_m = water content of manufacturing stage, W_{OPT} = optimum water content, W_p = water content at plastic limits and W_L = water content at liquid limit) (Hamard et al., 2016).

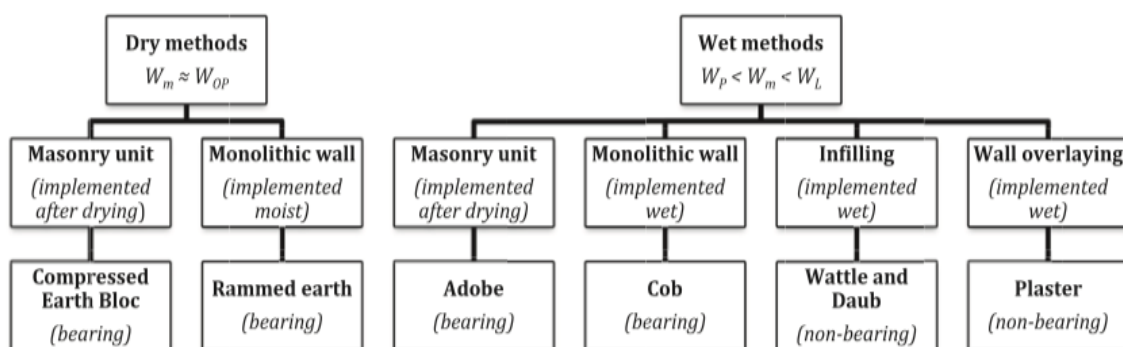


Figure 2.8. Classification of earth based construction techniques

These techniques and technologies are summarised as follows:

- Mortar: applied wet, utilised to lay bricks or stones.
- Plaster: applied wet, used to cover wall surfaces.

- Wattle and Daub: applied wet, non-load bearing in order to fill timber framework.
- Cob: applied wet, load bearing monolithic/free standing wall
- Adobe: moulded wet (at plastic limit) and dried, stacked for load-bearing/free standing wall
- Rammed Earth: layers applied in a formwork for load-bearing/free standing wall
- Compressed earth block: compacted at optimum water content and dried, stacked for load-bearing/free standing wall

2.4.1 Earth affinity with water

Understanding the relationship earth has with both water and temperature is imperative as research conducted by Padfield (1998) highlighted earth as a key material to be utilised and optimised for its moisture buffering properties. Not only this does earth have a high thermal inertia, consequentially it also reduces the heat flow fluctuations (Verbeke and Audenaert, 2018). Since then research has demonstrated in great detail the mechanisms behind heat and moisture transport within earthen construction materials. The relationship that earth has with its thermal and water are shown in Figure 2.9.

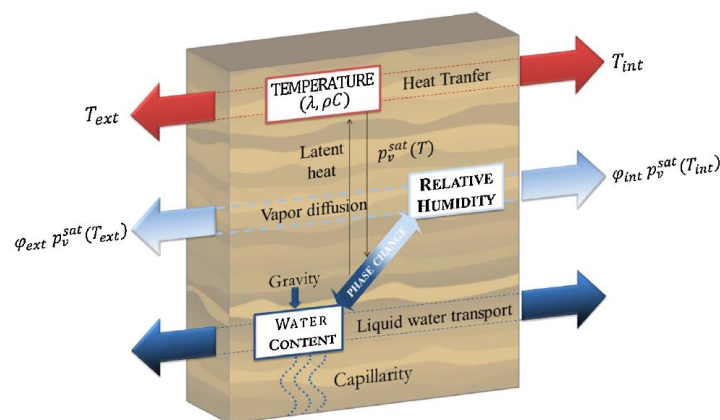


Figure 2.9. Moisture and thermal transfer within earth construction (where ϕ = relative humidity, T = temperature and p_v^{sat} = equilibrium vapour pressure) (Soudani et al., 2016).

As a raw material earth consists of clay, silt, sand, gravel and other biofibres/construction waste, when combined together the interlocking of these materials will inevitably create voids. These voids create a porous network within the earth and along with the individual intrinsic material characteristics creates a highly porous material. To understand the relationship between air and water within the earths pores can be calculated volumetrically using the saturation ratio, S_r by the following equation (2.1)

$$S_r = w_L \frac{\rho_d}{\phi \rho_w} \quad (2.1)$$

Where:

S_r = volume of pores within the material by water

ρ_d = dry density

ρ_w = density of water

$w_L = \left(\frac{m_L}{m_s}\right)$ where m_L liquid mass and m_s skeleton mass per unit of material volume

ϕ = porosity

Within Figure 2.9 the phase change between liquid water and water vapour. As earth is a hygrothermal material, it has the ability to adsorb and desorb water vapour so within the materials pores an exchange of water from vapour to liquid form (and vice versa) takes place. This is denoted by Kelvins Law as demonstrated in Soudani et al. (2015).

As this process of evaporation and condensation takes place, there is a variant in the capillary action pressure of the earthen material. Therefore the liquid water-vapour equilibrium equation can be denoted by equation (2.2)

$$P_G - P_L = \gamma_{LG} C_{LG} = f(w_L) \quad (2.2)$$

Where:

P_G = air pressure

P_L = liquid water pressures

γ_{LG} = Interfacial tension of the air against liquid water

C_{LG} = curvature of interface for pore

$f(w_L)$ = dependant on the porous network within the sample, liquid water content

At the phase change of water; at a constant pressure the average specific heat capacity can be calculated in equation (2.3):

$$\rho C_p = (1 - \phi) \rho_s C_{p,S} + \phi S_r \rho_L C_{p,L} + \phi (1 - S_r) (\rho_A C_{p,A} + \rho_V C_{p,V}) \quad (2.3)$$

Where:

ρ_s = density of solid material

ρ_L = density of liquid water

ρ_A = air mass concentration

ρ_V = water vapour (gas phase mass concentration)

At constant pressure:

$C_{p,S}$ = specific heat capacity of solid sample

$C_{p,L}$ = specific heat capacity of liquid water

$C_{p,A}$ = specific heat capacity of air

$C_{p,V}$ = specific heat capacity of water vapour

However, if there is a temperature differential between the internal and external temperature of the material it can be associated to latent heat (as demonstrated in Figure 2.9) which will be further discussed in section 2.5.2.

2.4.2. Hygrothermal ability of earth

Pore network and geometry have a large impact on the microstructural effect of the material as fully identified by Fabbri and Morel (2016). It was particularly highlighted the effect of water transport throughout the material and consequentially, its effect on hygrothermal performance of the material; particularly this is due to the chemical affinity that exists between the water and clay molecules (Hall and Allinson, 2009a). The ability to measure the effectiveness of how hygroscopic building materials function can be calculated via its Moisture Buffering Value (MBV) which will be further discussed within section 2.5.1.1.

2.4.3. Limitations using earth

Despite the environmental benefits, the use of earthen materials and construction has some drawbacks. These are generally associated to the exposure of buildings as earth is highly sensitive to deformation (Müller, Miccoli and Fontana, 2016) due to its hydrophilic behaviour. Buildings respond to their exposure conditions in a variety of ways as explored in Minke (2013); structural cohesion deformation and cracking are associated to having direct contact with water (Bui et al., 2009). Examples of deformation to earthen structures are: weathering, thermal expansion and shrinkage, mechanical impact and biological susceptibility (Gomes, Faria and Gonçalves, 2018). These key issues affecting earth construction can be grouped into three main categories: structural, environmental and chemical – which have been

organised within Table 2.1. Due to the inherently different physical and chemical properties of different earth, construction typologies and environmental conditions no two earth based buildings may face the exact same deformative issues (Ma, 2018). This deformation can occur in the short, medium and long term damage mechanisms at a micro or nano scale to create macro-sized cracks. Further to this, in terms of their implementation as building materials there is no current unified standard. Despite this, within 2016 a RILEM (International Union of Laboratories and Experts in Construction Materials, Systems and Structures) Technical Committee (274-TCE) has been set up to determine “testing and characterization of earth-based building materials and elements.

Table 2.1. Issues affecting degradation of earthen construction.

Structural	Environmental	Chemical
Thermal expansion/shrinkage causing cracking	Weathering (including rain and wind)	Delamination/Detachment due to incompatibility
Water adsorption/absorption	Poor construction/finish quality	Chemical attack
	Temperature change (Freeze thaw cycles)	
Crazing	Biological susceptibility (both pathological, vegetal and biological growth)	Salt crystallization
Settlement of walls		Disaggregation
Lack of physical connections with building components	Human and animal activity	Flaking
		Blistering

2.5. Moisture transport in bio-based building materials

2.5.1. Bio-based materials hygrothermal properties

The ability of bio based materials to relate relative humidity initiates the passive control of the local hygrothermal environment for which they are in (McGregor et al., 2016). By adding insulation as a retrofitting tool, to a residential building this also helps to reduce the heating energy in addition to acting as a view to reducing the demand of heating and cooling costs (Binici, Aksogan and Demirhan, 2016). Offsetting this energy requirement will act as a direct alleviation to the overall energy consumption of each home, city and overall countries efforts in an attempt to curb global warming.

As a fundamental basis, all materials are affected by parameters such as temperature and relative humidity explored in Jerman and Černý (2012). A high performing hygrothermal material have the ability to ‘self-regulate’ and buffer relative humidity. Bio-based insulation materials have hygrothermal characteristics, which make them ideal for indoor relative humidity buffering. Insulation materials respond to seasonal adjustments in temperature in relative humidity due to their specific thermophysical properties. As effective insulator materials, they must have thermal comfort of the occupants at the centre of their characteristics – to be cooling in the summer and reduce heat requirements within the winter. The heterogeneous nature of bio-based and evolving climatic conditions ensure that a ‘one size fits all’ approach is insufficient in order to maximise the intrinsically beneficial hygrothermal characteristics (Brás and Gomes, 2015). Therefore, the fit for purpose bio-based materials requires the analysis of relevant properties as presented below.

2.5.1.1. Moisture buffering

Understanding a materials ability to dynamically react to a changing hygrothermal environment can be calculated by finding its moisture buffering ability. Whilst it is known that there is a standard technique for determining this (by taking the mass of the sample within adsorption and desorption phases) the conditions surrounding it has come under disrepute. Current standards available for the MBV test are a German industrial normative DIN 18947 (DIN, 2013), NORDTEST Protocol (Rode et al., 2005), International standard ISO 24353 (ISO, 2008) and Japanese standard JIS A 1470-1 (JIS, 2002). As outlined in McGregor et al. (2016) and Roels and Janssen (2006). These standards utilise step changes in RH and regular mass taking to measure the gain in mass during absorption and loss of mass during desorption. However, the differences between these standards is within the hygroscopic parameters and length of time required for the step changes for adsorption and desorption phases are demonstrated in Table 2.2.

Table 2.2. Moisture buffering parameters.

Test	Preconditioning	Temperature (°C)	Adsorption phase RH range (%)	Desorption phase RH range (%)	Time steps Adsorption (hours)	Time steps desorption (hours)
DIN 18947:2013	50% at 23°C	23	80	50	12	12
NORDTEST Protocol	50% at 23°C	23	75	33	8	16
ISO 24353	(test conditions dependant) 43/63/83% at 23°C	23	55/75/95	30/50/70	12	12
JIS A 1470-1	(test conditions dependant) 43/63/83% at 23°C	23	55/75/95	30/50/70	12	12

Table 2.2. demonstrates that NORDTEST Protocol is the only protocol to not equally split the adsorption and desorption periods. It could be considered that as the occupant behaviour within resident dwellings ensures there is a dynamic environment that cannot be classified as simple as two equally weight lengths of time. Within a home, relative humidity could be raised due to a variety of factors such as cooking, breathing and showering. Therefore, when considering the moisture buffering behaviour of porous materials within these environments, the test conditions must be a true representation of the hygrothermal environment where it will be implemented within. The hygrothermal conditions that the experiments are conducted within are not unified which makes literature comparisons extremely difficult. Table 2.2 also shows that the JIS and ISO standard are the same, a further comparison of the methods demonstrates that all the tests operate at the same isothermal conditions of 23°C. In addition, different building materials will have different responses to the moisture loads they are surrounded by. The moisture loads materials are exposed to had a great effect on the materials MBV performance, as explored in Lengsfeld, Holm and Krus (2007); Yang et al. (2012). The number of cycles from initial to a stabilised MBV would therefore depend on moisture loading as moisture content within the samples would vary the outcome to the hygroscopic investigation as demonstrated within Cerolini et al. (2009) and Zhang, Yoshino and Hasegawa (2012). This hygroscopic response of the materials is attributed to the governing of the samples water vapour permeability and moisture capacity (Delgado, Ramos

and De Freitas, 2006). These were categorised by Ge et al. (2014) into three groups:

Group A: High moisture capacity and low vapour permeability

Group B: Low moisture capacity and high vapour permeability

Group C: High moisture capacity and high vapour permeability

This categorisation will give a better indication of the pore structure within the samples due to the moisture transport within it.

When reporting the results of the tests in Table 2.2, JIS and ISO require the reporting of the mass within the adsorption and desorption phases and the rate of each phase but only for the first 4 cycles. By comparison, NORDTEST protocol requires the calculation of Moisture Buffering Value (MBV) (equation (2.4)).

$$MBV = \frac{m_a - m_d}{A \Delta \phi} \quad (2.4)$$

Where:

m_a = Mass of sample at end of moisture adsorption stage (g)

m_d = Mass of sample at end of moisture desorption stage (g)

A = Exposed surface area of sample (m^2)

$\Delta \phi$ = Difference in RH between adsorption and desorption stage (%)

Within NORDTEST, MBV is calculated when samples are in a quasi-steady state over 3 cycles where samples mass change differs by no more than 5%. Once samples have stabilised they are then classified by their MBV as per Figure 2.10.

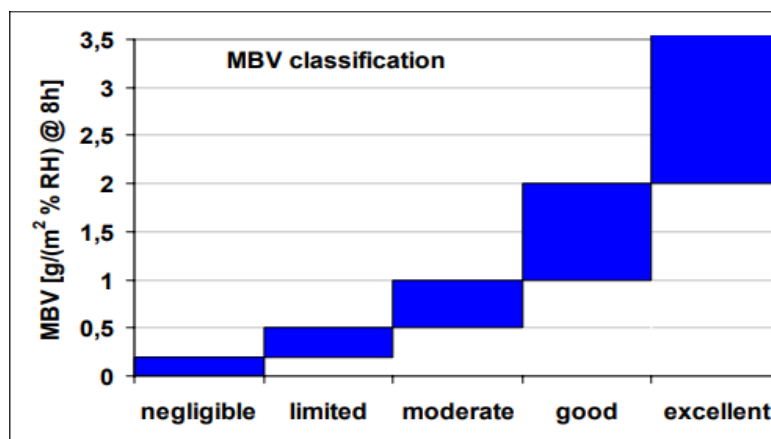


Figure 2.10. MBV Classification (Rode et al, 2005).

From calculating MBV, a comparative analysis of a materials performance is a greater MBV denoting a better performance. The MBV of common building materials was explored within Rode et al. (2007) and Collet and Pretot (2012) Particular difficulty comparing MBV of different

materials is that due to there not being a singular, streamlined test method with specific parameters whilst results could be discussed, studies cannot be directly compared.

It could be considered that MBV may not be a true classification tool but a factor in decision making of material benefits. This is as it only measures water absorption rather than understanding any other characteristics the sample may be affecting for example IAQ and reduction of VOCs (Kunkel et al., 2015). As previously mentioned, as JIS and ISO standards only require the first four phases which may not give a truly representative value for the materials as it has not reach equilibrium with its hygrothermal environment. Whilst the hygrothermal environment is arguably the most important variable for these tests other factors that can affect the moisture buffering ability include: exposed surface area and depth of samples, air velocity within climatic chamber and time taken to achieve the step change in relative humidity.

2.5.1.2. Water Vapour Permeability

This property demonstrates a porous materials ability to transfer moisture when exposed to a vapour pressure gradient as a nonlinear function of the equilibrium between the sample and environmental relative humidity. Collet et al. (2008) outline that this moisture movement is dependent on three factors: diffusion, effusion and liquid transfer. Values of water vapour permeability are calculated using wet or dry cup methods as per BS EN 12572-2016 (CEN, 2016) EN 1015-19 (BSI, 1999d) and BS EN 15803 (BSI, 2010). Osanyintola and Simonson, (2006) highlighted that when combining bio-based materials into a vapour permeable wall is beneficial to occupant IAQ. Further to this Zhang, Yoshino and Hasegawa (2012) demonstrated that the vapour permeability also reduced moisture build up which could potentially extend the service life of a building material. The vapour resistance within a sample is directly related to the interconnectivity of the pores within a material (tortuosity). Outlined by Padfield (1998) a low vapour resistance equates to an improved dynamic moisture buffering capability.

Another factor is that according to Zhang, Thiery and Baroghel-Bouny (2016) the diffusion of water within porous building materials is not only the tortuosity affects but also the remaining saturation within the materials microstructure. The literature has demonstrated that there is a significant dependency of WVP on the thickness of the sample (Vololonirina and Perrin, 2016; McGregor et al., 2017).

2.5.1.3. Sorption Isotherms

By exposing and stabilising samples to regular increases in relative humidity, the sorption isotherm can be created. This gives an indication of the hygroscopic and moisture storage capacity within the material. There are three layers of adsorption components which has been explored in Hill, Norton and Newman (2009a) and for this research project, within section 2.5.3. The difference between adsorption and desorption loops can be identified as the hysteresis phenomenon. Although this phenomenon is not greatly understood, it can be split into 6 groups as per International Union of Pure and Applied Chemistry (IUPAC) classification loops as per Figure 2.11 ((IUPAC), 1986; Thommes et al., 2015). These shapes demonstrate that due to capillary condensation, larger RH tends to impact and increase the hysteresis within a material.

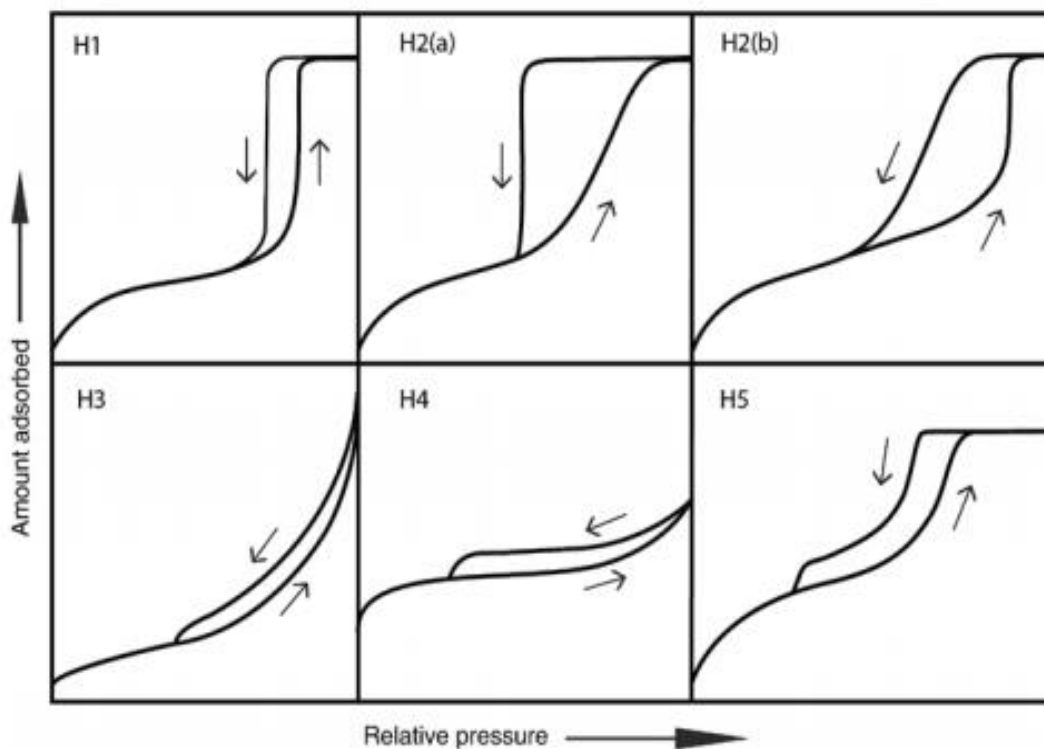


Figure 2.11. IUPAC hysteresis loop classification (Thommes et al., 2015).

Further to just the raw materials, other building materials and their water sorption isotherms have been investigated in Karoglou et al. (2005) and Růžička and Diviš (2019). Particularly for common building materials, Figure 2.12 demonstrates how the adsorption capacity is affected by relative humidity.

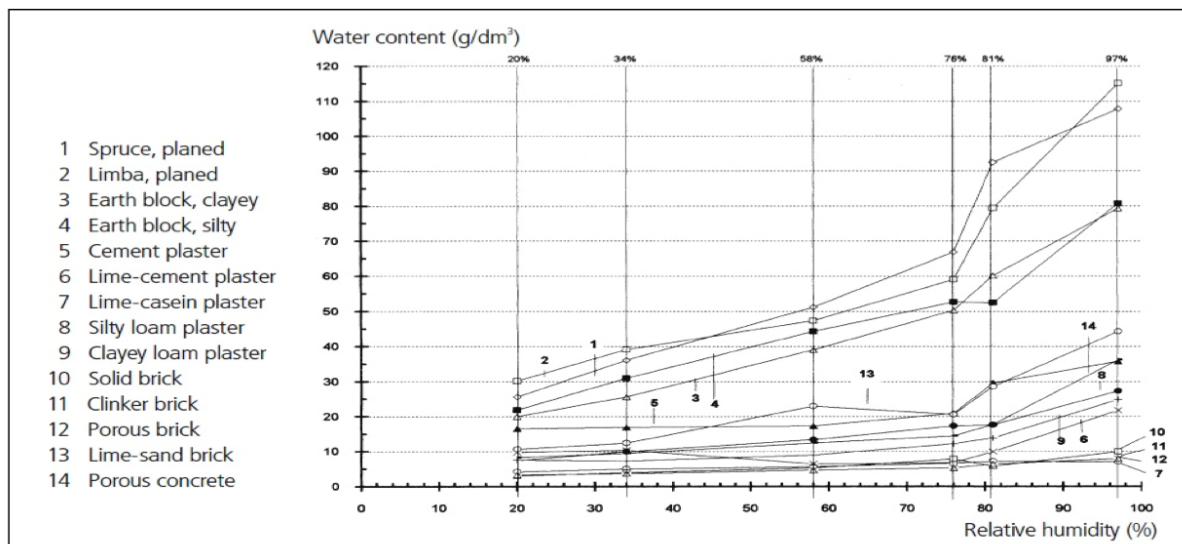


Figure 2.12. Isothermal adsorption curves for building materials (Minke, 2006).

2.5.2. Latent Heat

This is defined as the amount of heat that is required in order to facilitate a phase change in a material, without a change in temperature (Hawes, Feldman and Banu, 1993). The affects of latent heat has been relatively under researched but provides crucial information about how energy is exchanged within a sample. Within hygroscopic materials there is a constant dynamic state of vapourisation and condensing of water vapour on the surface of the material and as it travels through the pores of the sample. As the water changes state, latent heat is released; known as latent heat of condensation when water is on the surface of the material and adsorbed into the sample as liquid water (Rouquerol, 2014) and vice versa for latent heat of vapourisation. However, as this water is exchanged the latent heat that is produced during adsorption and desorption is not equal which can be attributed to the continual hysteresis as moisture is saturating throughout the sample (Callum et al., 2009).

Within a residential property, there is evidence by Qin et al. (2009) demonstrated how heating load is affected by the latent heat exchange within a 20m² office space. Where the interior

surface is covered with a hygroscopic finishing, heating energy was reduced by 6.5%. In addition Osanyintola and Simonson (2006) researched the effects that hygroscopic building materials have on latent heat exchange within a 12m² bedroom shared by two people. The effectiveness of these materials resulted in around a 10% reduction in energy consumption due to latent heat of condensation. Holcroft and Shea (2013) demonstrated that using bio-based composites can improve internal moisture buffering performance.

Bio-based materials and their coating perform differently dependant on the moisture loading conditions. Further to this, the paper also demonstrates how latent heat can be coupled with moisture buffering experiment. It can be shown that due to the implementation of these passive materials, the greater the latent heat exchanges are, energy demand is reduced however further literature within specific application of building materials is lacking.

2.5.3. Bio-based materials moisture transport mechanisms

The fundamental mechanisms and hygrothermal ability of these materials are not fully realised but are loosely attributed 'free' hydroxyl groups within the literature (Holcroft and Shea, 2013). Sorption behaviour of bio-based materials was explored in section 2.5.1.3. but on a molecular level, a water molecule consist of at least 2 hydrogen atoms and one oxygen which are polar and affects material properties as it is has a spatially-unbalanced distribution of charge – ensuring it is permanently polarised (which is visually represented in Figure 2.13). By comparison, hydroxyl groups are a functional group that consist of a hydrogen atom covalently bonded to an oxygen atom (denoted with -OH) and a valency charge of -1. As a highly reactive group, it is quick to interact with other molecules and the literature suggests that these groups provide a site for the hydrogen bonding on the surface of natural materials. This mechanism and 'likelihood' of hydroxyl groups to interact within these bio-based materials forms the basis of their theoretical hygrothermal background.

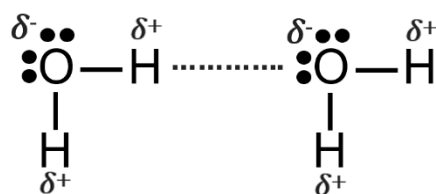


Figure 2.13. Dipole forces within water molecule.

Research has demonstrated that as temperature and time fluctuates, the number of hydrogen bonds that are formed in liquid water by a molecule varies (Jorgensen and Madura, 1985).

The fundamental knowledge behind the hydroxyl group within a bio-based insulation material is incredibly important to understand the hygrothermal characteristics of these materials. The mechanisms and methods of diffusion of water and the way in which it moves through samples is important to understand as this will contribute to the hygrothermal performance of the material.

Brunauer-Emmett-Teller (BET) theory on adsorption outlines three 'zones' of sorption in the isotherm curve (Rawat and Khali, 1999). Initially there is a monolayer adsorption, a multilayer adsorption and then capillary condensation. Within initial monolayer, adsorption is the critical element where water molecules initially bond with the different hydroxyl groups that exist within the surface layer of the material. The notion of different layers of adsorption within materials is also explained by Straube (2006) where the different sections for the moisture transport is within Figure 2.14. This Figure demonstrates that after initial adsorption of the top layer, moisture moves through a sample to its interconnected layers and then to capillary suction.

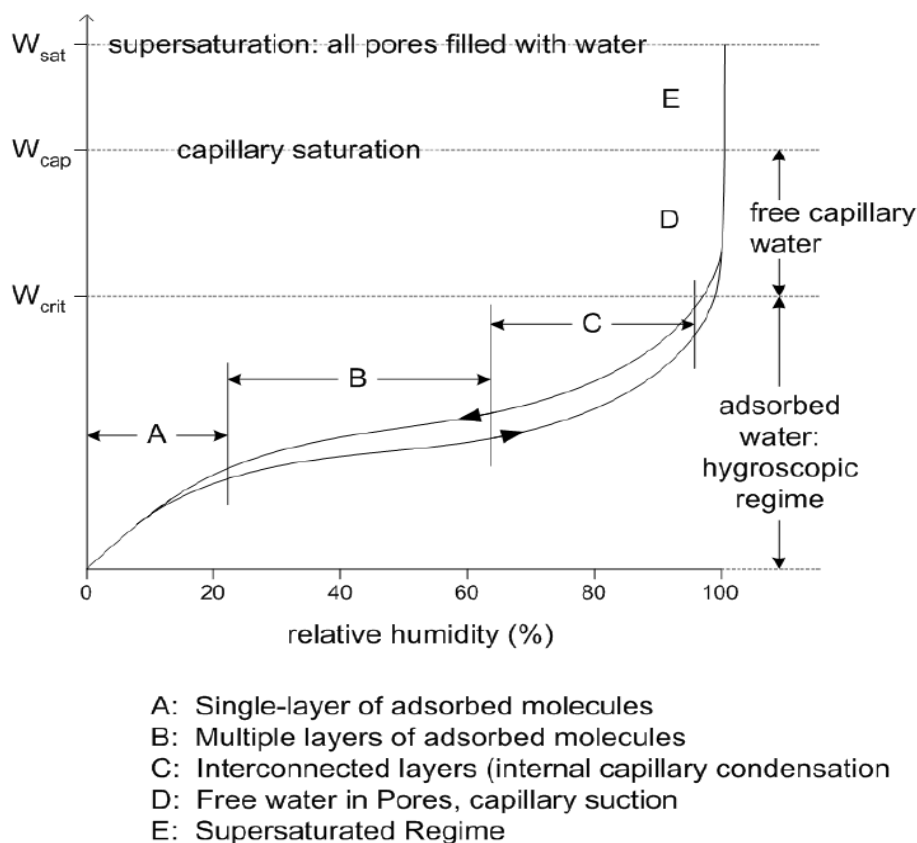


Figure 2.14. Moisture transport within hygroscopic materials (Straube, 2006).

Another way in which moisture moves and a transport phenomena from a high relative humidity environment to a low relative humidity environment is explained via the Ficks Law of diffusion and equilibrium, on the assumption of a uniaxial direction (Célino et al., 2013). The issues surrounding these theories are that they apply a 'blanket' mechanisms for hygric materials and do not account for a constantly varying hygrothermal environment over a sustained period of time. Hydroxyl groups activities seem to be related to the hygrothermal behaviour of bio-based materials. However, the chemical and physical mechanisms behind this macro behaviour are not explicitly outlined by the scientific community which emphasise the need for answers.

2.6. Understanding the differences between bio-based materials – the physicochemical impact

Aside from recycled plastics, as defined in EN 16575 (CEN, 2014) bio-based materials can be further categorised into 2 key groups: vegetable or animal fibres, but for the purpose this research will be denoted as cellulosic and keratin based. It has been well understood that bio-based materials have passive hygroscopic properties. To investigate the difference between these two groups of materials, a further review of their properties should be carried out.

As previously mentioned, bio-based insulation samples tend to be hygroscopic and therefore the moisture content greatly affects the materials thermal conductivity (as explored in (Gur'ev and Khainer (1999) and Jerman and Černý (2012)). Investigations into the characteristics of natural materials (such as wool) at daily, household temperatures was explored in Karamanos, Hاديarakou and Papadopoulos (2008) and offers an insight into when water becomes trapped within the wool it limits the materials ability to act as an insulator in its entirety. This is due to water having a much greater thermal conductivity value than that of air, so when materials are saturated in comparison to their dry state acts as a poor insulator – as explained in D'Alessandro et al. (2018). The effect of moisture having a linear relationship with thermal conductivity is also explained in Troppová et al. (2015) where wood and wood-based materials are characterised as the effects of moisture content on thermal conductivity value of wood-based fibre boards.

Understanding these bio-based materials on a microscopic level is as imperative as the macroscopic understanding as it will give an insights into why they intrinsically behave in a

certain way. Aside from recycled plastics/hydrocarbon bio based materials can be understood to be cellulose or keratin based and will be analysed separately.

2.6.1. Cellulose based

Within these type of materials, moisture mechanisms have not received sufficient research attention, where it has been demonstrated that cell wall polymers within have different bonding sites in including hydroxyl, carboxyl and sulfonic acid groups. Jiang et al. (2019) demonstrated how the microstructure and chemical composition could affect specifically the performance of fibres and shiv from hemp and flax. It also demonstrated that different parts of the material (i.e. the shiv compared to the fibre of the sample plant) had a different hysteresis behaviour and how different sorption sites affect their sorption performance.

The 'cellulose based' materials are manufactured from waste wood and these are utilised within these insulation materials as it comes from a variety of sources such as residual wood from industrial processes but also recycled wood (Yorulmaz and Atimtay, 2009). On a cellular level, the key chemical components of wood based materials rely on cellulose as the main strength element within the material, hemicellulose binds monocrystalline hydrophilic cellulose with amorphous hydrophobic lignin. Lignin is hydrophobic and its role within the material is for structurally support the materials whilst the carbohydrate (namely, cellulose) is hydrophilic. Formed by covalent bonds, cellulose maintains rigidity by transferring stress in order to reduce tensile stress and the formation of hydrogen bonds (Rahman, Hamdan and Hui, 2017). The structure of the cellulose within the material has a large and complex influence on the chemical reactions of this natural polymer.

Naturally a complex material, wood is considered a 'natural composite' consisting of lignin and carbohydrates but due to species variation there is an element of anatomical heterogeneity (Tarrío-Saavedra et al., 2011). Lignin is a one of the most naturally abundant polymers and is located in the cell walls. By utilising thermal methods, heat flow is applied to wood-based materials and pyrolysis products are produced which affects the thermal production. As an inherently diverse natural insulation material, wood is a heterogeneous and anisotropic cellular material which depends on variations within both species and interspecies dependant (Adl-Zarrabi, 2004). In addition the location of the wood sample from within the tree (for example branch, trunk or roots etc.) will give differing material properties (Cancellieri, Cancellieri and Leoni, 2009).

Understanding the molecular structure of a material is crucial to optimise its behaviour. Aside from identifying the functional groups bond behaviour, a key benefit of utilising Fourier Transform Infrared Spectroscopy (FTIR) for cellulose based materials is that the transmittance can indicate Total Crystallinity (TCI), Intensity of Hydrogen Bonding (HBI) and Lateral Order Index (LOI) (Yang et al., 2017). TCI is calculated as the infrared crystallinity rate from Nelson and O'Connor (1964) comparing absorption bands at C-H cellulose at 1370cm^{-1} and C-H bond of cellulose at CH_2 groups at 2900cm^{-1} . HBI considers the crystallinity of the molecule by examining the flexibility of the cellulose chains and the intensity of the hydrogen bonds within a sample (Poletto et al., 2012) by comparing the absorption bands at 3400cm^{-1} and 1320cm^{-1} . Finally, LOI determines the way in which the crystal lattice can vary within the crystal lattice (Corgié, Smith and Walker, 2011; Poletto et al., 2012) within crystalline zone at 1430cm^{-1} band and amorphous zone at 898cm^{-1} band. Cai et al. (2011) suggests that the thermal stability of samples which are cellulose based are affected by the order of the crystalline. Therefore, the greater the LOI the more thermally stable the sample is.

Outlined in the literature, wood is affected by high relative humidity as its hygrothermal and capillary characteristics are affected within increased environmental water vapour and takes this moisture into the cell wall and cavities of the wood. In turn, this affects the dimensional stability of utilising these materials in construction (Temiz et al., 2008) but actually boosts their utilisation as a hygrothermal buffer.

2.6.2. Keratin based

Wool consists of many different amino acids that are linked together by peptide bonds to form polypeptides. Within the wool formation, keratin is formed of a α -crystal and β crystal. From the keratin molecules, these amino acids are formed from the core elements of Carbon, Hydrogen and Oxygen, the fibres chemical composition are keratin proteins which contain Nitrogen, Sulphur, Ash (comprising of calcium, phosphorus and sodium) (McGregor, Liu and Wang, 2018). As an inherently complicated bio-based material, wools amorphous hygroscopic properties and as there is a polarity within the peptide groups of the macromolecule, salt linkages within the polymer (Micheal and El-Zaher, 2003; Osman and Abd El-Zaher, 2011; El-Amoudy and Osman, 2012). Due to intrinsically natural variations, wool insulation within this research is comprised of several different breeds of sheep and equally a variation in diet and age. Consequently, the amino acid and proteins within the wool will be heterogeneous.

Under normal atmospheric conditions wool contains around 15wt % absorbed moisture content. This relatively high moisture content within the material is a key consideration when investigating the hygrothermal conditions of these materials as this residual moisture may affect the material utilised in further experiments. Whilst the exterior of the material is hydrophobic, the interior is hygroscopic ensuring that the exchange of water can flow in and out of the sample but repels liquid water from the surface (Gibson, 2011). As outlined in Palumbo (2015) bio-based materials in hygrothermal environments are considered as a dynamic 3 phase system where there is the solid (sample matrix), liquid where the water vapour adsorbs to the surface of the samples (and therefore travels through the sample as liquid free water) and gas where the water vapour and air within the samples pores are. These materials ability to act as a hygric buffer is due to the continual equilibrium between these three dynamic states experience and their environment.

When the local hygrothermal and RH of the environment for which wool is in changes, the fibres exhibit a change in temperature, as the water vapour is adsorbed into the wools fibres it condenses and latent heat of sorption is produced as explored in Romano et al. (2019a) . Even as a bio-based material, wool is naturally flame resistant due to its protein structure and chemical composition associated with high content of nitrogen and sulphur (Üreyen et al., 2018) and when set alight is easily extinguished as it generally burns slowly (Johnson et al., 2003) – demonstrating this material’s natural flame retardant nature (Forouharshad et al., 2011).

2.6.3 Thermal methods for analysis for bio-based materials physicochemical characterisation

The thermal degradation of bio-based materials has been explored by different researchers regarding individual cellulose and keratin based materials but there is very limited literature using a combination of these materials. As explained within Jerman and Černý (2012) highlighted the importance of thermal energy storage or thermoregulation, an evaluation of thermal performance is important as thermal and hygrothermal parameters depend on both the temperature and moisture content of a material . By exploring the relationship between relative humidity and biochemical reactions within these materials it can be demonstrated how these bio-based materials fundamentally differentiate. Despite this, the drawbacks of using these materials are the inhomogeneity due to external factors that the bio-based materials may experience such as seasonal variations, location/climate and earth conditions etc.

Thermal methods enable to analyse the properties of materials as they change with temperature. Different methods can be used and they are distinguished from one another by the property which is measured as per Figure 2.15.

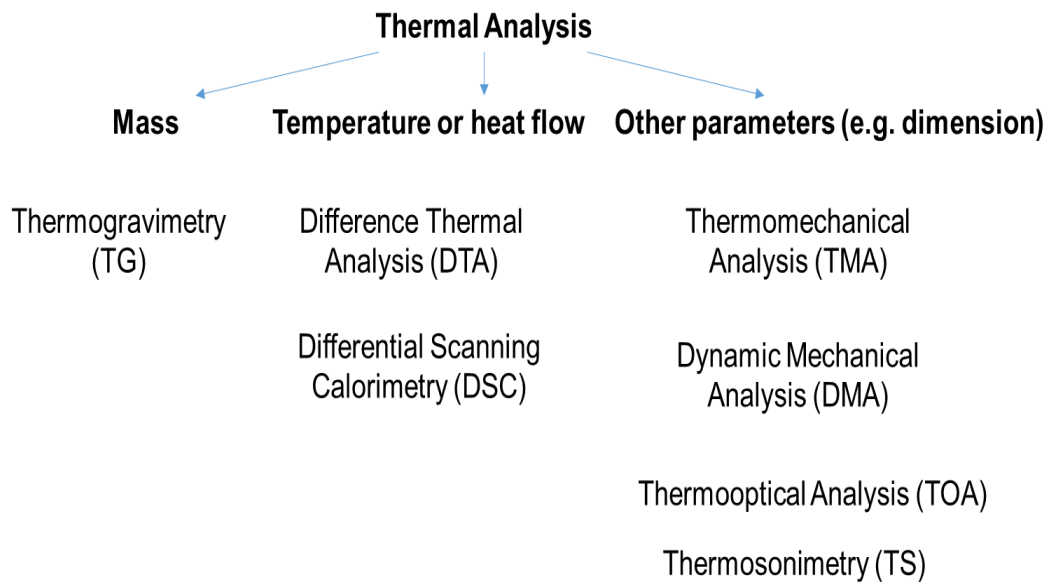


Figure 2.15. Parameter and methods of thermal analysis (based on (Feist, 2015)).

A key benefit of using thermal methods is that they provide quick and reliable results for the characteristics of materials. These include dehydroxylation which can be identified and denotes whereby heating a hydroxyl group is released and therefore a water molecule is formed (Frost and Vassallo, 1996). However a drawback of this method is that as there is such a natural variability of different bio-based materials, different thermal conditions in which they are experimented will give differing results (Bernal et al., 2017). Due to its repeatability, thermal analysis is utilised as a method of characterising heterogeneous organic materials (Tsujiyama and Miyamori, 2000). The importance/impact of the hydroxyl group on building materials properties could not be found within the literature.

2.6.3.1. Differential Scanning Calorimetry

For Differential Scanning Calorimetry (DSC) measure the heat flow changes versus temperature or time. From the thermograms that are produced, endothermic reactions demonstrate information from the samples melting and transitioning in their phases, pyrolysis and evaporation whilst exothermic reactions give information on crystallisation, combustion, chemical reactions and decomposition (Ball, C. McIntosh and Brindley, 1999). DSC thermograms consider the peak of an endothermic reaction as the melting point. Peaks whose area corresponds to the enthalpy involved within the process – the shape of this peak demonstrates if the phase change is exothermic or endothermic. A change in heat flow within a sample demonstrates a change in the heat capacity of the sample. This methodology uses only a small sample size (milligrams) and provides quick and reliable results (Tsujiyama and Miyamori, 2000).

2.6.3.1.1. Specific Heat Capacity

Specific heat capacity, C_p is the amount of thermal energy required to heat a substance by 1°C , therefore the greater the value of C_p the larger amount of energy required to increase the temperature of the material under consideration (Brown, 1997). This particular thermal parameter is important as it manages thermal properties including thermal mass and latent heat.

This methodology of C_p can be done so in two ways: statically and via DSC. Problems associated to utilising the static method is that the experiment is carried out at laboratory conditions. However, the benefit of utilising DSC this test ensures that a full temperature range within the materials service life is examined. This is particularly important for many different applications. Due to the wide-spread application of building materials across the world, the temperature range that these materials will experience is not always in line with the static conditions of the laboratory tests. Further to this, a continual increase in heating rate could be useful for fire engineering and assessing the flammability of samples. Huang et al. (2016) demonstrated the use of this methodology for raw Moso bamboo to calculate the C_p from $0-25^\circ\text{C}$. A key piece of literature for calculating C_p is by Pooley et al. (2019) which explores common building materials which is the only piece of literature of its kind.

2.6.3.2. *Fourier Transform Infrared Spectroscopy (FTIR)*

In different environments of electromagnetic radiation (EM), chemical bonds in organic compounds absorb at differing intensities at different frequencies causing peaks and signals to form a spectra. This method of spectroscopy aids the determination of chemical structure of bonding of functional groups, and can be split into two core sections: functional region and fingerprint region. For the functional region, its range is approximately 4000 – 1450 cm⁻¹ whereas the fingerprint region (specific for each material) is from 1450 – 600cm⁻¹ (Rees, 2010). The literature has demonstrated that each spectra demonstrate the functional groups according to the peak positions for every sample (Ferraro and Basile, 1978).

2.6.3.3. *Thermogravimetical Analysis (TGA)/ Derivative thermogravimetry (DTG)*

Thermogravimetical Analysis (TGA) measures mass change versus temperature or time. Performing thermal analysis such as TGA and derivative thermogravimetry (DTG) on these bio-based materials enables to develop the understanding for the way the reactions within the materials take place as a function of temperature and determines the thermal decomposition kinetic parameters (Prime et al., 2008).

Temperature changes cause alterations in the physical and chemical properties of bio-based materials, which can reflect on their hygrothermal behaviour and influence the overall properties of the final product. Chemical reactions such as hydrolysis, oxidation or reduction may be promoted, or physical changes, such as evaporation, melting, crystallization, condensation, etc may occur. A better understanding of the influence of temperature on the properties of bio-based materials enables to optimise processing conditions and tailor the product quality. It is therefore important to utilise analytical techniques to monitor the changes that occur in bio-based materials when their temperature varies. These techniques are often grouped under the general heading of thermal analysis.

More broadly, the thermal effects of a material are due to the re-distribution of internal energy within a system. This thermal response will ensure that the thermal behaviour of these materials will help an indicative understanding of these composites that previous research has neglected. Therefore, it is appropriate to ascertain some certainty for temperature-dependent

behaviour of these earth mortar composites over differing service life temperatures and beyond.

2.7 Limitations of bio-based building materials

2.7.1. Hysteresis phenomena

The inability for a material to ineffectively adsorb and desorb at the same rate and water becomes 'trapped' within the samples, these phenomena is known as hysteresis. From the literature it can be understood to be two causes of hysteresis where one is outlined by Hill et al. (2012) and within the inter-microfibrillar matrix there is a polymer relaxation that occurs when hygroscopic materials experience within a sorption isotherm. Another explanation examined by Engelund et al. (2013) demonstrates known theories of adsorption such as the ink bottle effect, capillary condensation hysteresis and contact angle hysteresis to the small linkages between large voids of adjoining pores because of the smaller diameter entry pores.

The behaviour of hysteresis was explored within Lelievre, Colinart and Glouannec (2014) where the optimal hygroscopic performance was reduced. In addition, the samples that are strongly hygroscopic will be affected the most which would demonstrate the effect of hysteresis more prevalently (Feng et al., 2015). These results also agree with work by Hall and Allinson (2009b) where there is a clear relationship linking saturation levels and an increase in thermal conductivity (Gourlay et al., 2017). The effect of hysteresis ultimately limits the functionality of the capacity to adsorb as it reaches saturation point, which limits functionality of the material as it will be unable to perform efficiency but is measured via moisture buffering value (MBV) and moisture buffering capacity (MBC). Understanding how hysteresis occurs but also how it affects performance is not a 'one size fits all approach'. However, the literature does not explicitly outline why a material has better hygric properties on a molecular level in order for the hysteresis effect to be optimised. Factors affecting the quantity of hysteresis within a material can be dependent on the materials hygric history but more fundamentally, Hill, Norton and Newman (2009a) explored how the water vapour sorption affects different bio-based fibres. It demonstrated that hysteresis between phases of adsorption and desorption isothermal is specifically dependant on the bio-fibre itself.

2.7.2. Legislation and Building Standards

The use of 'green energy' by countries intends to lower fossil fuel emissions and the overall global warming effect. To do so, protocols, regulations and the growing demand for the utilisation of bio-based building materials has never been greater (Liu et al., 2017; Burke and Stephens, 2018). Despite their low embodied energy, bio-based materials themselves have drawbacks due to the lack of European legislation surrounding embodied energy. Without sufficient regulation, the actual benefits of using such materials are much less measurable and classifiable (Scarlat et al., 2015). In spite of the legal pressures to reduce emissions within the U.K., Part L of the Building Recommendations are still yet to highlight and focus on the legislative significance of embodied energy and have tightened requirements for operational energy (Tingley and Davison, 2011).

By only considering the operational energy rather than also including the embodied energy, any Life Cycle Assessment (LCA) of a project cannot be sufficiently calculated and the true carbon footprint of the project is erroneous. In comparison to large scale construction projects such as bridges have a much larger embodied energy in comparison to smaller scale buildings such as residential houses so the requirement to highlight embodied energy is going to be even more exaggerated for these super structures (McAlinden, 2015). In addition to building regulations and passed legislation various assessment tools aim to act as a method for defining a building's performance (Jones and Brischke, 2017). There is currently no one, singular, harmonised assessment method for building performance however there are many European schemes that aim to do this such as: BREEAM (British Research Establishment Environmental Assessment Method), LEED (Leadership in Energy and Environmental Design), DGWB (Deutsche Gesellschaft für Nachhaltiges Bauen) and HQE (Haute Qualité Environnementale). BREEAM is currently the most widely used for environmental assessment in the world (Crawley and Aho, 1999; BREEAM, 2008) however, a singular unified scheme (such as a Eurocode like assessment method) may still take a long while to come to fruition. As there is yet to be a singular method, the true benefits of using biobased materials cannot be truly demonstrated which is important to consider as this may impact their wider use within the construction industry at the moment.

2.8. Earth Composites

Understanding the limitations of a material is extremely useful as it means that utilising the limitations in Table 2.1 can be utilised beneficially by other materials to be included, to improve the material properties. By combining raw bio-based materials within an earth based matrix to create this composite will potentially enhance the performance of the fibres. It will also improve the versatility of the material as a mortar panel will be much more useful than the fibres on their own. The ability to use earth as a part of an earth mortar contributes to its use as an extremely eco efficient and sustainable building material (Melià et al., 2014). In comparison to other (standard) mortars, an earth mortar composite is much more environmentally efficient as it has a lower embodied energy (Swan, Rteil and Lovegrove, 2011). The limitation outlined in Table 2.2 for high deformation under water adsorption/absorption (Fratini et al., 2011) will be utilised as a positive characteristic to enhance hygrothermal properties.

2.8.1. Stabilisers

To counteract this, a stabiliser must be used to further inherently improve structural strength and shrinkage cracking. The use of stabiliser has been notified as a requirement for improving the mix design of bio-based composites. Aside from organic binders such as outlined in Matalkah et al. (2017), Coppola et al. (2018) and Mukherjee and Achal (2015), however due to the lack of consistent and focused research, these have been discounted for this project. The main three binders utilised within construction materials are gypsum, lime and cement. Due to the high energy consumption of cement-based mortars, the search for a more environmentally conscious binder for earth mortars was required. The use of natural hydraulic lime has been utilised as it has many beneficial characteristics such as: a lower energy consumption compared to cement based mortars when created and its hygrothermal characteristics (as outlined by Cardoso, Eires and Camões (2013); (Iucolano, Liguori and Colella, 2013)). Similar to previous research, Gomes et al. (2017)) used both air-lime and hydraulic lime with varying weight of earth, increasing binder also increased water absorption coefficient. (Faria et al., 2015) investigated the behaviour of different binder content within an air-lime earth mortars, displaying increased thermal conductivity.

These hygrothermal characteristics enable the mortar to permeate vapour transport within the matrix where cement would not be able to facilitate this movement. Whilst lime comes in many forms, to generalise, 'limes' are manufactured at 900-1100°C whilst their equivalent Portland cement is fired at 1200 to 1500°C (Naktode, Chaudhari and Waghe, 2014). This difference in

temperature between the materials demonstrate that the carbon dioxide (CO₂) emissions are greater in Portland Cement due to higher energy input required to increase firing temperature. Further to this, whilst the lime also emits CO₂ during the curing of lime mortars, CO₂ is also partially adsorbed and therefore sequestration occurs –the net CO₂ is lowered. The differences between using lime and cement as a stabiliser within a mortar has been explored by Srinivasa Murthy (2014)

Further to the addition of earth and stabilisers, the incorporation of fibres to a mix design has been proven to be beneficial in terms of improving thermal characteristics by reducing thermal conductivity (Fabbri, Morel and Gallipoli, 2018) and improving compressive strength (Palumbo et al., 2016). As outlined in Laborel-Préneron et al. (2016) there are clear benefits of stabilising earth based samples but a balance should be struck between improving the materials properties versus the environmental impact. When combining the bio-fibres within an earth mortar matrix it creates a composite material. The creation of such composites has had a lot of research attention as it boosts the materials overall properties.

2.8.2. Natural Hydraulic Lime (NHL) Composites

Produced by heating a limestone with naturally occurring impurities and clay, NHL has been used for constructions purposes for thousands of years. Uniquely to NHL and unlike Portland cement, it has an innate water vapour permeability which gives it its unique hygrothermal properties (Ramamurthi and Sophia, 2016). Utilising the A further benefit of utilising NHL is its burning temperature is approximately 1000-1250°C and by comparison to Portland cement which is 1400-1450°C (Sabbioni, Bonazza and Zappia, 2002). This difference in temperature means that NHL has an innate lower embodied energy before the production of any mortar has begun. Within this research project, the utilisation of a binder that can transport moisture molecules from the external environment to within the sample is crucial for boosting the moisture buffering potential. As a NHL, a pozzolanic admixture and hydrated lime and ability to continually sequester carbon dioxide during carbonation, makes it an ideal building material. Research conducted by Lanas, Sirera and Alvarez (2006) demonstrated that this ability of NHLs to utilising water vapour from its environment that when cured in different RH conditions, strongly enhances the tensile strength of the sample. Further to its mechanical properties, at different RH samples durability was also improved due to the porosity of the structure. Di Bella et al. (2014) demonstrated that when combined with natural/bio-based fibres, the mechanical performance of NHL mortars was just as good if not surpassed by comparison to fossil fuel derived fibres such as polypropylene.

2.8.3. Influence of bio-fibres within earth mortar matrix

2.8.3.1. Thermal behaviour

There has been extensive literature, which demonstrates that adding bio-based materials reduces the thermal conductivity and optimises the insulative properties of an earth mortar matrix. Fundamentally, as the fibre content is increased, the mortar matrix is reduced and as the bio-based material replacement has a lower density it reduces the overall composites density and thermal conductivity. Values for the thermal conductivity of these mortar matrixes vary from 0.067-1.21 (W/(m.K)) ((Benmansour et al., 2014; Millogo et al., 2014; Labat, 2016; Mazhoud et al., 2017; Viel, Collet and Lanos, 2017). Aside from review papers, the characterisation of earth mortar includes either cellulose or keratin based materials. It is difficult to cross compare these types of composites due to the differences across the testing methodology and procedure.

2.8.3.2. Mechanical properties

Traditionally, fibres have been used as a reinforcement for earth based construction where straw has been used to reduce shrinkage cracks and optimised throughout the literature (Ghavami, Toledo Filho and Barbosa, 1999; Bouhicha, Aouissi and Kenai, 2005; Segetin, Jayaraman and Xu, 2007).

These studies have demonstrated how the inclusion of fibres improves tensile strength but reduces compressive strength. As demonstrated in Table 2.2 a problem affecting the degradation of raw earth materials is the issue of shrinkage (especially during drying) leading to cracks which is combatted by improving the matrixes plastic behaviour by incorporating bio-based fibres which was investigated by Eid (2018). The other structural properties and how the earth mortar and bio-based materials interact to enhance these properties are demonstrated in Achenza and Fenu (2006), Galán-Marín, Rivera-Gómez and Petric (2010), Dove, Bradley and Patwardhan, (2016); Menasria, Perrot and Rangeard (2017) and Perrot et al., (2018).

Other literature has also explored the use of other fibres in order to reinforce earth mortars with materials such as hemp (Hussain et al., 2019), hibiscus (Millogo et al., 2014), coir (Anggraini et al., 2015) and other raw bio-based materials as outlined in Laborel-Préneron et

al (2016), Mesbah et al. (2004) and Fabbri, Morel and Gallipoli (2018).

2.8.4. Fibre to Matrix Adhesion

A limitation of the earth mortar and fibre interaction is the lack of bonding between the two materials. Due to the hygroscopic nature of the fibres, initially when combined within the matrix, the fibres swell with water and as they dry out a void between the fibre and matrix is left (see Figure 2.16). The poor adhesion between fibre and matrix, resulting in an overall reduction in strength characteristics (John and D. Anandjiwala, 2008). The interface between bio-based materials and the matrix it is surrounded in (specifically earth mortar within this context) is extremely important and within research conducted by Ghavami, Toledo Filho and Barbosa (1999) is governed by three key parameters. These are:

1. The resistance of the earth in shear due to the surface morphology/surface roughness of the fibre
2. As the earth shrinks, the compressive friction forces this creates on the surface of the fibre
3. The earth's cohesive properties

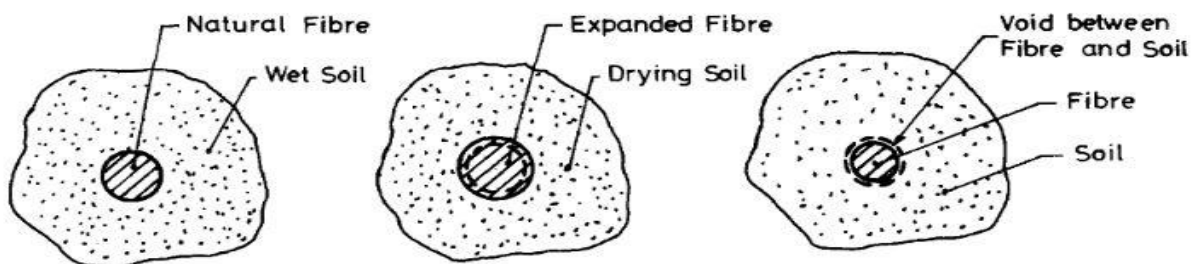


Figure 2.16. Bio-fibre to matrix adhesion (Ghavami et al 1999).

However it was also explored in Naaman and Najm (1991) that the compatibility with the mix designs will be examined outlined that there are 4 key elements which affect the compatibility and strength of bonds between fibres and the surrounding matrix: 1) chemical and physical adhesion 2) mechanical component of the bond 3) interlocking of fibre to fibre and 4) friction. As natural fibres degrade within specifically alkali conditions (Guo et al., 2019) this affects both structural and hygrothermal capability of the sample.

In terms of the quality of adhesion, outlined in Alvarez and Vázquez (2006), it demonstrated how this can be evaluated by tensile/flexural testing but an Scanning Electron Microscope (SEM) image would demonstrate the morphology between the fibre and matrix. The improvement between this interaction has been researched and if necessary, acetylation is used (where alkali solutions are used to strip the initial surface layer, waxes or oils within a

fibre to improve the texture for adhesion) as used in Fatma et al. (2019). Other treatments that have been researched include the boiling of samples in water and oils (Ledhem et al., 2000; Merzoud, Fertikh and Habita, 2011; Achour, Ghomari and Belayachi, 2017; Fadele et al., 2019).

2.8.5. Thermal analysis

The way in which ancient mortars have been analysed using chemical techniques as outlined in Elsen (2006) and how different sample types and methods of preparation are explored Middendorf et al. (2005). Middendorff outlines the different ways in which samples can be utilised in to optimise the investigation of the constituent materials. Corti et al. (2013) also outlines several different analytical techniques to categorise these complex mortars and research that has already utilised them. The utilisation of bio-based fibres in stabilised earth mortars has received much research attention. As outlined in B. Armel et al. (2017) the physicochemical properties of these materials and resultant effect on the mechanical properties of the final product has been the focus of little research. Further to this, the methodology has been traditionally used for conservation tasks and understanding heritage building materials but not for understanding the hygrothermal performance of construction materials.

2.8.6. Alternatives to bio-based earth mortar composites

Generally, 'green' insulation panels can be realized by employing 'Phase Changing Materials' (PCMs) as outlined in Cui et al. (2015) and Baetens, Jelle and Gustavsen (2010) and bio-based composite materials as outlined in Laborel-Préneron et al. (2016). Due to their large specific heat capacity, PCMs can increase thermal comfort as they have the ability to regulate indoor temperature (Al-Saadi and Zhai, 2013). Yet the energy required for the material to change phases (i.e. superheating) limits their application (Chen and Qin, 2016), enhancing the need to optimise bio-based composites. Bio-fibre composites can be developed using agro-waste which is widely available. Internal wall bio-based panels optimisation has been studied by other researchers (Arnaud, 2009; Pavlik et al., 2011; Latif et al., 2016; Latif et al., 2018). However, the knowledge on the passive mechanisms and the hygroscopic characteristics associated to these materials is not fully realised. Further to this for their utilisation in the U.K, according to Mathis et al. (2019) the majority of melting temperatures (over 25°C) is higher than the average temperatures so would be ineffective for use within British climate.

2.9. Conclusion

This literature review has aimed to understand the current typography, problems and requirement for a moisture buffering panel in residential properties and to understand the differences in bio based and earthen materials. From this literature review, it is demonstrated that following research will have to ensure that the bio-fibre and earth mortar are optimised independently before combining the two materials together to create the composite. It is also clear that latent heat has a clear effect on the passive usage of these materials.

Further to this, to the author's understanding there is no research that demonstrates how relative humidity affects both cellulose and keratin fibres and also how they perform within earth mortar and their physicochemical properties. From this literature review, the following research gaps have been found:

2.9.1 Knowledge gaps in current literature

- The effect of latent heat has on the hygrothermal performance of a bio-based material has not fully been realised.
- The thermal stability of bio-fibres and their composites, especially within different relative humidities (RH) cannot be found in the literature.
- Understanding how temperature effects the specific heat capacity (C_p) of bio-fibres and their composites over their service life temperature range cannot be found within the literature.
- Bio-fibres and composites exhibit hygrothermal behaviour, but how their structural alters because of this cannot be found within the literature.

Chapter 3 – Characterisation of bio-fibres

3.1. Introduction

Within Chapter 2, it is demonstrated how bio-fibres have an innate ability to passively control indoor relative humidity as well as improving air quality and increase thermal comfort. To produce a panel that optimises the performance of these materials, it is crucial to understand which bio-fibres perform the most effectively and efficiently. This chapter will use laboratory experimentation to classify the physical (but in particular the hygrothermal and thermal) properties of 10 bio-based and 1 recycled thermoplastic polymer insulation samples, currently available on the market in the U.K. The best performing samples were selected for further experimentation in Chapter 4.

3.2. Materials

3.2.1. Materials Characterisation

Ten samples of natural bio-based insulation materials and one thermoplastic polymer were analysed: four different types of (Sheep and recycled) Wool insulation, Hemp, Wood Wool Board (WWB), Saw Mill Residue (SMR), Wood Fibre (WF), Straw, Insulated Cork Board (ICB) and Polyethylene terephthalate (PET). All materials are currently available on the market within the U.K. (Figure 3.1a-k). For each test, samples were utilised 'as received' and where required for fibrous samples (such as wool), cut to size. For experiment, 5 measurements were taken. The properties of each type of bio-based material are listed in Table 3.1.

Table 3.1. Raw bio-fibre material characteristics.

Sample ID	Photo reference letter	Sample Thickness (mm)	Density (kg/m ³)	Thermal Conductivity (W/m.K)																								
Wool 1	a	65	18	0.039																								
Wool 2	b	75	31	0.035																								
Wool 3	c	50	45	0.04																								
Wool 4	d	40	30	0.039																								
Hemp	e	50	25	0.04																								
WWB	f	15	0.065	SMR	g	55	50	0.038	WF	h	60	145	0.041	Straw	i	60	200	0.0397	ICB	j	65	120	0.04	PET	k	10	13	0.04
SMR	g	55	50	0.038																								
WF	h	60	145	0.041																								
Straw	i	60	200	0.0397																								
ICB	j	65	120	0.04																								
PET	k	10	13	0.04																								



Figure 3.1. Natural bio-based insulation materials and one thermoplastic polymer tested, according to the information presented in Table 3.1.

3.3. Methodology

3.3.1 Surface Morphology

Once samples were selected, the surface morphology and material characteristics were investigated at micro-level. This was conducted by using a Scanning Electron Microscope (SEM) Quanta Inspect S device. The accelerating voltage of the SEM was 20 kV, with a filament voltage of 2.0 – 2.3, Emission Current (EC) of ~100 and a set auto-bias to an EC of 100. Before testing, samples had a sputter coating in gold to prevent any charging of electrons to the sample.

3.3.2. Density

To compare the effect of moisture on the samples, both the dry and saturated density of the materials were calculated as per should be BS EN 1015-10 (BSI, 1999c). For each type of material, three specimens were analysed. Density of saturated materials was determined by completely immersing samples in water, periodically recording weight gain until mass was constant and saturation point was reached.

3.3.3. Moisture Buffering Value (MBV)

The Moisture Buffering Value (MBV) is a manifestation of the ability of a material to efficiently adsorb and desorb moisture in a dynamic hygrothermal environment. To prepare the samples, all materials were cut to ensure the same exposed surface area of 0.01m². Samples were exposed to cyclic step changes of RH between 75% and 53% every 8 hours and 16 hours, respectively, at a constant temperature of 23°C. This is in accordance with both NORDTEST protocol (Rode et al., 2005) and ISO 214353 (ISO, 2008) – Figure 3.2 demonstrates the step change in RH over a single 24 hour cycle.

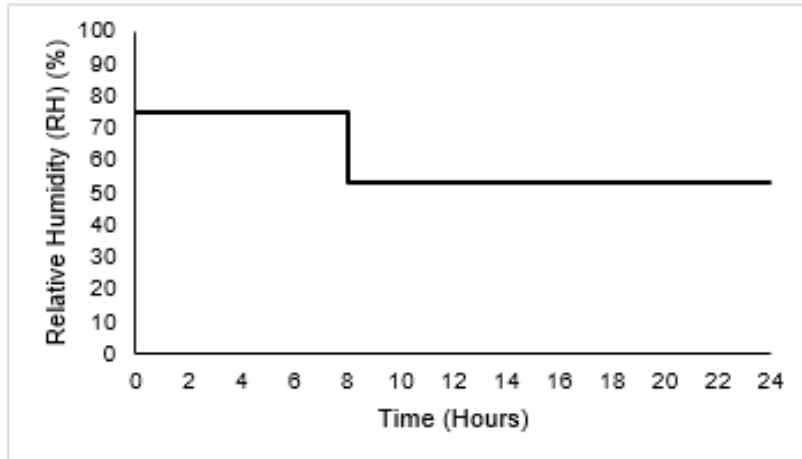


Figure 3.2. Step change in RH within climatic chamber over a singular, 24 h cycle

To determine the Moisture Buffering Value (MBV) the following equation was adopted (Equation 3.1):

$$MBV = \frac{m_a - m_d}{A \Delta \phi} \quad (3.1)$$

Where:

m_a = Mass of sample at end of moisture adsorption stage (g)

m_d = Mass of sample at end of moisture desorption stage (g)

A = Exposed surface area of sample (m^2)

$\Delta \phi$ = Difference in RH between adsorption and desorption stage (%)

Apart from satisfying the two test conditions, the adopted hygrothermal conditions mimic a residential household and the occupant's behaviour within the U.K. Samples were placed horizontally within the climatic chamber and wrapped in aluminium foil tape. All samples had a singular exposed surface area $0.01m^2$ (where other surfaces were covered in aluminium foil tape).

3.3.4. Thermal Conductivity

Thermal conductivity values of the as-received and moisture-saturated samples were recorded. This was carried out by using a thermal conductivity meter (ISOMET 2114) that features a 60mm diameter circular contact probe (see Figure 3.3). Thermal conductivity measurements were conducted at laboratory conditions of $21^\circ C$ and 54% RH.

The thermal conductivity was measured in three differing states: dry, saturated and how the samples dynamically react to a changing hygrothermal environment within a climatic chamber. When in the chamber, thermal conductivity of the samples was recorded during at time intervals of 0, 8 and 24 h during the absorption and desorption phases.



Figure 3.3. Saturated bio fibre thermal conductivity reading.

3.3.5. Temperature evolution during transient behaviour

To detect the temperature changes within the samples, thermocouples were located on both the surface and at 50% of the depth of the sample (as per Figure 3.4a). The K type thermocouples and data loggers are functional at temperature ranges of -40°C to 260°C and -250°C to 1370°C respectively, with a maintained resolution of $\pm 0.04^{\circ}\text{C}$.



Figure 3.4a. Bio-based samples with thermocouples attached.

Samples within 'Run 1', were exposed to 10 cycles of 24 hours, where temperature values were recorded in 30 sec time intervals. The selection of 10 cycles is assumed to be the minimum number for a representative analysis of hygrothermal behaviour of each sample. According to Holcroft (2016) and Padfield (1999), there appears to be an optimum zone within the sample for detecting temperature changes. This area is an approximately 15-16mm thick material zone that starts from the surface of the sample towards its core (Padfield, 1999). This 'optimum zone' is hypothesised to be the active layer of the sample (McGregor et al., 2017). Therefore, for the next cycle of testing ('Run 2'), samples were scanned with thermocouples

on both the surface and at a depth of 15mm (see Figure 3.4b), where 22 cycles represents the final stabilisation of samples.

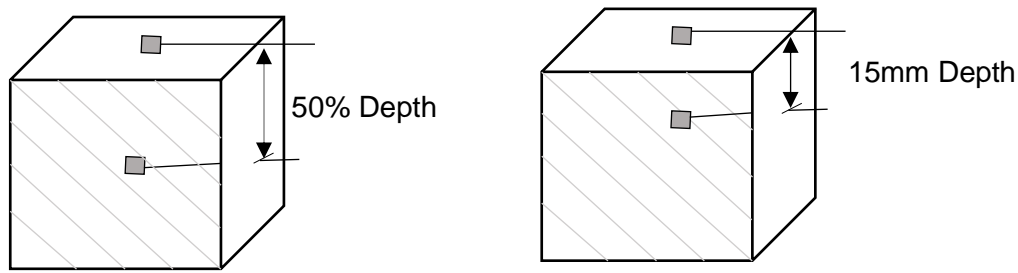


Figure 3.4b. (L) 'Run 1' thermocouples arrangement and (R) 'Run 2' thermocouple arrangement.

3.4. Results and Discussion

3.4.1. Density of the materials

The density values of the samples are illustrated in Figure 3.5a and 3.5b. When comparing density data from both dry and saturated samples, it is evident that moisture (and particularly when saturated) increases significantly with density of the sample. This is attributed to voids or air gaps between fibres, within the bio-based material, that are filled by water molecules rather than free flowing air. Low density values of dry samples indicate that the material is permeable enough as bonding sites for water molecules are readily available.

As can be seen in Figures 3.5a and 3.5b, it is evident that the density values of Wool 1,2,3 and 4 exhibit a substantial increase when samples are saturated. The increase in density can vary to values between 1.5 to 8 times of the dry density. It has been hypothesised by Swift and Smith (2001) that this could be attributed to the microscale structure of wool itself and the hygrothermal conditions the sample is exposed to. Swift and Smith (2001) highlighted that depending on the hygrothermal conditions, the lipid layers that are disordered and dynamic may change positions. Therefore, as a direct response of being saturated, lipid layers may change positions and when in contact with water may swell to as many as 7 times of their original size. ICB exhibited the lowest dependency on changes between dry and saturated states. This could be attributed to the extremely slow water adsorption of water into cork cells in comparison to other bio-based materials such as the wood fibres (Rosa and Fortes, 1993).

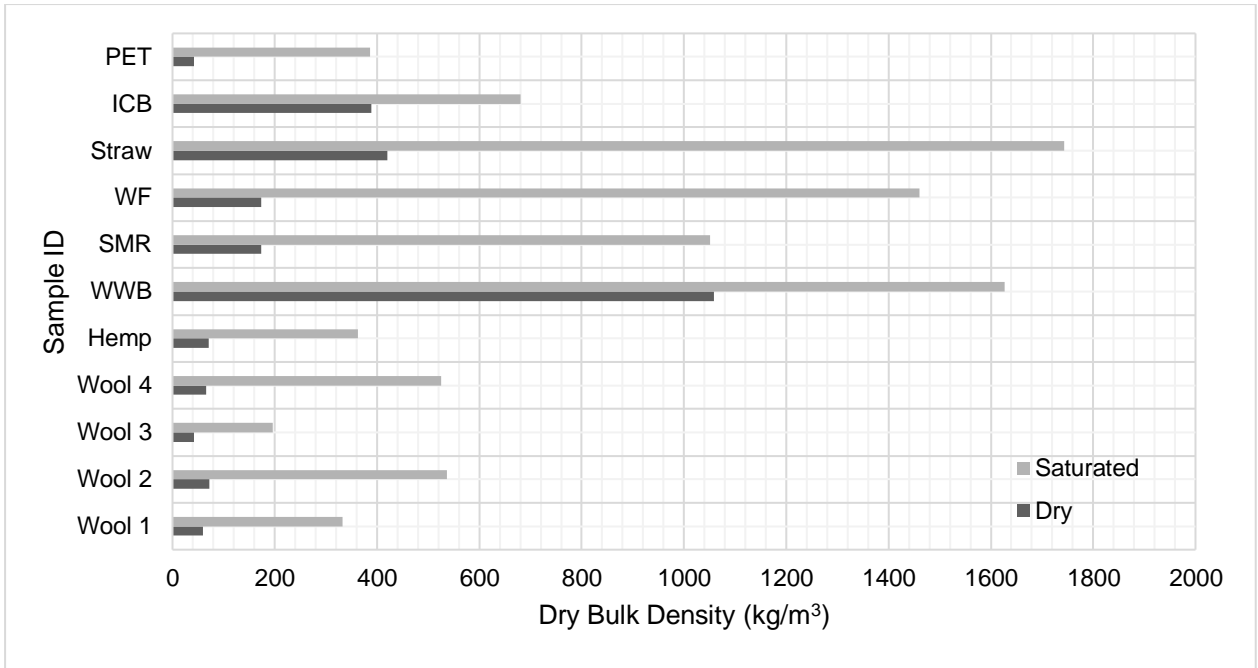


Figure 3.5a. Bulk density variation of samples in dry and saturated states.

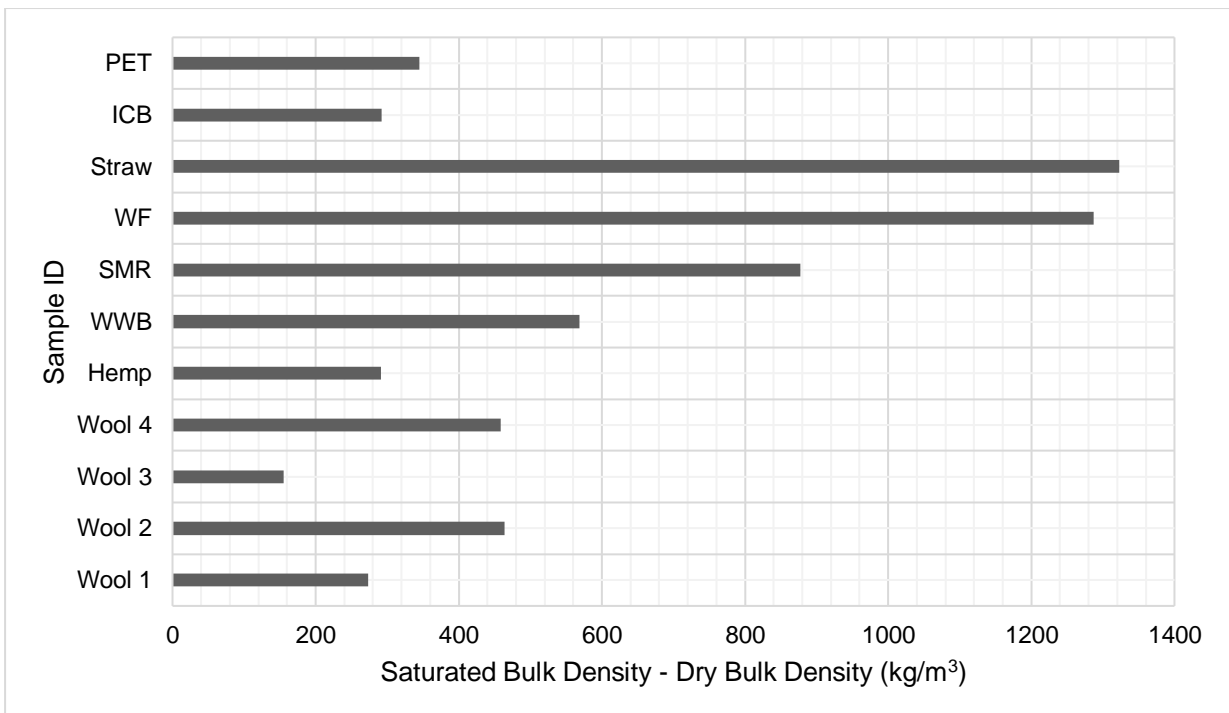


Figure 3.5b. Difference between saturated and dry density of examined materials.

3.4.2. Moisture Buffering Value (MBV)

The MBV of the examined samples were determined for each individual cycle. The MBV for 10 cycles is illustrated in Figure 3.6. MBV measurements were taken manually and due to accessibility issues to the climatic chamber over weekends, cycles 4, 5 and 6 have been excluded from Figure 3.6.

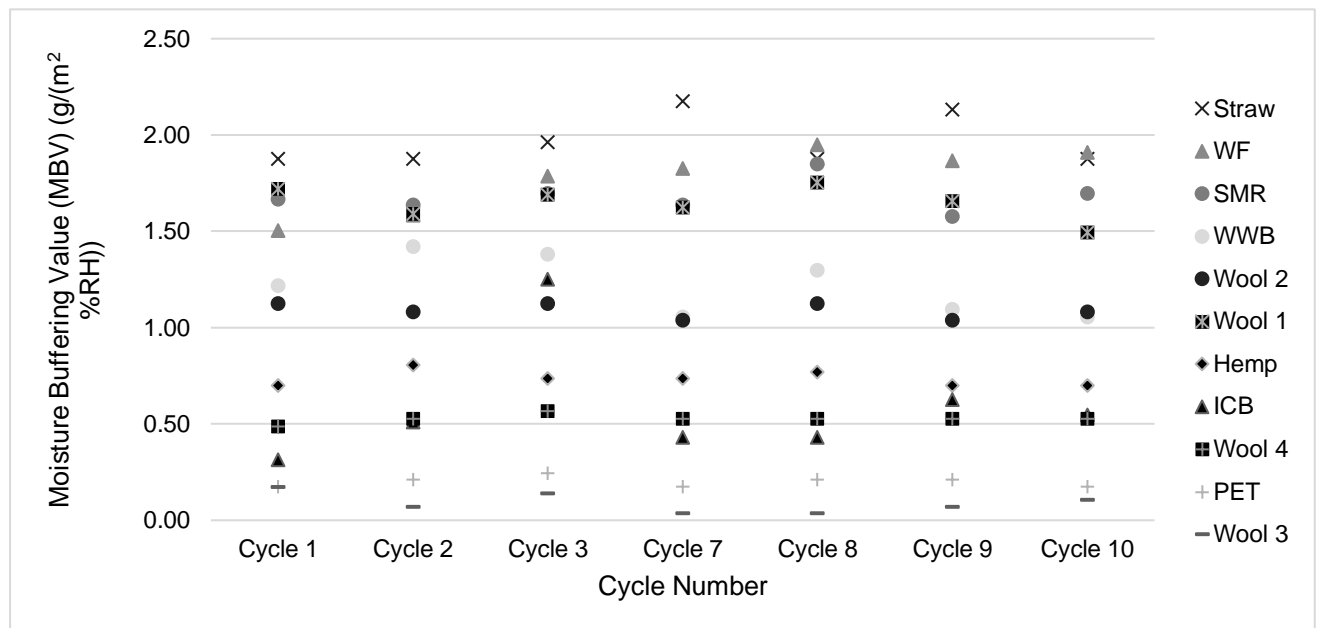


Figure 3.6. MBV variation of each sample per cycle.

In Nordtest Protocol (Rode, 2005) test, materials must be in a quasi-steady state, demonstrated by a variation in mass of less than 5% for 3 consecutive cycles. Due to the inherently variability of bio-based and recycled materials, all samples except for ICB, Straw, Wool 1, Wool 4, SMR and PET are in a quasi-steady state within 10 cycles. This is demonstrated within Figure 3.6 as it demonstrates MBV values fluctuation over the course of the hygrothermal cycles. It may be postulated, that the variation between each bio-based sample is a result of a probable micro-capillary network formations created during water molecules adsorption and desorption. As this process continues, for samples that are cellulose based, transient micro-capillary networks are formed within cellulose and lignocellulose fibres. Whilst in a constant cycle of adsorption and desorption within the chamber, capillary condensation becomes more apparent (Hill, Norton and Newman, 2009b). Due to their fundamental and inherently variable characteristics, different bio-based materials stabilise at different rates (McGregor et al., 2016). This explains the increased scattering within the MBV values for the different studied samples to sample as they react to the hygrothermal environment.

In addition to MBV values, the shape of the adsorption/desorption curve has received little attention. The adsorption/desorption curves can be seen in Figures 3.7a and 3.7b. These graphs demonstrate that some samples are losing mass from the start of the experiment. This is potentially due to moisture within the sample being greater than the extra hygrothermal environment. Water molecules will then move across this moisture gradient and will begin to adsorb once samples have acclimatised.

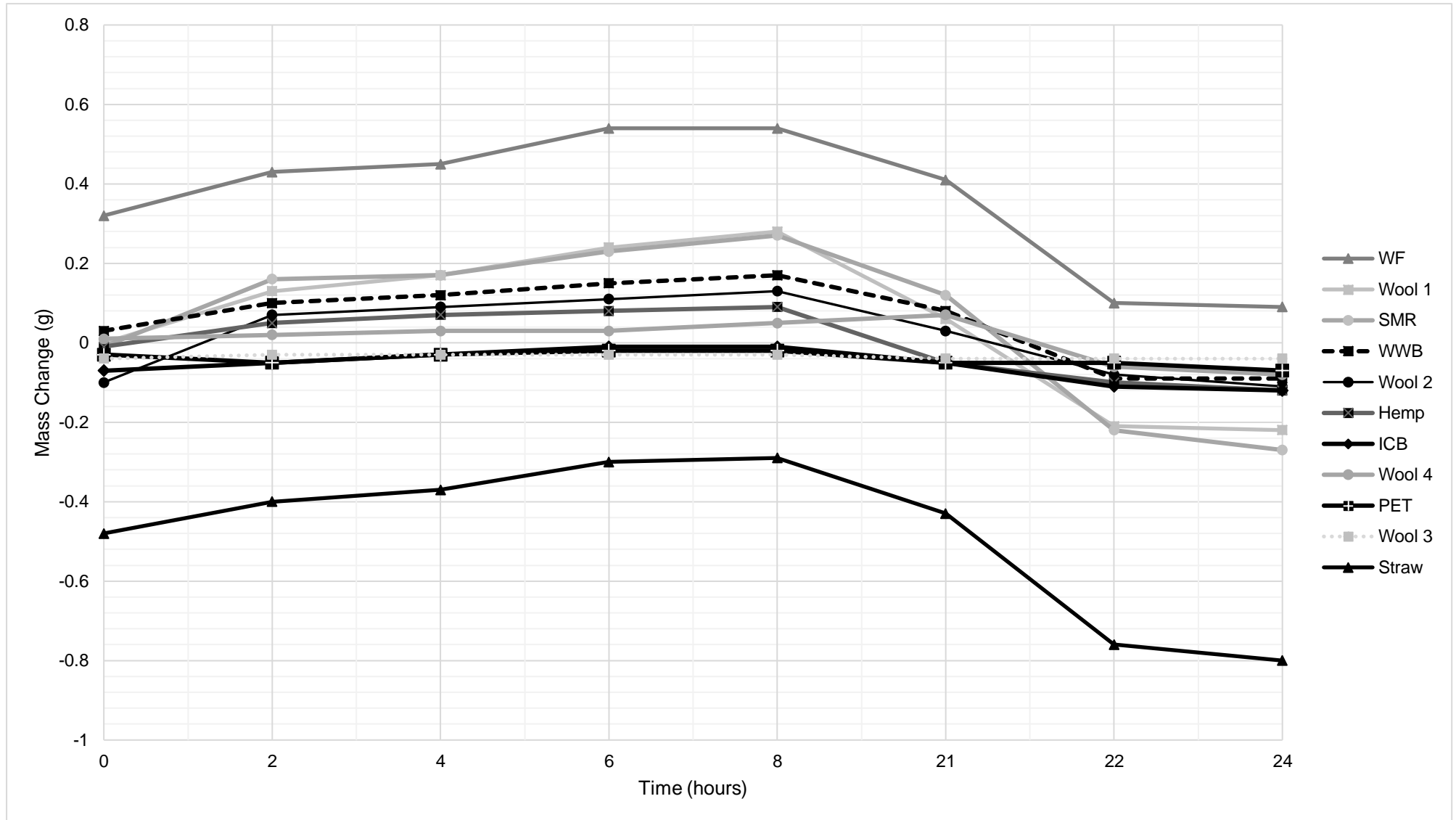


Figure 3.7a. Change in mass during the 7th cycle of the 10 bio-based materials and 1 recycled plastic during a 24-hour cycle.

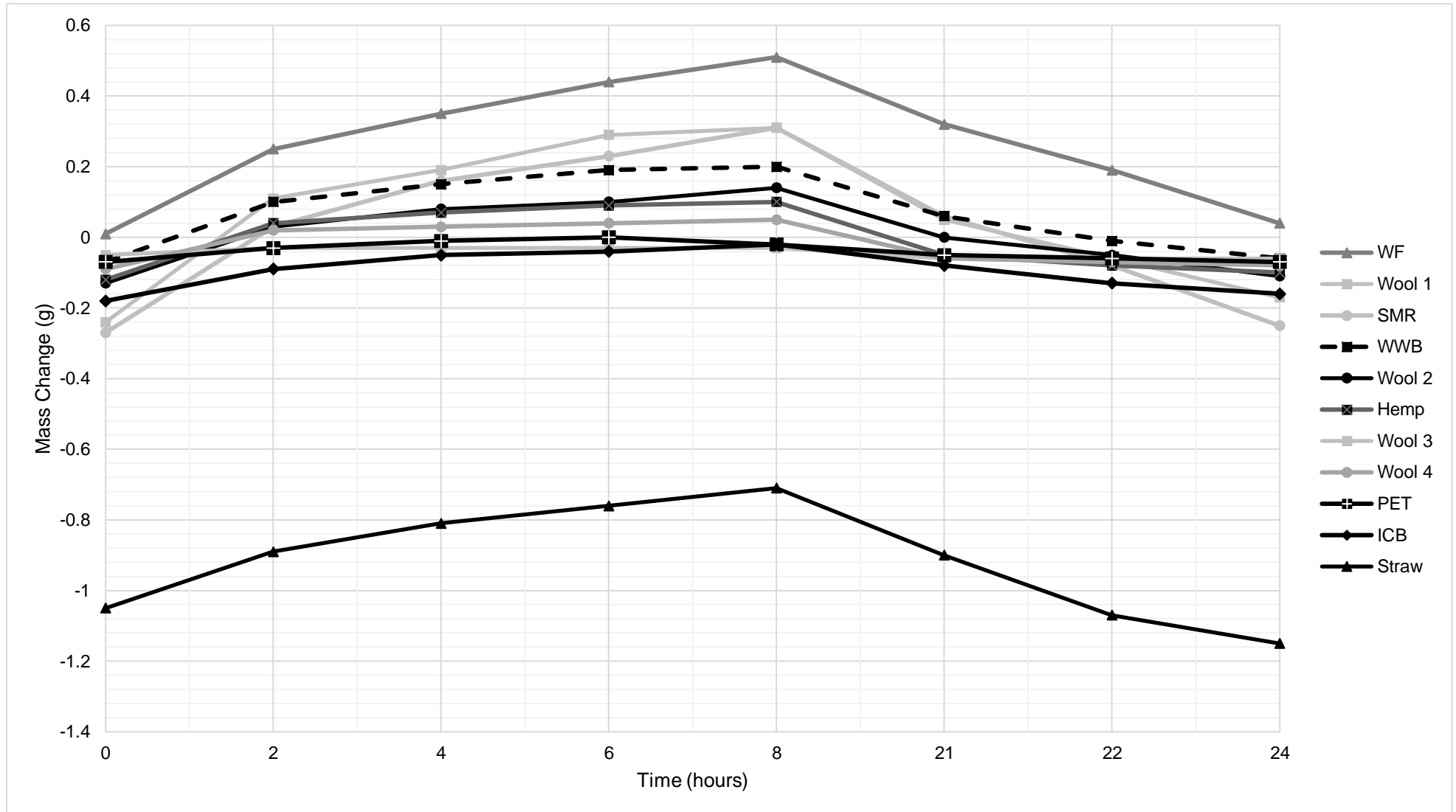


Figure 3.7b. Change in mass during a 10th cycle of the 10 bio-based materials and 1 recycled plastic during a 24-hour cycle.

From Figures 3.7a and 3.7b it is demonstrated that the moisture adsorption and desorption process vary for the various studied materials. The comparison of cycle 7 and cycle 10 helps to demonstrate the differentiation of shapes materials experience before they are in a quasi-steady state. Figures 3.7a and 3.7b also demonstrate the natural variation and evolution between the different materials throughout the entirety of the experiment. By comparing the differences between the graphs, they show a range of shapes; this explores the variety of ways in which water enters (during adsorption) and exits (during desorption). Previous research has solely focused on the prominence of MBV but doesn't highlight the mechanisms of water transport. By understanding this, it would give a greater insight into the specific material hygrothermal properties; the different adsorption/desorption curves for each material and can be categorised into the following groups:

'Group 1'

Within this group, all samples initially adsorb moisture at a high rate for a period of 8 h and mass is constantly increasing (see Figure 3.8a). After 8 h, samples desorb moisture in a similar manner. This is mirrored in the desorption stage. Samples within Group 1, exhibit clear adsorption/desorption phases, having a peak after 8 h of exposure, which denotes the end of the adsorption phase. This adsorption/desorption curve shape corresponds to an instantaneous reaction to differential hygrothermal conditions. This behaviour clearly demonstrates the hygroscopic nature of the material having the ability to manage dynamic moisture changes. This is evidence that the material can dynamically react to differing hygrothermal environments.

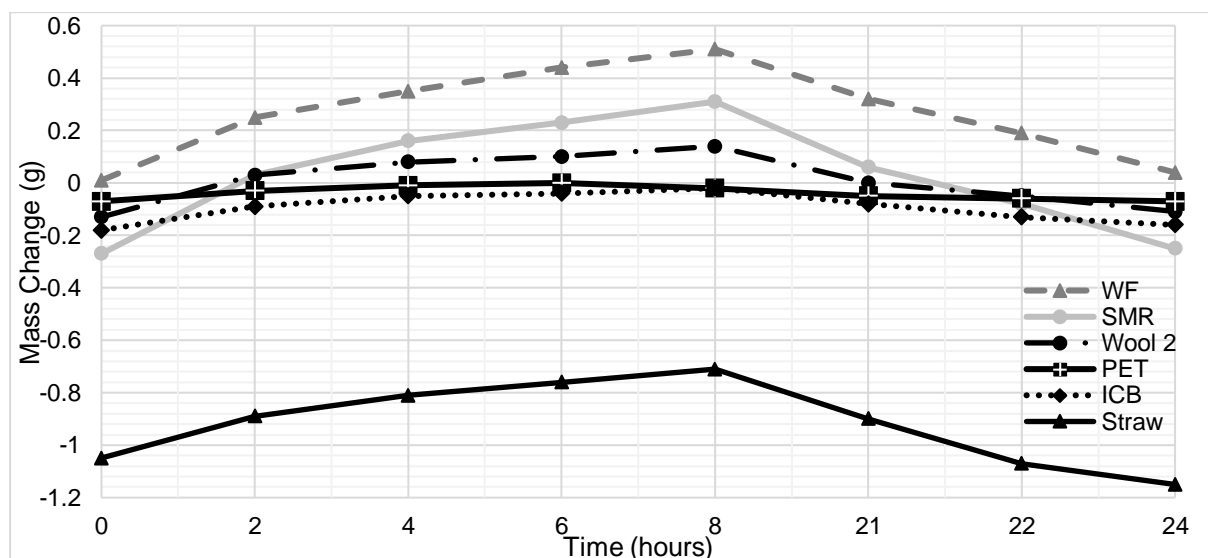


Figure 3.8a. Adsorption and desorption curves to show the categorisation of 6 samples within 'Group 1' (Romano et al, 2018).

'Group 2'

The shape of the adsorption/ desorption curves of 'Group 2' samples exhibit an initially high absorption rate (see Figure 3.8b) for the first 2 h of exposure. After that, a clear change in the adsorption curve rate is depicted. The materials desorb moisture in a similar manner. The adsorption and desorption phases in this class of materials are distinct and separated by a peak in after 8 h of exposure. Although, the rate reduction is an evidence of the material losing its ability to efficiently manage moisture. This effect indicates that the material starts saturating as it can no longer retain water as efficiently. In the desorption phase, the material desorbs moisture less efficiently demonstrating its inability to remove efficiently moisture. Moisture retention will eventually lead to unwanted material decomposition.

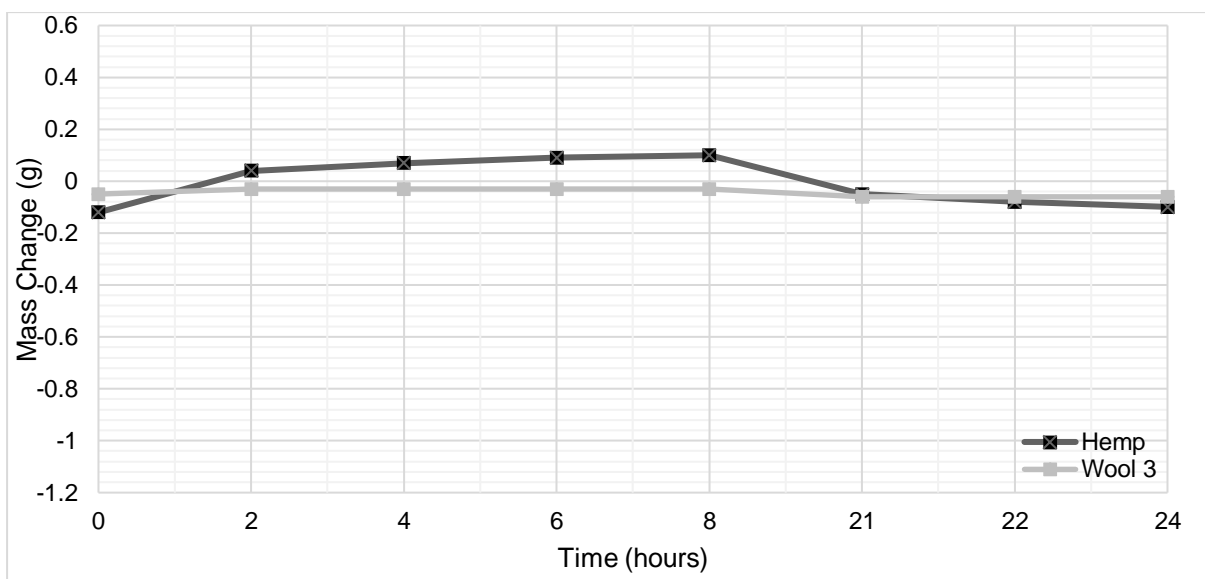


Figure 3.8b. Adsorption and desorption curves to show the categorisation of 2 samples within 'Group 2'.

'Group 3'

Similar to 'Group 2', samples in this group adsorb moisture at a high rate for the initial 2 h of exposure. After that, moisture adsorption slows down significantly (see Figure 3.8c). On the contrary to the other groups exhibiting a peak after 8 h of exposure, – most of the samples within this group begin to desorb before the step change in RH. The adsorption/desorption curve of the samples in this group reaches saturation (a plateau within their adsorption/desorption curve) which corresponds to the inability of the material to exchange

moisture.

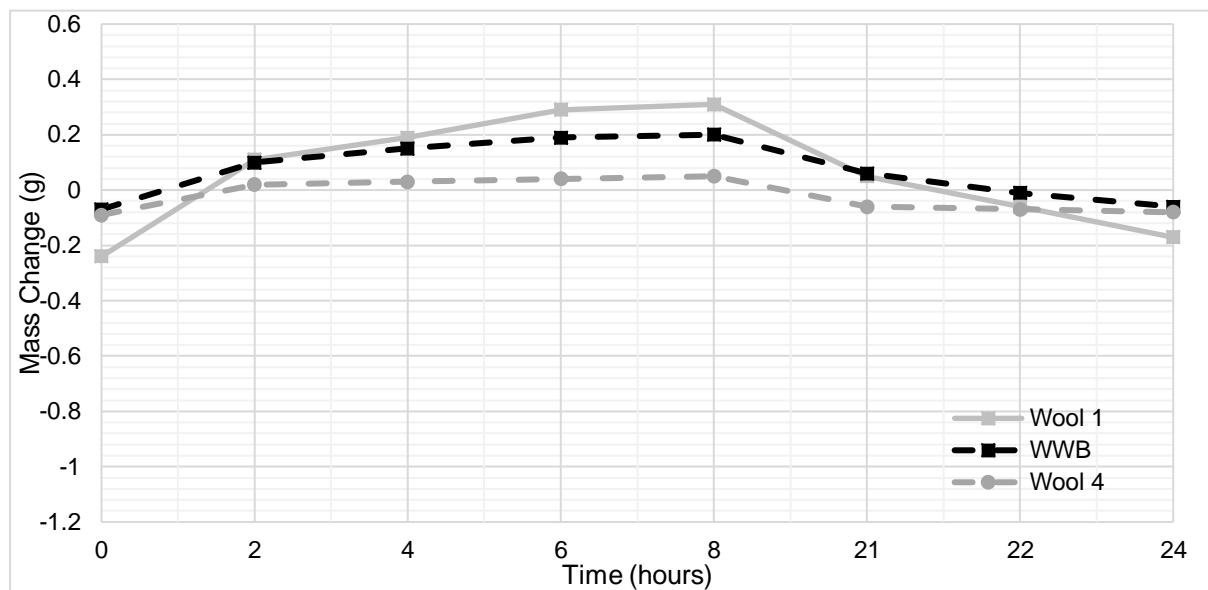


Figure 3.8c. Adsorption and desorption curves to show the categorisation of 3 samples within 'Group 3'.

For optimal results, materials are expected to continuously exchange moisture in a dynamic manner. Thus, samples of 'Group 1' respond efficiently to differing hygrothermal environments, which is of primary importance when considering panels for indoor environmental comfort. The shape of the adsorption/ desorption curves has been used to categorize the samples within Figures 3.8a - c (see Table 3.2).

Table 3.2. Categorisation of materials 7th Cycle and 10th Cycle through the adsorption/ desorption curve.

Sample ID	Group Categorisation	
	7 th Cycle	10 th Cycle
Wool 1	2	2
Wool 2	2	2
Wool 3	3	3
Wool 4	2	2
Hemp	2	2
WWB	2	2
SMR	1	2
Wood Fibre	1	2
Straw	2	2
ICB	2	3
PET	2	3

Table 3.2 demonstrates that during the 7th cycle, this is not always the same group number as the final cycle categorisation. When differentiating between materials, the MBV may not be sufficient information to decipher one material from another. However, by being able to categorise a materials adsorption/desorption pattern, a more informed decision of the selection of a material will be possible based on the desired characteristics.

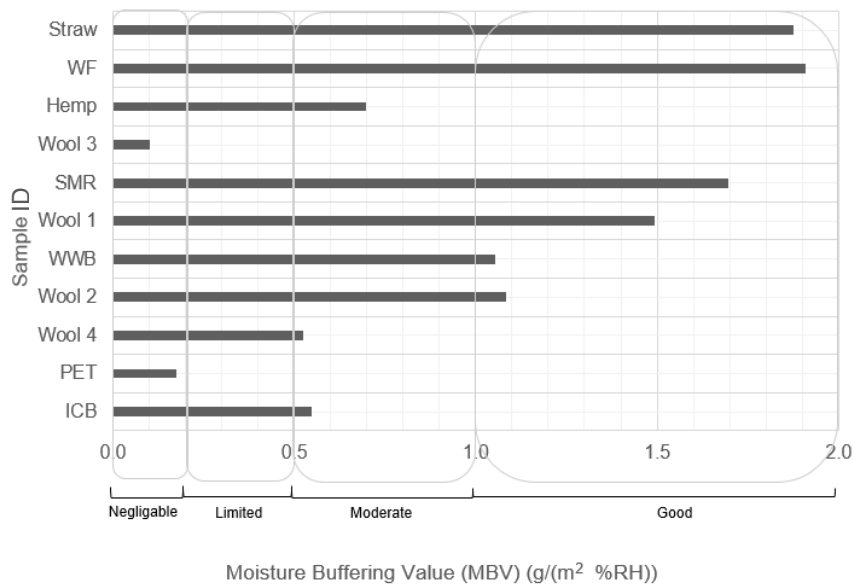


Figure 3.9. MBV of each material and its rating according to NORDTEST protocol, during the 10th cycle within climatic chamber.

Figure 3.9 demonstrates the classification of materials within this study employing a methodology outlined in Rode et al. (2005). Out of 11 samples, 6 were categorised as ‘good’; these bio-based materials were studied more extensively. Samples were put back into the chamber for 22 hygrothermal aging cycles as outlined in Romano et al. (2018). The categorisation of samples from their final cycle are illustrated in Table 3.3.

Table 3.3. Mortar composites moisture buffering properties.

Sample ID	22 nd Cycle Group Number	Mean MBV Value (g/ (m ² %RH))	MBV Classification (as per(Rode et al., 2005))
Wool 1	1	1.88	Good
Wool 2	1	1.23	Good
WWB	2	Did Not Stabilise	-
SMR	1	2.06	Excellent
WF	2	1.25	Good
Straw	2	Did Not Stabilise	-

From the six bio-based materials that were within the chamber, only four materials stabilised and therefore have a MBV for comparison. SMR has the most desired grouping of all the materials, whilst Wool 1, Wool 2 and WF have the same categorisation. When comparing their MBV, Wool 1 has the highest whilst Wool 2 and WF have very similar values. As there is only 0.02 g/ (m² %RH) between them, this is not a sufficient differentiation between materials in order to select a preferential material. Because of this, the cycle group number must be considered in order to make a decision between Wool 2 and WF. As previously mentioned, Group 1 is the most preferential group due to its efficient moisture exchange. After 22 cycles, Wool 2 has a group classification of Group 1 rather than WF, which is in Group 2.

3.4.3. Thermal Conductivity and SEM micrographs

For an insulating material to be successful, it needs to buffer the way heat is exchanged via radiation, convection and conduction (Callen, 1985). By measuring thermal conductivity, this acts as an indication of the ability for a material to conduct heat. As aforementioned, the thermal conductivity of the investigated samples was analysed. Figures 3.10a – 3.10v demonstrate the thermal conductivity of each sample within a single 24 h hygrothermal aging cycle, the samples surface morphology was investigated using SEM.

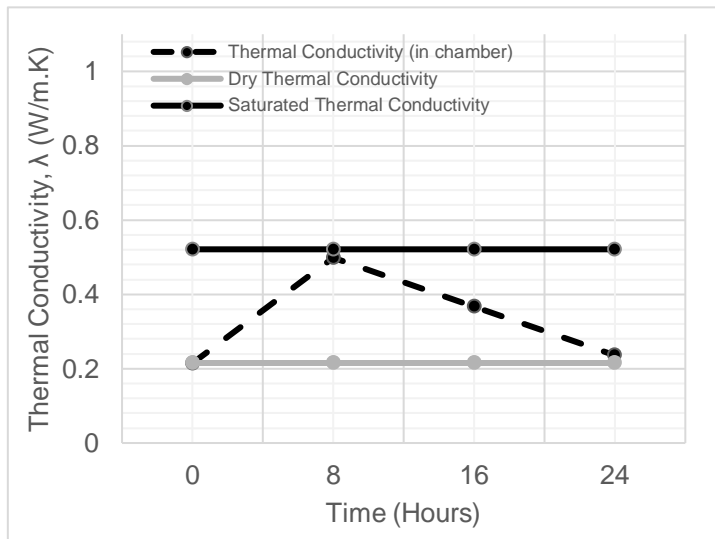


Figure 3.10a. PET - thermal conductivity of dry, saturated within a climatic chamber during a 24-hour cycle

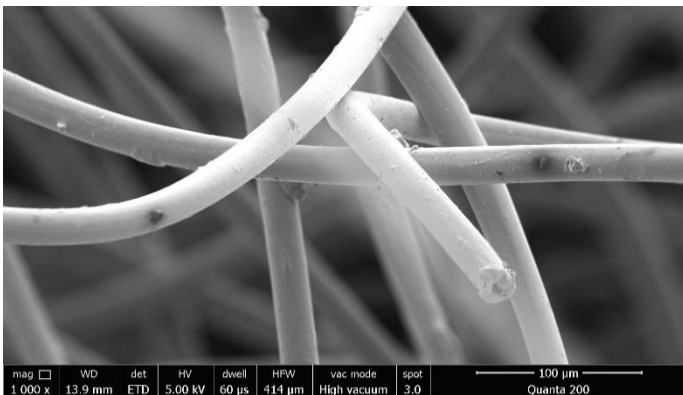


Figure 3.10b. SEM Image of PET

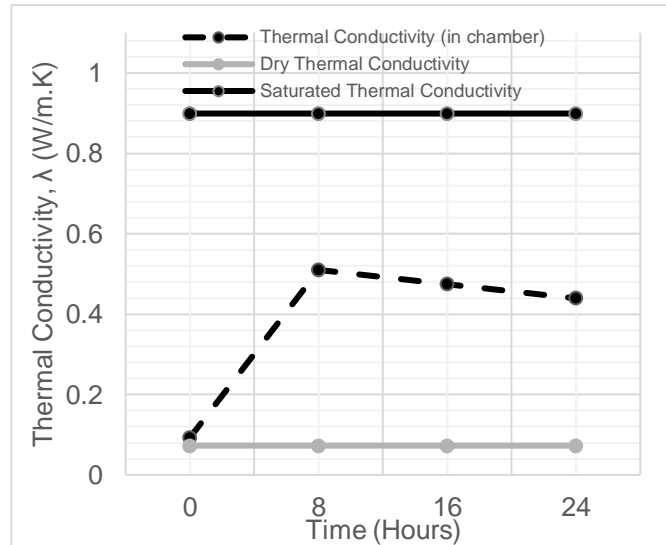


Figure 3.10c. Wool 2 thermal conductivity of dry, saturated within a climatic chamber during a 24-hour cycle

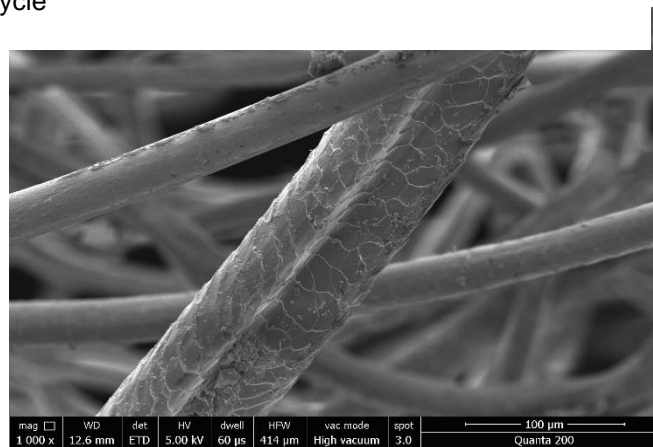


Figure 3.10d. SEM Image of Wool 2

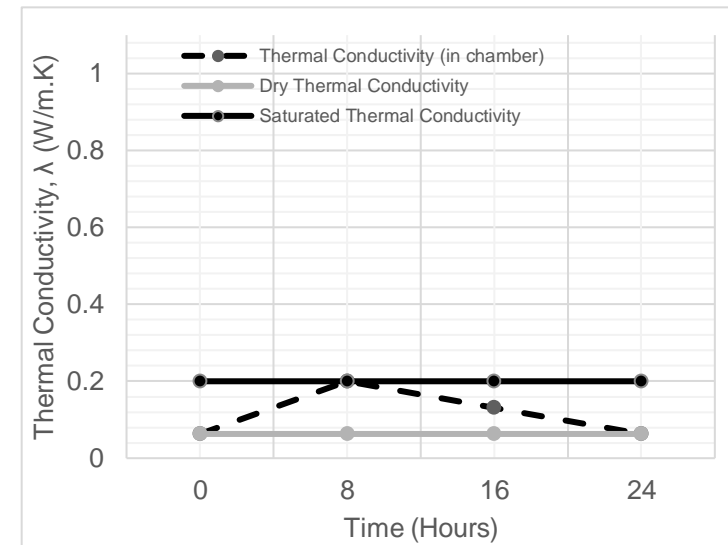


Figure 3.10e. WF thermal conductivity of dry, saturated within a climatic chamber during a 24-hour cycle

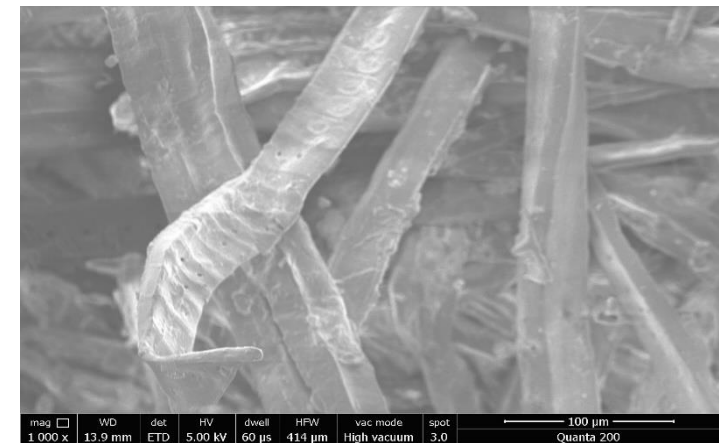


Figure 3.10f. SEM Image of WF

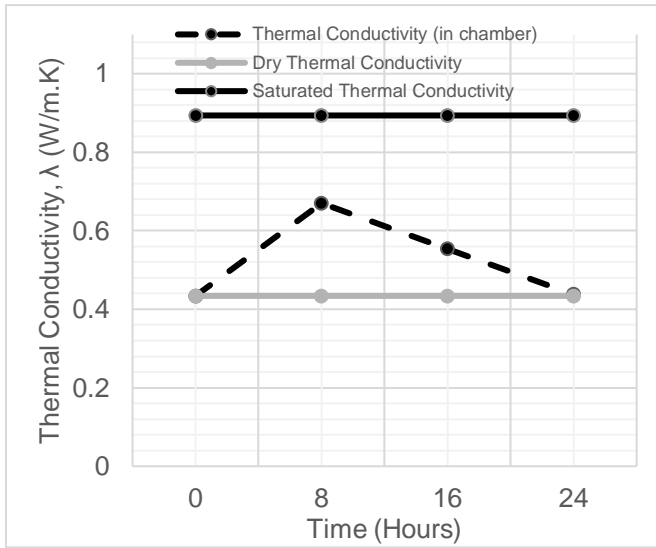


Figure 3.10g. Wool 3 thermal conductivity of dry, saturated within a climatic chamber during a 24-hour cycle

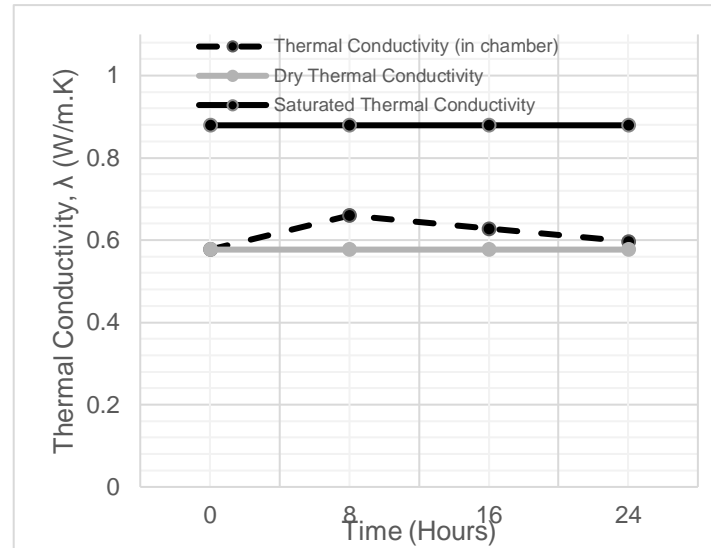


Figure 3.10i. Hemp thermal conductivity of dry, saturated within a climatic chamber during a 24-hour cycle

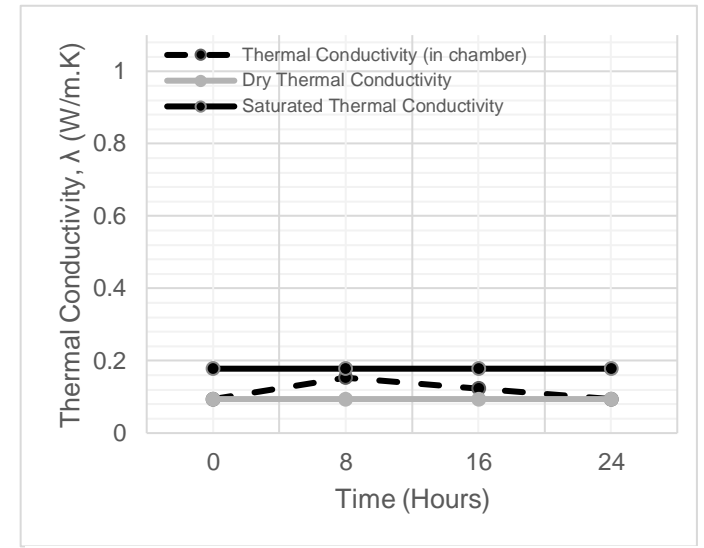


Figure 3.10k. SMR thermal conductivity of dry, saturated within a climatic chamber during a 24-hour cycle

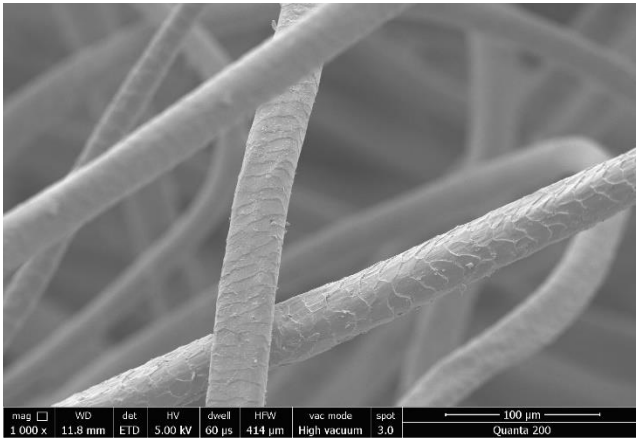


Figure 3.10h. SEM image of Wool 3.

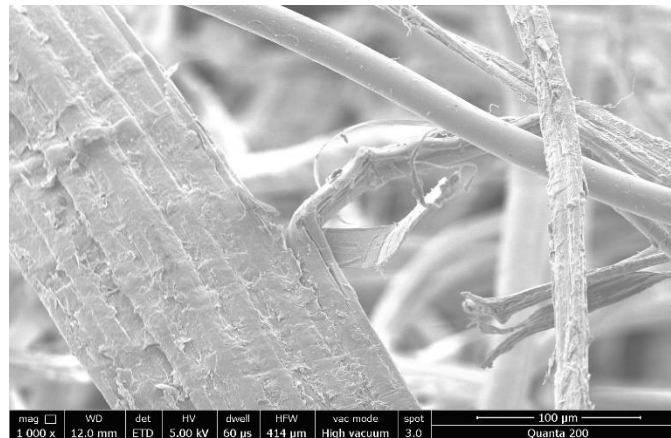


Figure 3.10j. SEM image of Hemp

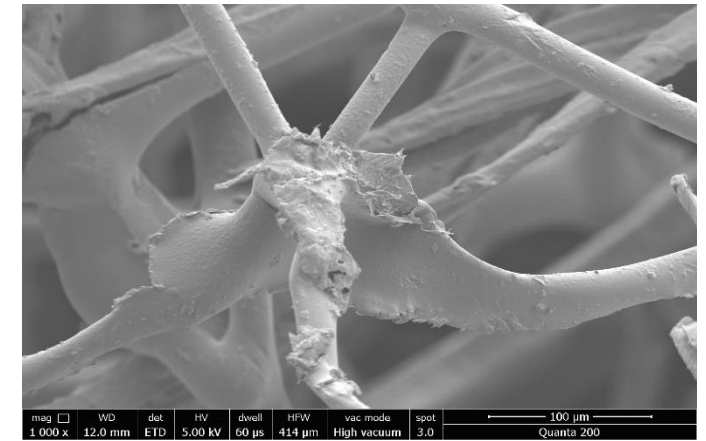


Figure 3.10l. SEM image of SMR

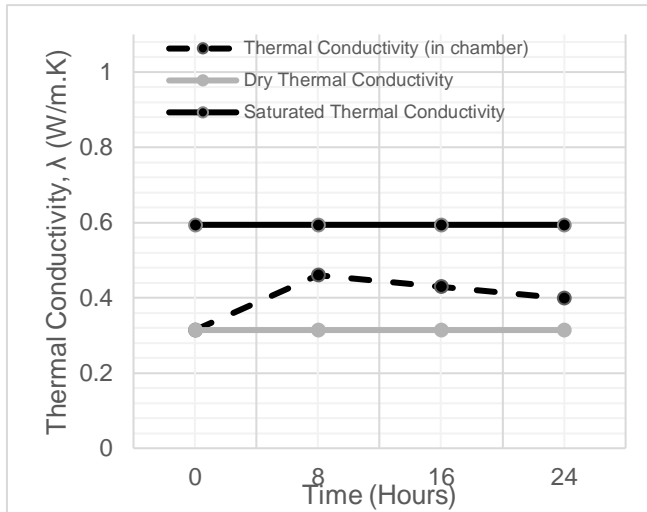


Figure 3.10m. Wool 1 thermal conductivity of dry, saturated within a climatic chamber during a 24-hour cycle

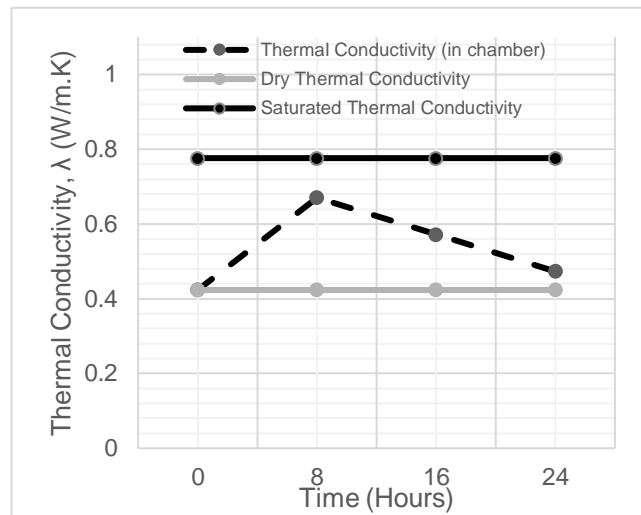


Figure 3.10o. Wool 4 thermal conductivity of dry, saturated within a climatic chamber during a 24-hour cycle

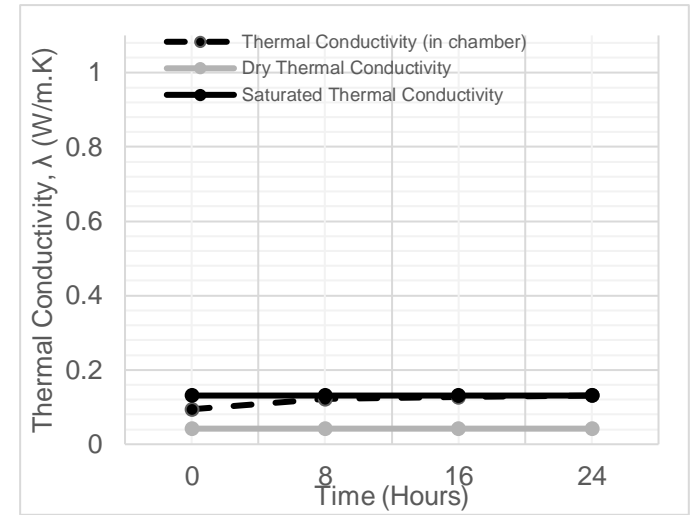


Figure 3.10q. ICB thermal conductivity of dry, saturated within a climatic chamber during a 24-hour cycle

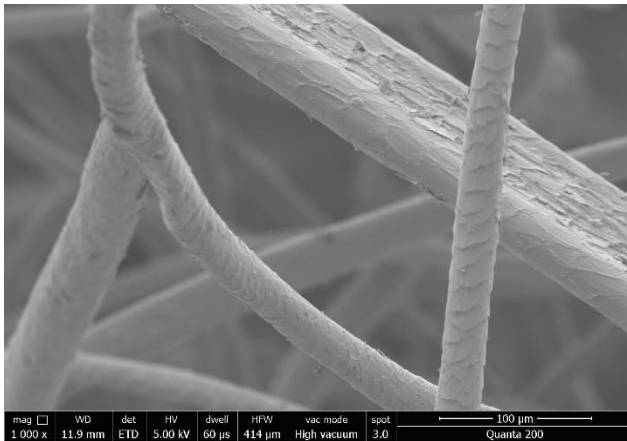


Figure 3.10n. SEM image of Wool 1.

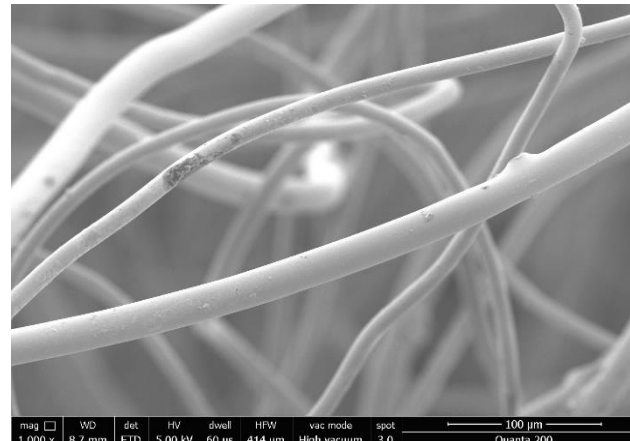


Figure 3.10p. SEM image of Wool 4.

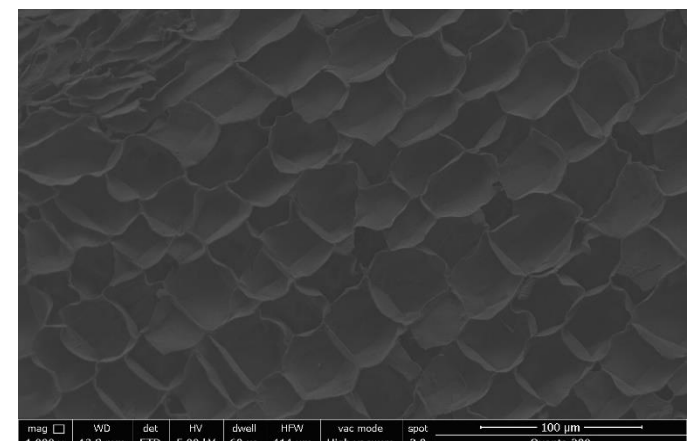


Figure 3.10r. SEM image of ICB.

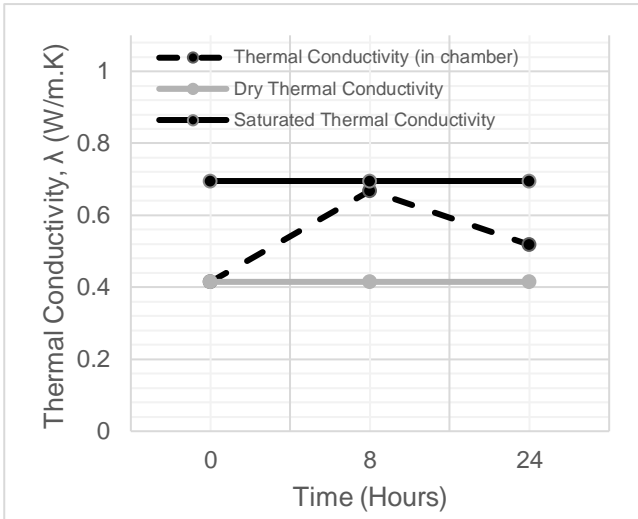


Figure 3.10s. WWB thermal conductivity of dry, saturated within a climatic chamber during a 24-hour cycle

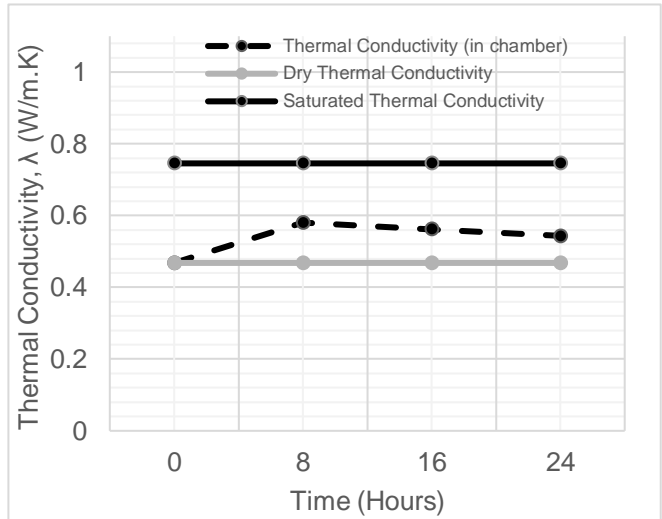


Figure 3.10u. Straw thermal conductivity of dry, saturated within a climatic chamber during a 24-hour cycle

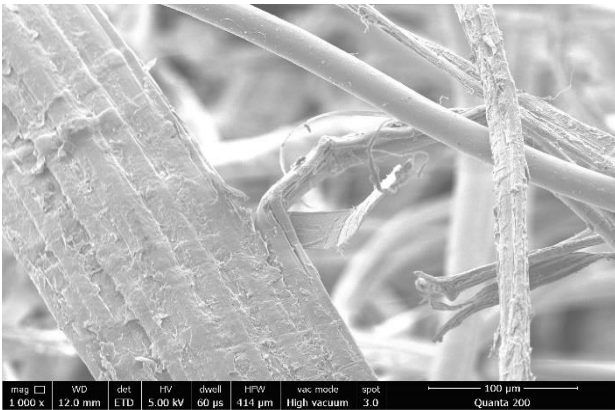


Figure 3.10t. SEM image of WWB.

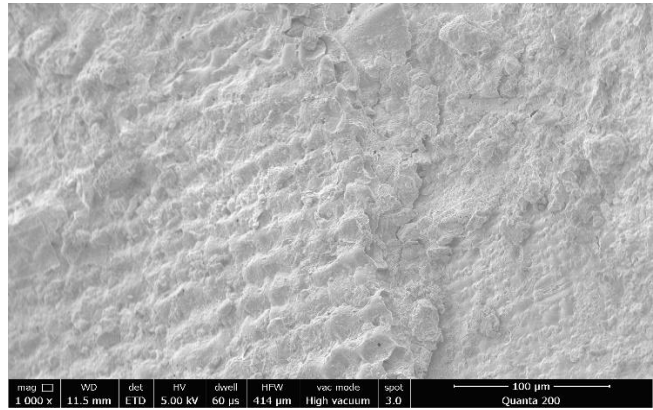


Figure 3.10v. SEM image of Straw.

By comparing the thermal conductivity of dry and moisture-saturated samples, it could be concluded that the material loses its inherent insulating ability when saturated (Shea, Wall and Walker, 2013). The thermal conductivity measurements obtained from the 11 studied materials can be classified into two different groups: those that exhibited identical and non-identical thermal conductivity values before and after hygrothermal cycling. Specifically, the samples that exhibited identical thermal conductivity values were: Wool 2, Wool 4, WFs, Hemp, PET and SMR. Whilst, the samples that revealed dissimilar thermal conductivity after exposure were: Wool 1, Wool 4, Straw, ICB and WWB.

The materials that revealed identical thermal conductivity values after exposure demonstrate a dynamic response to external hygrothermal changes. On the contrary, materials' inability to return their initial hygrothermal state (even if exposed for only hours and later remained at low RH for 16 h), retain water molecules within the structure, which reduces their ability to buffer

moisture and function as an insulator. The latter case refers to non-hygroscopic materials as highlighted in Zhang et al. (2017).

Further experimentation would be required to demonstrate the impact on measurements through more cycles and to understand whether the difference between 8-h peak and dry thermal conductivity readings. As the difference between the materials will either exaggerate throughout the experiment as the water molecules potentially become trapped and degrade /dissolve the bio-fibres or as the hygrothermal conditions change, the gap is at its largest and then lessens as the materials stabilises within the environment.

Figure 3.11a and 3.11b demonstrate the difference in thermal conductivity values as density varies within the two different states, that of dry and moisture-saturated samples. Within Figure 3.11a there appears to be no general trend, however within Figure 3.11b a linear trend demonstrates that thermal conductivity increases linearly with density increase. There are a few of exceptions to this, where bio-based materials exhibit an unexpected behaviour to hygrothermal exposure due to their heterogeneous nature (McGregor et al., 2016).

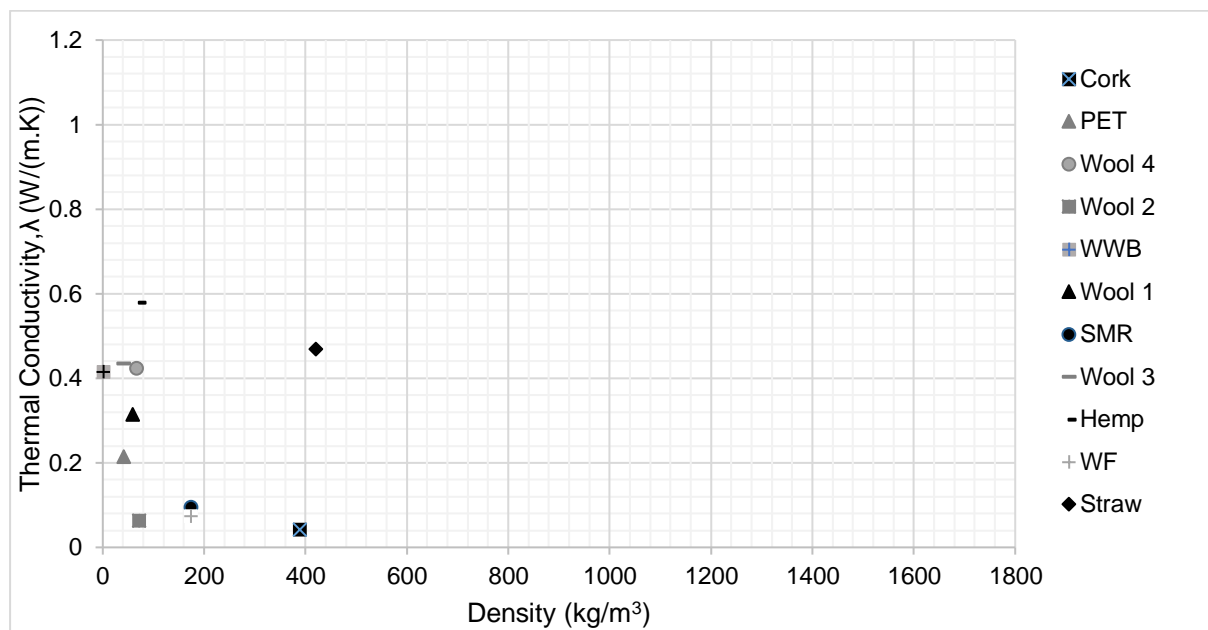


Figure 3.11a. Thermal conductivity against bulk density.

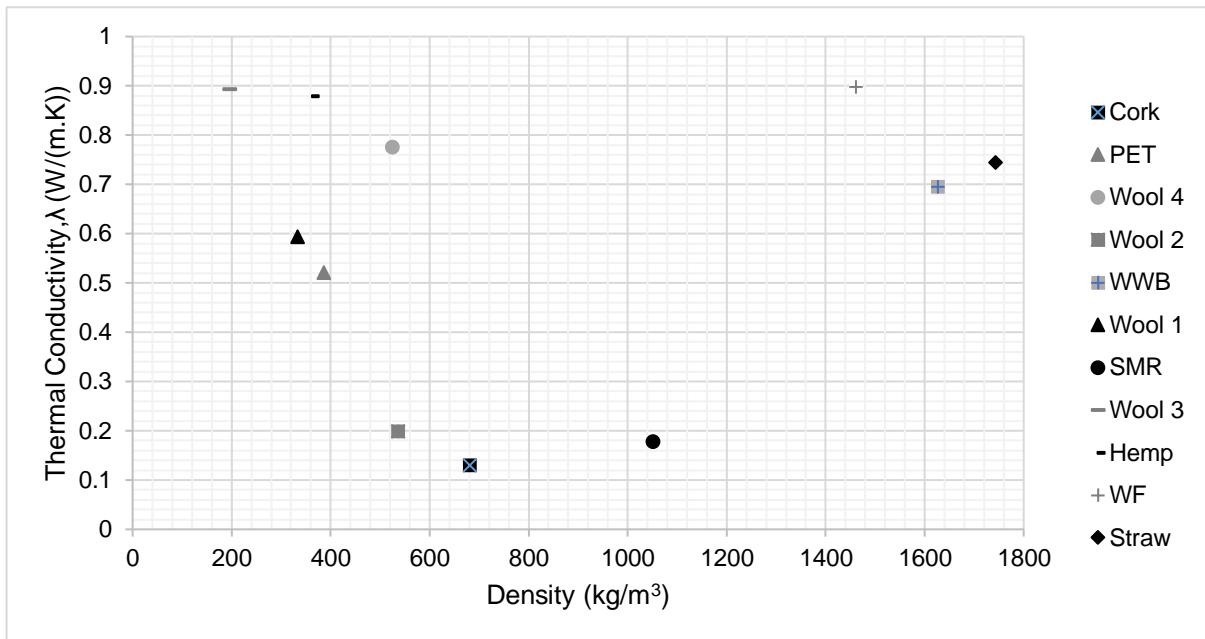


Figure 3.11b. Thermal conductivity against saturated density.

However, some of the outliers in Figure 3.11a (such as ICB), could be attributed to the naturally occurring trapped air pockets and voids between ICB granules (see Figure 3.12). As presented within Brás, Leal and Faria (2013) not only this, but the microstructure of ICB is similar to a honeycomb providing further microscopic voids within the material (demonstrated in Figure 3.10r). Furthermore, having such a relatively low saturated thermal conductivity value exhibits the difficulty of water ingress to ICB cells in comparison to other materials (such as WF). So, although this material has inherently low thermal conductivity value, its ability to be used within a 'green panel' with hygrothermal benefits is limited due to its low hygroscopicity.



Figure 3.12. ICB with naturally occurring air pockets and voids on the surface of the sample circled.

In comparison to other materials such as wool (see Figures 3.10c, 3.10g, 3.10m and 3.10o), the voids are within the microstructure of the material rather than just between fibres. This contributes to how in the dry state, ICB can have a high density but equally low thermal conductivity. By comparing to previously conducted studies such as Millogo et al. (2014) and Bouguerra et al. (1998) the results within these papers align with them. When comparing Figures 3.10a and 3.10b it is clear that this data also correlates to the works of (Zach et al., 2012), where the higher the bulk density of a sample results in a more restricted air flow through and between the fibres of a material, leading to less convection and therefore a higher thermal conductivity value.

When comparing SEM images, it is evident that samples can be divided into 2 categories, those that demonstrate homogenous structure (see Figure 3.10r and 3.10v) and a more fibrous structure (in particular Figure 3.10p). A much more fibrous material indicates a multitude of plains for the material water molecules have a most 'free space' and voids to potentially fill and therefore more air pockets, equating to a lower thermal conductivity value.

Table 3.4. Bio-fibres and dry thermal conductivity values in a dry state.

Sample Name	Dry Thermal Conductivity (W/ (m.K))
Wool 1	0.31
Wool 2	0.063
Wool 3	0.43
Wool 4	0.42
Hemp	0.58
WWB	0.42
SMR	0.094
WF	0.47
Straw	0.47
ICB	0.042
PET	0.21

In comparison to data produced by Thieblesson et al. (2017) where thermal conductivity ranges from 0.09 to 0.045 W/(m.K) for samples, the data of this study represent high thermal conductivity values which would render the studied materials as poor thermal insulators. However, when considering the thermal conductivity readings for both dry and moisture-saturated samples, it is important to consider that these materials have been through two sets of experiments within a climatic chamber in addition to being kept in a laboratory for week of fluctuating hygrothermal conditions. Furthermore, the results displayed in Table 3.4 are much higher than that of the thermal conductivity values as stated by manufacturers (as per Table

3.1). Because of this, it is understood that samples can be affected by long exposure to hysteresis.

3.4.4. Temperature evolution during transient behaviour

Moisture buffering characteristics of bio-based materials renders them ideal materials for passive energy reduction management (Simonson, Salonvaara and Ojanen, 2004; Osanyintola and Simonson, 2006; Qin et al., 2011). A reduction in energy requirements can be attributed to the latent heat exchanges within the sample. Within this research work, due to the continuous adsorption and desorption of water vapour within the bio-based samples there is an expectant latent heat exchange inherently to the structure of the bulk sample. Here, latent heat is attributed to the changing state of water (Hens, 2017). During the phase change between liquid water molecules and water vapour, latent heat is identified, especially during the step change in RH values.

Figure 3.13 demonstrates the results from the thermocouples placed both on the surface and within the bio-based samples. It is evident from the Figure that there has been no change in temperature throughout the experiment. However, there is a distinct difference between the internal and external temperatures of the sample meaning that there is a heat flow.

From a dynamic perspective, Figure 3.13 demonstrate that even after shifting the thermocouples the materials exhibit no changes in temperature per sample throughout the duration of the experiment. From a static perspective, there are some detected changes in temperature of samples when surface is compared to the temperature in the centre. This directly contradicts previous research that exhibits a change in temperature at a step change in RH (James et al., 2010; Holcroft and Shea, 2015). When comparing the duration of experiments, 'Run 1' lasts for 10 cycles of 24 hours whilst 'Run 2' lasts for 22 cycles of 24 hours. It is evident from both runs that there was a clear difference in temperature. The clear differentiation in temperature from within the sample to the surface and as there is no external heat source; the elevated temperature can only be attributed to latent heat.

Figure 3.14 displays that there is a multitude of characteristics between the different bio-fibres. Due to the temperature difference and due to their being no external heat source the temperature differential is due to latent heat. When considering the positive and negative values represented in Figure 3.14, these can be attributed to the latent heat vapourisation and condensation for which are not equal within all materials. SMR, Wool 1 and Wool 2 have equal temperature differential between Run 1 and Run 2 which demonstrates the ability for the material to stabilise within 22 cycles. However, WWB and Straw Run 2 demonstrates a high value in comparison to Run 1, despite Run 2 being 22 cycles is unable to stabilise within 10

cycles. Comparatively, WF exhibits a sustained negative temperature difference throughout both runs.

Considering the thermodynamics within the samples, generally (with exception to only WF) Run 1 demonstrates that the surface temperature is greater than the temperature at the centre of the sample (displayed as a positive value in Figure 3.14). Therefore, heat flow absorption into the sample is vapourised and as latent heat of vapourisation is an endothermic reaction and requires enthalpy to complete the process, the heat is absorbed by water to vapourise it. Run 2 is the converse, where the temperature at 15 mm from the surface is greater than that of the surface temperature so there is a heat flow release from the sample – (displayed as a negative value in Figure 3.14). WF demonstrates constant latent heat of condensation throughout both Run 1 and exaggerated particularly within Run 2. It is hypothesised that due to the very nature of bio-based materials being intrinsically heterogeneous this could attribute that WF may not stabilise until after 22 cycles.

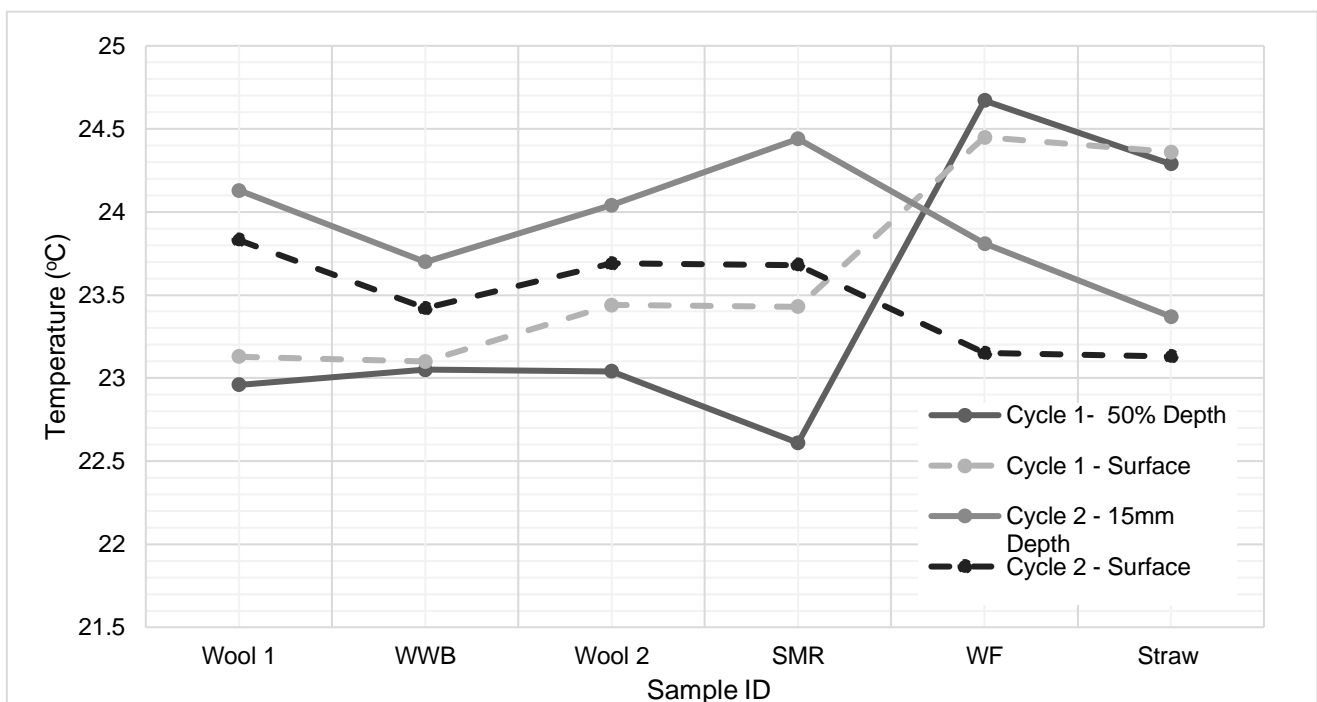


Figure 3.13. Temperature change on the surface and within samples throughout 2 experimental campaigns.

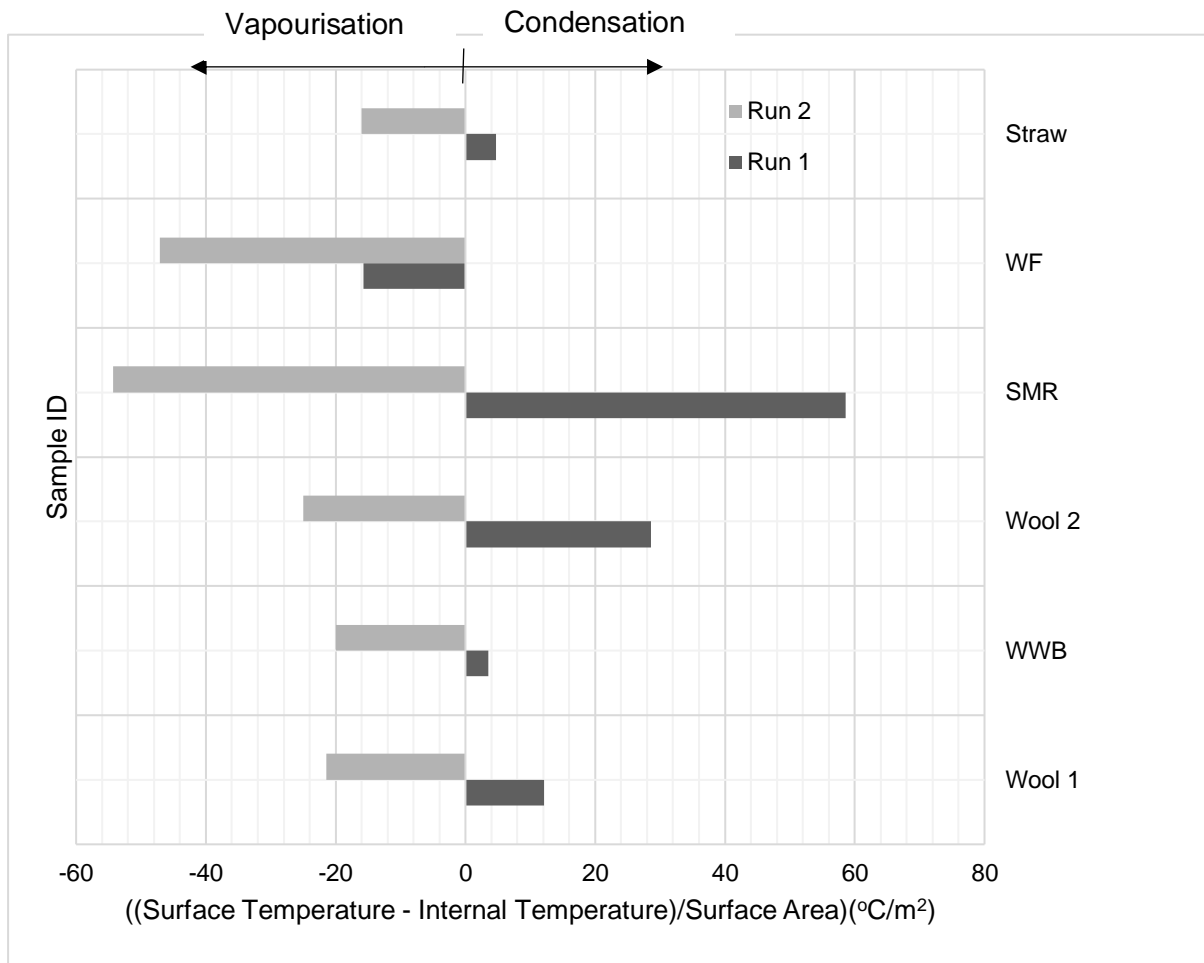


Figure 3.14. Temperature difference between surface and internal temperature per m² of bio-based insulation sample.

3.5. Conclusion

As hygrothermal conditions are an integral factor to this research, the MBV results are considered of primary importance. The highest MBV value in addition to lowest group number categorisation ensures the material is efficient and effective in terms of moisture exchange. Results indicate that in to select a bio-based building material, simultaneously consideration of MBV and the shape of the final mass change graph is necessary to demonstrate adsorption/desorption characteristics of the sample. It was also found that only samples from SMR and Wool exhibited acceptable (MBV from 1 to 2 g/ (m² %RH)) are one of the most promising as materials respond dynamic response to hygrothermal changes. Only half of the samples (Wool 2, Wool 4, WF, Hemp, PET and SMR, Wool 1, Wool 2) have the equivalent efficient moisture transfer to be able to desorb the same quantity of water. 'Green panels' made of bio-based materials are expected to passively control hygrothermal conditions.

From the initial MBV, a total of 11 materials were tested, of which 6 that were categorised as 'good', were tested further: Wool 1, Wool 2, WWB, SMR, WF and Straw. After these samples were then retested within the climatic chamber, the MBV categorisation results for Wool 1, Wool 2, SMR and WF were categorised as either 'Good' or 'Excellent' (see Table 3.3). Considering the shape of the final cycle, WF are categorised as 'Group 2' rather than 'Group 1', showing the other three samples as having superior characteristics. Thermal conductivity analysis demonstrates that on saturation, values rises of samples increase, where material dependant, samples cannot desorb water as efficiently as it is absorbed (as demonstrated in Figures 3.10a-3,10v). On a microstructural level, the properties of each bio-based insulation material provide an explanation of their performance. After experimentation, two categories of samples were created. Preferable characteristics were revealed by the sample category that at the end of the cyclic exposure (whilst in the climatic chamber), the samples reverse back to their dry thermal conductivity values.

From the SEM images taken of the bio-fibres, it is demonstrated that the more fibrous samples have more potential air pockets, which would give an inherently lower thermal conductivity value. The SEM images demonstrate the fibrous nature of the samples and diversity of surface characteristics of the microstructure of bio-based materials.

This chapter also demonstrates that latent heat can be detected in addition to also being further analysed and the categorisation of latent of vapourisation or condensation. When considering the temperature evolution during transient behaviour, materials can equally vapourise and condense (see Figure 3.14). This efficiency are the most preferable properties - the bio-fibres that demonstrated this are Wool 1, Wool 2 and SMR. Each of the different bio-fibres will have a slightly different mechanism for reacting to the hygrothermal environment due to the intrinsic properties and characteristics of bio-based materials. Future experimentation will demonstrate the combination of the bio-based fibres with other environmentally conscious materials in to boost their thermal properties. For Chapter 4, the best performing top 6 samples (W1, W2, SMR, WF, WWB and STW) will be taken forward to understand their thermal properties utilising thermochemical analysis techniques.

Chapter 4 - Physicochemical characterisation of bio-based insulation to explain their hygrothermal behaviour

4.1. Introduction

From Chapter 2 there is clearly a wide range of research on the hygrothermal properties of bio-based materials. Chapter 3 further explored their physical properties, but particularly their hygrothermal characteristics. However, a gap in the knowledge within this sector is what actual mechanisms are undergone by these materials and how they physically and chemically alter under different relative humidity's. The challenge is to understand the movement of heat and moisture through a material. Temperature changes can cause alterations in the physical and chemical properties of bio-based materials, which reflects on their hygrothermal behaviour and influence the overall properties of the final product. A better understanding of the influence of temperature via the thermal analysis on the properties of bio-based materials enables to understand the behaviour and optimise the material. This chapter will explore the physicochemical differences between the best performing bio-fibres from Chapter 3 and contribute to the fundamental knowledge of these mechanisms.

4.2. Materials

The bio-based materials utilised within this work are that of: Saw Mill Residue (SMR), Straw (STW), Wood Wool Board (WWB), Wood Fibre (WF), Wool 1 (WL1) and Wool 2 (WL2) (as outlined in 3.2.1).

4.3. Methods

4.3.1. Preparation and Stabilisation of Samples

Samples were cut to approximately 5mm size pieces and were initially dried to BS EN ISO 12570 (ISO, 2000). Each sample was tested 'as received' and untreated, then conditioned and stabilised within a climatic chamber for 24 hours prior to testing. The hygrothermal conditions of 53% and 75% were selected as they are utilised in Romano et al. (2019b) and reflect the results of full-scale laboratory environmental conditions testing of a residential property. Before samples were tested, the same mass for all materials was used where each material was tested 5 times to ensure accurate results.

4.3.2. Thermogravimetry Analysis (TGA) and Derivative Thermogravimetry (DTG)

As a quantitative technique thermogravimetric analysis (TGA) measures the mass change in a substance, as a function of temperature. As volatile compounds are lost, mass loss is demonstrated where the shape appears sigmoid in nature and graphically as a 'step'. Utilising

this type of thermal analysis enables a deeper understanding of the thermal stability of the bio-based insulation materials.



Figure 4.1. TA Instruments, TGA Q50.

For this research a TA Instruments, TGA Q50 was used (see Figure 4.1), where samples were under scan conditions of 25 to 300°C at a linear rate of 20°C min⁻¹ under a Nitrogen atmosphere, using a circular, platinum crucible.

4.3.3. Differential Scanning Calorimetry (DSC)

As another quantitative method of thermal analysis, DSC measures heat flow rate Q (W/g), differences from the samples being tested to an inert reference material as a function of the temperature and time taken. This enables the thermal properties such as melting/freezing temperature, sample specific heat capacity and the latent heat capacity of the sample to be measured. A Perkin Elmer DSC 7 was utilised (see Figure 4.2) with a temperature range of 25 to 300°C and heating conditions of 20°C/min in an oxygen free, nitrogen environment.



Figure 4.2. A Perkin Elmer DSC 7.

4.3.4. Fourier Transform Infrared Spectroscopy (FTIR)

This method of analysis utilises a wide spectral range simultaneously to collect an infrared spectrum, where each spectra demonstrates the functional groups according to the peak positions for every sample. Using an Agilent Technologies Cary 630 FTIR with a diamond crystal (see Figure 4.3), where each spectra was averaged over 128 scans and a 4000-650 cm^{-1} range.

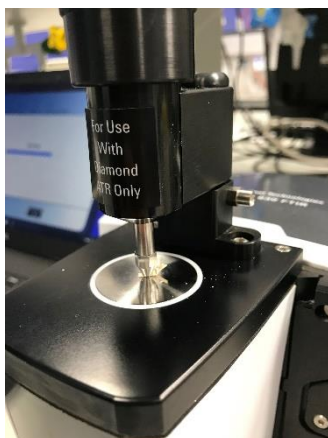


Figure 4.3. Agilent Technologies Cary 630 FTIR.

4.3.5. Scanning Electron Microscopy (SEM)

To understand the surface morphology of the bio-based materials, SEM was utilised as per the methodology for section 3.3.1 and within Figure 4.4.

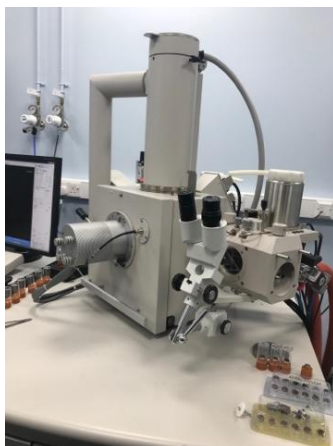


Figure 4.4. FEI Inspect S SEM.

4.4. Results and Discussion

4.4.1. TGA and DTG

Performing thermal analysis on these bio-based materials enables to develop the understanding for the way the reactions within the materials take place as a function of temperature and determines the thermal decomposition kinetic parameters. For each sample results, the TGA and DTG will be presented (where DTG is the first derivative of TGA). For the purpose of these insulation materials to act as a hygric buffer, it is important to understand the reaction mechanism to heat them and how effectively bound water molecules evaporate.

This is vital to know, in addition to their hygrothermal performance, to give a more comprehensive understanding of these materials rather than just at laboratory conditions. Factors affecting the maximum decomposition rate and the location of the TGA curve are the heating rate. Therefore, similar conditions to other works have been selected in order align with them. For each sample results, the TGA and DTG will be presented (where DTG is the first derivative of TGA).



Figure 4.5. WWB sample on crucible before entering furnace.

The TGA/DTG data for all samples can be found in Figures 4.6a to 4.6l. The objective of this analysis is to understand the thermal stability of the samples at different hygrothermal conditions (53% and 75% RH). By examining this at the specific temperatures within Table 4.1, it will provide an adequate comparison of the material's behaviour. Comparing the performance of the samples at different temperatures demonstrates the nature of the materials crystallinity. Due to the clear variation in mass loss between the samples, a comparison between temperatures of 100°C and 300°C are shown in Table 4.1, for 53% and 75% RH for

cellulose and keratin based materials. Bio-based samples utilised within this research work are that of: Saw Mill Residue (SMR), Straw (STW), Wood Pellets (WF), Wood Wool Board (WWB), Wool 1 (WL1) and Wool 2 (WL2).

Table 4.1. Weight loss of all samples at 100°C and 300°C.

Sample	Weight loss % at 100°C		Weight loss % at 300°C	
	53% RH	75% RH	53% RH	75% RH
SMR	7.129	5.155	34.112	34.699
STW	4.403	8.846	32.731	26.176
WF	6.565	6.268	15.033	15.278
WWB	3.719	5.398	8.398	13.678
W1	5.080	5.324	13.849	14.310
W2	4.895	10.298	11.459	23.586

4.4.1.1. Cellulose based analysis regarding TGA and DTG

The thermal degradation of wood-based insulation materials within this inert atmosphere is restricted by the proportions of constituent main components of hemicellulose, cellulose and lignin (Alén, Kuoppala and Oesch, 1996). The degradation of this material is a three-step process. Due to the wide variation in species and that the 'waste wood' may include different species of wood, the inherent differences between them the quantity and time taken for different mass loss of different samples will vary.

For cellulose based samples, initial mass loss can be attributed to evaporation within the fibre from the adsorption of both intra and intermolecular reactions (Fairbridge and Ross, 1978; Martin et al., 2010; Liu et al., 2013). Extraction of water (by evaporation) can be demonstrated in cellulose samples up to 160°C (Gašparovič, Koreňová and Jelemenský, 2010). However, after this cellulose degradation occurs at approximately 185°C (Jabbar et al., 2016) and as temperatures reach approximately 220°C the total degradation of cellulose begins. This degradation of the cellulose marks to beginning of the degradation of the two step thermal degradation pathway of the fibre (Alabdulkarem et al., 2018). As temperatures increase, hemicellulose continues to degrade and further exposure to temperatures at approximately 360°C begins the full degradation and charring of cellulose (Haiping et al., 2007; Ali and Alabdulkarem, 2017). It is evident from the Figures 4.6a to 4.6d that the degradation of these materials often overlaps and occurs in similar places.

Table 4.1 demonstrates that SMR and WF, shows no significant differences between the temperatures at which water evaporates within the sample. However, there is a difference between STW and WWB for water evaporation at 100°C and 300°C. Samples have a larger weight loss when stabilised at 53% by comparison to those at 75%. This demonstrates that for these materials, a differing hygrothermal environment alters their thermal properties. When comparing the amount of weight lost, STW at 75% has the largest initial mass loss (in addition to both samples of WWB). This shows their initial highly hygric properties, affecting the mass loss of WWB samples but not as significantly as 75% STW. From these 4 samples, SMR and WF are the most thermally stable are those which have not altered, despite the dynamic hygrothermal environment.

DTG was also used to understand the thermal stability of the cellulose based samples and samples experience three different steps: dehydration, active and pass pyrolysis (Fengel, 1989). As previously mentioned, the degradation of these materials initially is absorbed water (dehydration), the second stage of peaks correspond to cellulose and hemicellulose (active pyrolysis). Hemicellulose is usually a smaller 'shoulder peak' to the cellulose 'main peak' (Gašparovič, Koreňová and Jelemenský, 2010). When lignin degrades, it exhibits (simultaneously) both active and passive pyrolysis over such a wide range of temperatures. Therefore it is extremely difficult to attribute what process is being observed for the curve within the curve (Haiping et al., 2007). The differences in temperature due to the different species of wood is outlined in González-Díaz and Alonso-López (2017) but is evidently a clear factor when considering the DTG curves in the following figures. For SMR, Figures 4.6a demonstrates that from 200-250°C when stabilised at 75%, the derivative peak is much more elongated and occurs over a shorter temperature range. By comparison to SMR at 53% this range is much larger and broadened demonstrating the results that in a differing hygrothermal environment there is a physicochemical change in SMR which will directly affect its hygrothermal ability. Understanding this offers fundamental knowledge for the mechanisms that affect these materials' moisture buffering capability within an indoor environment.

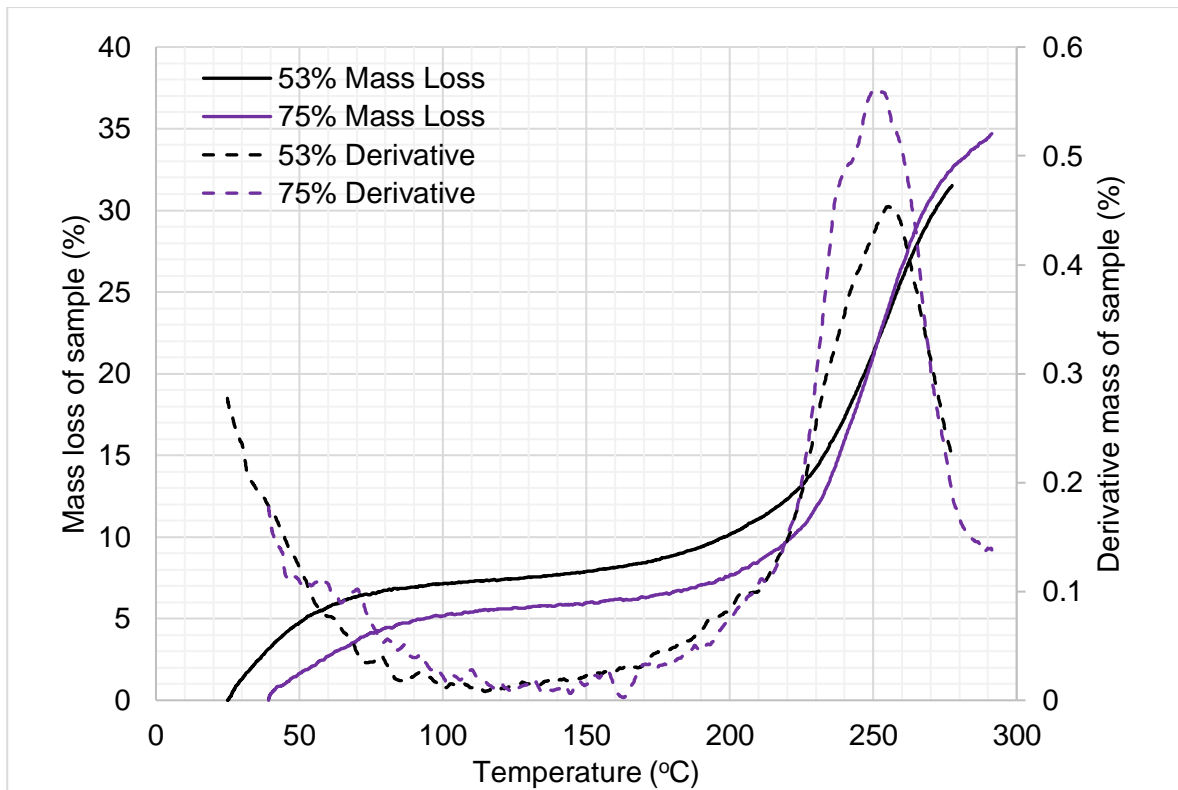


Figure 4.6a. TGA (solid line) and DTG (dashed line) for SMR at 53% and 75% RH.

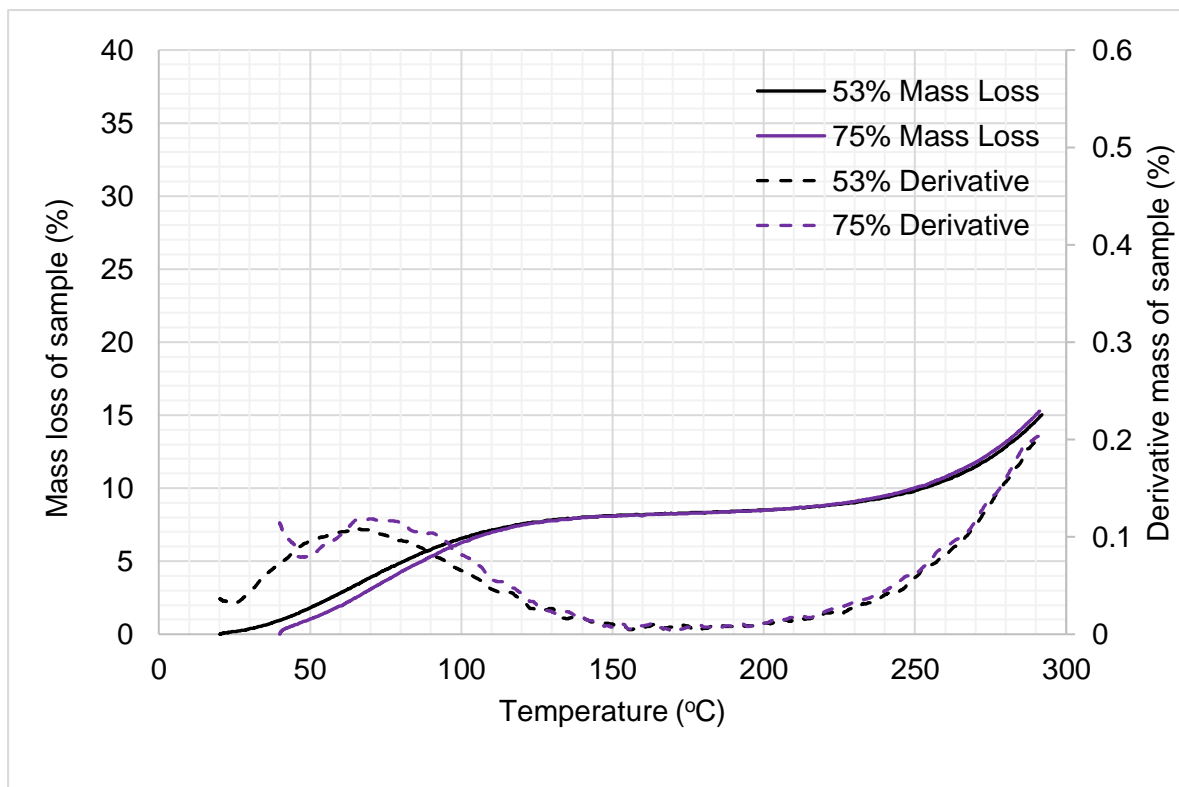


Figure 4.6b. TGA (solid line) and DTG (dashed line) for WF at 53% and 75% RH.

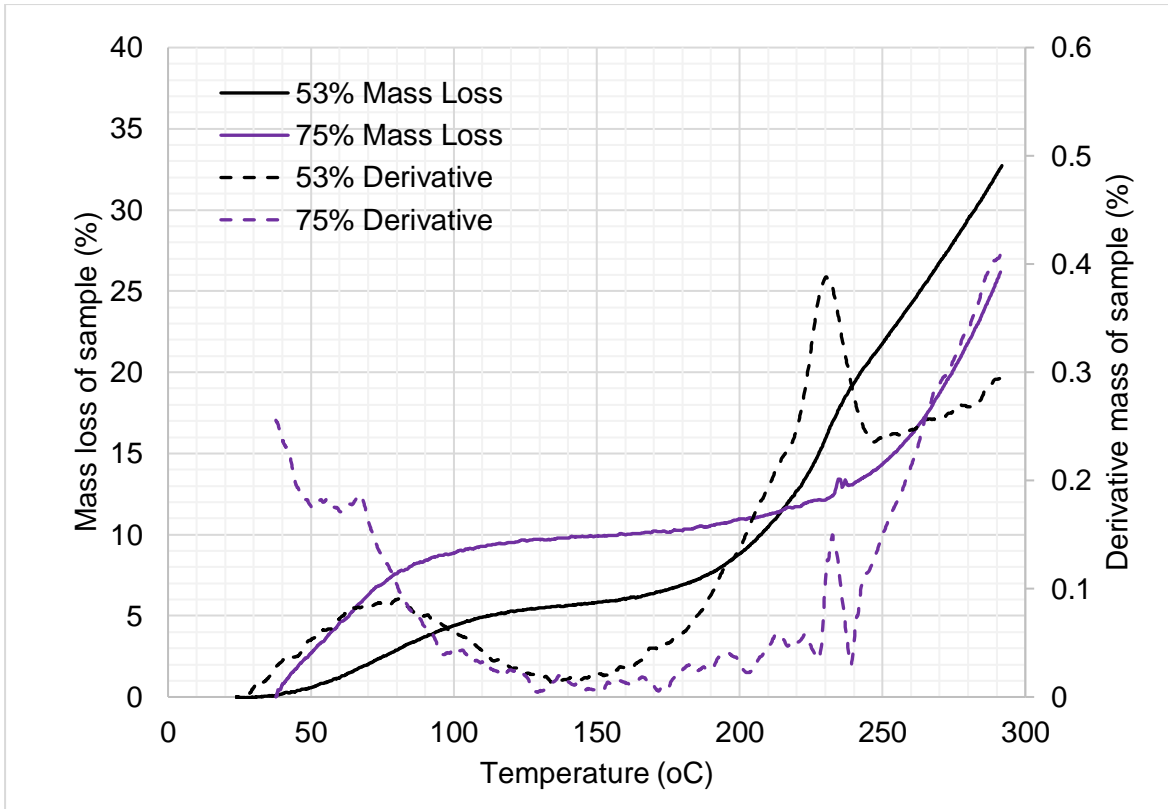


Figure 4.6c. TGA (solid line) and DTG (dashed line) for STW at 53% and 75% RH.

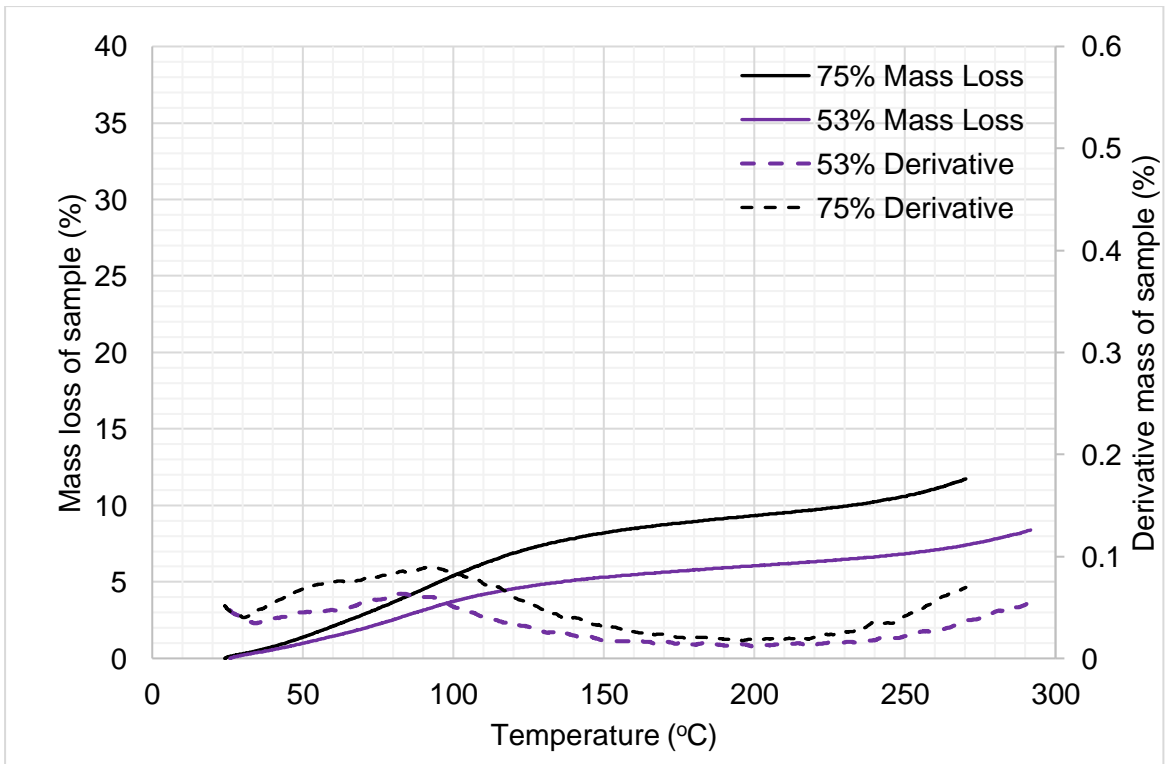


Figure 4.6d. TGA (solid line) and DTG (dashed line) for WWB at 53% and 75% RH.

4.4.1.2. Keratin based analysis regarding TGA and DTG

TGA and DTG for W1 and W2 at 53% and 75% are demonstrated within Figures 4.6e to 6f. Research for the thermogravimetric analysis of wool mainly comes from the textile industry where it has been examined that the melting point of wool decreases with increasing moisture content (Cao and Bhoyro, 2001; Romano et al., 2019a) - outlined by Flory's theory (Cao, 1997). This is when wool encounters water molecules and interacts with the polypeptides when crystallites melt. Another factor affecting melting point is the stability of structures, the more stable the structure the higher the melting temperature as it can resist a greater amount of thermal degradation (Li, Hurren and Wang, 2019).

Initial mass losses within sample W1 are overall lower than that of W2 and the derivative of W1 at both RH's are similar. However, there is a greater increase in mass loss within 53% than 75% RH. By comparison, W2 has a larger peak for 75% at approximately 100°C associated to the moisture release within each sample. Water within samples takes 3 different forms: chemically bound water, loosely bound water and free water. Within a TGA curve these different types of water and the way in which it leaves the sample overlaps making it difficult to precisely identify (Rahman, Hamdan and Hui, 2017). The actual thermal and chemical degradation of wool molecules occurs at approximately 200°C (Price and Horrocks, 2013). So, when comparing weight loss after the release of water (within Table 4.1) within the sample (before the chemical depletion of the molecule), it demonstrates that W1 has lost the least amount of mass therefore demonstrating its thermal stability. Overall it could be stated that due to the strong inner cross-linkages that the macromolecules have, W1 is less sensitive to a dynamic hygrothermal environment by comparison to W2 as outlined by concepts in Nelson and O'Connor (1964); Cancellieri, Cancellieri and Leoni (2009). Although this method is useful for investigating the behaviour of these materials, it is not a "finger print" technique and can only indicatively mark the 'typical' behaviours in order to identify a sample therefore FTIR will be utilised in conjunction with TGA (Haines et al., 2002).

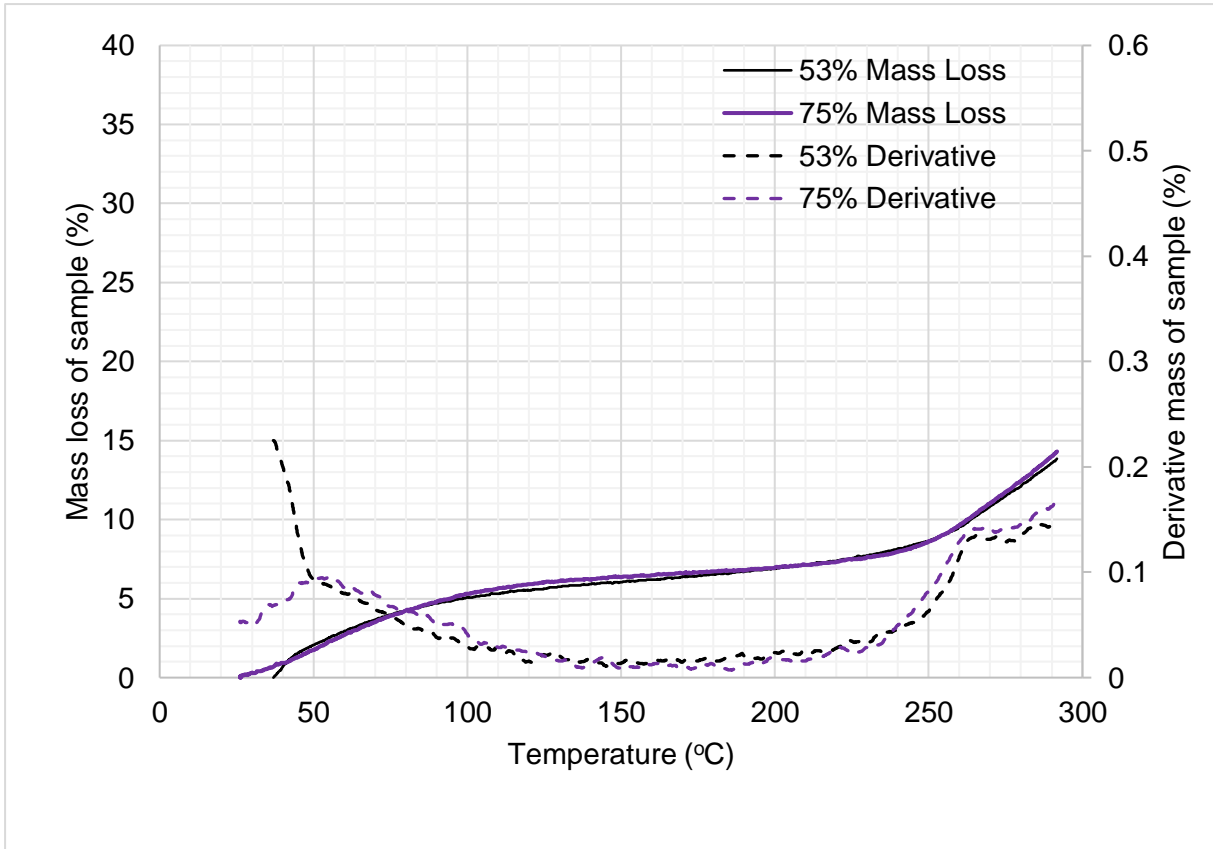


Figure 4.6e. TGA (solid line) and DTG (dashed line) for W1 at 53% and 75% RH.

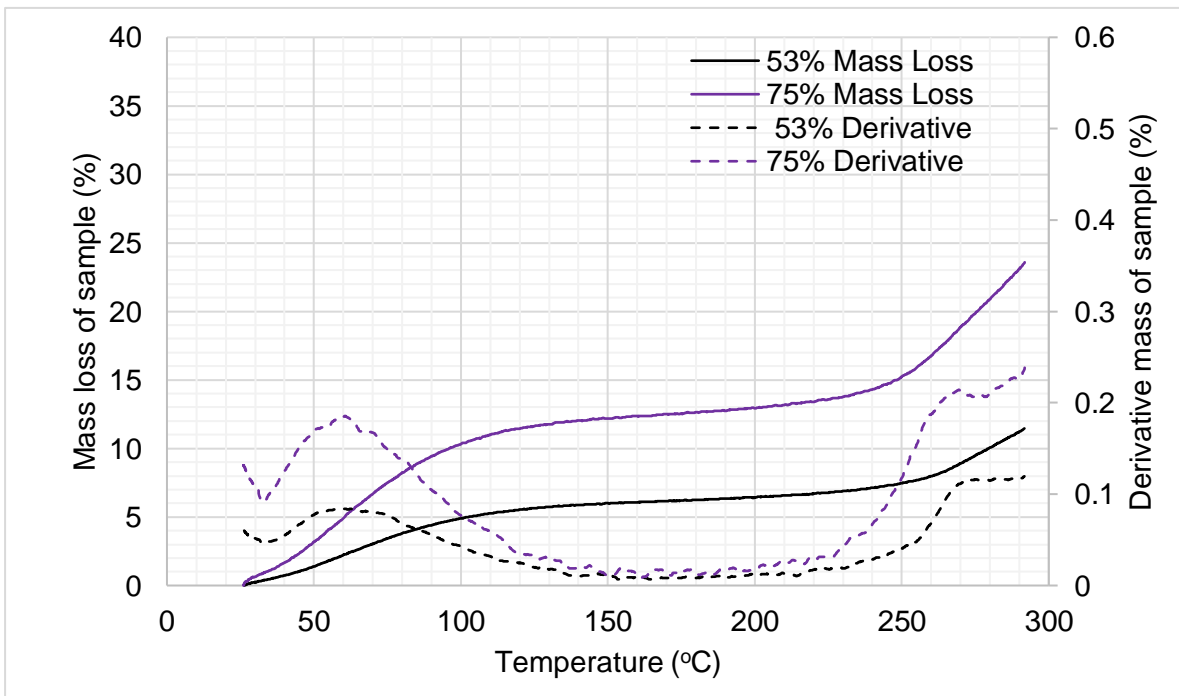


Figure 4.6f. TGA (solid line) and DTG (dashed line) for W2 at 53% and 75% RH.

4.4.2. DSC

DSC will be utilised as a single step diagnostic tool for identifying and analysing patterns within phase transitions and understanding information about components within a sample (Reh, Kraepelin and Lamprecht, 1986). Key thermal events that a DSC curve can map are: the evaporation of water, denaturation and glass transition (Martí et al., 2007). This demonstrates that a physical transition or chemical reaction is taking place within the sample, the shape of the DSC curve is critical for deciphering the characteristics of the sample. The DSC thermograms for cellulose and keratin based samples will be analysed separately.

4.4.2.1. Cellulose Based analysis with DSC

The DSC thermograms for plant derived, cellulose based samples are demonstrated in Figures 4.7a to 4.7d. The temperatures for key phase changes to the samples can be found within Table 4.2. In cellulose based fibres (STW, WF, WWB, SMR) (with the exception of hydrogen bonding which are required for breaking and rebonding), there are no cross-linkages between molecules (Lewin, 2006). Between 25°C and 100°C, these hydrogen bonds are broken which give a greater range of freedom but less stillness and elasticity for the cellulose within the macromolecule (Xia et al., 2016).

Table 4.2. DSC phase transition temperatures for cellulose based samples.

Sample		Water Evaporation Temperature (T_{eva})	Denaturation Temperature (T_d)
SMR	53%	131.34	239.27
	75%	131.73	260.47
STW	53%	89.40	-
	75%	97.47	-
WF	53%	131.34	-
	75%	110.34	-
WWB	53%	126.47	-
	75%	133.47	-

Following the glass transition, the water evaporation temperature (T_{eva}) occurs and due to the relationship between the water content of the fibres and water evaporation enthalpy this is an important link to the effect that relative humidity has on these samples. From the literature, it

is evident for all samples that an endothermic peak demonstrates the release of adsorbed water at approximately 100°C (Martin et al., 2010). This is due to the vaporisation of water that is both within the sample's fibres and the interstitial spaces (Belaadi et al., 2014). When comparing the evaporation temperatures of the different cellulose based samples (from Table 4.2), it is evident that there is a wide difference in the way that water is released from the sample. STW has a lower evaporation temperature than the 'wooden based' samples SMR and WF. On the outer layer of STW, there are epidermal cells, which create a thin 'waxy' layer on the surface of the STW, makes water vapour penetration difficult (Pizzi and Mittal, 2011).

The denaturation temperature (T_d) is the temperature at which materials lose their quaternary, tertiary and secondary structure. For SMR there is a shift in the gradient of the heat flow, this step demonstrates an endothermic peak at 239.27°C for 53% and 260.47°C for 75% stabilised sample. This difference is substantial enough in order to suggest that there is a change within the SMR molecule when stabilised at differing RH. It is evident from Table 4.2 that within this research work, the DSC was run to 300°C and for STW and WF this temperature is not sufficient for denaturation to occur, implying that they are thermally the most stable out of all cellulose based samples. At further alleviated temperatures, (approximately 330-360°C) cellulose based samples experience the degradation, dehydration and therefore the depolymerisation of cellulose (Fairbridge and Ross, 1978; Shafizadeh and Bradbury, 1979) leading it to char (Rahman, Hamdan and Hui, 2017).

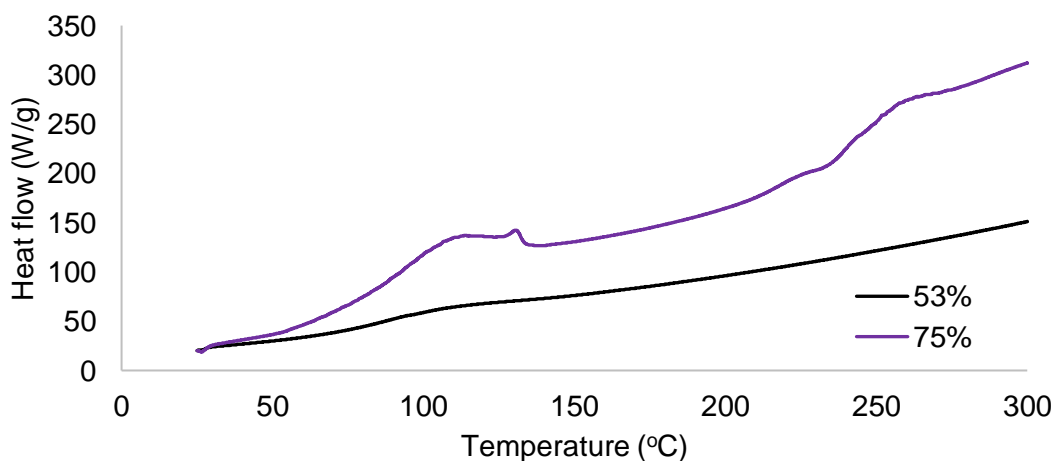


Figure 4.7a. SMR DSC thermogram.

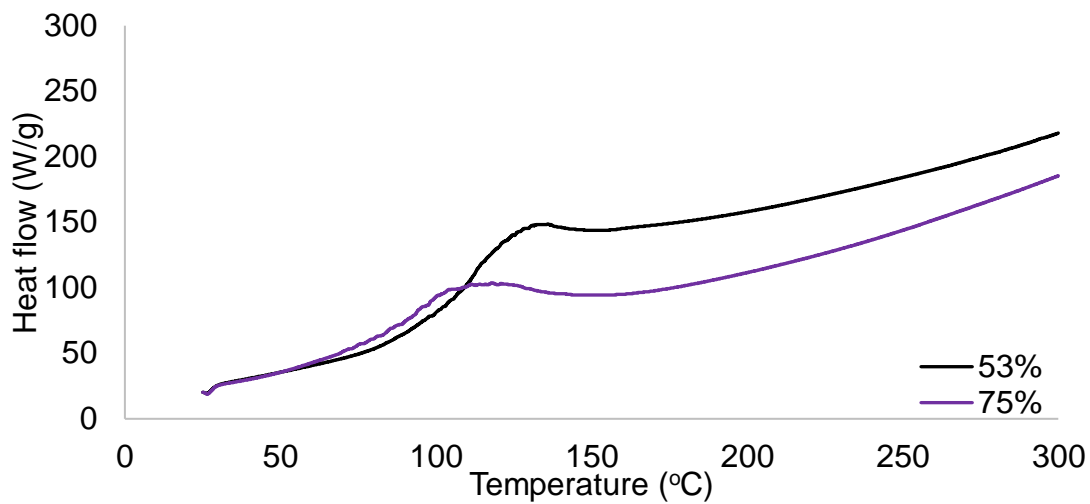


Figure 4.7b. WF DSC thermogram.

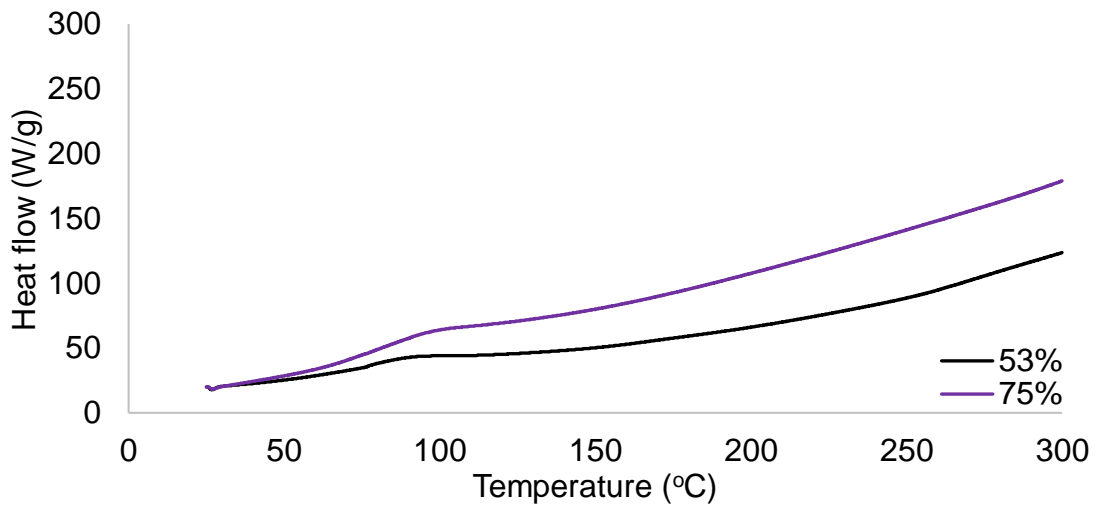


Figure 4.7c. STW DSC thermogram.

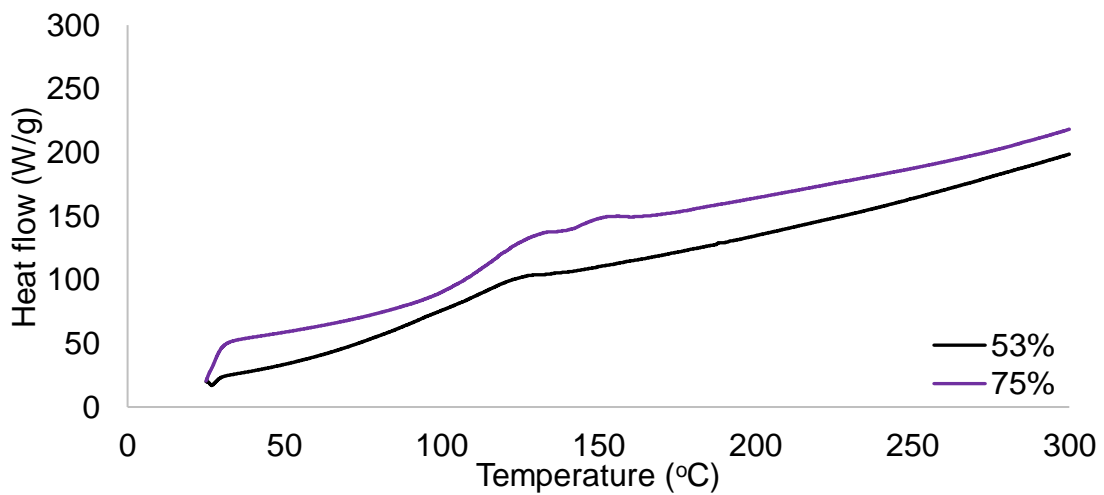


Figure 4.7d. WWB DSC thermogram.

4.4.2.2. Keratin Based analysis with DSC

For keratin-based materials, their thermograms are shown within Figures 4.7e and 4.7f. Key information for the different phases that the samples experienced are provided in Table 4.3. Glass transition is the first noted characteristic of this curve is between 40-60°C but overlaps with the initial water evaporation within the sample and therefore is difficult to analyse. Further to this, as a second order transition, glass transition occurs due to a relaxation of chain sections located within the amorphous part of the polymer (Osman and Abd El-Zaher, 2011). Due to the fibrous nature of the wool, it can be difficult to accurately measure glass transition via DSC in comparison with cellulose based samples which were discussed earlier (Marti et al., 2007).

Table 4.3. DSC phase transition temperatures for keratin based samples.

Sample		Water Evaporation Temperature (T_{eva}) (°C)	Denaturation Temperature (T_d) (°C)
Wool 1	53%	124.60	256.94
	75%	89.60	253.60
Wool 2	53%	121.53	256.27
	75%	107.87	256.00

More broadly, thermal analysis within Table 4.3 demonstrates that from approximately 25-100°C there is no degradation in the molecular chain due to there being no clear thermal events. As previously described water bonded to the fibre will evaporate from 30-150°C (Xia et al., 2016). Table 4.3 shows that the water denaturation temperature is greater when samples are stabilised at higher RH's. It could be suggested that samples stabilised at a higher RH are less sensitive to temperature changes as the cross linkages within the inner macromolecules are stronger. When considering W1 and W2, as the evaporation temperature increases (T_{eva}) the interaction between the specific fibre and water molecules are stronger. When the wool based fibres adsorb more moisture, the interactions become more consistent and stronger.

Within Figure 4.7e and 4.7f it is evident that there is a secondary, small abrupt endotherm at approximately 250°C. This can be associated to the inner α -crystal within the wool molecule spilling and decomposing (Cao and Bhoyro, 2001; Hsieh et al., 2004). Once the α -crystal has

decomposed, if temperatures continue to rise further decomposition of β -keratin structure would be demonstrated (Xu et al., 2007).

Denaturation of the sample can be exhibited within the samples at approximately 250°C (Marti et al., 2007; Zargarkazemi et al., 2014). Despite the difference in RH both W1 and W2 have very similar denaturation temperatures, suggesting that the RH has no effect on this property of the material. This could indicate that keratin based samples do not experience a change in permanent chemical characteristics (when stabilised at different RH). After the denaturation temperature, the different components of the wool sample are decomposing (Cao, 1999). Although this experimentation was from 25°C to 300°C, the literature explains how further increased temperatures would have exhibited the thermal breakage of intermolecular bonds and main chain degradation of the wool macromolecule (WI, 2003) and further structural degradation up to 600°C.

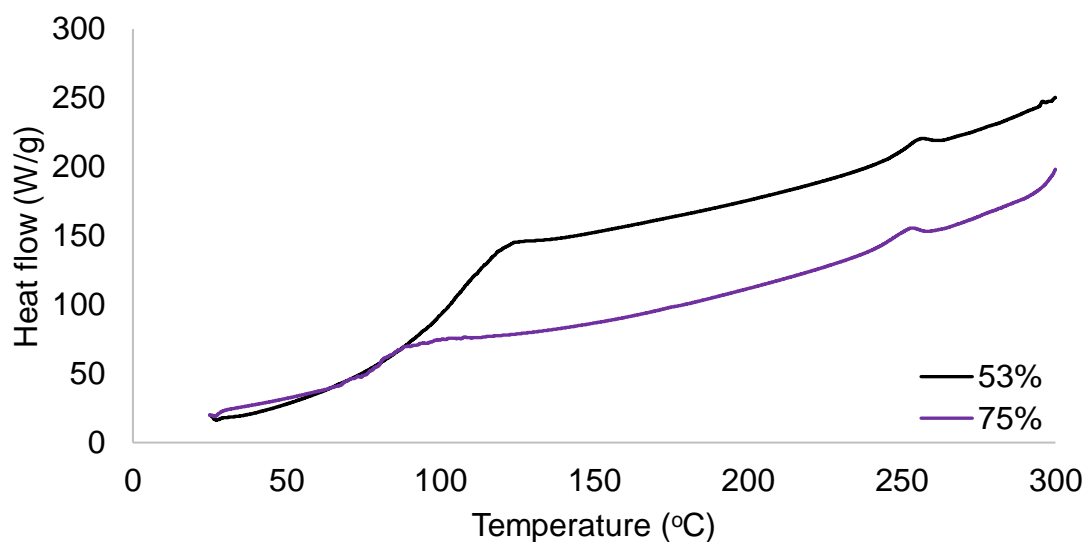


Figure 4.7e. Wool 1 DSC thermogram.

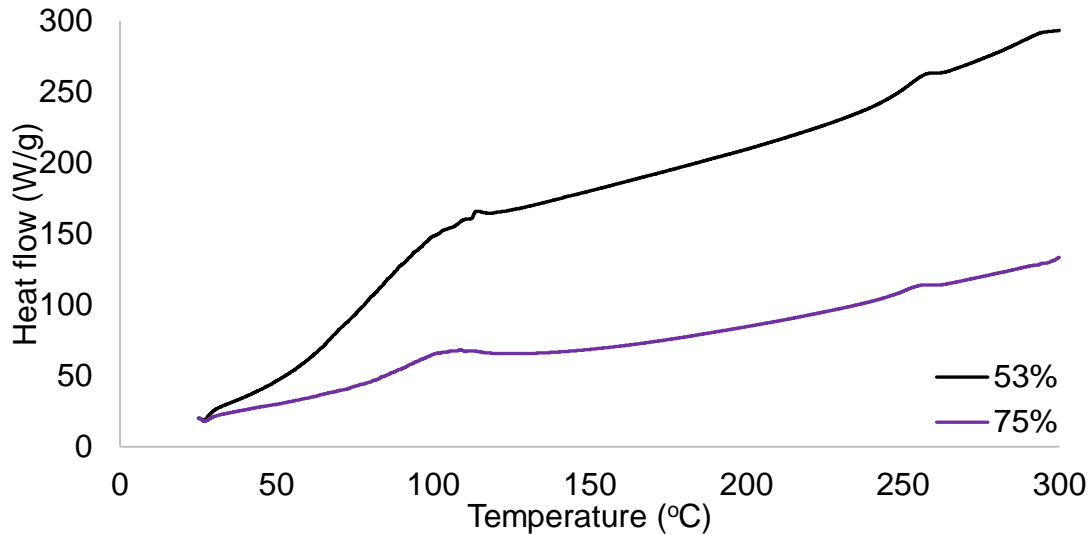


Figure 4.7f. Wool 2 DSC thermogram.

4.4.3 FTIR

This investigational technique enables to examine the molecular structure of the materials and to determine the chemical compositions via the demonstration of specific bonds as peaks or bands within a spectra. Within this experimentation, it will mainly focus on the functional group region of each spectra.

4.4.3.1. Cellulose Based analysis with FTIR

The 4 different cellulose based samples spectra can be found in Figures 4.9a to 4.9d. Within their core structure, all the bio-based materials within this research work have hydroxyl groups which hydrogen bond with water in to exhibit their hygrothermal characteristics. The fundamental mechanisms behind the way in which they do this has not been fully researched however, the assignment of bonds for each of the cellulose based samples can be found in Table 4.5.

As highlighted in Maskell et al. (2015), FTIR highlights the ability of materials to adsorb water as a measure of the absorption of hydroxyl groups. Both inter- and intra- hydrogen bonds formed within the cellulose to water of each bio-fibre has demonstrated big differences on hydroxyl reactivity solubility and physical properties as outlined by Fan, Dai and Huang (2012). All samples exhibit OH- stretching vibrations and sample have a larger adsorption band when stabilised at 75% by comparison to those at 53% (Maréchal and Chanzy, 2000). The broadening of hydroxyl groups is due to the inter and intra hydrogen bonding taking place

within the molecule (Abdel-Kareem and Elnagar, 2005). The hydrogen bond network in cellulose is observed by Garside and Wyeth (2003) and despite the transmittance being relatively low, a weak 'hump' at approximately 1640cm^{-1} indicates carbon to carbon vibrations. However, as indicated by Xia et al. (2016), this is masked by water adsorption at the same frequency. At this point for all cellulose based insulation materials, the hydroxyl groups are stretching and at higher relative humidity, this gain in water molecules increases the length of cellulose molecules and reduces intermolecular hydrogen bonding. Due to the location of these (-OH) groups within the cellulose their affinity to water is high.

When comparing all four samples to one another, there is a whole spectral difference in all samples which demonstrates how the spectra is affected by a difference in relative humidity and therefore water within the sample. For the cellulosic materials, there is a broadened absorption peak around 3000cm^{-1} when the materials are conditioned at a higher relative humidity. This adsorption peak can be associated to the inter and intramolecular hydrogen bonding as well as free/bound water within the material and free hydroxyls within the cellulose of the macromolecule.

Figures 4.9a - 4.9d show that there are different sections of the spectra that are greatly affected by relative humidity by comparison to others. SMR, WF and STW all experience differences in adsorption intensities between $2935\text{-}2900\text{cm}^{-1}$ assigned to the CH bond stretching, which is in line with Céline et al. (2014) and demonstrates that this bond is affected by a differentiation in local hygrothermal environment.

In addition to this, from the works completed by Carter and Kibler (1978), this work further supports that water molecules may coexist within each sample within both adsorption and desorption. Water exists in samples as 'free' and 'bound' water where free and bound water is exhibited at around 3000cm^{-1} whilst free water is exclusively found at approximately 1630cm^{-1} . These molecules bind to not only hydroxyl sites but also carboxyl function and the free water can diffuse into the porous bio-based fibres.

For SMR the transmittance is quite low and there are no major, strong bands within the material. However, there is a clear differentiation between the two different RH's for the same sample. Similarly to SMR, WF demonstrates that it is very affected in the hydroxyl region and this band is now much greater at 75% than 53% stabilisation. STW and WWB show that whilst the hydroxyl groups are affected, the rest of the molecule is not as affected by its hygrothermal conditions in the same way that SMR and WF are. Table 4.4 demonstrates Total Crystallinity

(TCI), Intensity of Hydrogen Bonding (HBI) and Lateral Order Index (LOI) for the 4 cellulose-based samples.

Table 4.4. Total Crystallinity Index (TCI), Hydrogen Bonding Index (HBI) and Lateral Order Index (LOI) for 4 cellulose based samples.

Sample ID	TCI						HBI						LOI					
	I1370		I2900		I1370/ I2900		I3400		I1320		I3400/ I1320		I1430		I898		I1430/I898	
	53%	75%	53%	75%	53%	75%	53%	75%	53%	75%	53%	75%	53%	75%	53%	75%	53%	75%
SMR	92.09	86.83	90.64	85.18	1.02	1.02	94.02	85.63	92.27	87.13	1.02	0.98	91.50	85.06	88.23	82.09	1.04	1.04
WF	92.96	89.87	94.85	92.15	0.98	0.98	93.62	87.83	92.98	90.25	1.01	0.97	93.64	90.81	90.17	86.07	1.04	1.06
WWB	91.55	79.12	99.17	97.56	0.92	0.81	98.03	95.67	95.67	89.17	1.02	1.07	89.94	77.20	97.07	91.75	0.93	0.84
STW	74.96	77.76	79.28	81.65	0.95	0.95	80.88	76.94	77.50	79.24	1.04	0.97	79.04	81.28	67.24	65.78	1.18	1.24

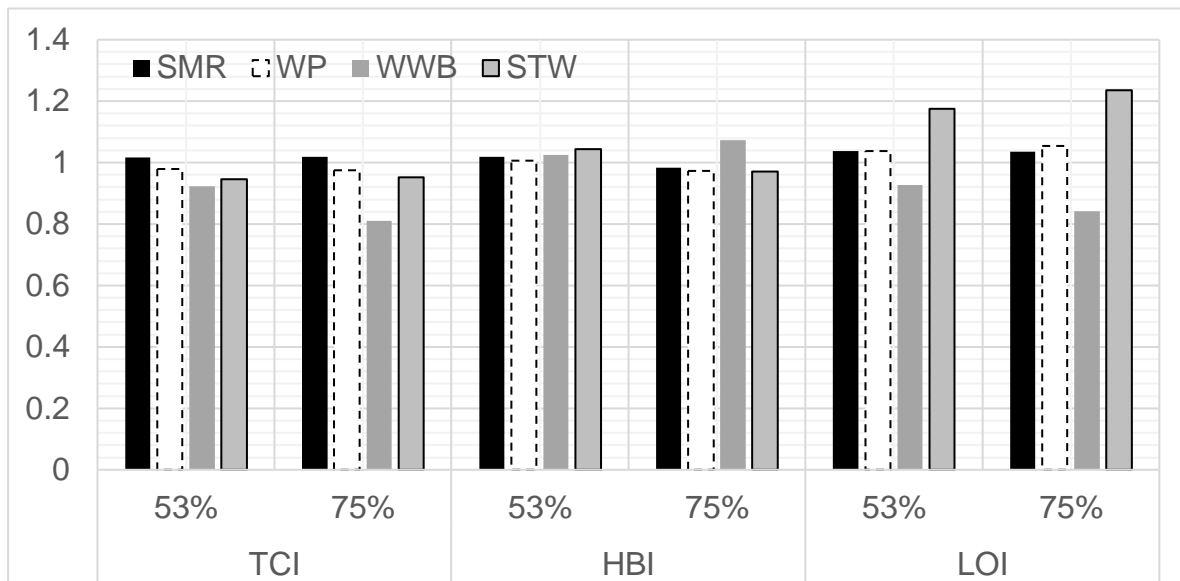


Figure 4.8. Total Crystallinity Index (TCI), Intensity of hydrogen bonding (HBI) and Lateral Order Index (LOI) for cellulose based samples.

When comparing the results from Table 4.4 and Figure 4.8, SMR has the highest TCI at both RH (1.016 for 53% and 1.019 for 75% RH) by comparison to the WWB with the lowest (0.923 for 53% and 0.811 for 75%). By comparison to Yang (2017) (where TCI ranges from 0.46-0.58) the values for TCI within Figure 4.8 are considerably greater. As the literature suggests, a great value of TCI indicated more crystalline material in the cellulose. However, as TCI decreases HBI increases and for all samples except for WWB, at 75% RH reduces the HBI. At 53% RH it is notable that all bio-based insulation samples have extremely similar HBI values. The LOI is particularly high in STW at both RH suggesting the molecule has a larger variation of the crystal lattice. Cai et al. (2011) suggests that the thermal stability of samples which are cellulose based are affected by the order of the crystalline. Therefore, from Figure 4.8 it can be suggested that due to having the largest total crystallinity index, SMR is the most thermally stable bio-insulation sample.

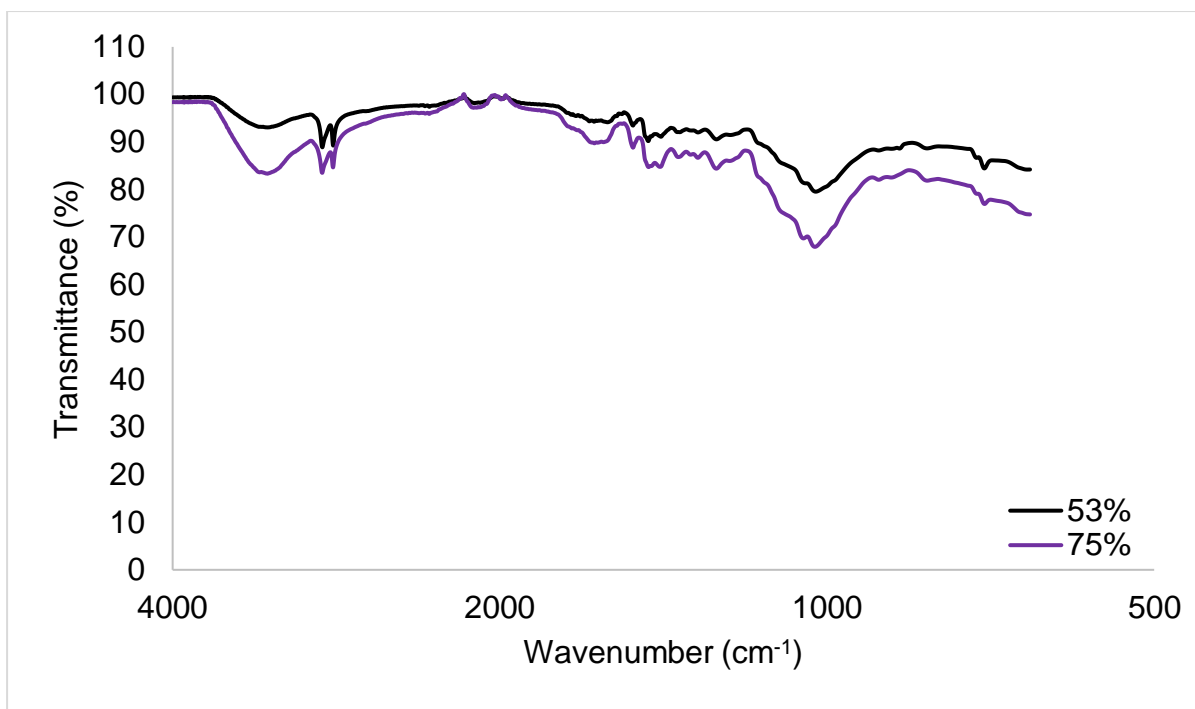


Figure 4.9a. SMR FTIR spectra.

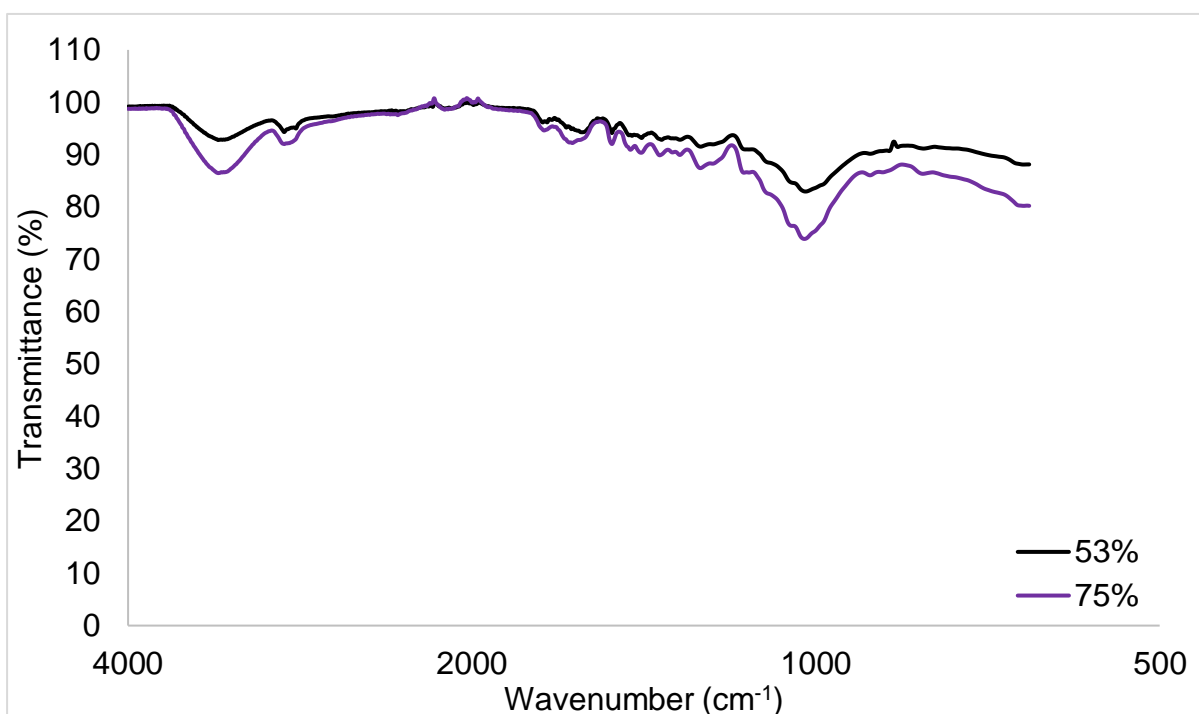


Figure 4.9b. WF FTIR spectra.

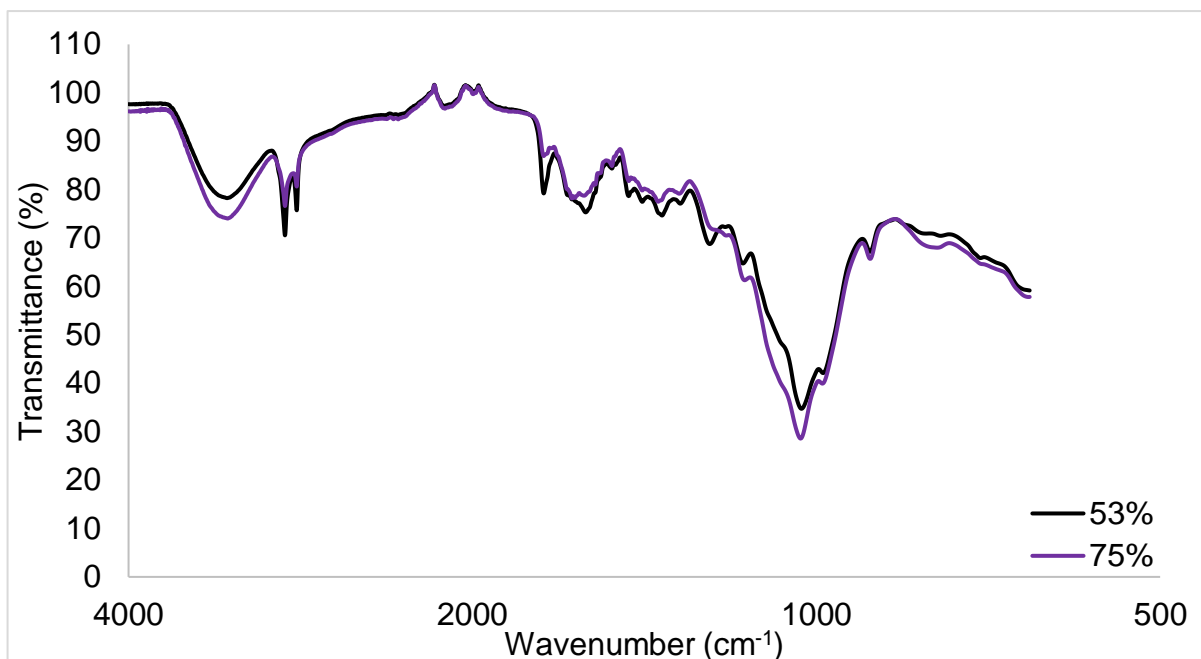


Figure 4.9c. STW FTIR spectra.

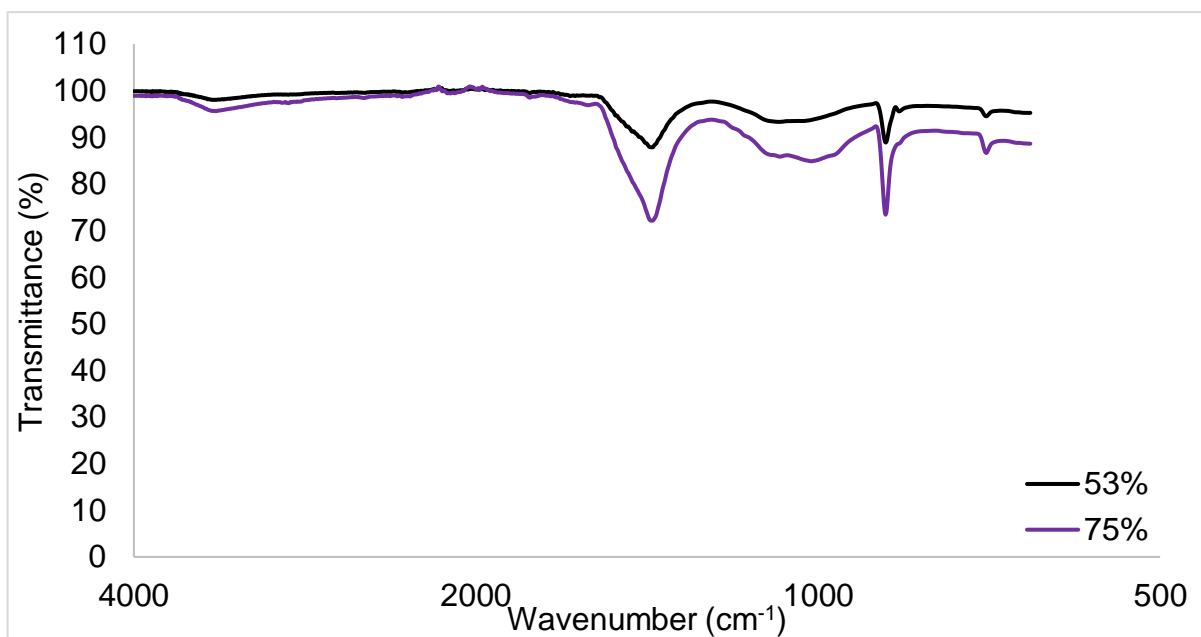


Figure 4.9d. WWB FTIR spectra.

Table 4.5. FTIR analysis of cellulose based samples and associated assignment of bonds at 53% and 75% RH.

SMR position of band (cm ⁻¹)		WF position of band (cm ⁻¹)		STW position of band (cm ⁻¹)		WWB position of band (cm ⁻¹)		Assignment for bond
53%	75%	53%	75%	53%	75%	53%	75%	
3270.739	3272.603	3335.967	3335.967	3280.057	3276.33	3408.65	3410.514	(OH) stretching vibration due to intermolecular hydrogen bonded and free groups (Owen and Thomas, 1989; KONDO, 1997; Hinterstoisser and Salmén, 1999; Dai and Fan, 2010) and stretching vibration of cellulose and lignin of the fibre (Brigida et al., 2010) (Schwanninger et al., 2004)
2912.915	2914.778			2847.686	2849.55			CH symmetrical stretching due to hemicellulose and cellulose components (Wojciechowska, Włochowicz and Weselucha-Birczyńska, 1999)
		2920.369	2920.369	2916.642	2918.506			Stretching vibrations of V(C=O) ester of cellulose and hemicellulose (Morshed, Alam and Daniels, 2010) and free hydroxyl group (Rana et al., 2010)
						1401.479	1399.615	C-O bond elongation of hemicellulose and cellulose (Hori and Sugiyama, 2003; Popescu et al., 2007; El Hajam et al., 2019)
1025.018	1025.018	1021.291	1023.154	1021.291	1026.882	872.1971	872.1971	P(-CH-) bending vibration in cellulose (Garside and Wyeth, 2003)
				987.7445	987.7445			

4.4.3.2. Keratin Based analysis with FTIR

The spectra for WL1 and WL2 can be found in Figures 4.9e and 4.9f (respectively) and assignment of bonds is demonstrated within Table 4.6. Within FTIR, the main characteristic bands appear between 1000 and 1700 cm^{-1} including: Amide I and Amide II (Church, Corino and Woodhead, 1997; Wojciechowska, Włochowicz and Wesełucha-Birczyńska, 1999). Amide I and Amide 2 are characteristic within the wool protein and the shape of this band is associated to the quantity and nature of hydrogen bonds within the molecule. Bands around 2900 and 1400 cm^{-1} represent CH_2 bonds and 2800 cm^{-1} is due to CH bonds (Wojciechowska, Włochowicz and Wesełucha-Birczyńska, 1999) but due to Amide II forms a stretching vibration of C=O at approximately 1620-40 cm^{-1} (Vasconcelos, Freddi and Cavaco-Paulo, 2009).

Due to inter and intra-hydrogen bonding, when placed in differing hygrothermal environments the hydroxyl group will fluctuate so becomes imperative to measure. The nature of these hydrogen bonds that are occurring will give a variety in the quantity and strength that the intermolecular interactions have. This varies greatly within the samples and causes the hydroxyl band to be broad (by comparison), when intermolecular reactions are weaker and therefore there is 'less' of a chemical environment for reactions to take place, bands are smaller and narrower. A bigger peak intensity from one sample to another (with the same peak position) demonstrates that there is more quantity of that specific type of bond. Any shifting or movement of the peak demonstrates an interaction has occurred. Further to this, if the band shape has changed (e.g. has broadened) displays interactions have occurred which is generally attributed to hydrogen bonding. For samples stabilised at 75%, their OH- absorption peak becomes bigger and broader indicating water gain, reducing the restraints of the hydroxyl group movement (Xia et al., 2016). This is examined within W1 much more evidently than in W2 where in W1 the band has increased by comparison to the sample stabilised at 53%.

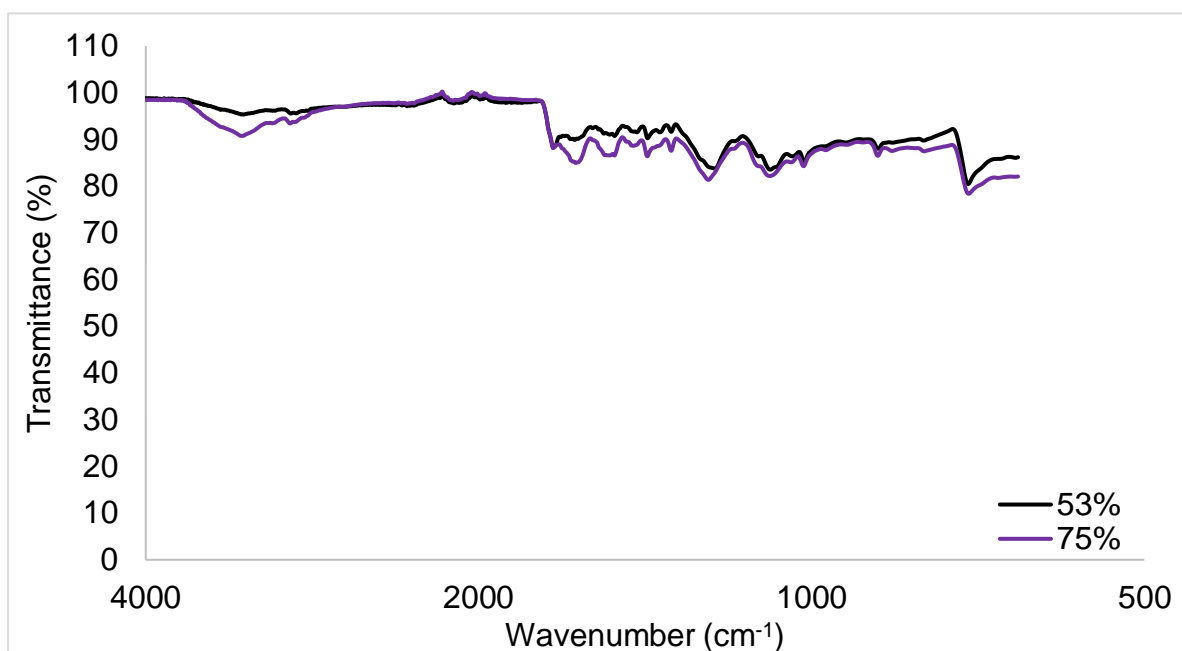


Figure 4.9e. W1 FTIR spectra.

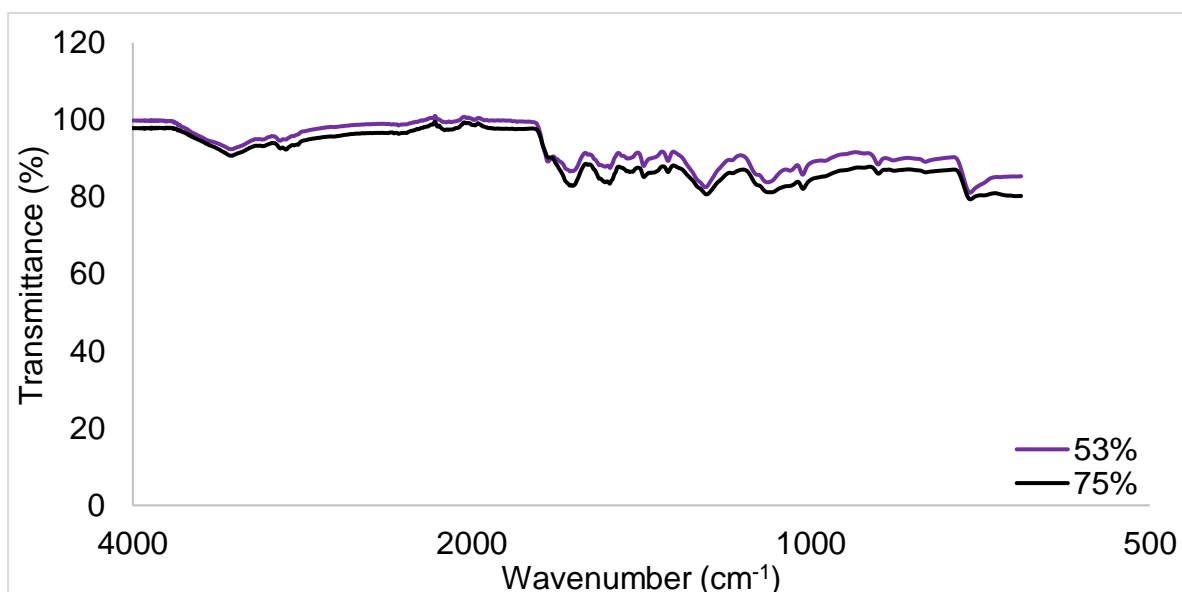


Figure 4.9f. W2 FTIR spectra.

Table 4.6. FTIR analysis of keratin-based samples and associated assignment of bonds at 53% and 75% RH.

W1 position of band (cm ⁻¹)		W2 position of band (cm ⁻¹)		Assignment of Bond
53%	75%	53%	75%	
3265.148	3276.33	3263.284	3274.466	Presence of hydroxyl groups (-OH)
1626.983	1626.983	1636.301	1634.438	Stretching vibrations of C=O (Amide I) (Liu X. et al., 2008 and Pelton and McLean, 2000)
1507.708	1507.708	1524.481	1522.618	Bending deformation peak of C-N-H (Amide II) (Gallagher, 2005)
1237.376	1239.34	1222.567	1239.34	Carbonyl oxygen C-O (Gallagher, 2005)

Regularity of the molecular chain (ROM) within these molecules can be calculated by utilising the intensity of the band at 1240cm⁻¹ and 1450cm⁻¹ (Li, Hurren and Wang, 2019). These results are displayed in Table 4.7 and Figure 4.10. The lower the ROM value is, the more disorder there is within the molecule (Huson, Church and Heintze, 2001). W1 and W2 generally have very similar ROM values, however W2 generally has a lower value and is only slightly affected by the differing hygrothermal environment. By comparison, W1 is initially more ordered than W2 but after being conditioned at 75% becomes more disordered.

Table 4.7. ROM of keratin based molecules at 53% and 75%.

Sample ID	I1240		I 1450		I1240/ I 1450	
	53%	75%	53%	75%	53%	75%
W1	80.84	82.56	86.54	90.01	0.93	0.92
W2	84.27	81.40	91.71	88.68	0.92	0.92

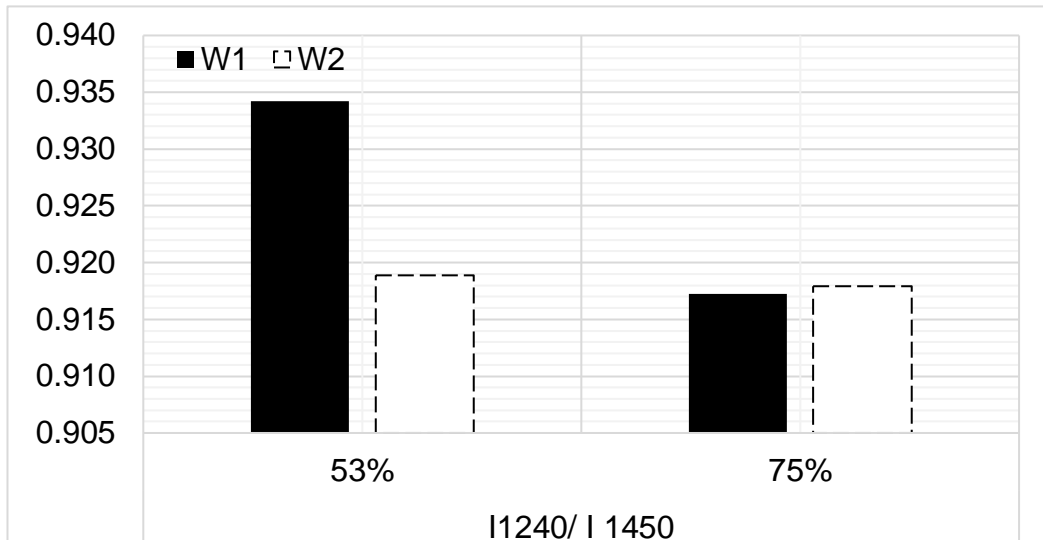


Figure 4.10. Regularity of the molecular chain (ROM) for keratin-based samples.

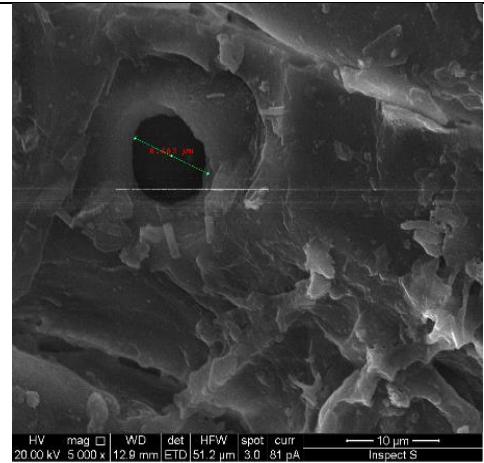
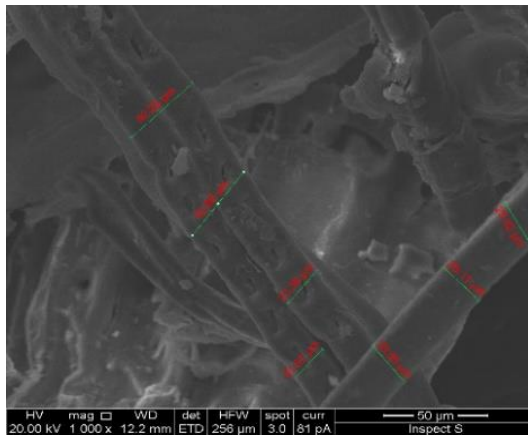
4.4.4 SEM

Providing three-dimensional, high resolution imagery of samples, SEM is important as it allows the user to understand morphological, topographical and physical properties of the materials. Table 4.8 presents all insulation materials stabilised at 53% and 75%. It is evident that all samples have a complex surface morphology. For W1 and W2 it is evident from Langley and Kennedy (1981) that the individual strands of fibre demonstrate even size and scale length. When considering the each strands surface texture, wool has an irregular, 'naturally crimped' surface morphology (Yao et al., 2008). This fibrous morphology and irregular pattern on multiple planes by which these fibres intertwined with each other, makes this material suitable for good adhesion within a matrix (i.e. a mortar or grout). When considering SMR, WF, WWB and STW there is no clear and obvious optical differentiation between those stabilised at 53% and 75%.

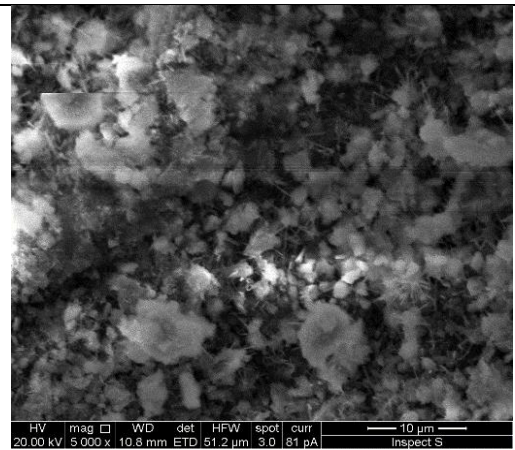
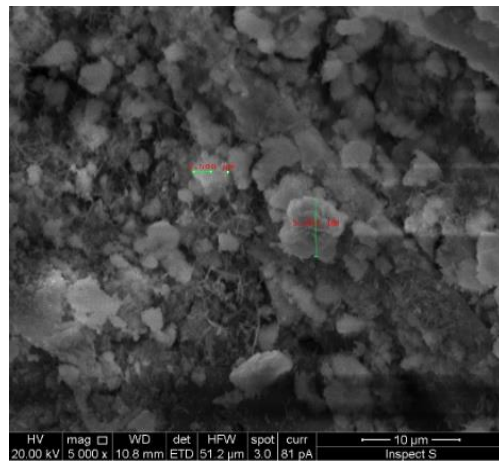
Table 4.8. SEM Images of samples stabilised at 53% and 75% taken at 1000 and magnification.

Sample ID	53%	75%

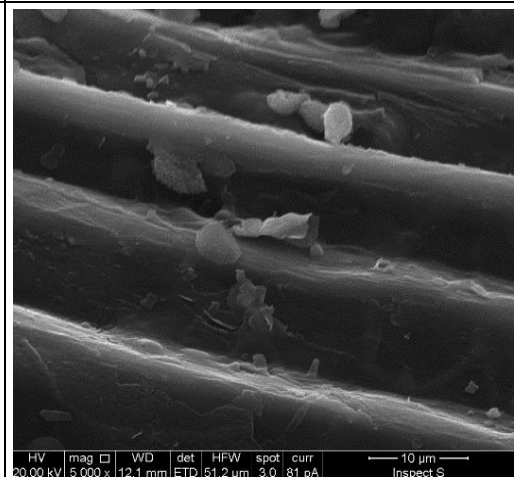
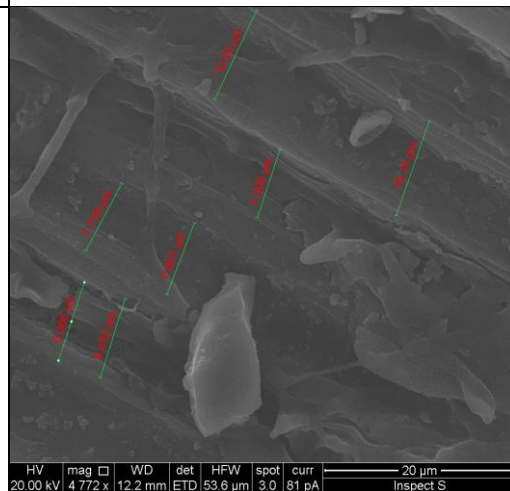
SMR



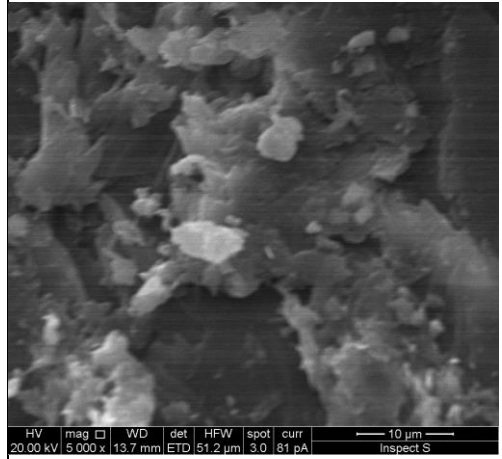
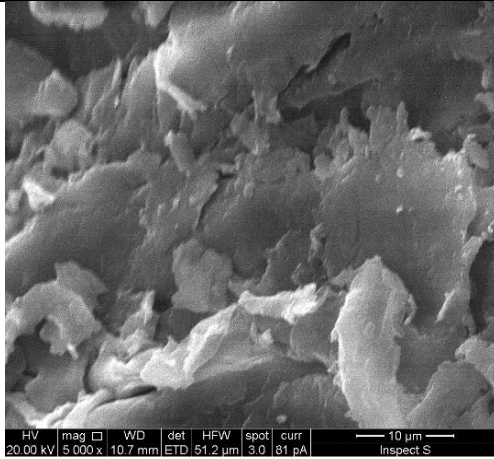
WWB



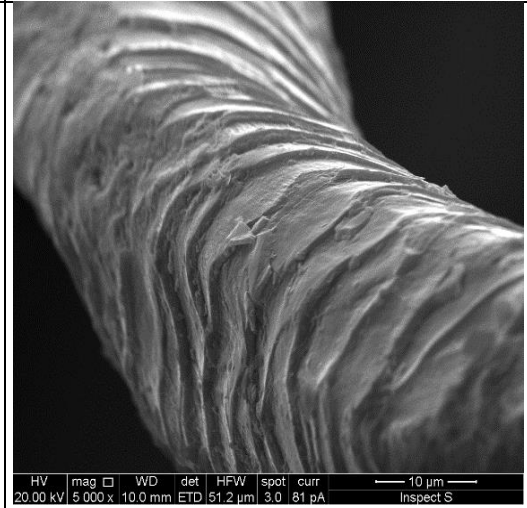
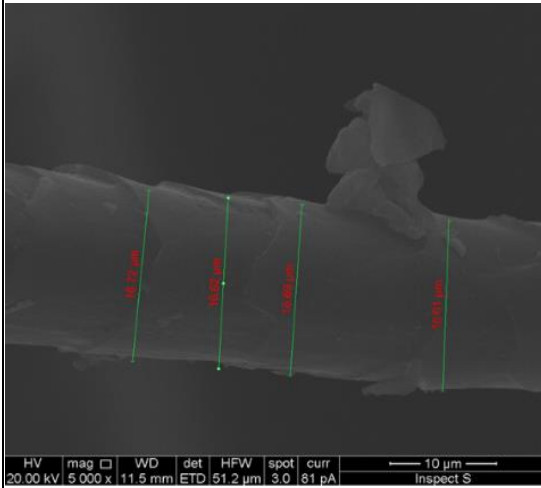
STW



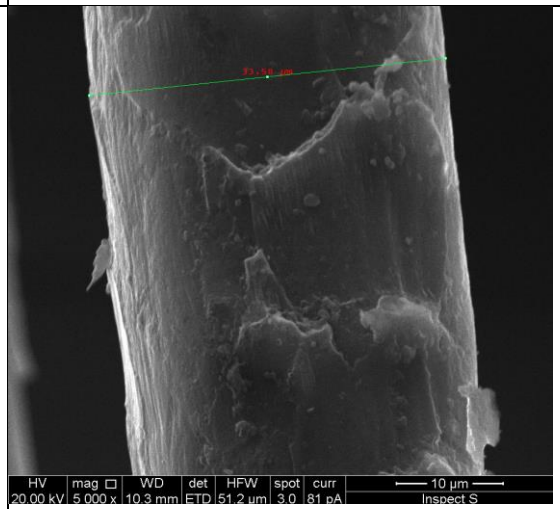
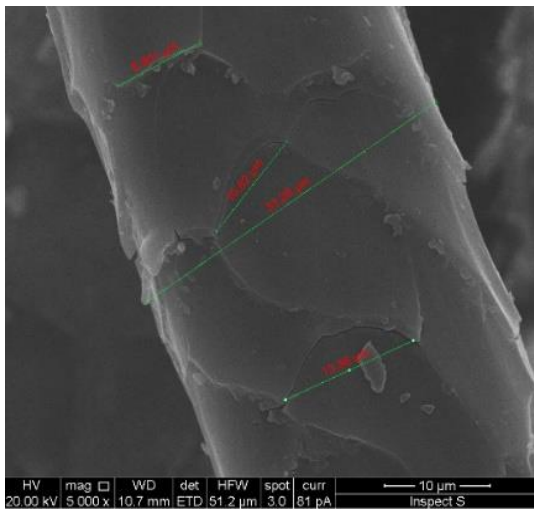
WF



W1



W2



4.5. Conclusion

This research work has demonstrated multiple different thermochemical methods in order to detect differences between 6 different bio-based insulation samples, stabilised at 53% and 75%. Consisting of two fundamentally differing structures, the samples were divided into cellulose (SMR, STW, WWB, and WF) and keratin (W1 and W2) based materials.

- Using TGA, it was demonstrated that in a dynamic hygrothermal environment SMR and WF are the most hygrothermally stable and for keratin-based materials W1 is the most stable.
- DSC demonstrated that whilst STW and WF did not reach their denaturation temperature within this experimentation SMR and WWB temperature remained the same, despite their different stabilisation RH. Whereas wool based materials demonstrated little differentiation between the two samples.
- In terms of FTIR for cellulose based materials, when comparing spectra and absorbance's at different frequencies shows the overall crystallinity index. This indicates that SMR has the highest thermal stability for cellulose based samples. For the keratin-based samples when conditioned at 75%, W2 has the more ordered structure but W1 is affected more in terms of hydroxyl absorbance from the spectra.
- When comparing using SEM to compare samples, despite having a greater understanding of their surface morphology, there are not significant and obvious differences between samples conditioned at different RH.

It is evident from this experimentation that the differences between bio-based samples conditioned at different RH fundamentally affects their physical properties and interactions but is difficult to generally quantify due to their heterogeneous nature. In terms of cellulose based materials, SMR has demonstrated that it is the most thermally stable and due to being little differentiation between the samples except for in TGA – W1 demonstrates the most thermally stable characteristics.

Chapter 5 - Bio-Based Earth Mortar

5.1. Introduction

Within the literature in Chapter 2 it outlines that by combining bio-fibres within an earth mortar matrix it can boost the properties of both materials. Chapter 2 also outlined how the addition of bio-fibres into an earth mortar can reduce cracking and improve moisture buffer properties, so the addition proactively problem solves the materials issues. From understanding the bio-fibre physical properties in Chapter 3 and the physicochemical and thermal properties in Chapter 4, this chapter will outline, investigate and identify the most suitable mix design for the best performing bio-based materials.

Initially, some preliminary experimentation were completed to focus the scope of the research into mix designs. The materials used and testing methodology that will be utilised to select the best performing mix designs will be outlined in the preliminary experimentation. These experiments were initially selected to give a general understanding of the materials typical behaviour before the addition of bio-fibres. Further testing procedures to analyse the performance of the composites will be outlined within the main experimentation section.

5.2. Initial Mix Design Selection

To fully realise the bio-fibre earth mortar composite, an initial set of experimentation will ensure that the performance of the panel is optimised. Before creating the mortar mix, the constituent materials are presented in section 5.2.1.

5.2.1. Materials

The sand that has been used within this project was supplied by a national builders merchant where its particle grain size distribution is demonstrated in Figure 5.1.

5.2.1.1. Binders

5.2.1.1.1. Earth

For this study, the earth was collected from a construction site in central Liverpool (North-West England) from a depth between 1.5-2m. Due to an abundance of construction waste materials, the earth was sieved at 2mm to disregard any large pieces of aggregate and to ensure the creation of a homogenous material. The earth was characterised in accordance with EN 1015-1 (BSI, 1999a) and its grain size distribution is displayed for both earth and sand in Figure 5.1.

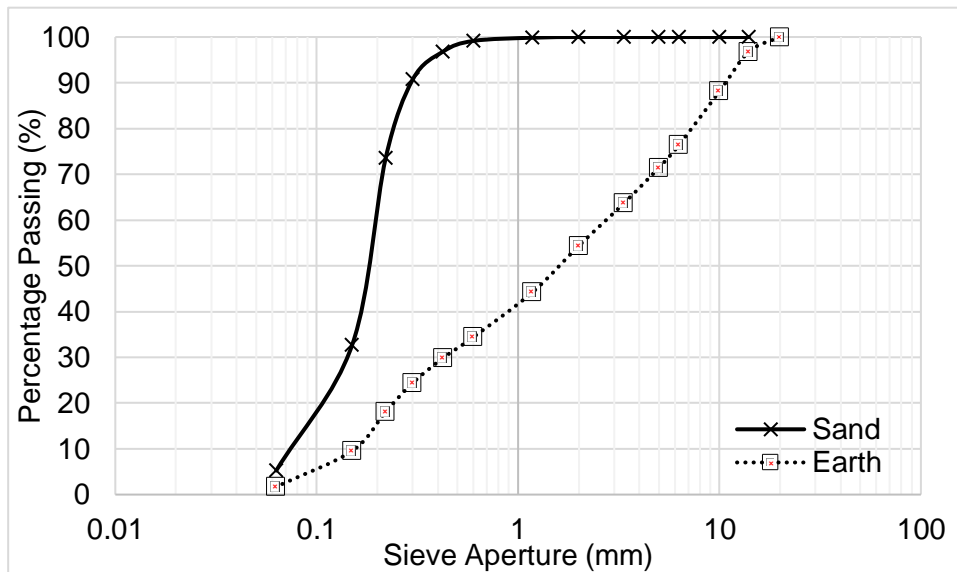


Figure 5.1. Dry grain size distribution of earth and sand.

XRD Analysis for earth characterisation

The earth was dried (as per BS EN ISO 12570 (ISO, 2000)) and after being passed through a 2mm sieve, the fine fractions were placed into a Rigaku Miniflex (see Figure 5.2), at a scanning speed of 2 degrees per minute in continuous scan mode from 5° to 65°. With Cu-K α x-ray radiation at a voltage of 30kV and a current of 15mA. This device produced a qualitative analysis of the material, where peak patterns were matched to identify the minerals. This was conducted to understand what type of crystalline components are within the earth. The methodology was used as technique that can rapidly analyse the material to give a better understanding of the sample. Figure 5.3 demonstrates that the main mineralogical constituents in the earth are Calcite, Dolomite and Quartz. It could be suggested that due to the earth being sourced from a construction site, calcite and quartz could be attributed to the intrusion of these materials in the raw earth. Another potential explanation of such levels of calcite could be due to the abundance of Carboniferous and Triassic rocks within the geological profile of Liverpool (Aitkenhead. N. et al., 2002; Rawlins et al., 2012).



Figure 5.2. XRD Rigaku Miniflex.

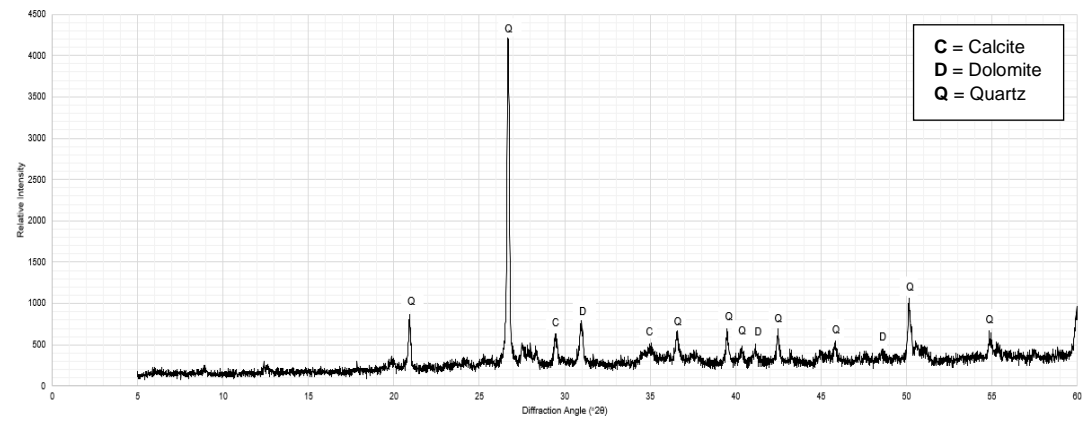


Figure 5.3. Diffractogram of earth samples.

5.2.1.1.2. Lime

In terms of using binders, there is limited literature to correlate the hygrothermal properties of earth-lime composites, so its characterisation is restricted. Despite being relatively less so than cement, lime is still an energy intensive binder, the use of lime is ideally limited to as smaller quantity (without compromising on material performance) as possible in order to reduce the carbon footprint of each mix design. By reducing the amount of lime used within this research chapter, it also reduces the embodied energy of the overall produced panel. This research utilises Natural Hydraulic Lime (NHL) supplied from a national builders merchant (Tarmac Limite NHL 3.5) where the requirements are defined within EN 459-1 (CEN, 2015). Further to this, the dry bulk densities (as per BSI (2017)) for lime, sand and earth can be found within Table 5.1.

Table 5.1. Dry Bulk Density of mix design components.

Binder	Dry Bulk Density (kg/m³)
Earth (after passing 2mm sieve)	2527
NHL	940
Sand	1593

5.2.2. Mix Design

Based upon the literature in Chapter 2, the mix designs selected within this preliminary experimentation can be found within Table 5.2. However, the water content and therefore the consistence should be set to calibrate the viscosity of each mix design.

Table 5.2. Mix design proportions (by mass).

Mix Design	Lime	Earth	Sand
NHL1	1	0	7.7
NHL2	1	0.1	8.6
EM0.3	1	0.3	10.3
EM7	1	7.7	0
EM5	1	0.05	8.15
EM2	0	2	6.5
NHL3	0.5	0.25	9.95

5.2.3. Formulation

Each mix design (as outlined in Table 5.2) was formulated as per EN 1015-2 (CEN, 1999a) where all dry ingredients (including bio-fibres) are mixed to homogenise (and reduce agglutination) before adding water. Before mixing (and due to the fibrous nature of samples) bio-fibres were pulled apart to ensure that the mix is as consistent as possible. Both prismatic (40mm x 40mm x 160mm) and MBV square (100mm x 100mm x 35mm) were cast.

5.2.4. Curing

Throughout their curing, samples were covered with plastic sheeting to maintain hygrothermal conditions. After 14 days of curing, samples were demoulded and elevated to ensure that all surfaces of the sample can dry and then left to cure for a further 14 days (28 days total curing time). Samples were cured in laboratory of environmental conditions of approximately 21°C

and 54% Relative Humidity (RH). Cast samples for both prismatic and MBV squares can be seen in Figure 5.4.



Figure 5.4. Casting of (L) prismatic and (R) MBV square samples.

5.2.5. Methodology

5.2.5.1. Consistence

The optimisation of the flow capacity of the mortars was carried out by using a flow table test as per EN 1015-3 (BSI, 1999b), where both mix designs were calibrated to a 180mm consistence. This was completed by gradually adding 10ml of water to determine the optimum water content. The dimension was selected due to the hygroscopic nature of the bio-fibres that when they are included into the mix design would reduce the consistency to around 155mm \pm 5mm. To ensure all samples had the same consistency, bio-fibres were added incrementally to the mix design until a spread value of 150mm was achieved.

5.2.5.2. Compressive and Tensile Strength

As a measure of the prismatic samples structural strength, compressive and flexural strength was measured in accordance with EN 1015-11 (CEN, 1999b) using a Tinius Olsen H25KS as per Figure 5.5.

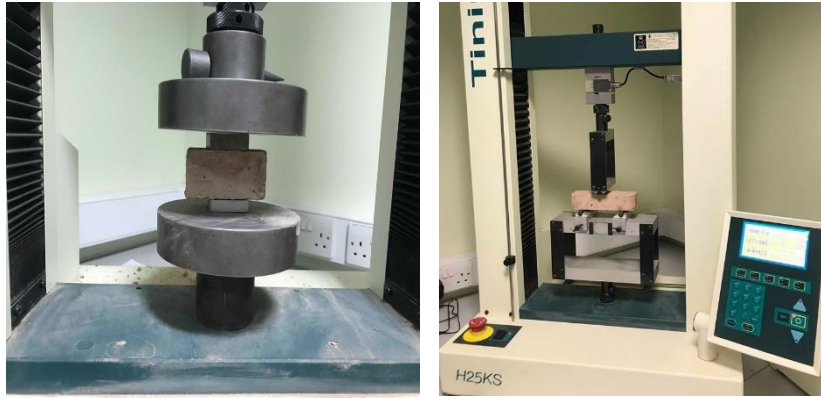


Figure 5.5. (L) Compressive and (R) tensile strength equipment.

5.2.5.3. Capillary Action

To demonstrate the capacity of a material to absorb in the short and medium term, prismatic samples were partially submerged in accordance with EN 1015-18: 2002 (CEN, 2002).

5.2.5.4. Moisture Buffering Value (MBV)

To adequately assess the ability of a material to adsorb and desorb water vapour from a local hygrothermal environment, a combination of NORDTEST protocol (Rode et al., 2005) and ISO 21453 (ISO, 2008) was used. Samples were wrapped in aluminium tape, laid horizontally with an exposed surface area of 0.01m^2 . After an initial stabilisation period of 24 hours in conditions of 23°C at 60% RH samples were exposed to a cyclical step change in RH of 75% for 8 hours and 53% for 16 hours (as per Figure 5.6).

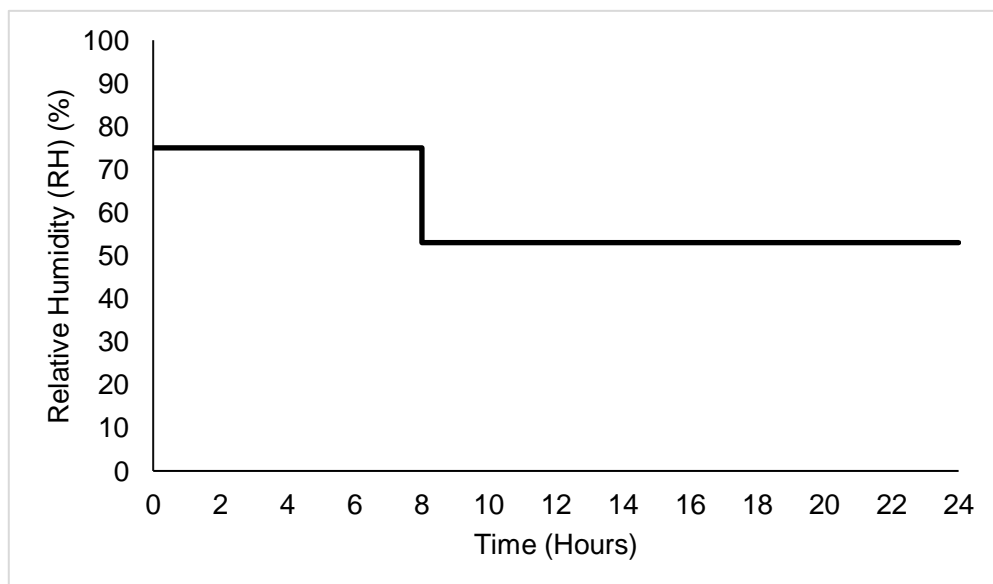


Figure 5.6. Step change in RH within climatic chamber over a singular, 24 h cycle.

These hygrothermal condition are those of measured conditions in full scale laboratories at LJMU, for residential properties within the UK. The Moisture Buffering Value (MBV) was calculated as per Equation 5.1.

$$MBV = \frac{m_a - m_d}{A\Delta\phi} \quad (5.1)$$

Where:

m_a = Mass of sample at end of moisture adsorption stage (g)

m_d = Mass of sample at end of moisture desorption stage (g)

A = Exposed surface area of sample (m²)

$\Delta\phi$ = Difference in RH between adsorption and desorption stage (%)

5.2.6. Results and Discussion

5.2.6.1. Consistence

After incrementally adding water to the mix design, the resulting consistence value that falls within the limits set out in section 5.2.5.1. is presented in Table 5.3.

Table 5.3. Quantity of water added to mix designs.

Mix Design	Quantity of water added (ml)	Consistence (mm)		
		D1	D2	Average
NHL1	180	181	182	181.5
NHL2	240	186	184	185
EM0.3	270	183	181	182
EM7	300	181	183	182
EM5	210	184	183	183.5
EM2	240	185	181	183
NHL3	320	183	185	183

Figures 5.7 presents an image of the consistence test being carried out. From Table 5.3 there is a large range in quantities of water added – which varies by 140ml from the minimum (NHL1) having 180ml added and the maximum (NHL3) requiring 320ml. It could be suggested that as NHL3 has the largest amount of sand, the specific surface area of the mix design is larger and therefore requires more water to penetrate and fully incorporated into the mix.



Figure 5.7. Flow test of plain earth mortar.

5.2.6.2. Compressive and Tensile Strength

By testing both the compressive and tensile strength it will help to give an understanding of the panels structural properties - displayed in Figure 5.8. Compressive strength varies from 0.51 to 0.79 MPa and tensile flexural strength from 0.18 to 0.34 MPa. Aside from NHL1 (at 0.79 MPa) (but with no earth contents), EM0.3 has the best compressive strength (0.67MPa). When considering the tensile strength, EM7 (0.31 MPa) and NHL2 have the greatest values (0.29 MPa). Samples were cured and tested after 28 days. As the mix design incorporated natural hydraulic lime as a stabiliser, it is currently acting as a filler rather than a structural component of the mix. As 28 days is insufficient time for the process of carbonation to occur, this will directly affect not only structural properties but also the porosity, capillary action and thermal conductivity of the sample. Further experimentation, with longer curing period of the mix designs would give a better indication of the long term structural strength.

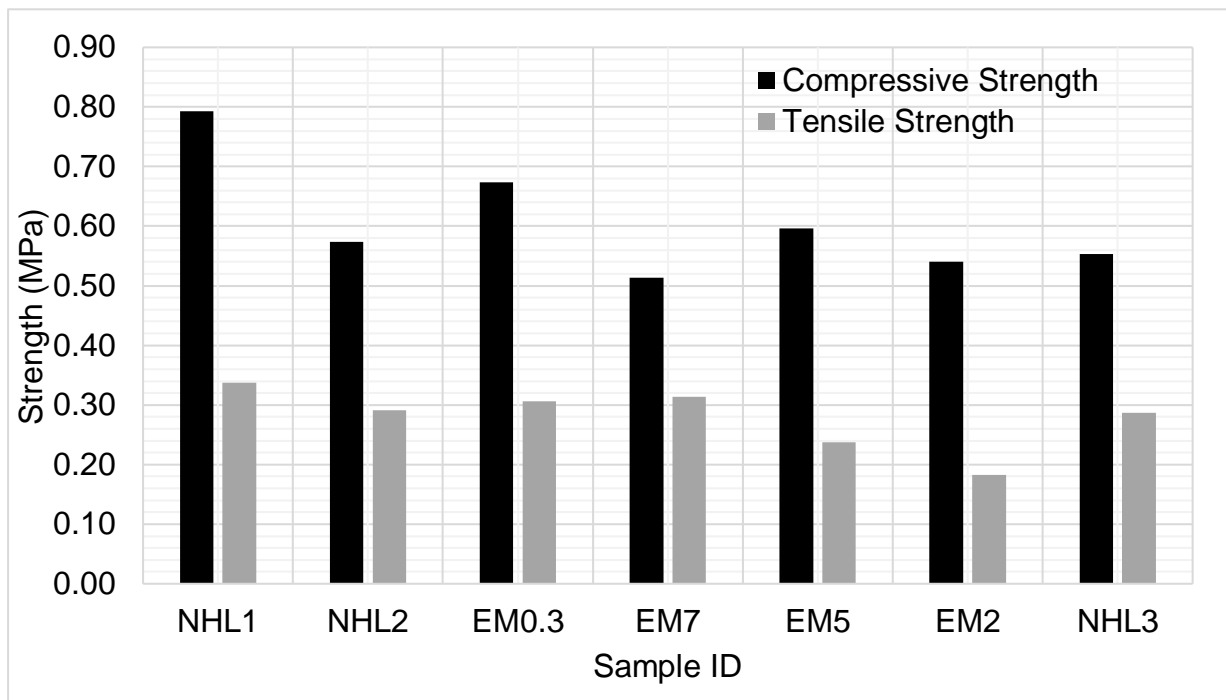


Figure 5.8. Compressive and Tensile Strength of initial 7 mix designs.

5.2.6.3. Capillary Action

As highlighted in Chapter 2, a key disadvantage of using earth within construction materials is due to it being highly sensitive to water causing deformation. To understand the transport of water throughout the sample via capillary action, results can be shown in Figure 5.9.

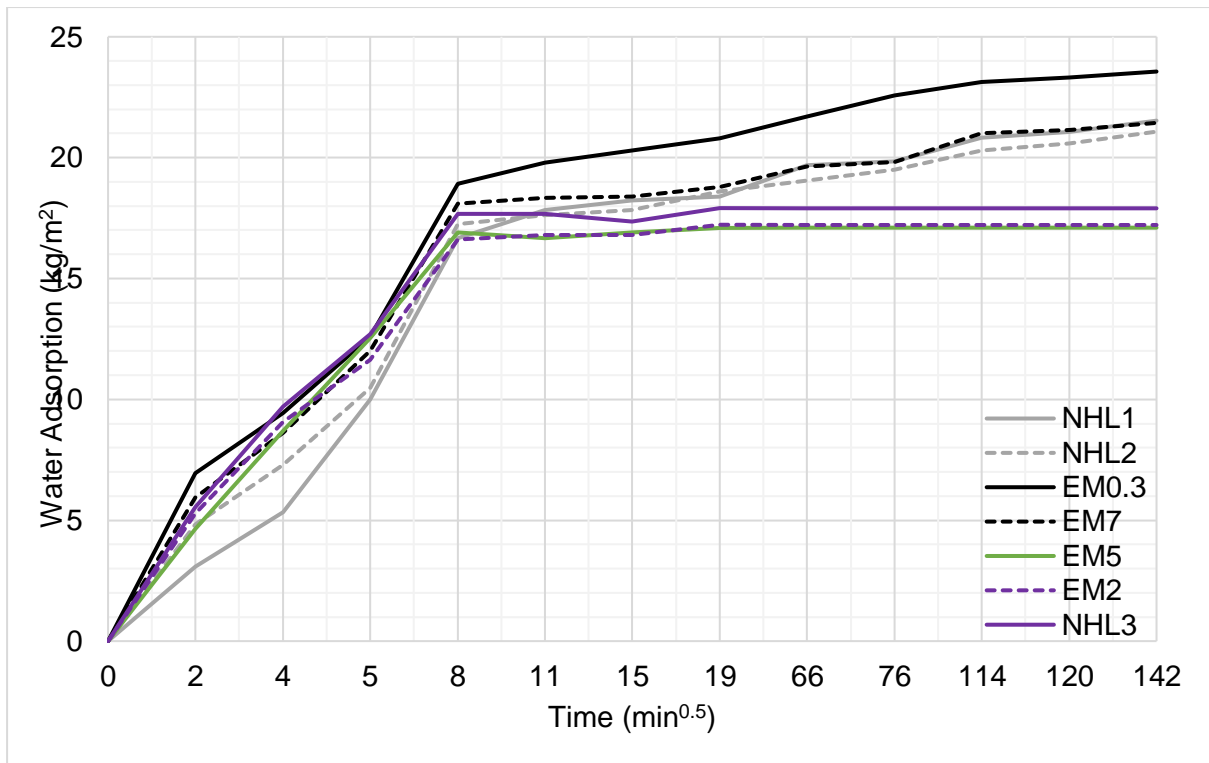


Figure 5.9. Capillary action of mix designs.

Understanding the sorption capabilities of the mortar in both the short and medium term is important to consider so Figure 5.9 should be analysed in two stages. When the mortars are initially added into the water, the initial sorption is high. Within this period, NHL1 has the lowest adsorption but EM0.3 has the largest. When comparing all of the different mix designs, mixes NHL2, NHL3, EM2 and EM7 all have a similar initial adsorption quantities. However, when considering the medium term constant adsorption of water within these samples it is not as clustered in comparison to the initial adsorption. Figure 5.9 demonstrates that EM0.3 has the highest adsorption (23.2kg/m²) whilst EM5 has the lowest (17.1kg/m²).

5.2.6.4. Moisture Buffering Value (MBV)

The utilisation of this experiment helps to understand how in a dynamic hygrothermal environment, the exchange of water vapour within the sample between adsorption and desorption phases. Samples were placed inside a climatic chamber which is shown in Figure 5.10. After stabilising within the climatic chamber, the MBV of samples can be found in Table 5.4. The MBV characteristic is important to understand as when the bio-fibres are added to the mix design, they will enhance the performance. Therefore, it is important at this stage to select the best performing mix designs for further experimentation. Table 5.4 shows that all 7 mix designs have a 'good' classification (Rode et al., 2005) and range from 1.024-1.368 g/(m² ·%RH). The highest MBV is from EM0.3 (1.363 g/(m² ·%RH)) and lowest NHL1 (1.024 g/(m² ·%RH)), this mix design has no earth within the mix design so can be considered a control sample. From the seven mix designs, the top three performing mixes are EM0.3, EM7, and EM2 have the best MBV values.



Figure 5.10. Earth mortar samples within climatic chamber

It is of note that these MBV values are not as high as the literature in Chapter 2. It was also outlined within Chapter 2 that the utilisation of lime as a binder has many benefits. However, as mentioned in section 5.2.6.2., this addressed the structurally associated issues, the use of lime acting as a filler at 28 days will affect MBV. It could be suggested that a reduced carbonation may also contribute to a reduction in MBV but carbonation effect is probably irrelevant during the first 28 days.

Table 5.4. MBV values for initial mix design samples.

Sample ID	Average Moisture Buffering Value (g/(m² · %RH))	NORDTEST Classification (as per (Rode et al., 2005))
NHL1	1.02	Good
NHL2	1.26	Good
EM0.3	1.36	Good
EM7	1.29	Good
EM5	1.12	Good
EM2	1.27	Good
NHL3	1.26	Good

5.2.7. Initial Mix Design Conclusion

Overall, to select the best two performing mix designs, a combination of the analysis for all experiments within this section should be considered. As the panel will be non-load bearing, the low strength values from Figure 5.6 can be accepted. Another main focus of this research project is to contribute to an overall reduction in carbon emissions for residential properties by creating a moisture buffering panel. Therefore, if two materials have a comparably similar performance, a slight compromise of performance offsets a reduction in the embodied energy and costs of using more materials.

Based upon this and their performance throughout the experiments within this preliminary experimentation, NHL2 and EM0.3 have been chosen within this experimentation and have been renumbered in Table 5.5.

Table 5.5. Renumbered Mix Design Proportions

Original Mix ID	New Mix ID	Lime	Earth	Sand	Lime/Water Ratio
NHL2	1	1	0.1	8.6	2.4
EM0.3	2	1	0.3	10.3	2.7

From the preliminary experimentation, an initial 7 mix designs, the best two performing mix designs were selected for further experimentation. To understand their physical and hygrothermal properties, these two mix designs will have best performing bio-fibres from

Chapter 4 incorporate within them. This will be incrementally added within each mortar to meet a fixed consistence value of 150-160mm.

5.3. Further Experimentation of Best Performing Mix Designs

5.3.1. Materials

For these materials, all of the same mix design constituent parts were exactly the same as those outlined in section 5.2.1.

5.3.1.1. Bio-Fibres

Three different types of bio-based materials were used within this chapter (the selection of these bio-fibres was based on the results from investigation to bio-fibres in Chapters 3 and 4) these are: Wool 1 (W1), Wool 2(W2) and Saw Mill Residue (SMR) (images of these bio-fibres are in Figure 5.11). The material properties of these bio-fibres can be found within Table 5.6.



Figure 5.11. (L) SMR (Centre) W1 (R) W2

Table 5.6. Material properties of bio-fibres.

Bio-Fibre	Dry Bulk Density (kg/m ³)
W1	59
W2	72
SMR	173

5.3.2. Methodology

The following methodologies were completed as per the experiment outlined in section 5.2.5.

Consistence

Compressive and Tensile Strength

Capillary Action

Moisture Buffering Value

The following experiments utilised new equipment for this section as outlined below:

5.3.2.1. Surface Morphology and elemental analysis

After 28 days of curing SEM was utilised to explore the surface morphology of samples as outlined in section 5.2.4. Simultaneously, energy dispersive spectrometry (EDX) was also utilised to give a greater insight into the elemental composition of the composites.

5.3.2.2. Dry Bulk Density

Using callipers to an accuracy of 0.01mm dimensional readings were taken of prismatic samples to determine bulk dry density and carried out in line with EN 1015-6 (BSI, 1999c).

5.3.2.3. Open Porosity

As a method of calculating the void space within the sample, open porosity gives an indication of how much water a substance can retain. Circular samples of diameter (40mm) were cast, and the test method was performed as per EN 1936:2006(CEN, 2007).

5.3.2.4. Thermal Conductivity

Assessing a materials' ability to act as an insulator and specific heat capacity was measured using an ISOMET 2114 with a 60mm diameter circular contact probe with a range of 0.04-2.0 W/(m.K) (as per Figure 5.12) within laboratory conditions of approximately 21°C and 54% RH.



Figure 5.12. Thermal conductivity equipment for samples.

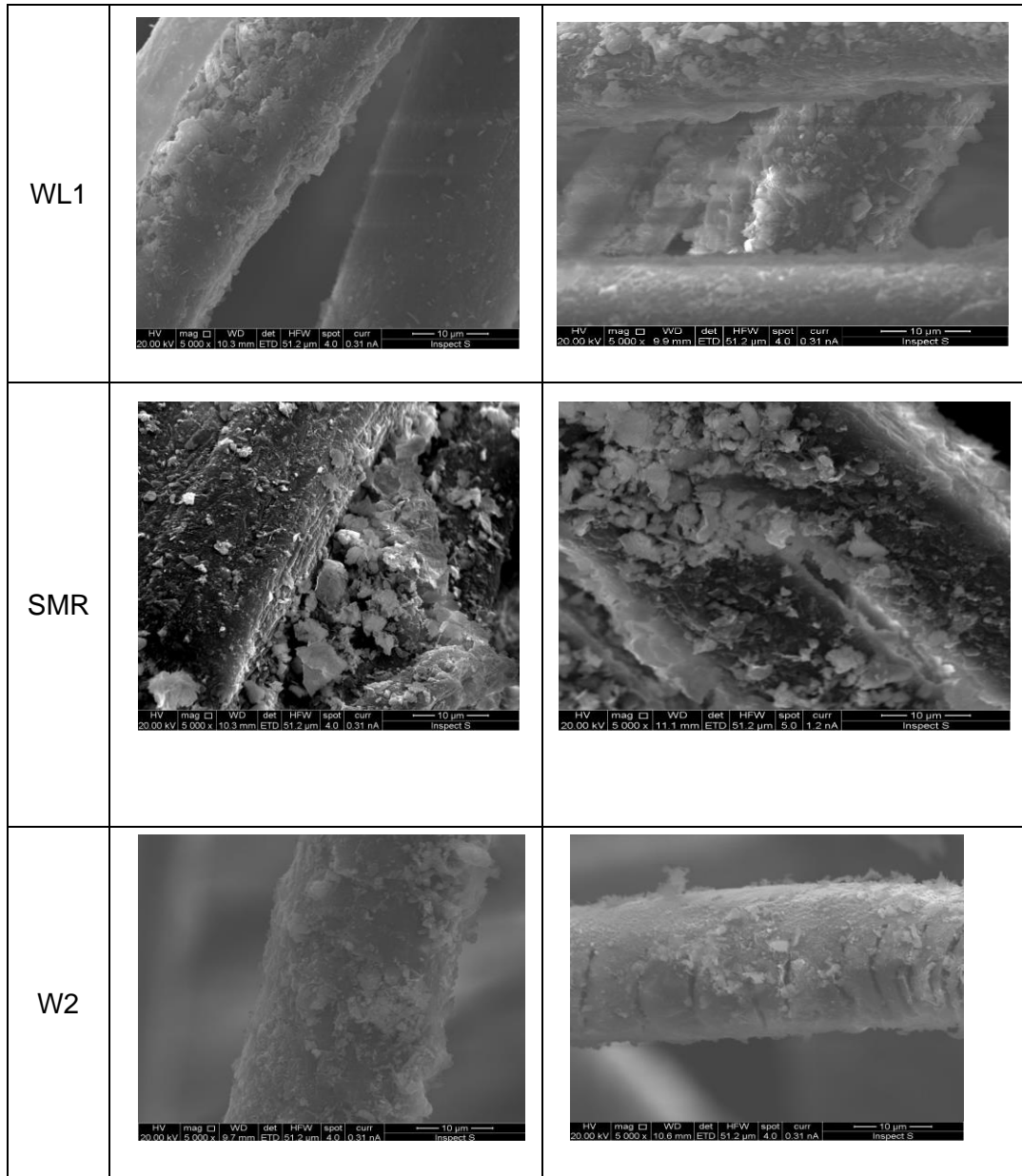
5.4. Results and Discussion

5.4.1. Surface Morphology and elemental analysis

After curing, fractions were taken from prismatic samples before being inspected under SEM and elemental. The images taken from the samples can be found in Table 5.7. Simultaneously, energy dispersive spectrometry was carried out on the samples where the results are demonstrated in Table 5.8.

Table 5.7. SEM Images for mixes 1 and 2.

Bio-Fibre	SEM Image	
	M1	M2
PL		



As outlined within section 3.4.3., the different bio-fibres have unique surface morphologies, particularly as their base constituent materials of cellulose and keratin are so fundamentally different. Table 5.7 demonstrates that within M1 PL there seems to appear lighter coloured/white particles, which have been identified as lime. Comparing this to M2 PL it could potentially be an explanation that M1 PL has had more carbonation, the consequences of this would be enhanced structural and hygrothermal performance. The images of WL 1 for both mix designs demonstrate a multitude of fibres surface morphology, especially in comparison to WL 2. M2 WL 1 shows that there is generally a better surface cohesion of the earth mortar matrix to the fibres than M1 WL1. When evaluating WL2 for both mix designs, the mortar matrix is much more similar than that of WL 1.

Table 5.8. Elemental composition of the composites.

Sample ID		Element Percentage (%)							
		O	Mg	Al	Si	K	Ca	Fe	S
1	PL	72.26	0.59	3.06	16.18	1.98	5.52	0.41	-
	W1	82.27	-	1.55	10.25	0.35	5.08	0.5	-
	SMR	90.22	0.97	1.21	2.33	0.21	4.75	0.31	-
	W2	82.81	1.38	1.15	4.97	0.37	7.54	0.48	1.29
2	PL	70.49	0.94	3.07	20.9	0.72	3.18	0.8	-
	W1	80.86	-	1.46	3.53	0.76	10.91	0.91	1.58
	SMR	87.03	1.3	1.6	3.67	1.06	4.39	0.95	-
	W2	87.97	0.9	1.52	4.27	0.53	4.81	-	-

5.3.2. Consistence

As mentioned in section 5.2.2.1. the initial consistence without any bio-fibres was 180-190mm however from the literature in Chapter 2 to have a good workability, with bio-fibres the mortar should have a spread value of 150-160mm. Due to the varying hygroscopicity of bio-fibres (as explored in McGregor et al. (2016)) despite having the same basic mix design, differing bio-fibres required differing percentages to have the same flow table value. Building on the initial consistency values from section 5.2.5.1, fibres were incrementally added into the mix design until the consistence value was achieved. The results for this can be found in Table 5.9. When incorporating the bio-fibres into the mix designs it was initially particularly difficult to disperse the fibres evenly and consistently – especially with the wool based materials having such long and thin fibres. To ensure that these were dispersed as evenly as possible throughout the wet mix all fibres were pulled apart from another to reduce agglomeration. Before mixing, all dry ingredients were initially combined before adding any water to ensure that the bio-fibres were distributed throughout the mortar.

Table 5.9. Consistence values of mix designs.

Mix Design ID	Quantity of Water Added (ml)	Quantity of bio-fibres added (by mass of dry ingredients) (%)	Quantity of bio-fibre added (g)	Consistence (mm)		
				D1	D2	Average
1	PL	0	0	180	182	181
	W1	0.5	4.85	149	154	152
	W2	0.5	4.85	149	153	151
	SMR	1	9.7	149	152	151
2	PL	0	0	179	183	181
	W1	0.25	5.8	148	151	150
	W2	0.5	5.8	151	150	151
	SMR	0.5	11.6	154	151	153

Utilising this quantity of bio-fibres, the final mix design quantities each mix can be found in Table 5.10.

Table 5.10. Mix design quantities (by weight).

Mix Design ID	Lime	Earth	Sand	Lime/Water	Bio-fibres	
					Sample ID	Lime/Biofibre
1	1	0.1	8.6	2.4	PL	-
					W1	0.0243
					W2	0.0485
					SMR	0.0243
2	1	0.3	10.3	2.7	PL	-
					W1	0.0145
					W2	0.029
					SMR	0.029

5.4.3. Dry Bulk Density

The dry bulk density results for both mix designs are demonstrated within Figure 5.13. For M1 dry bulk density values range from 14010 – 1707 kg/m³ and 1575-1615 kg/m³ for MD2. By utilising the dimensional characteristics of each sample, it is clear from Figure 5.13 that the addition of bio-fibres reduces the dry bulk density for all samples from both mix designs. This is due to the fibres having a lower density than the PL mortar, which would usually occupy the same space as the fibres - these findings are in line with experimentation by Gomes, Faria and Gonçalves (2018). M1 SMR has the lowest overall density (1409.747 kg/m³) and is therefore the most lightweight and by comparison to M1 PL, a 17.44% reduction in dry bulk density. In contrast to earlier findings for M1, although M2 demonstrates a drop in dry bulk

density it is not as extreme. Despite the addition of bio-fibres, for M2 dry bulk density remains relatively similar.

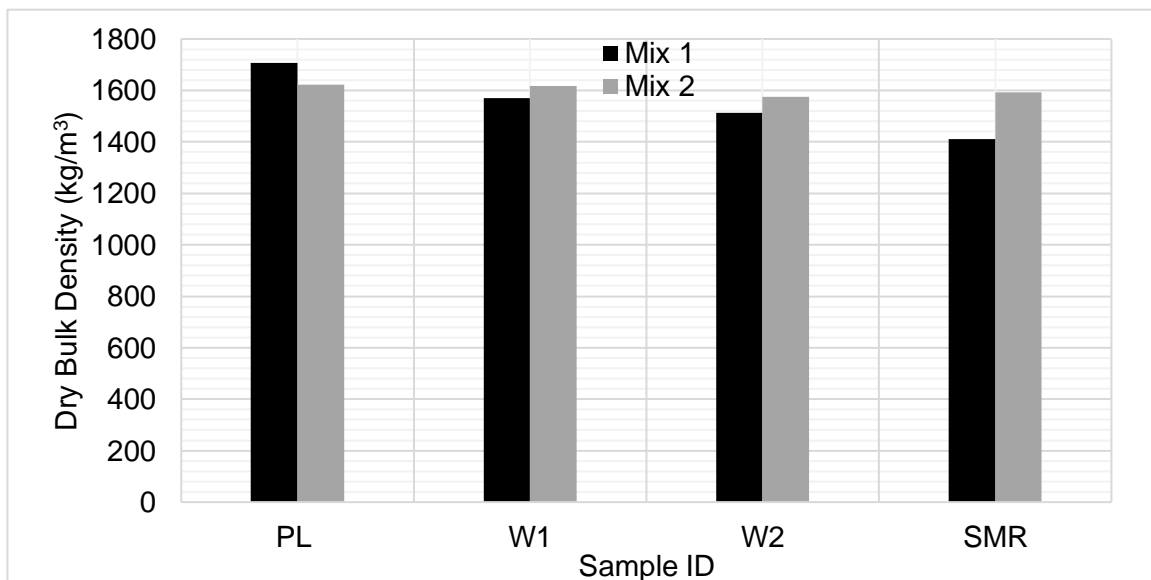


Figure 5.13. Dry Bulk Density of earth mortar samples.

5.4.4. Compressive and Tensile Strength

Data in Figure 5.14 presents the compressive and tensile strength values for the bio-earth mortar composites. With the exception of M2 W1, all samples with bio-fibres across both earth mortars performed better than that of their respective plain mix. Comparing both mix designs, M1 performed better and had greater compressive and tensile strength values than that of their M2 counterparts. The mix design with the highest compressive strength value was M1 W2 (0.517 MPa) and M1 SMR (0.507 MPa). By comparison, the addition of W2 fibres to M1 compared to M1 PL increases compressive strength by 79.31%. In terms of tensile strength, M2 W2 has the highest value (0.400 MPa) but this value is also higher than its compressive strength (0.330 MPa). This could be associated with wool fibres being able to resist tensile forces by being able to disperse the loading through the fibres before deformation (by comparison to the PL mix). However, the initial swelling of fibres due to water in the mix design and consequential drying has left air voids and reduces compressive strength.

For all other mix designs, the resulting compressive and tensile strength due to addition of fibres to the matrix is evidence that this interaction promotes 'toughness' within the sample. Despite an improvement in general strength, it is evident from Figure 5.14 that the values of these structural tests are not particularly high and would limit the dimensions of this hygrothermal buffering panel however as it is intended for it to be an indoor, non-structural panel a high strength capability is not a limiting factor of this design. In addition, the flexural results presented within Figure 5.14 are only slightly lower than that of the results demonstrated within (Grilo et al., 2014).

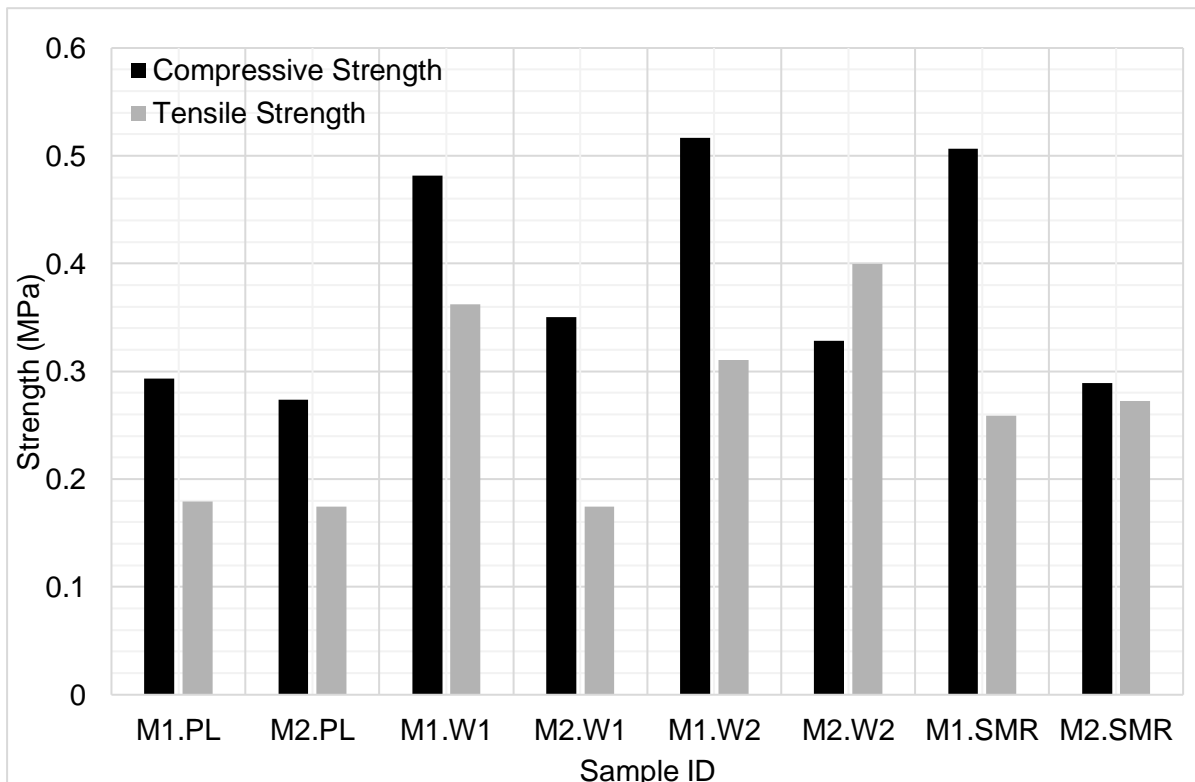


Figure 5.14. Compressive and tensile strength of all mix designs.

There are also several different factors that could be affecting the structural strength of these samples. One could be that as there being natural hydraulic lime included into the mix design and the testing date of the samples is only 28 days, the lime may only be acting as a filler. It could be understood that the strength indicated within Figure 5.14 may not be the mix designs fully realised strength capacity. With prolonged exposure and a sufficient length of time for carbonation to occur in air drying conditions, it is hypothesised that these mix designs will all experience higher compressive and tensile strength values.

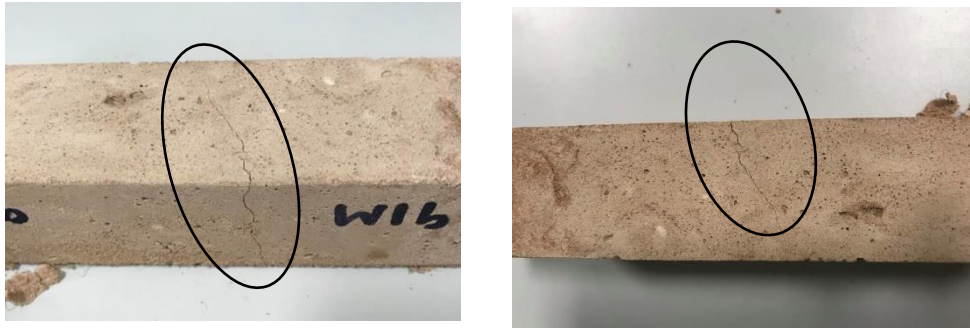


Figure 5.15. Samples after tensile strength testing, hair line fractures circled.

After each tensile strength test was completed and failure had been achieved within the sample, upon visual inspection there was only a hairline crack of the prisms. An image of this is demonstrated within Figure 5.15. Due to the incorporation of the bio-fibres within the mix, samples were held together by the bio-fibres and therefore these fibres would act as a hinge between them. As explored in Raj et al. (2017) when bio-fibres are included in the mix, during the tensile flexural strength testing there are 2 key points of failure. Firstly, it is that of the mortar but then secondly the bio-fibres “reinforce” the mortar to create a secondary failure point. Another limitation of utilising bio-fibres is controlling the dispersion of fibres throughout the matrix. As bio-fibres have hygroscopic characteristics, they are prone to forming agglomerates during mixing, making the uniformity of mixtures difficult (John and D. Anandjiwala, 2008).

5.4.5. Open Porosity

As a measure of the ratio of the quantity of open spaces which have the ability to be filled with a fluid within a materials microstructure to the whole volume of the sample, open porosity gives an indication of the earth based construction durability and resistance to deform. The results for open porosity can be found within Figure 5.16. Except for M1 PL compared to M1 W1, the addition of fibres increase porosity in all samples.

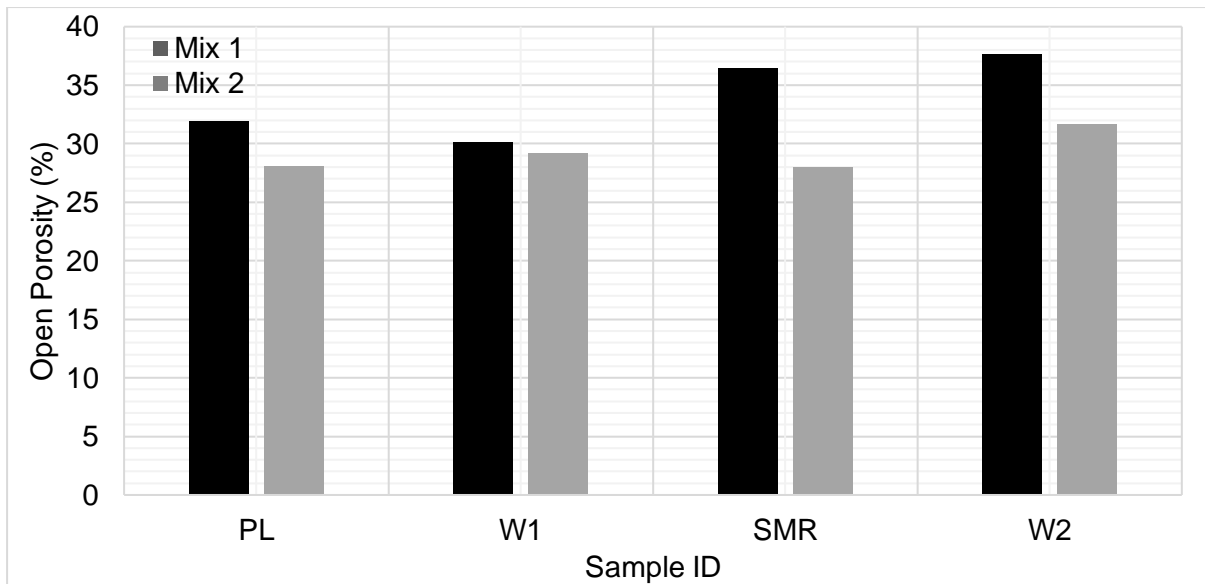


Figure 5.16. Open porosity for samples.

As previously mentioned, the incorporation of lime into both mix designs and the cure time for these samples being only 28 days dictates that the lime is currently acting as a filler rather than a key structural element of the mix. As the carbonation process is yet to occur within the mix, it has been evidenced the effect of carbonation on cement based mortars lowers the open porosity, this has been explored in Lawrence et al. (2007) and this process will also occur in earth based mortars. As a consequence of this, the open porosity values outlined in Figure 5.16 may reduce after a longer cure length where carbonation has taken place.

As porosity increases dry bulk density tends to decrease. Demonstrated within Figure 5.17, it is evident that dry bulk density has a moderately inversely proportional relationship (where Pearson Correlation Coefficient (PCC) $r = -0.65$) with open porosity. This relationship between porosity and dry bulk density and other material characteristics follows other research as explored in Bouguerra et al. (1998) and Laborel-Préneron et al. (2016).

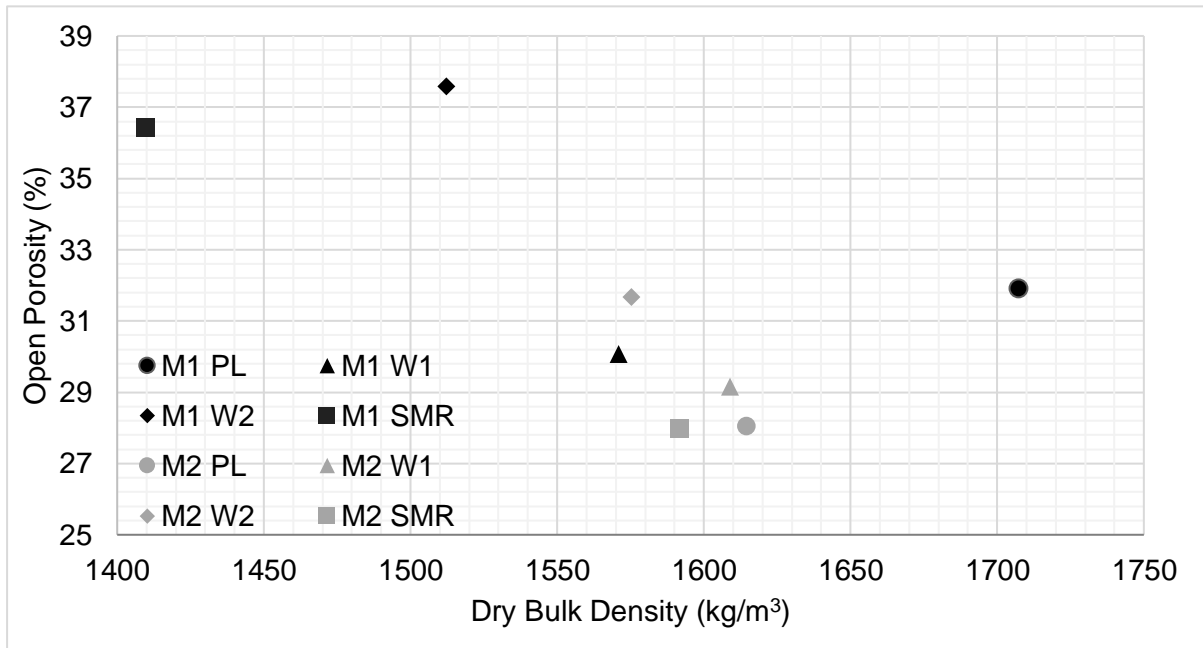


Figure 5.17. Relationship between open porosity and dry bulk density for samples.

Understanding Figure 5.17 enables the establishment of a relationship between bulk density and open porosity due to incorporation of bio-fibres within the mix design and the resulting microstructure of the mortar. Figure 5.18 forms a relationship between compressive strength and open porosity. As outlined within section 2.8.3., when a bio-fibre is incorporated into a mix design this reduces the homogeneity of the samples microstructure. When initially mixed, fibres swell due to the free water within the mix design and during curing as this free water dries, the fibre shrinks and a void is created. These air voids create cavities within the matrix, reducing the compressive strength. However, Figure 5.18 shows that an increase of porosity does not necessarily decreases the compressive strength (it is detected a strong positive correlation where for PCC, the value of R is 0.78). A potential explanation for this could be that by comparison to the fibres explored within the literature, the interfacial bonding between the matrix and fibres are enhanced. This is particularly prevalent in Figure 5.18 for M1 W2 and M1 SMR.

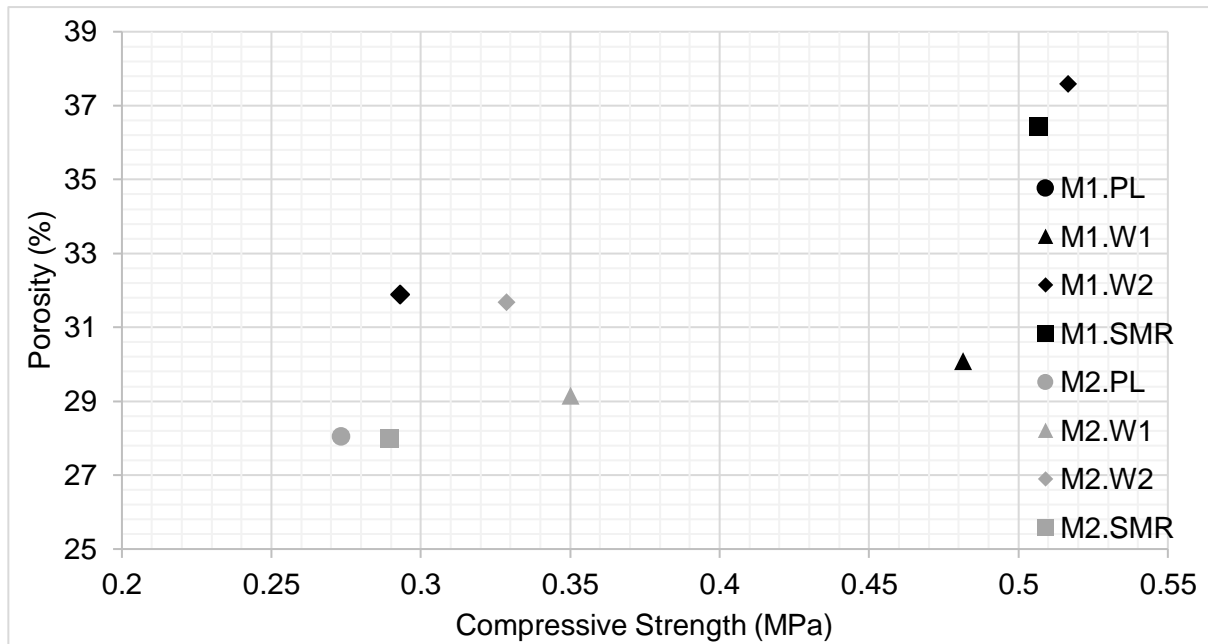


Figure 5.18. Relationship between porosity and compressive strength of samples.

5.4.6. Capillary Action

A key disadvantage of using earth based construction is its high deformation with exposure to water (as highlighted in Table 2.1). Figure 5.19 demonstrates the capillary action curve for all samples. During the initial absorption, water is rapidly absorbed which understood to be due to the control of capillary pores (Neithalath, 2006). As the water travels through the capillary pores, the rapid adsorption ends and water rises through to the top of capillary pores and water absorption is constant. During this phase, water transitions out of the capillary pores and into the gel pores due to diffusion (Zhao et al., 2014 and Yang, 2019).

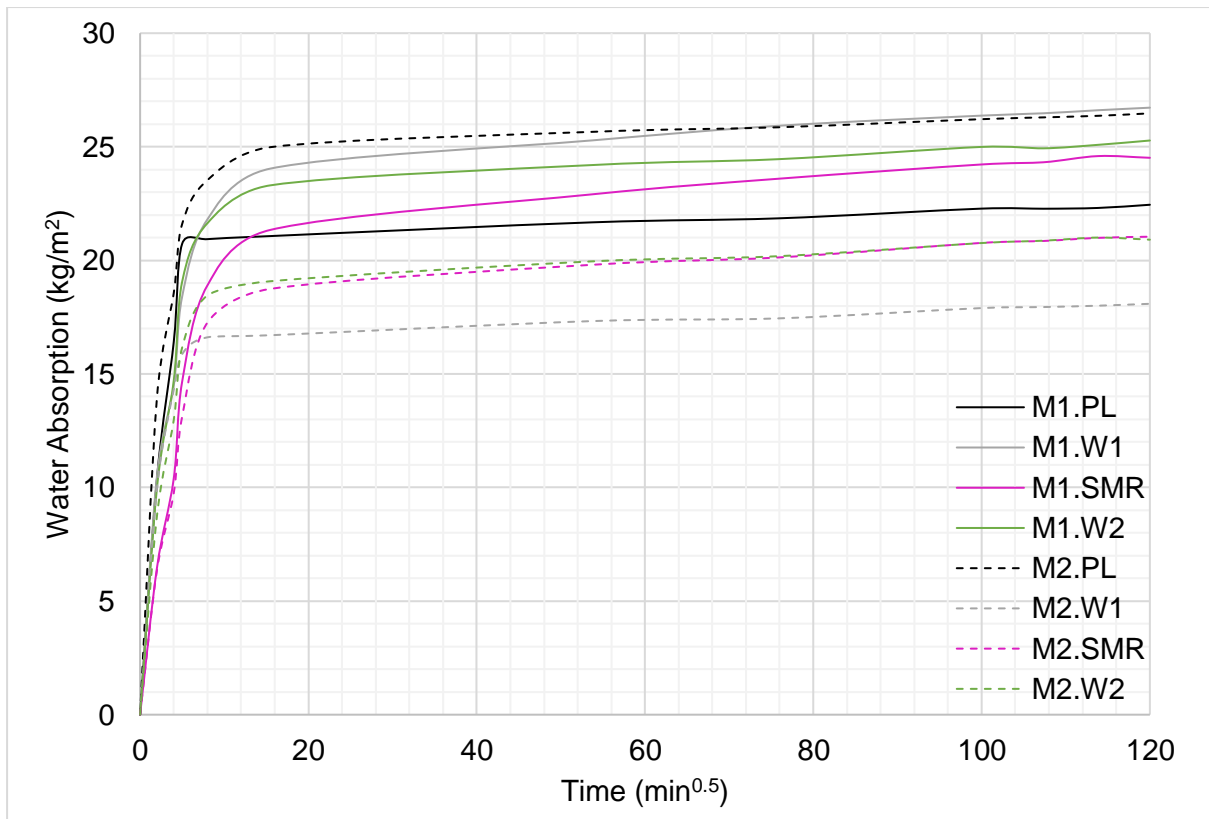


Figure 5.19. Capillary action curve for earth mortar samples.

From Figure 5.19, the capillary coefficient can be calculated, outlining (as a function of time) how far the water travels/is up taken within the sample results, this can be found in Table 5.11. This is derived by investigating the gradient of the initial rapid absorption phase for each sample. From this Table 5.11 it can be shown that for M1, SMR ($2.376 \text{ m/s}^{0.5}$) had the lowest capillary coefficient but PL, W1 and W2 all have a very similar values ($2.646, 2.654$ and $2.638 \text{ m/s}^{0.5}$ retrospectively). By comparison, M2 has a much greater range of values. M2 PL has a substantially larger capillary coefficient value ($2.809 \text{ m/s}^{0.5}$) than the other bio-fibres within the same mix design as seen in Table 5.11.

As the aim of this research project is to create a panel which will remain indoors, the low durability of earthen construction, the long-term adsorption and its effect on service life must be considered. Concerning a mix design with bio-fibres, for Mix 1, SMR had the lowest initial water adsorption and sustained water adsorption within the plateau region. For Mix 2, W1, had the smallest initial and constant water adsorption (plateau region). All M1 samples have a greater initial and sustained water adsorption in comparison to M2. This demonstrates that in terms of initial and sustained water adsorption, M1 W1 has the most preferable characteristics. By comparison to the investigation by Santarelli et al. (2014) these values are significantly

lower however due to the other mechanical properties demonstrate a higher performing mortar mix.

Table 5.11. Capillary coefficient for mix designs.

Sample ID		Capillary coefficient (m/s ^{0.5})
Mix 1	PL	2.646
	W1	2.654
	SMR	2.376
	W2	2.638
Mix 2	PL	2.809
	W1	2.006
	SMR	2.140
	W2	2.277

5.4.7. MBV

To evaluate the hygrothermal behaviour of these mix designs, MBV was selected as an appropriate way to understand the samples effectiveness for exchanging water molecules for 22 cycles of 24 hours. Samples were placed horizontally within a climatic chamber as per Figure 5.20.



Figure 5.20. Samples within climatic chamber.

The MBV for each cycle was calculated and is displayed within Figure 5.21. It is evident that initially all samples have a fluctuating MBV especially when comparing M1 and M2. MBV measurements were all taken manually and due to accessibility to the climatic chamber over weekends, some cycles have been omitted from Figure 5.21. This figure also demonstrates

an MBV fluctuation over all the cycles that the water transport within each sample varies. The stabilised MBV values for the mix designs can be found in Table 5.12.

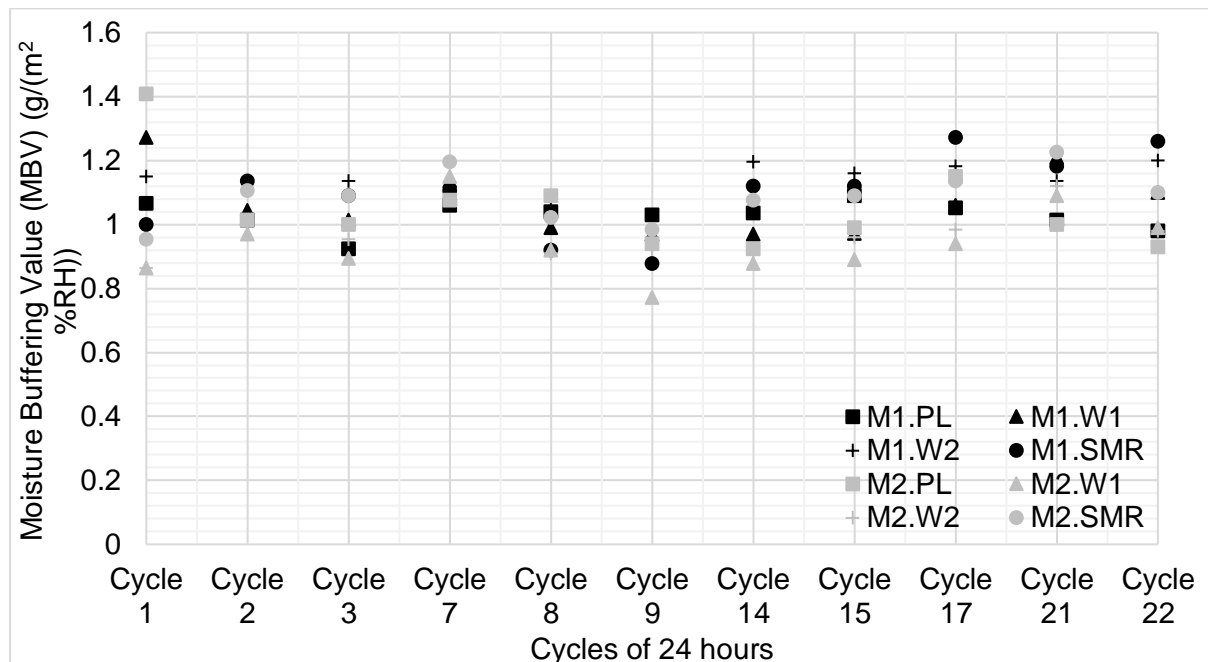


Figure 5.21. Average MBV per cycle for each mix design

Table 5.12. Stabilised Average MBV for samples.

Sample ID		MBVave (g/(m ² %RH))
Mix 1	PL	0.98
	W1	1.10
	SMR	1.26
	W2	1.21
Mix 2	PL	0.93
	W1	0.99
	SMR	1.10
	W2	1.01

By comparison to the MBV results from Chapter 3 when encapsulated within an earth mortar, MBV values are lower than those of just the plain bio-fibre samples. After 22 cycles all the mix designs were classified via the NORDTEST protocol within Figure 5.22. Another factor that could affect the MBV values is that pore accessibility can be limited due to the crystal growth within the carbonation of the lime (McGregor et al., 2014). The resulting consequence of this

would be the potential to affect the rate of moisture adsorption. However, the samples with the best MBV after 22 cycles was M1 SMR and M1 W2.

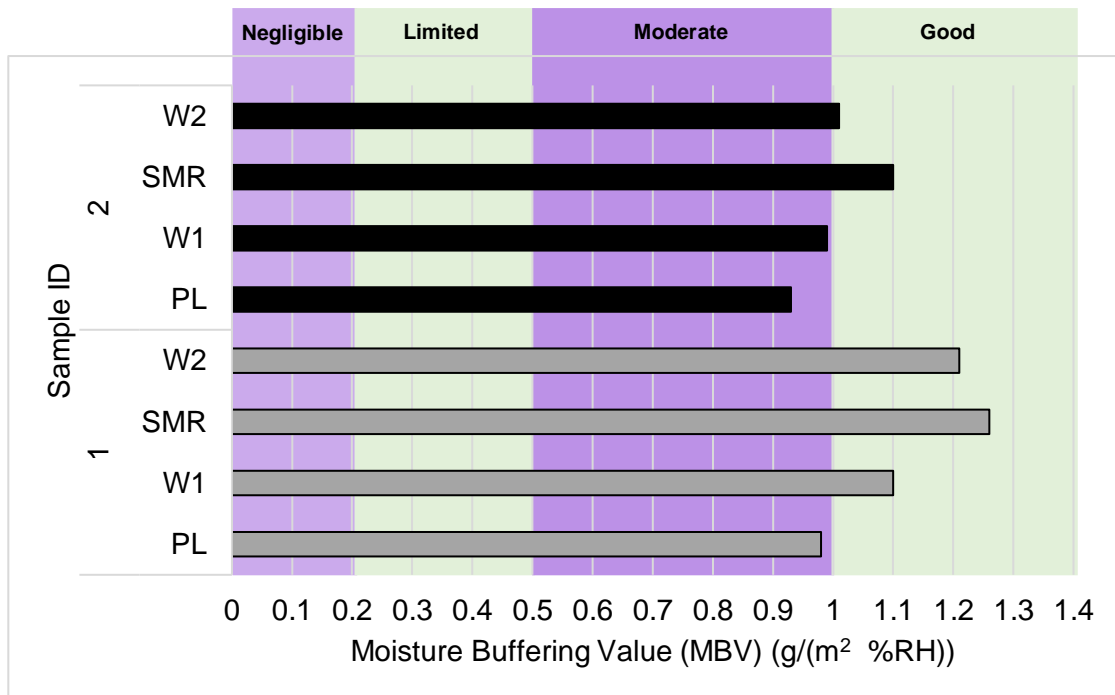


Figure 5.22. MBV classification of samples according to (Rode et al., 2005).

When considering Table 5.12, there is a variation in the stabilised MBV of the samples which could be explained due to there being a smaller amount of water within mix design that after 28 days of curing has still not fully evaporated. Another explanation for the rationale of the materials behaviour would be that due to there being less ‘bonded’ water within the mix design. Further to this, the densities for M2 (as side from M2 PL) are higher than that of its M1 counterpart. Therefore, the fibres will have swelled a lot less and therefore the ‘gap’ between the interfacial bonding site will be smaller by comparison to M1 which has a lot more water within the mix.

Although the stabilised MBV has been analysed, as outlined in section 3.4.2 the MBV itself is not enough of a differentiation between samples that have similar or the same MBV. Therefore, by having the same exposed surface area within the sample, the mass change graph per m² can be utilised to demonstrate the mass variation for each cycle. The mass change graph for cycle 1, 14,15 and 22 (respectively) are presented within Figures 5.23 to 5.26. Initially, Figure 5.23 demonstrates that adsorption and desorption is continuous over the first cycle, with peak adsorption values all being at the end of the adsorption phase where M1 W2 had the largest increase in mass (and therefore held the biggest quantity of water) (22.67g/m²).

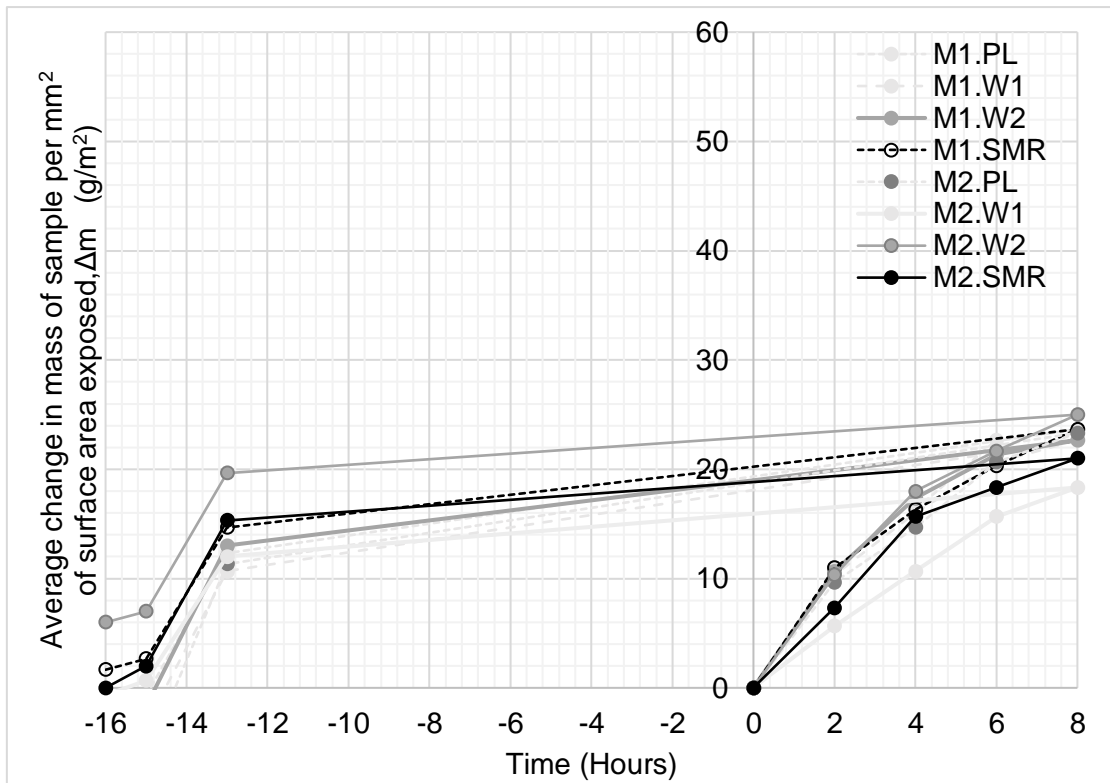


Figure 5.23. Adsorption/Desorption graph for all earth mortar samples after 1, 24 hour cycle.

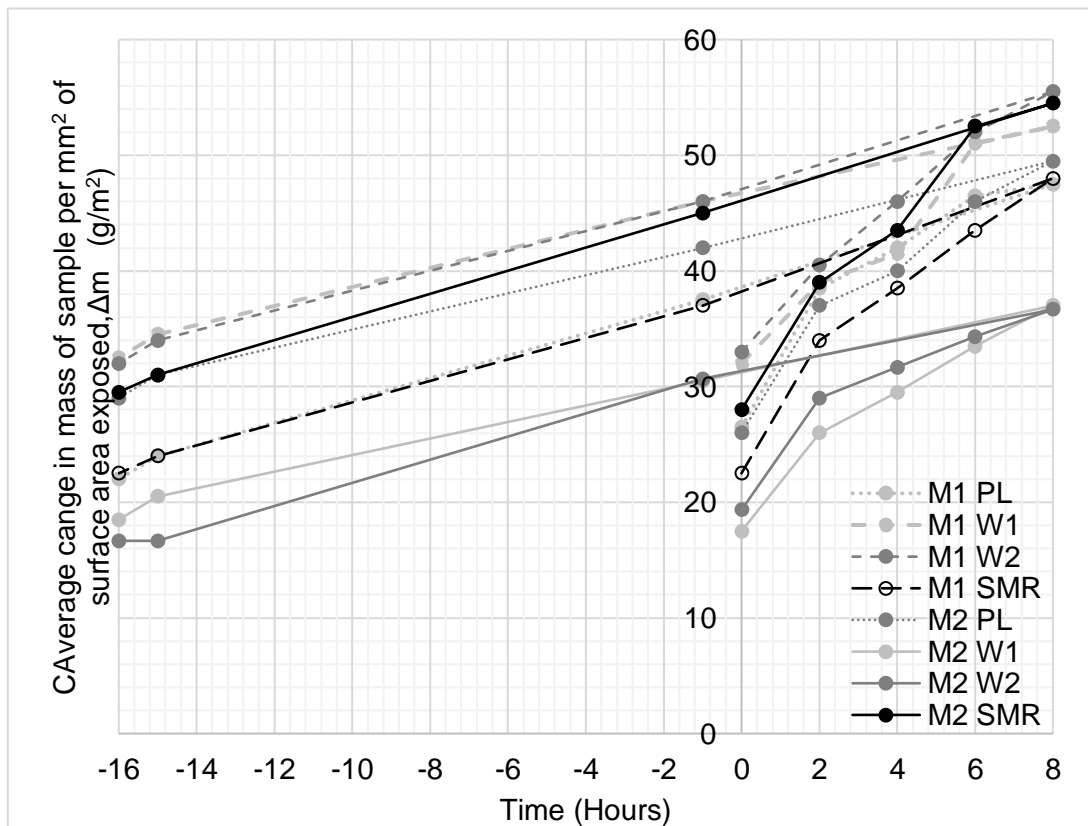


Figure 5.24. Adsorption/Desorption graph for all earth mortar samples after 14, 24 hour cycles.

After 14, 24 hour cycles it is evident that all mix designs have not remained at their original mass. All samples have increased in mass, this is sufficient evidence to suggest that as the samples have adsorbed in high RH, they are unable to desorb the same quantity of water in low RH periods. This water has become ‘trapped’ and is retained within the sample, an efficient exchange of water molecules within the sample is integral for this panel to function as a RH regulator.

Despite this behaviour of ‘trapping’ water molecules, Figure 5.24 also demonstrates all samples are still able to adsorb and desorb via clear increases in mass within 8 hours of adsorption and high RH (75%) and then lose mass during 16 hours of desorption and low RH (53%). Whilst the samples examined are still hygrothermally functional, the efficiency at which the water molecules are exchanged has reduced. Figure 5.24 shows that samples such as M1 SMR and M2 SMR can adsorb water at a much higher rate in comparison to the other samples. It is evident that M1 SMR has progressively increased in mass over the length of the experiment thus far but is able to return to the approximate same mass as at the beginning of the cycle. M2 W2 demonstrates that at the end of cycle it is beginning to lose mass in doing this demonstrates that the water molecules ‘trapped’ within the sample are now dissolving the fibres and the sample is now beginning to decompose.

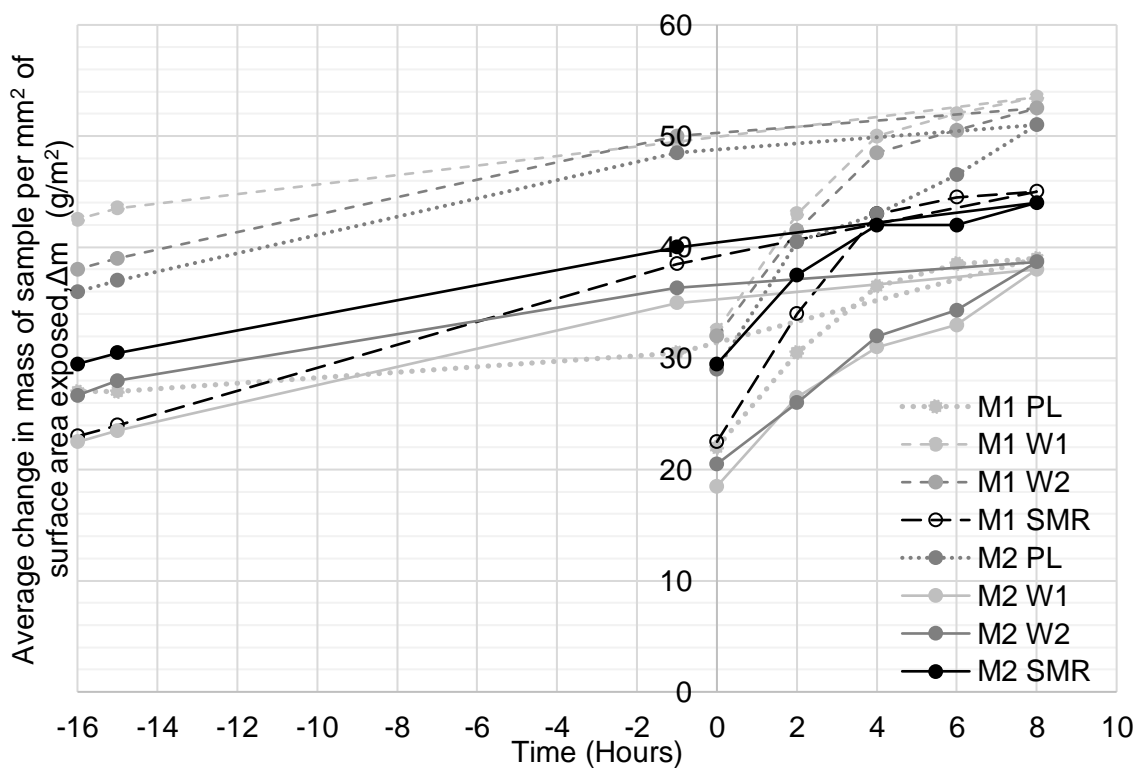


Figure 5.25. Adsorption/Desorption graph for all earth mortar samples after 15, 24 hour cycles.

Similar to Figure 5.24, Figure 5.25 demonstrates the vast range of the changes in mass throughout the 15th cycle of 24 hours. When comparing M1 W1 to M1 W2 there is initially a high adsorption level, however during the desorption phase the samples are not able to sufficiently lose the water molecules they originally gained. Much like that of Figure 5.24, Figure 5.25 shows that M1 SMR has a clear high adsorption and are able to desorb to the approximate same mass as the start of the cycle. When comparing M1 PL and M2 PL it is evident that both samples are able to initially adsorb but during desorption phase M1 PL is able to reduce to its original mass but has a much lower original adsorption.

When considering the evolution and change in mass of the samples from the first cycle (Figure 5.23) to the final, 22nd cycle (Figure 5.26) the mass adsorbed over a 24 hour period has increased. Further to this, it is clear that there is a substantial amount of ‘trapped’ water molecules within the sample that from the previous cycle the initial gain in mass is above 0. Further to this, the rate at desorption after 8 hours decreases after 22 cycles, demonstrating the reduction in the capacity for a effective moisture exchange mechanism.

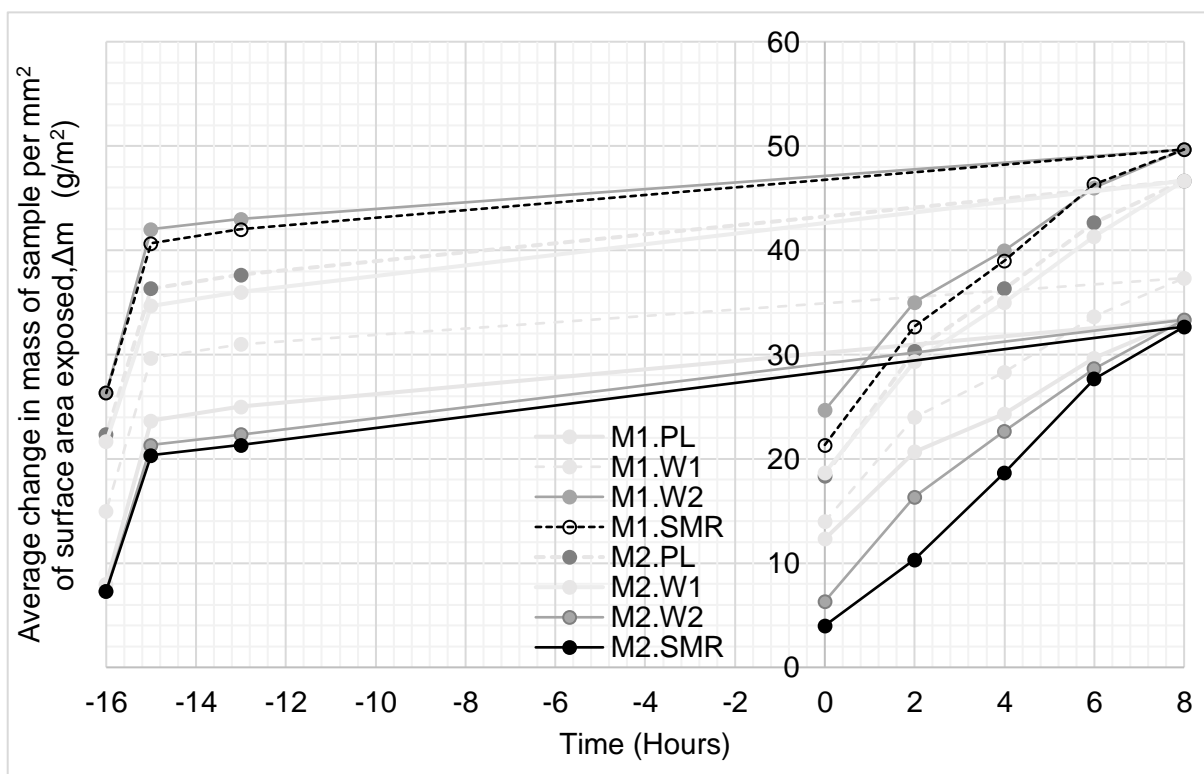


Figure 5.26. Adsorption/Desorption graph for all earth mortar samples after 22, 24 hour cycles.

5.4.8. Thermal Conductivity

Understanding the way heat is exchanged within the sample is important as thermal conductivity investigates the conduction of heat. At laboratory conditions, the thermal conductivity of samples is demonstrated within Table 5.13.

Table 5.13. Thermal Conductivity values for samples.

Sample ID		Thermal Conductivity, λ (W/(m.K))
Mix 1	PL	0.203
	W1	0.183
	SMR	0.179
	W2	0.189
Mix 2	PL	0.203
	W1	0.191
	SMR	0.189
	W2	0.192

From Table 5.13 the range of thermal conductivity is from 0.1786 to 0.2026 W/m.K. Where M1.SMR has the lowest reading (0.1786 W/m.K) and M2 PL has the largest thermal conductivity but M1 PL is negligibly similar (0.2026 and 0.2025 W/m.K respectively). The literature within Chapter 2 has evidenced that there is a clear relationship with the addition of fibres to an earth matrix which results in a reduction in thermal conductivity. This is because the fibre within the earth mortar matrix has a lower thermal conductivity value than if it was just the mortar itself.

As highlighted within Chapter 3, section 3.4.3. and within the literature of Chapter 2 there is a relationship between density and thermal conductivity. This is due to the air voids within a matrix having a lower density than if they were filled with the material, which lowers the thermal conductivity as heat cannot travel as easily through it. For the bio-fibre earth mortar composites this has been explored by comparing dry bulk density and thermal conductivity within Figure 5.27. It is clear from Figure 5.27 that there is a very strong correlation (PCC, R = 0.91) between the dry bulk density and thermal conductivity for samples within this research.

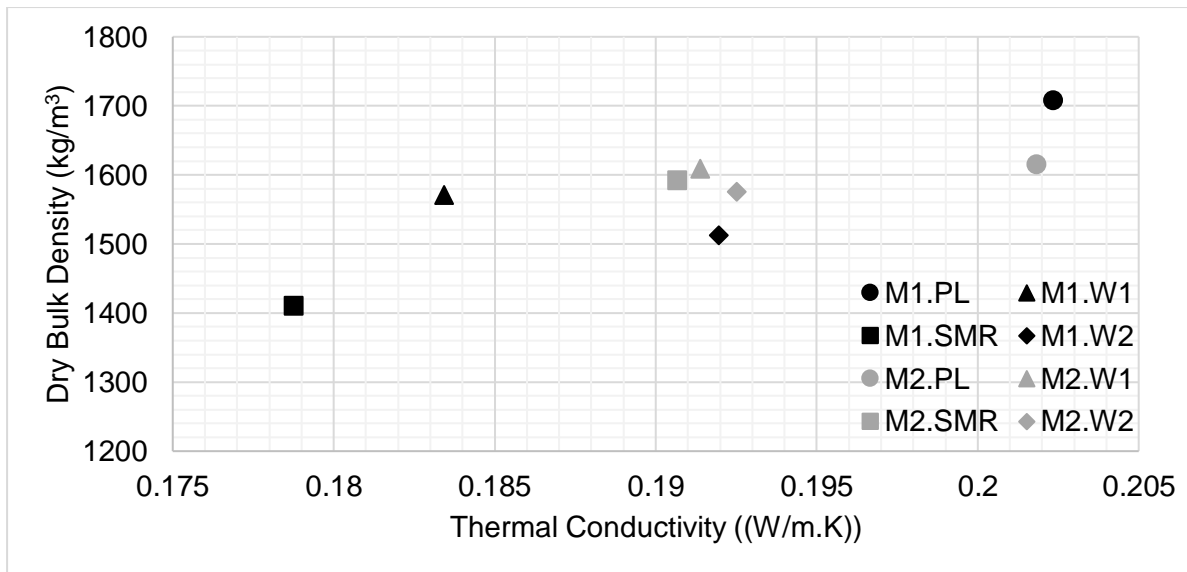


Figure 5.27. Relationship between dry bulk density and thermal conductivity of samples.

By investigating the composites thermal conductivity, the thermal resistivity can also be easily calculated. The r value of a material demonstrates the resistance of the sample to all types of heat flow and is calculated as per equation (5.2).

$$\text{Thermal Resistivity, } R = \frac{l}{\lambda} \quad (5.2)$$

Where:

R = Resistivity of element, 'r value' ($\text{m}^2.\text{K}/\text{W}$)

l = thickness of material (m)

λ = thermal conductivity ($\text{W}/\text{m}.\text{K}$)

Further to this, the r value (thermal resistivity) can also be used to calculate 'u-values' of these samples, when used in the BRE exemplar houses in the LJMU campus.

Table 5.14. Calculated r for samples.

Sample ID		R value, m ² .K/W (at 0.035m thickness of samples)
Mix 1	PL	0.173
	W1	0.191
	SMR	0.196
	W2	0.182
Mix 2	PL	0.173
	W1	0.183
	SMR	0.184
	W2	0.182

5.5. Conclusion

The optimisation of both mix design and different bio-fibres executed within this paper will enable the next step towards an indoor, passive RH regulating panel to be brought to fruition. Capillary action demonstrates that M1 has a larger capillary coefficient values, however in terms of plateau regions, M1 generally has the larger water absorption. Bulk density is reduced by approximately 30% by comparison to M1 PL mix and due to the relationship between open porosity and dry bulk density as demonstrated within this chapter M1 SMR has the most desirable features. With the lowest thermal conductivity, M1 SMR (0.1786 W/m.K) was also able to remain hygrothermally effective after over 22, 24 hour cycles by comparison to the other mix designs. M1 SMR had the best MBV value (1.26 g/(m² %RH)) this mix design will be selected as the best performing to continue with the creation of the RH buffering panel.

Chapter 6 - Physicochemical characterisation of bio-earth mortar composites to explain their hygrothermal behaviour

6.1. Introduction

Chapter 4 demonstrated that according to the RH of bio-based fibres samples, their chemical properties change which was investigated by comparing to their MBV performance. Following this, Chapter 5 demonstrated that when comparing the performance of these bio-fibres combined within an earth mortar matrix this also alters their physical and hygrothermal properties differ. Out of the mix designs investigated, Mix 1 had most desirable characteristics. To incorporate the works of Chapter 4 and 5, this chapter will investigate the physicochemical effects of these bio-earth mortar composites, in order to provide a greater insight into their chemical and hygrothermal characteristics.

This analysis is required due to the inadequate research attention that has been given to the influence of earth and bio-fibres at a micro level to the thermal performance of mortars. There is limited knowledge on the thermal degradation of mortars, where the majority of the situations tested are related to the behaviour of ancient mortars (Ramacciotti et al., 2018). Thermal analysis are well established methods of investigation. However, there is still no official standard or regulation for this methodology in this specific context.

More broadly, the thermal effects of a material are due to the re-distribution of internal energy within a system. Understanding the thermal response will minimise the knowledge gap and ensure that the thermal behaviour of these materials will effectively contribute to the hygrothermal optimisation of these composites. Therefore, it is appropriate to ascertain some certainty for temperature-dependent behaviour of these earth mortar composites over differing service life temperatures and beyond. The physicochemical characteristics of Mix 1 (the best performing mix design) earth mortar, must be explored to understand the difference in these composites at different RH, the nature of adhesive bonds and how this affects their hygrothermal behaviour.

6.2. Materials

The mix design and bio-fibres used within this chapter are those outlined in Mix Design 1 within Chapter 5 and tested after 28 days of curing. Due to the nature of the testing equipment, prismatic samples (160mm x 40mm x 40mm) would have been too large for the machinery,

consequently samples were crushed and ground. For these experiments, the results are based on fine fractions of the mortar upon grinding. Understandably, grinding the composite mortars may affect the material properties and may not be truly accurate of the results. However, the results shown will give a representative indication of the material characteristics.

6.3. Methods

The following methodologies were completed as per the experiment outlined in 5.3.

Fourier Transform Infrared Spectroscopy (FTIR)

The following experiments have different procedures as outlined below:

6.3.1. Thermogravimetry Analysis (TGA) and Derivative Thermogravimetry (DTG)

Despite having the same linear heating rate as within section 4.3.2. (20°C min⁻¹ under a Nitrogen atmosphere, using a circular, platinum crucible), the heating range is from 25-700°C. This increase in range is to incorporate the difference in material properties of the composite in comparison to the raw bio-based fibre.

6.3.2. Differential Scanning Calorimetry (DSC)

The same equipment and heating rate were used as within section 4.3.3 (25 to 300°C and heating conditions of 20°C/min) a comparison of the effect RH has on the earth mortars material properties. Whilst still using the Perkin Elmer DSC 7, specific heat capacity (C_p) was also calculated at a range of 5-50°C and at a heating rate of 3°C min⁻¹. This range of temperatures was selected as this is what the material would experience throughout its service life and help to give a much broader understanding of the materials performance within dynamic working conditions. This compares to standard testing of specific heat capacity at a static temperature, usually in laboratory conditions.

Samples were initially dried as per BS EN ISO 12570 (ISO, 2000), then stabilised at 53% for 24 hours in a climatic chamber at 23°C. After this test run was complete, the samples were dried then stabilised at 75% for 24 hours at the same isothermal conditions for testing (conditions as per Huang et al. (2016)). The specific heat capacity of bio-earth mortar composites (c_p^{sp}) (kJ.kg⁻¹.K⁻¹) was calculated as per ISO 11357-4 (ISO, 2014), using α -alumina (synthetic sapphire) as a known, standardised material using Equation 6.1.

$$c_p^{sp} = c_p^{cal} \times \frac{m^{cal}(P_{specimen\ run} - P_{blank\ run})}{m^{sp}(P_{calibration\ run} - P_{blank\ run})} \quad (6.1)$$

Where:

c_p^{sp} = Specific Heat Capacity of sample ($\text{kJ}\cdot\text{kg}^{-1}\cdot\text{K}^{-1}$)

c_p^{cal} = Specific Heat Capacity of calibration material ($\text{J}/(\text{K kg})$)

m^{cal} = mass of calibration material (g)

$P_{specimen run}$ = Heat flow rate of sample (W/g)

$P_{blank run}$ = Heat flow rate of blank/empty crucible (W/g)

m^{sp} = mass of sample (g)

$P_{calibration run}$ = Heat flow rate of calibration material (W/g)

6.4. Results and Discussion

6.4.1. Thermogravimetry Analysis (TGA) and Derivative Thermogravimetry (DTG)

TGA and DTG have been used within this chapter as a method of determining the rate of weight loss within the sample. For this chapter, the utilisation of TGA/DTG is to understand the thermal stability of the bio-earth mortar composites at 53% and 75% of RH. The experimental set up for these methods is demonstrated within Figure 6.1.

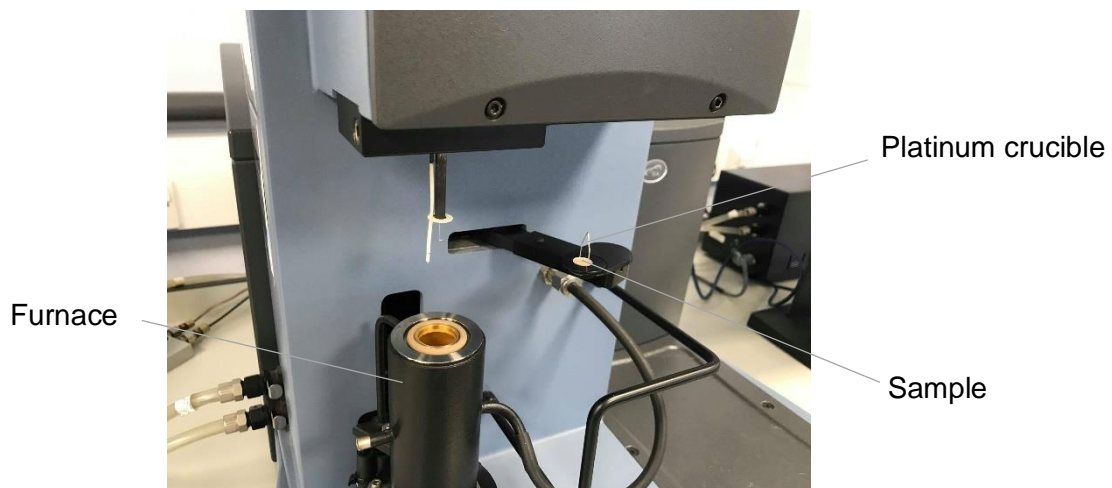


Figure 6.1. Image of bio-earth mortar composite entering furnace.

It has been outlined by several authors that the different ranges of temperatures where weight loss occurs within the mortars indicate the release of specific molecules within the samples

(Bakolas et al., 1998; Paama et al., 1998 and Frankeová and Slížková, 2016). These are in the following groups:

- 25-120°C adsorbed / hygroscopic water begins to evaporate
- 120-200°C
- 200-600°C chemically bound water release and depolymerisation begins
- >600°C loss of carbon dioxide (CO₂) due to decomposition of carbonates

Chemically bound water refers to any compound that has been hydrated. This variation in potential identification of compounds over such a large temperature range adds complexity for distinguishing each specific compound. As outlined in Ellis (2000), the environmental conditions that the mortars have been in will affect the shape and peaks exhibited in Figures 6.2a-d.

Where the samples have lost mass, the percentage of weight loss per temperature range are demonstrated in Table 6.1. In addition to the weight loss, by using the ratio of >600 °C and 200-600 °C it will enable an understanding of the natural hydraulic lime binder within the material by comparison to the chemically bound water. This could help to give an understanding of the quantity of bound water within the sample and its ability not only to adsorb, but also to bind with the sample.

Table 6.1 also indicates that for the majority of samples, their mass loss is predominantly split over 200-600°C and over 600°C. By comparison to the PL (plain) sample, all mix designs with bio-fibres have a much larger percentage of weight loss within 200-600°C range. Weight loss within 200-600 °C range is associated with chemically bound water and denotes that there are more hydraulic compounds being released, which occur from the presence of organic matter. The amount of weight loss for bio-fibre samples is approximately double that of the PL sample, demonstrating the relevant effect of bio-fibres to thermal stability for within this region.

When comparing the quantity of weight loss under 120°C, all samples except for SMR have a reduced value when stabilised at 75%. For most of the samples, when stabilised at a higher RH the weight loss of adsorbed/hygroscopic water is not as easily evaporated. However, SMR initially presents more water evaporation than any other sample in particular at 75%. When comparing the rest of the weight loss across the test it experiences a larger loss in 200-600 °C and >600 °C range. Both stabilised PL samples have the lowest weight loss between 200-600°C, but highest values over 600°C. Within the range of 200-600°C denotes chemically bound water within hydraulic compounds, where clay minerals within the composite contribute to the pozzolan (He, Osbaeck and Makovicky, 1995 and Tomassetti et al., 2015). Similarly to this research, Karatasios et al. (2012) outlines the differences in thermal properties of

materials cured at different humid conditions. Likewise, to Karatasios et al (2012) results, Figure 6.2d demonstrates that despite there are some differences between the curves, these are not significant.

Further to the thermal analysis of water within the sample, the thermal degradation of the other constituent elements within the mortars are important to understand other constituent elements. From the literature Ellis (2000), the oxidation of organic materials at approximately 490°C. All samples except PL (Figure 6.2a) exhibit a curve in this region. A limitation of this experiment is the temperature range as there may be further reactions taking place after this value. For example, a wider temperature range will give the CO₂ peak (which could be over 700°C) (Moropoulou, Bakolas and Bisbikou, 1995). This methodology is used when investigating and analysing the type of binder used in historic mortars. Due to this being known at the point of casting, a wider range for this experiment isn't required. In addition the values obtained will give a clear enough indication of the material properties.

As a component of the mix design, utilising natural hydraulic lime as a binder will have an important influence on the nanostructure of each sample. Within the structure of the composite, there is a reaction between the Ca(OH)₂ in an aqueous medium and the atmospheric CO₂ which then forms CaCO₃. Under thermal analysis, formed of Ca(OH)₂ dehydration is detected between 400 and 520°C (Moropoulou, Bakolas and Bisbikou, 1995). In addition, the composites were analysed after 28 days of curing. Whilst the lime will eventually boast structural benefits after only 28 days the carbonation process has not yet peaked. As previously mentioned in Chapter 5 (and how this affects structural properties), the lime was acting as a filler. Despite this, there will still be a thermal analytical information for how the different bio-fibres interact within the composite (Oates, 2007; Ševčík et al., 2015).

Table 6.1. Overall weight loss percentages for earth based mortar composites.

Sample ID			Weight loss per temperature range (%)				
			<120°C	120-200 °C	200-600 °C	>600 °C	>600°C /200-600 °C ratio
Mix 1	PL	53%	11.27	5.47	36.95	46.31	1.23
		75%	11.12	15.20	37.65	35.99	0.96
	W1	53%	11.61	3.17	60.46	24.76	0.41
		75%	3.19	3.06	66.54	27.20	0.41
	SMR	53%	7.34	2.15	70.50	20.01	0.28
		75%	10.66	2.74	60.52	26.07	0.43
	W2	53%	6.49	2.77	61.73	29.01	0.47
		75%	3.34	2.59	64.77	29.3	0.45

A comparison for the weight loss of each sample helps to understand the thermal stability of the material. This comparison can be made as each material experienced the same isothermal conditions. W2 at 75% lost the most mass throughout the duration of the experiment. Compared to the other mix designs, PL at both 53% and 75% had a significantly less weight loss which is demonstrated by a shallow, consistent mass loss curve.

The amount of CO₂ released by the degradation of carbonates is at approximately 600°C, from classification proposed by Moropoulou, Bakolas and Anagnostopoulou (2005). From the samples within Table 6.1, these samples are in accordance with the research by Moropoulou et al (2005), demonstrating their reliability.

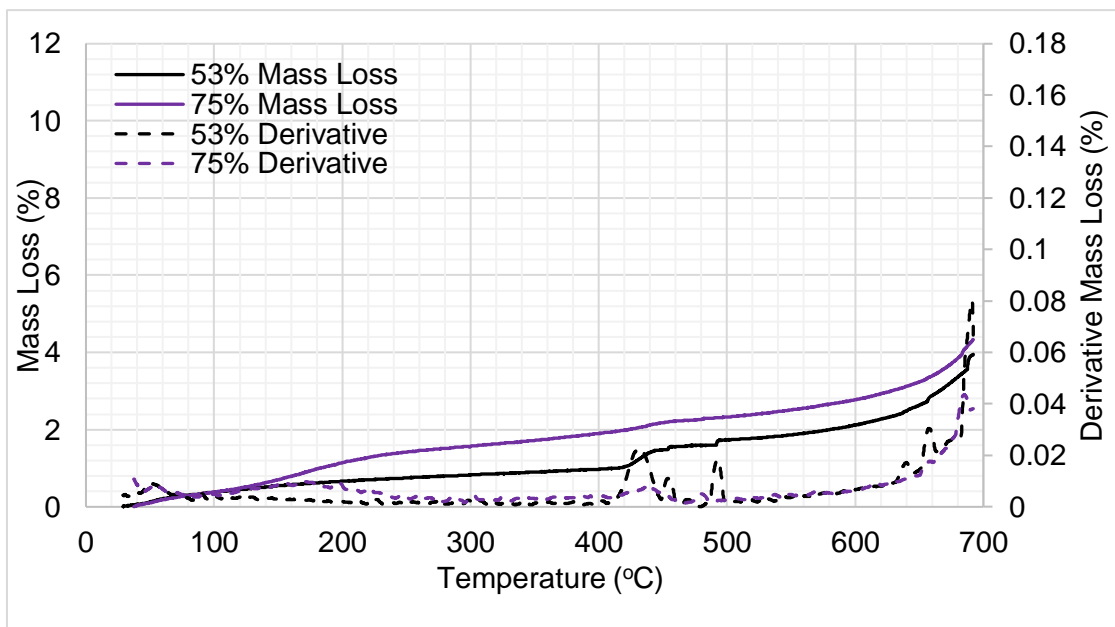


Figure 6.2a. TGA (solid line) and DTG (dashed line) for Mix 1 PL at 53% and 75% RH.

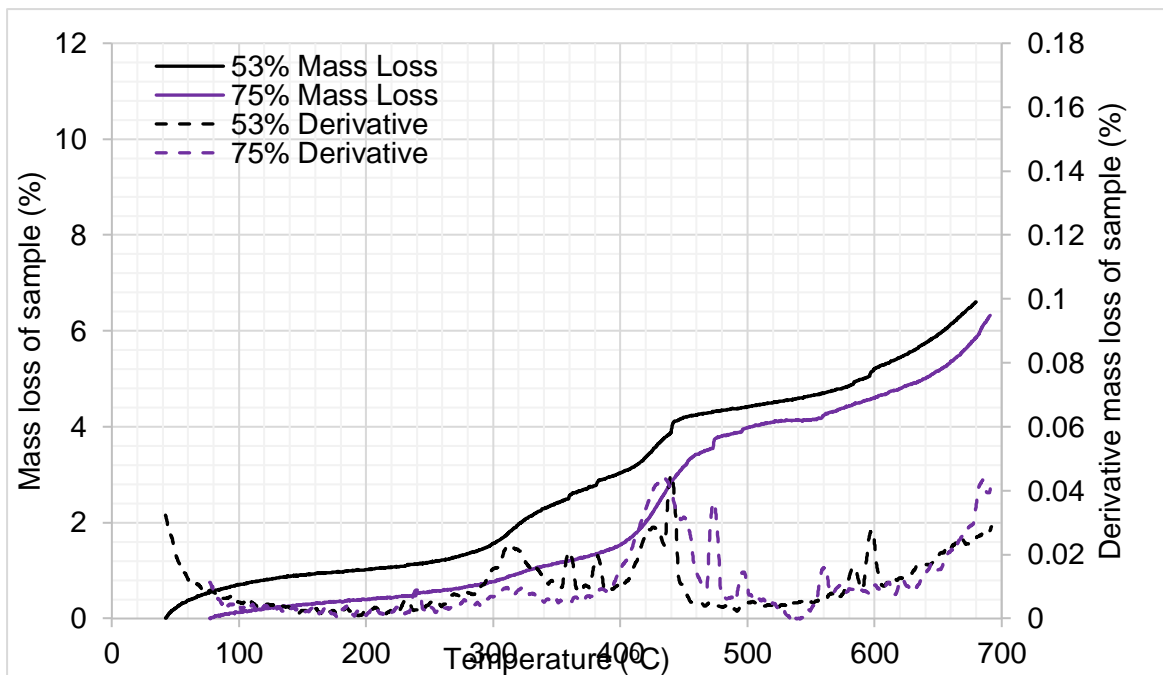


Figure 6.2b. TGA (solid line) and DTG (dashed line) for Mix 1 WL1 at 53% and 75% RH.

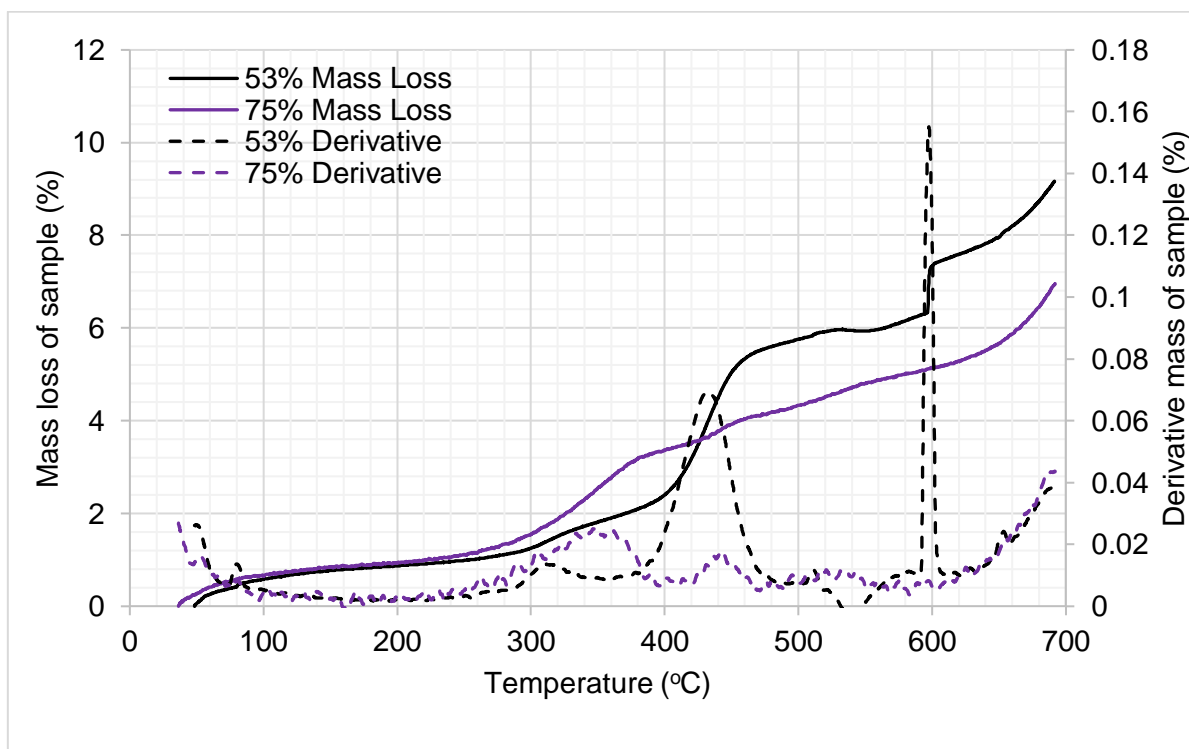


Figure 6.2c. TGA (solid line) and DTG (dashed line) for Mix 1 SMR at 53% and 75% RH.

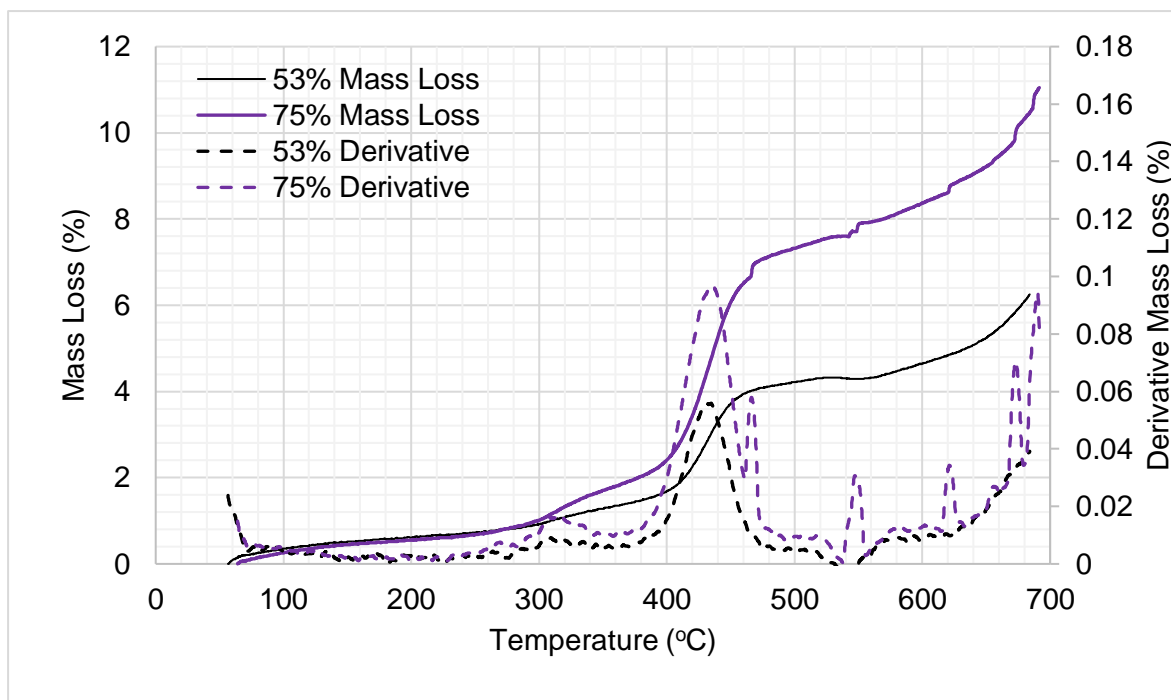


Figure 6.2d. TGA (solid line) and DTG (dashed line) for Mix 1 W2 at 53% and 75% RH.

6.4.2. Differential Scanning Calorimetry (DSC)

DSC provides a quick and relatively easy method of measuring how energy changes within a sample upon heating. By comparing to the samples examined in Chapter 4 (Figures 4.4a, 4.4e and 4.4f), Figures 6.3a to 6.3d within this chapter demonstrate that there are clearly less endotherms. In line with Liu, Ma and Zhang (2016) until 300°C there are no obvious endotherms. However, despite not being any major transitional endothermic peaks or differences, the samples are clearly experiencing thermal effects throughout the experiment which is important to investigate. Figures 6.3a to 6.3d demonstrate curved endotherms where thermal events are occurring, so the reaction is not linear and there are transition temperatures. These have been investigated and presented in Table 6.2.

As temperature constantly increases, Figure 6.3a demonstrates that there is a clear difference between 53% and 75% stabilisation, where 53% requires a comparatively larger heat flow. Initially the difference in heat flow is sustained (for example at 50°C is 12.83 W/g), however, as temperature increases, rather than the difference in heat flow being maintained it decreases. The change in gradient for the two stabilisation RHs occurs at 86.55 °C, then 190.53 °C for 53% and 85.97 °C and 190.33 °C for 75%. As the difference between these two values is so small, it can be considered negligible. This point (~190.4 °C) could be considered a 'transition temperature' where the gradient of the curve changes for both lines. After this

point, the two lines converge and difference in heat flow is greatly reduced (for example at 275°C is 6.22 W/g).

Table 6.2. DSC phase transitions temperatures for bio-earth mortar composites.

Sample ID		Water Evaporation Temperature (T_{eva}) (°C)	Transition Temperature (T_t) (°C)	Denaturation Temperature (T_d) (°C)
PL	53%	86.44	190.53	-
	75%	85.97	190.34	-
W1	53%	85.43	176.93	-
	75%	125.93	177.80	-
SMR	53%	96.20	-	227.00
	75%	96.20	-	227.00
W2	53%	81.66	198.4	254.93
	75%	86.13	178.01	254.93

By comparison, Figure 6.3b initially has a similar heat flow (for example at 50°C the difference in heat flow is 3.63 W/g) but with 75% RH sample having a larger heat flow. As temperature increases, heat flow continues to rise the difference between the samples continually rises. At approximately 85.43°C the 53% sample experiences a transition in the gradient of the line. From an initially steep incline to a flatter, slower increase in heat flow with temperature (for example at 275°C difference in heat flow is 20.01 W/g). This is also experienced for the 75% sample, but this change in gradient occurs at a much higher temperature of 125.94°C. In general, the heat flow within Figure 6.3b is larger than that of Figure 6.3a which can be assumed to be because of the addition of bio-fibres. Similar to Figure 6.3a, there is a point within Figure 6.3b where the trend line majorly transitions, for 53% is 176.93 °C and 75% 177.80°C; as these points are so similar they can be considered the same temperature. Figure 3a demonstrates that there is an endothermic peak at 282.2 °C and 253.2 °C for 53% and 75% retrospectively. In comparison to Chapter 5, Figure 6.3b also shows the same endothermic peak at 253.2°C. Therefore, within Figure 6.3b the small abrupt endotherm can be assigned to the inner α -crystal within the wool molecule spilling and decomposing – the denaturation of wool.

Interestingly, Figure 6.3c differs again to the thermograms in Figures 6.3a and 6.3b due to both RHs demonstrating an almost identical curve. Initially, samples have some differentiation where the 75% RH sample has a slightly elevated heat flow by comparison to 53% RH stabilised sample. This curve also features two ‘transition points’, this curve alters in gradient

at 96.20°C and 227.00°C. When comparing Figure 6.3c to Figure 6.4a (the earth mortar composite is similar to the 53% RH curve).

Initially like Figure 6.3a, Figure 6.3d has a consistently differing heat flow between the two stabilised samples. At 50°C the difference in heat flow between 53% and 75% samples is 33.39 W/g. In comparison to the other mix designs, the difference in heat flow is nearly consistent for the entire experiment as at 275°C heat flow is 53.506 W/g. For both stabilisation curves, there are 3 points where the curve changes gradient for 53%: 81.66 °C and 198.4 °C and for 75% 86.13 °C and 178.01 °C. 75%. Within Figure 6.3d there is a small, endothermic peak for both stabilisation curves. At 53% stabilisation this peak is observed as a peak with a shoulder curve at 254.93 °C and 262 °C but 75% only displays a singular peak at 255.93°C. By comparison to Figure 6.4a, Figure 6.3d there is an established different between the two curves at both RHs.

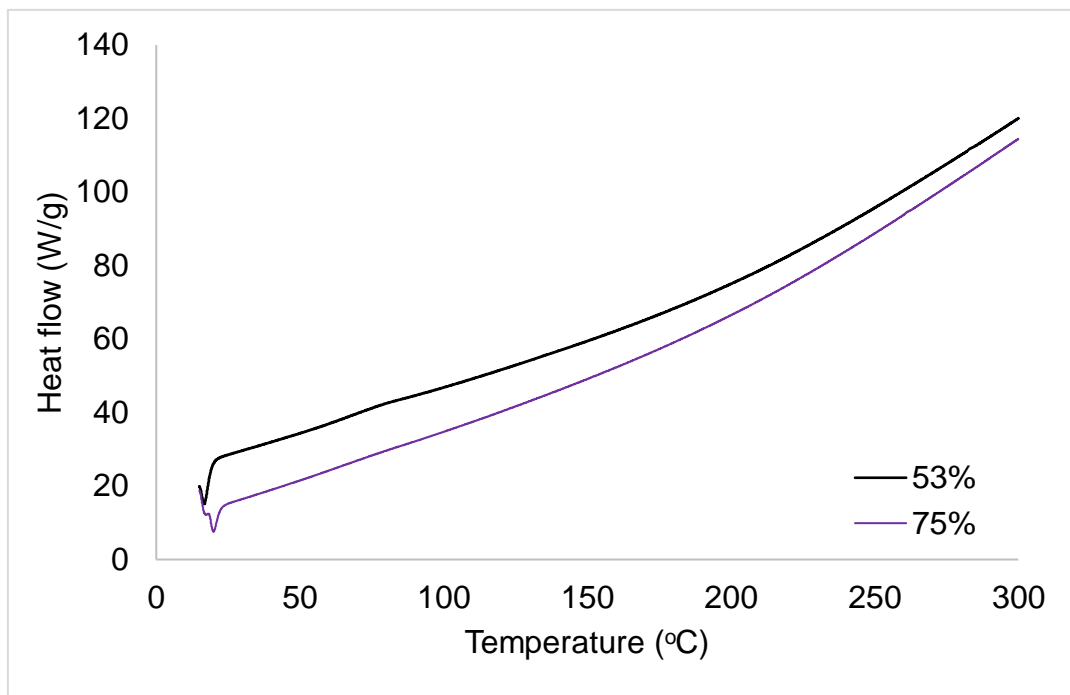


Figure 6.3a. Mix 1 PL DSC thermogram.

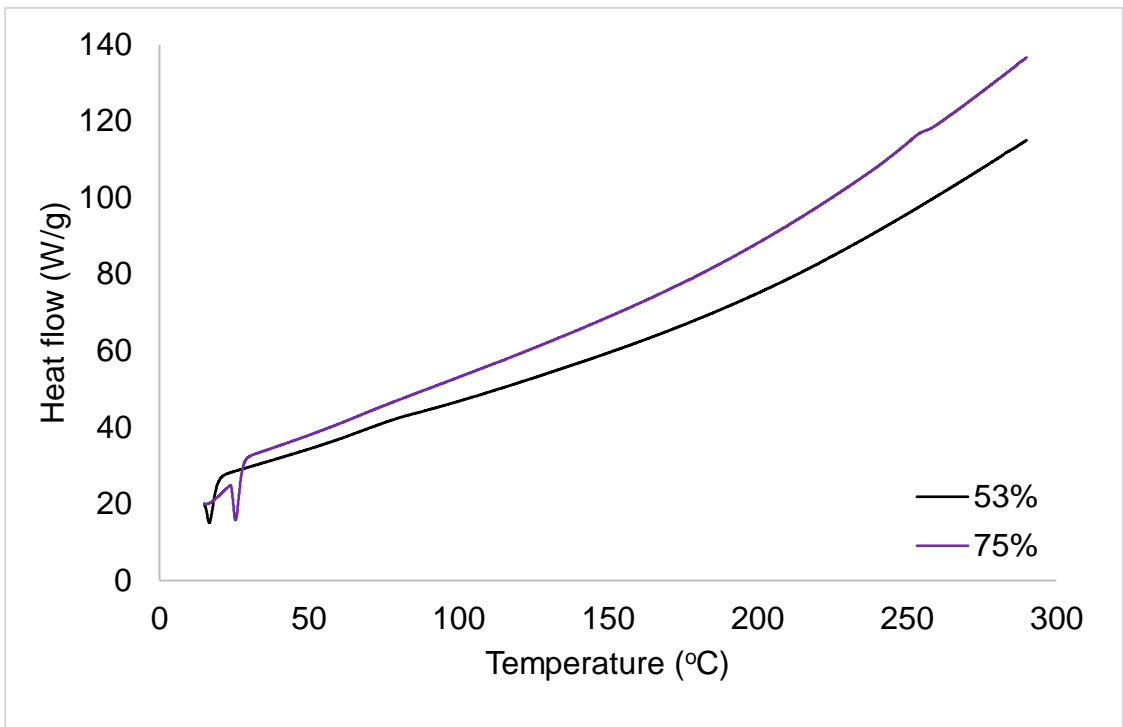


Figure 6.3b. Mix 1 W1 DSC thermogram.

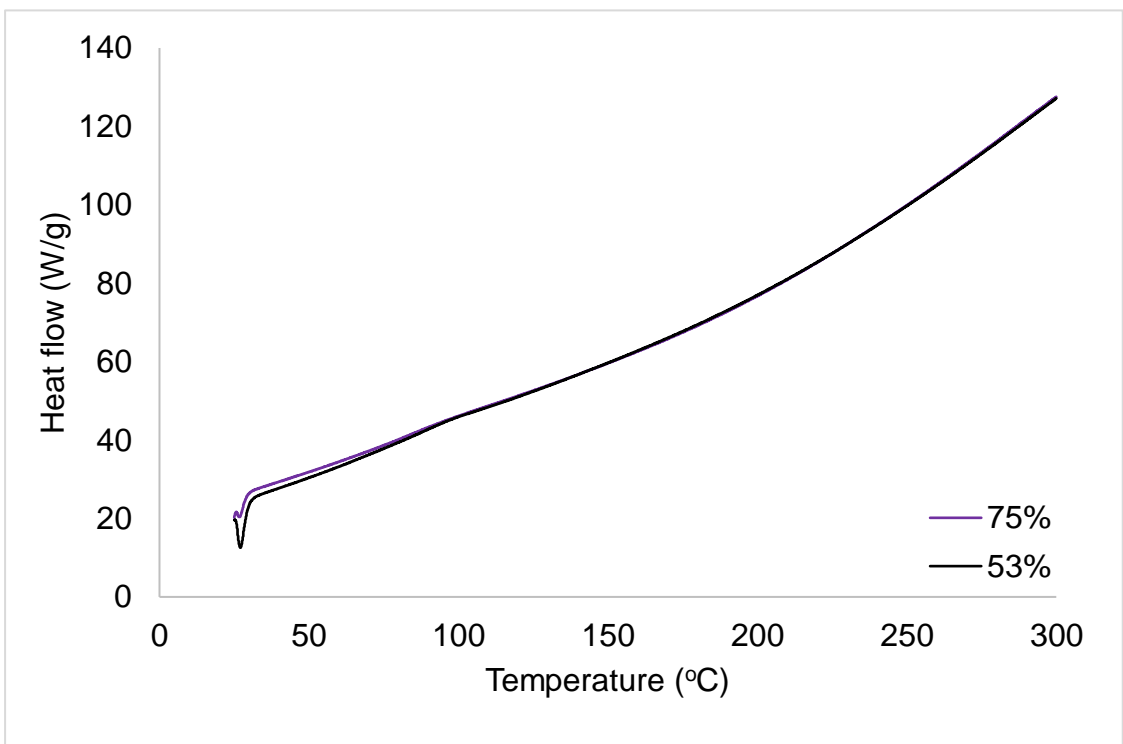


Figure 6.3c. M1 SMR DSC thermogram.

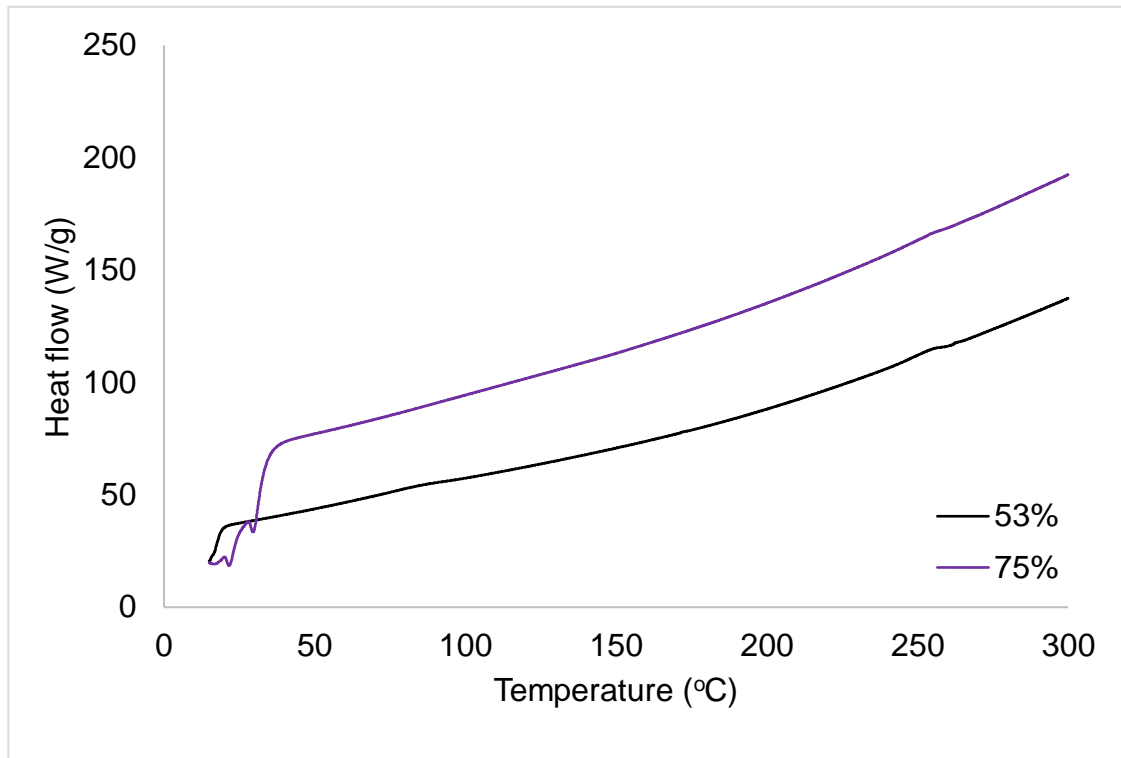


Figure 6.3d. M1 W2 DSC thermogram.

6.4.2.1. Specific Heat Capacity

Utilising the DSC equipment, specific heat capacity (C_p) (kJ/kg.K) was calculated for the mix design from 5-50°C for samples stabilised at both 53% and 75% RH. By utilising this temperature range it gives an indication of the materials performance over its dynamic service use temperatures. By comparison, most C_p values are taken in static laboratory conditions which will not always be truly representative of what the material may experience. As samples were stabilised at two different RH, the values for C_p can be found for 53% RH in Figure 6.4a and 75% RH in Figure 6.4b. For Figures 6.4a and 6.4b it is demonstrated that for all samples (including PL) the C_p increases with temperature. Figure 6.4a differs from Figure 6.4b in a number of important ways, which will be explored throughout this section.

In both wood and wool based composites, there is a relationship of increasing temperature and increasing C_p . This phenomena has been explored by several authors (for cellulose based materials (Koch, 1969; Beall, 1971; Simpson and Ten Wolde, 2009; Radmanović, Đukić and Pervan, 2014)) and keratin based materials ((Haly, Abu-Isa and Dole, 1965; Deliski, 2011). For 53% PL has consistently the smallest value of C_p throughout the experiment and

W2 has the largest. When stabilised at 75%, PL still has the smallest value but SMR has the largest Cp value.

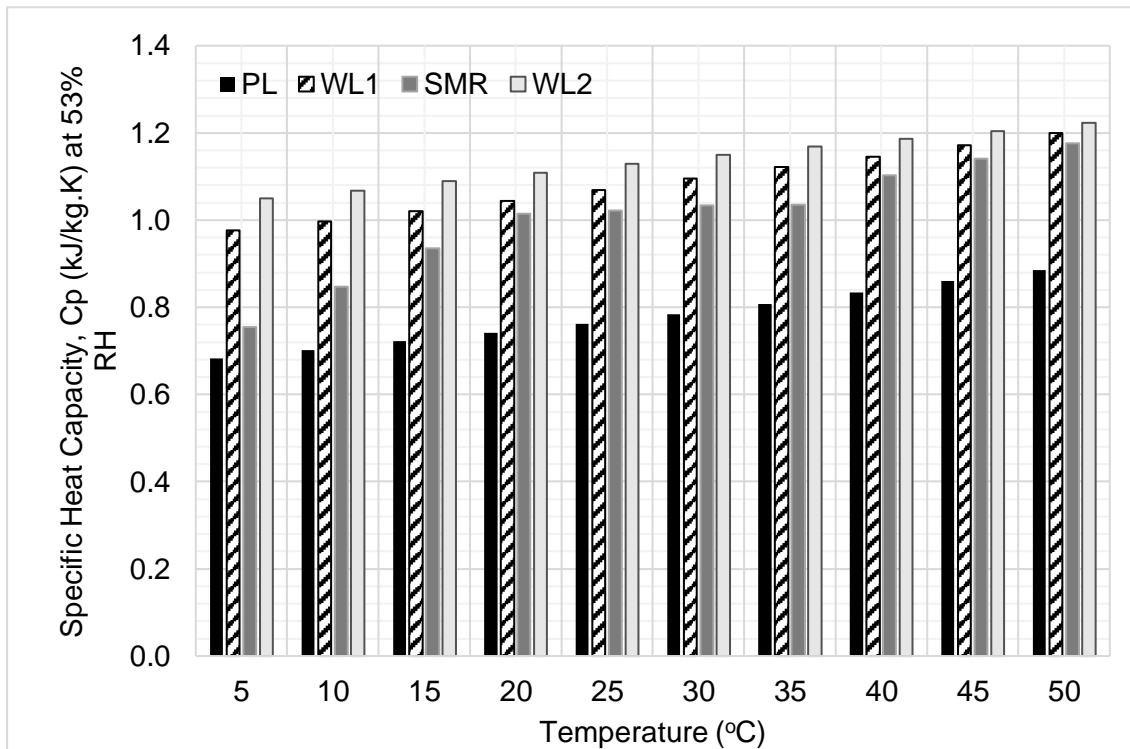


Figure 6.4a. Specific heat capacity for Mix design 1 from 5-50°C at 53% RH.

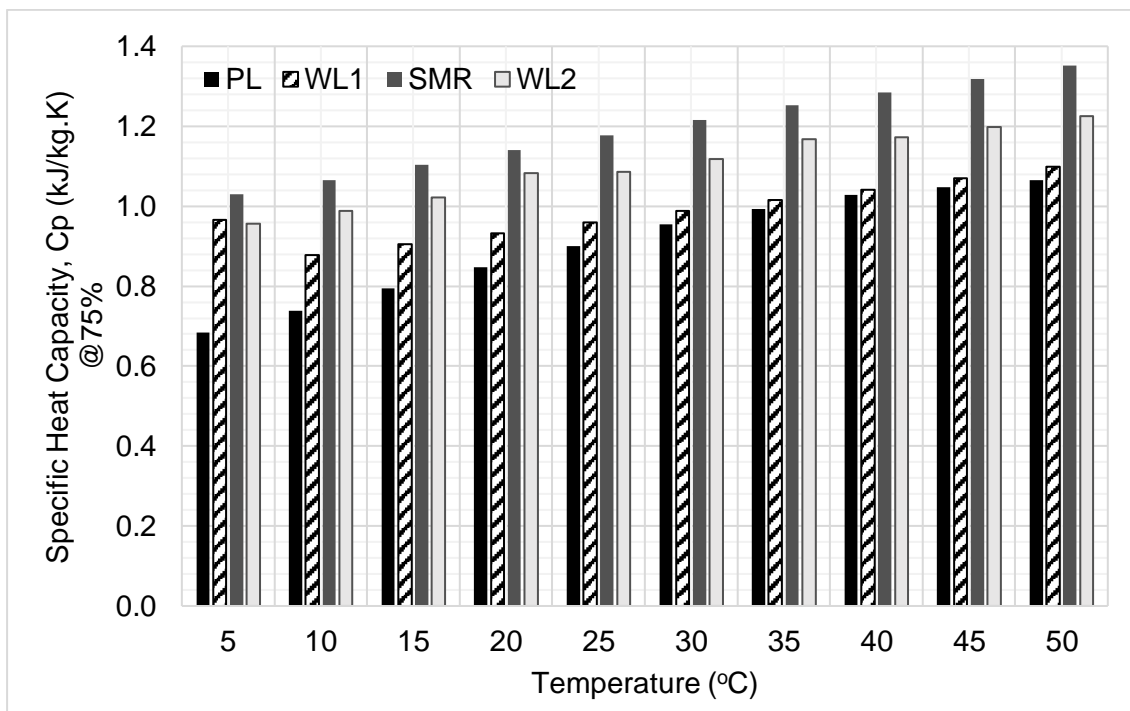


Figure 6.4b. Specific heat capacity for Mix design 1 from 5-50°C at 75% RH.

From Figure 6.5 it is clear that when stabilised at a higher relative humidity, only 2 of bio-fibre earth composites have a higher Cp. Out of all 4 mixes, SMR has the greatest Cp values at 75% (1.141kJ/kg.K) (see Table 6.3). A greater Cp value represents that this composite is affected the least by temperature change. There is also a difference between the value of Cp which is demonstrated in Table 6.4. When comparing the 4 mixes, SMR has the largest difference in Cp where W2 is the least affected by the stabilisation RH.

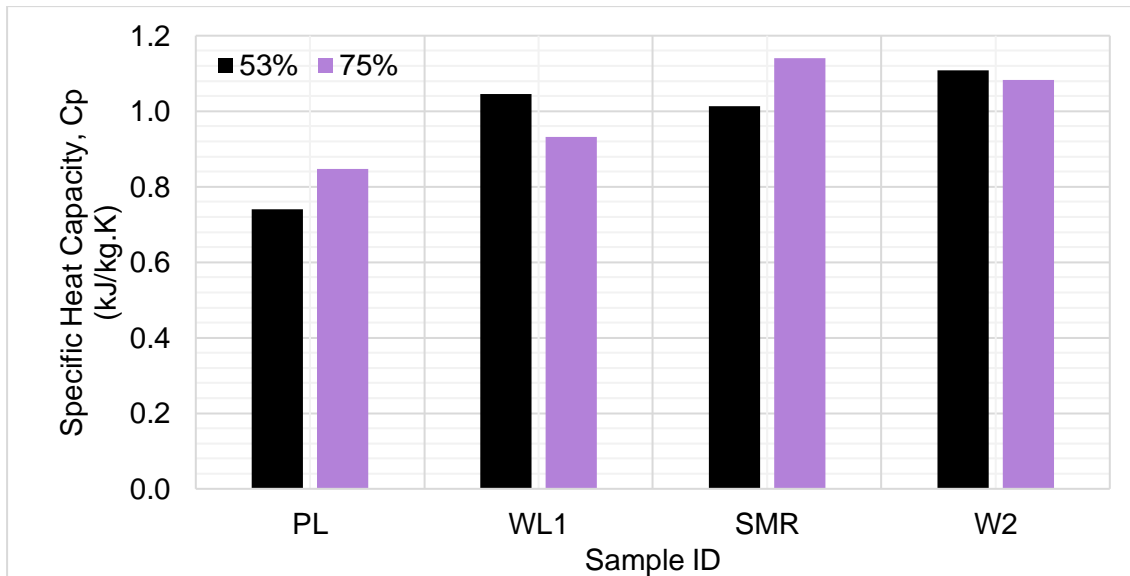


Figure 6.5. Average specific heat capacity, Cp of samples at 53% and 75% RH at 20°C.

Table 6.3. Specific heat capacity Cp values for samples at 20°C.

Specific Heat Capacity, Cp (kJ/kg.K) at 20°C		53% RH			75% RH		
		Sample ID	Minimum	Maximum	Average	Minimum	Maximum
Mix 1	PL	0.707	0.771	0.741	0.792	0.902	0.847
	W1	0.960	1.161	1.045	0.921	0.940	0.932
	SMR	0.927	1.197	1.014	0.991	1.291	1.141
	W2	1.010	1.201	1.109	0.998	1.116	1.083

Table 6.4. Difference in Cp values for 53% and 75% stabilised samples at 20°C.

Sample ID	Difference in Cp at 20°C (kJ/kg.K)
PL	0.106
W1	0.113
SMR	0.127
W2	0.026

Deliski (2011) outlines that for porous materials, the specific capacity ($C_{p,ps}$) is the sum of the specific heat capacity of the dry porous material ($C_{p,d}$), specific heat capacity of the free water ($C_{p,fw}$) and specific heat capacity of bound water ($C_{p,bw}$) as outlined in Equation (6.2)

$$C_{p,ps} = C_{p,d} + C_{p,fw} + C_{p,bw} \quad (6.2)$$

Where:

$C_{p,ps}$ = Specific heat capacity of a porous material (kJ/kg.K)

$C_{p,d}$ = Specific heat capacity of a dried porous material (kJ/kg.K)

$C_{p,fw}$ = Specific heat capacity of free water (kJ/kg.K)

$C_{p,bw}$ = Specific heat capacity of bound water (kJ/kg.K)

It could be proposed that the higher the stabilisation RH, the higher the value of Cp due to the environment that the materials are stabilised in has a larger quantity of water vapour. However, the results demonstrated in Figure 6.5 show that this is not always the case. Due to the samples only being stabilised for 24 hours, the ratio of bound and free water that the material has within its structure could differ. Therefore for some materials', for example W1 and W2, when stabilised at a 75% RH presents a lower Cp when compared to stabilisation at 53% RH. It could be hypothesised that this is due to the materials ability to readily accept water molecules. So, the same material could have more 'free water' within the capillary pores of the material and upon heating is easier to release these water molecules. By comparison, composites such as PL and SMR when stabilised at a higher RH present a larger Cp. Indicating that this material can not only initially adsorb water molecules but also bind to the samples chemical structure. Compared to Huang (2016) the values within Figure 6.5 demonstrate that at 20°C, the mortar has a lower Cp than the raw bamboo samples within the paper.

From a practical perspective and in the context of buildings, the storage capacity of a composite is related to the specific heat capacity and the volume of the materials used in a building envelope. Nevertheless, the storage capacity of the envelope is also related to the composition of the walls and the technological solutions.

Utilising this equation to understand the earth mortar composites is interesting as due to their stabilisation RHs it is inevitable that the quantity of free water and bound water would differ. Further research would be interesting to quantify the affect the specific heat capacity of free and bound water has on the bio-earth mortar composites. For an initial understanding of the role water has within the sample can be identified by using FTIR which will be explored in section 6.4.3.

Utilising this method also helps to give a broader understanding of the materials potential performance in differing climate conditions. Therefore, this would enable a 'prescription' of the material rather than simply selecting the 'overall' best performing material. Understanding the material properties via DSC has many benefits over other hygrothermal methods such as Moisture Buffering Value (MBV) not only for the speed of the test but also the multifaceted results per thermogram.

6.4.3. Fourier Transform Infrared Spectroscopy (FTIR)

This methodology of analytics spectroscopy will enable the identification of organic materials but adsorption and transmittance of infrared radiation. Figure 6.6 demonstrates how the bio-earth composite samples were tested.

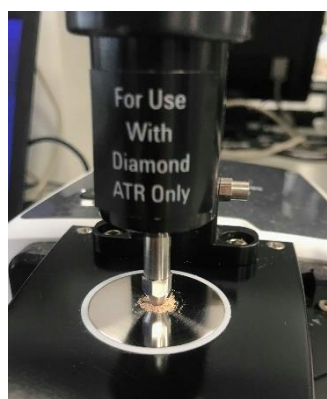


Figure 6.6. FTIR equipment analysing a bio-earth mortar composite sample.

Figures 6.7a to 6.7d demonstrate the spectra's for the mix designs stabilised at 53 and 75% RH. The assignment for bonds that have been detected within these spectras have been collected and are demonstrated within Table 6.5.

Table 6.5. FTIR analysis of earth mortar composites and associated assignment of bonds at 53% and 75% RH.

Mix 1								Assignment for bond
PL position of band (cm ⁻¹)		W1 position of band (cm ⁻¹)		SMR position of band (cm ⁻¹)		W2 position of band (cm ⁻¹)		
53%	75%	53%	75%	53%	75%	53%	75%	
3606.20	3650.93	3641.61	3641.61	3641.61	3636.01	3641.61	3639/75	Stretching and bending O-H (hydroxyl) group (Rampazzi et al., 2016) (Man, Haque and Chen, 2019) (Ammari et al., 2018)
		3388.15	3384.42	3416.11	3311.74	3401.70	3401.20	
		2961.37	2950.19					C-H bond stretching and bending (Rampazzi et al., 2016)
		2329.59	2320.27	2320.27	2320.27	2322.99	2324.00	Carbon Dioxide (CO ₂) (Millogo, Hajjaji and Ouedraogo, 2008)
1763.03	1763.03	1712.71	1710.85	1414.52	1407.07	1418.25	1407.07	Vibration bands of calcite (CaCO ₃) (Ammari et al., 2018)
				1634.44	1626.98	1643.78	1643.75	Stretching absorbances of C=O and C-O bonds (Rampazzi et al., 2016)

On initial inspection, Figures 6.7a and 6.7b do not appear to have much differentiation when considering the two stabilisation RHs. Especially when comparing the differences between the spectra's as observed in these figures with comparison to Chapter 4 Figures 4.9a (SMR), 4.9e (W1) and 4.9f (W2). However, to understand the discreet changes, a magnified image of the spectra is displayed just beneath the measured values in Figures 6.7a - 6.7d.

As carbonates are formed within the earth mortar, it could be suggested that this is due to the bio-physical chemical conditions of the earth. As natural hydraulic lime has been utilised as a binder in the mix design (in addition to water and sand) it facilitates the formation of calcite. Calcite sets quickly within the mortar matrix and it has the ability to agglomerate to inert materials such as quartz (Millogo et al., 2008). Other materials found within lime rich mix designs is carbon dioxide as it is extensively dissolved (Millogo and Morel, 2012). The release of this molecule is outlined in TGA/DTG experimentation.

To understand the differences between the bands, it is important to understand what they represent. Affecting the intensity of the absorbency bands can be associated to a dipole moment and/or the quantity of bond. To analyse the Figures within this thesis it is understood that the lower the transmittance (and therefore greater the absorbance) the "stronger" and/or quantity of bonds there are. The major peak for the hydroxyl (O-H) group within each composite is clearly visible through all Figures 6.7a to 6.7d. By understanding how the key bands which are associated for hydroxyl bands observes the hydroxyl reactivity. For PL, Figure 6.7a at 3606.20cm^{-1} and 3650.93 cm^{-1} (for 53% RH and 75% RH retrospectively) demonstrates that there is no differentiation between the band width and transmittance. However, for the rest of spectra there is a clear, sustained difference between the two different stabilised samples.

By contrast, W1 in Figure 6.7b shows a peak for hydroxyl group at 3641.61 cm^{-1} for both 53 and 75% which fall at difference percentages of transmittances. The samples stabilised at 75% have a lower transmittance and therefore a greater amount/intensity of hydroxyl bonds. Although they vary in transmittance, the form of the peak is exactly the same. This effect is directly comparable to W2.

When considering the peaks within SMR, it is clear that there is a difference in the transmittance and also the shape of the peak. At 53% stabilisation it is observed a shallow peak. However, 75% shows a much broader peak with a larger transmittance value. Considering all of the other mix designs, in this hydroxyl region, there is a clear change in the chemical arrangement of SMR. Due to the lack of research in this area it is difficult to understand if the difference in the hydroxyl group can be attributed to 'free' or 'bound' water.

The difference between the hydroxyl peak values for W2 is 0.17% whereas W1 is 0.12% and PL is 0.09%. In contrast, SMR has a difference of 0.8%. Even when there are no bio-fibres within the composite there is still a slight difference in the hydroxyl group stability within the compound. Due to the repeated sampling and averaging of 128 scans for each samples it can be emphasised that these numbers are representative of the materials. Therefore, out of all 4 mix designs it can be concluded that in terms of their FTIR spectra, when exposed to a differing hygrothermal environment, SMR has the largest impact on the hydroxyl stability of the mortar composite.

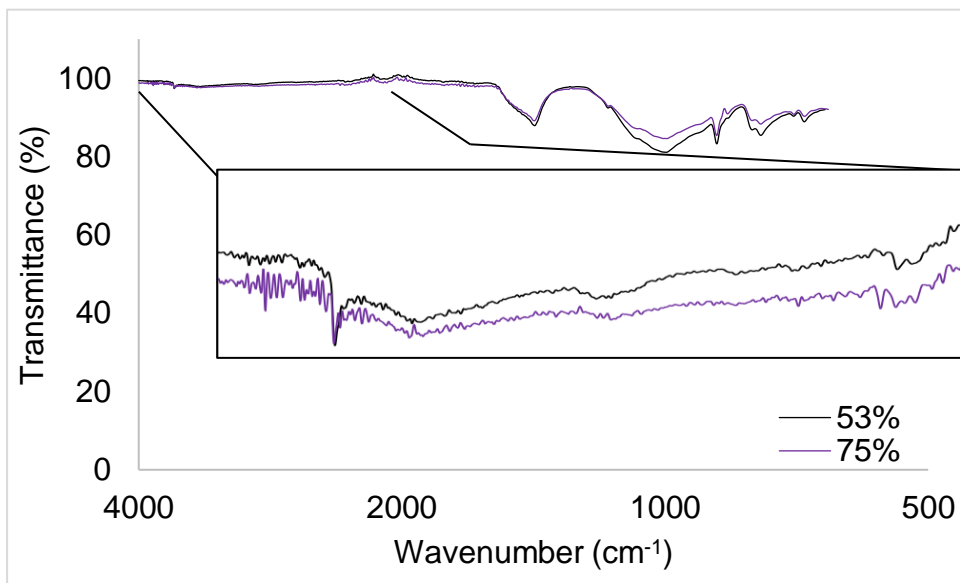


Figure 6.7a. M1 PL FTIR spectra.

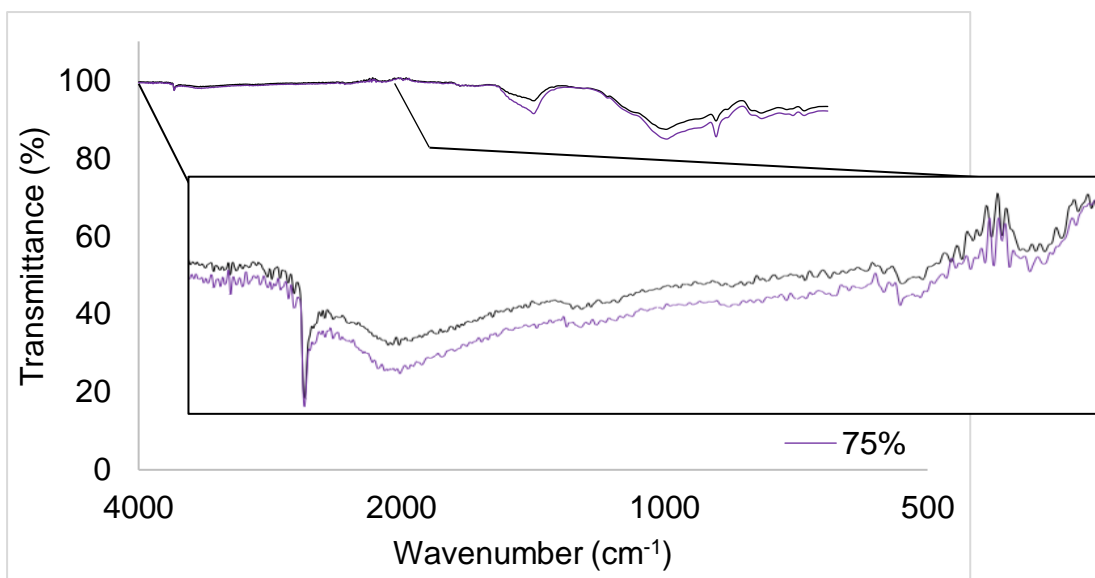


Figure 6.7b. M1 W1 FTIR spectra.

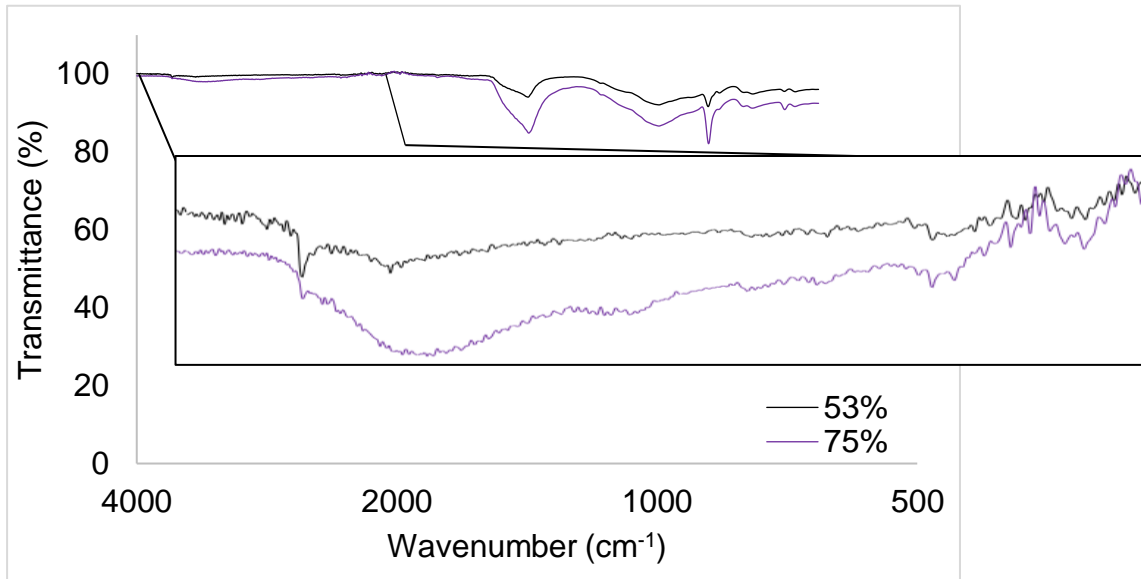


Figure 6.7c. M1 SMR FTIR spectra.

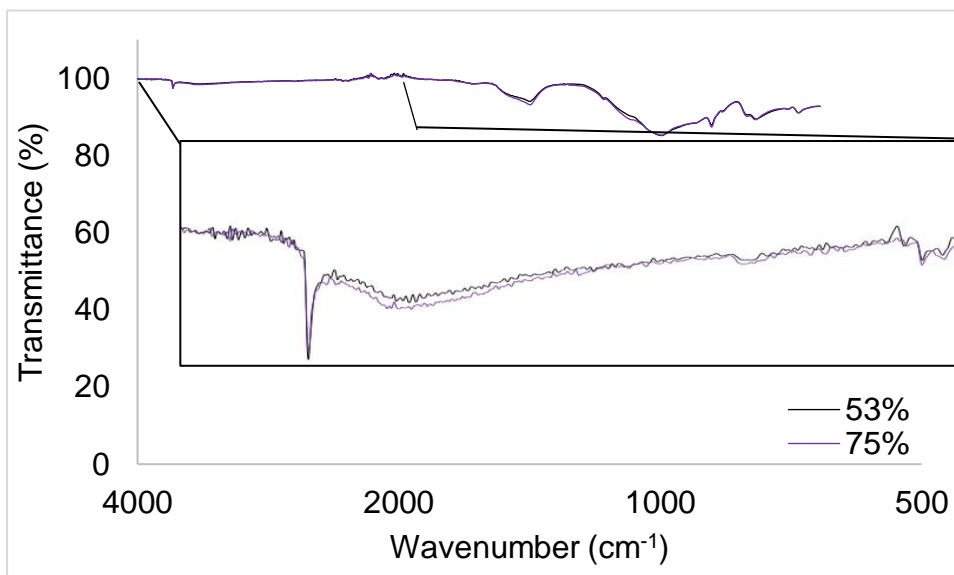


Figure 6.7d. M1 W2 FTIR spectra.

6.5. Conclusion

This chapter presents both thermo-chemical and chemical spectra for 4 different bio-fibre earth mortar composites, W1, W2 and SMR in addition to a PL as a constant. These samples were stabilised in a climatic chamber at 53% and 75% RH. Temperature changes can cause alterations in the physical and chemical properties of bio-based materials, which reflects on their hygrothermal behaviour and influence the overall properties of the final product, including the ability to storage energy.

The use of TGA/DTG enables the thermal stability of materials to be analysed. Within mortars the weight loss at different temperatures can be aligned to the bonding nature of water within the matrix. PL had the least overall weight loss, but this can be attributed to the lack of organic materials. However, of the bio-fibres W1 has the smallest weight loss. DSC was utilised in two different capacities; firstly to understand the heat flow and temperatures of key transition phases. These different mix designs exhibit three different reactions to both a rise in temperature and stabilisation percentage. SMR has the lowest denaturation temperature but remains unaffected by RH stabilisation. In terms of water evaporation temperature, W2 has the lowest value (81.88°C at 53% and 86.13°C).

Secondly, DSC was used to calculate the Specific Heat Capacity, C_p which demonstrated that C_p increases with temperature. When stabilised at different RH, the difference in C_p also varies and affects the composites differently. These differences could potentially be attributed to the materials ability to readily accept water molecules. It also demonstrates the differences of the samples adsorption and absorption of water in differing hygrothermal environments. SMR has the largest C_p for 75% at 20°C was 1.141 kJ/kg.K.

The use of FTIR, this demonstrates a difference between both stabilisation RHs, it is not as significant as just the bio-fibres as explored in Chapter 4. Despite this, there is still a difference in transmission in addition to a change in the main hydroxyl group peak for SMR. This indicates SMR has the largest impact on the hydroxyl stability of the mortar composite.

Overall, these experiments have shown that much like just the bio-fibres, these bio-fibre composite mortars demonstrate that when stabilised at different RH fundamentally affects their properties.

Chapter 7 – Dynamic moisture movement within bio-earth composites

7.1. Introduction

The hygrothermal behaviour of earth mortars was outlined in Chapter 5 and consequentially, how this affects its chemical structure was explored in Chapter 6. However, the mechanisms behind this moisture movement within the sample are also important, as they will enable a greater understanding of which hygrothermal conditions the mortar will operate most efficiently. Comparative literature studies such as Navarro et al. (2016) demonstrate that the moisture transfer mechanisms will also be indicative of the climates or building fabrics the panel will be most suited.

7.2. Materials

The mix design and bio-fibres used within this chapter are mix design 1 and are outlined within Table 7.1. For Water Vapour Permeability and sorption isotherm, samples were cast into circular disc moulds with a diameter of 80mm and depth of approximately 25mm. For latent heat of sorption, samples were cast into square moulds (100mm x 100mm x 35mm) and after 28 days of curing, samples were tested.

Table 7.1. Mix design proportions (by mass)

Lime	Earth	Sand	Lime/Water	Bio-fibres	
				Sample ID	Lime/Bio-fibre
1	0.1	8.6	2.4	PL	-
				W1	0.0243
				W2	0.0485
				SMR	0.0243

7.3. Methodology

7.3.1. Water Vapour Permeability

Water Vapour Permeability (WVP) was conducted by wet cup method as per BS EN 12572-2016 (ISO, 2016) BS EN 1015-19 (BSI, 1999d) and BS EN 15803 (BSI, 2010) and bio-earth

mortar samples were stored within a plastic container (with 5 circular samples with a thickness of approximately 25mm). To ensure there was no vapour movement around the sides of the sample, sealant was used (see Figure 7.1).

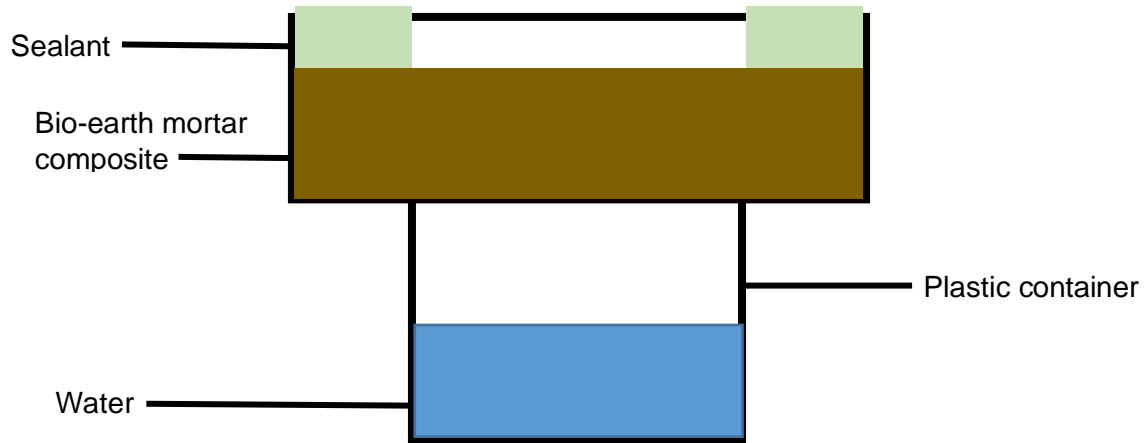


Figure 7.1. WVP experimental set up.

Initially samples were conditioned at 23°C at 50% RH to ensure a constant mass was achieved. The experimental set up for this was under isothermal conditions (23°C) using the wet cup method at 40% RH. The samples were sealed for there to be a unidirectional moisture flow. The set up for this experiment can be found within Figure 7.1. An issue that should be considered for this method is that it does not consider how surface vapour resistance of the material may affect the overall result. Due to the gradient of moisture between the lower and upper surface of the sample, this drives a moisture gradient within the cup and the vapour is released from the sample. Every 24 hours the sample was measured until a three successive values were within $\pm 5\%$ of the mean value. The rate of change in mass of the sample (G) (mg/hr) was calculated in Equation 7.1.

$$G = \frac{(m_1 - m_0)}{(t_1 - t_0)} \quad (7.1)$$

Where:

G = mean of at least 3 successive determinations of $G_{1.0}$ (mg/hr) given $G_{1.0}$ is within $\pm 5\%$ of the mean value

m_1 = mass of test assembly at time t_1 (mg)

m_0 = mass of test assembly at time t_0 (mg)

Water vapour transmission rate (g) (mg/m^2) was calculated in Equation (7.2)

$$g = \frac{G}{A} \text{ (7.2)}$$

Where:

g = water vapour transmission rate (mg/m^2)

G = rate in change of mass (mg/hr)

A = the upper exposed surface area of test specimen (m^2)

Water vapour permeance (W) ($\text{mg}/\text{m}^2.\text{hr.Pa}$) was calculated in Equation (7.3)

$$W = \frac{G}{A.\Delta P} \text{ (7.3)}$$

Where:

W = water vapour permeance (W) ($\text{mg}/\text{m}^2.\text{hr.Pa}$)

A = the upper exposed surface area of test specimen (m^2)

ΔP = pressure difference (Pa) as outlined in BS EN 12086

Water vapour resistance (Z) ($\text{mg}/\text{m}^2.\text{hr.Pa}/\text{mg}$) was calculated in Equation (7.4)

$$Z = \frac{1}{W} \text{ (7.4)}$$

Where:

Z = water vapour resistance ($\text{mg}/\text{m}^2.\text{hr.Pa}/\text{mg}$)

W = water vapour permeance ($\text{mg}/\text{m}^2.\text{hr.Pa}$)

Water vapour permeability (δ) ($\text{mg}/\text{m}.\text{hr.Pa}$) is calculated in Equation (7.5)

$$\delta = W . d \text{ (7.5)}$$

Where:

δ = water vapour permeability ($\text{mg}/\text{m}.\text{hr.Pa}$)

W = water vapour permeance ($\text{mg}/\text{m}^2.\text{hr.Pa}$)

d = thickness of sample (m)

Water vapour diffusion resistance factor (μ) was calculated in Equation (7.6)

$$\mu = \frac{\delta_a}{\delta} \text{ (7.6)}$$

Where:

μ = water vapour diffusion resistance factor

δ = water vapour permeability of insulation material ($\text{kg}/(\text{m}.\text{s.Pa})$)

δ_a = vapour permeability of air ($\text{kg}/\text{m}.\text{s.Pa}$)

7.3.2. Sorption Isotherm

Also known as moisture storage function, sorption isotherms demonstrate a relationship between the relative humidity of the environment and equilibrium moisture content of a sample. As these materials are porous, their ability to dynamically alter to their hygrothermal environment is of great importance. These samples were dried in accordance with BS EN ISO 12570 (ISO, 2000) where a constant mass (with less than a 0.1% of total mass) was achieved over three consecutive weighing at least 24 hours apart. Adsorption isotherms were calculated in line with BS EN ISO 12571 (ISO, 2013) in a climatic chamber at a temperature constant of 23°C, where moisture content by mass by mass, u (kg/kg) was calculated as with Equation 7.7.

$$u = \frac{m - m_0}{m_0} \quad (7.7)$$

Where:

m = mass of sample (kg)

m_0 = mass of dried test specimen (kg)

7.3.3. Latent heat of sorption

As explored in section 3.4.4, during the phase change between water molecules in the liquid and vapour state, latent heat was identified over 10 cycles of the raw bio-fibres. For this experiment, each mix design were cast and a thermocouple inserted into the wet mortar on the surface at 15mm from the surface (approximately half way through the sample) (see Figure 7.2). Once cured, composites were placed within a climatic chamber (see Figure 7.3) where the latent heat of sorption was measured dynamically and continuously every 30 seconds for 21, 24 hours cycles with cyclical RH step changes between 75% and 53% for 16 and 8 hours respectively.

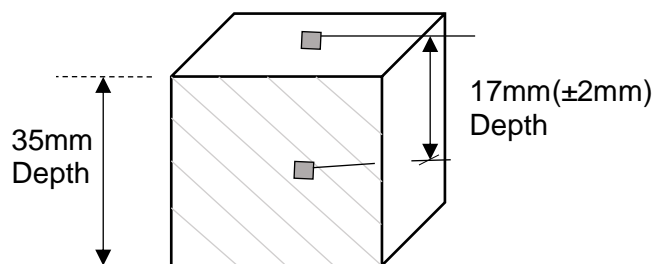


Figure 7.2. Experimental set up of thermocouples within earth mortar composite.



Figure 7.3. (L) Thermocouple cast on the surface (R) Thermocouple cast 15mm from surface of earth mortar composite.

7.4. Results and Discussion

7.4.1. Water Vapour Permeability (WVP)

WVP of a material indicates the ‘breathability’ of a material - a larger value of water vapour permeability indicates an enhanced transport of water throughout the composite as capillary condensation leads to the microscopic pores to fill. The results for the WVP and water vapour diffusion resistance factor in Table 7.2.

Table 7.2. WVP values for bio-earth mortar composites.

Sample ID	Water Vapour Permeability, δ ($\times 10^{-11}$) ($\text{kg}\cdot\text{m}^{-1}\cdot\text{s}^{-1}\cdot\text{Pa}^{-1}$)	Water Vapour Diffusion Resistance Factor, μ
PL	1.6	4.21
W1	2.01	2.83
SMR	2.5	2.44
W2	2.12	2.55

Understanding the permeability of water vapour into the sample is important for anticipating the potential risks of moisture build up within the composite (Zhang, Yoshino and Hasegawa,

2012). The greater the ability for water vapour to enter and exit the sample indicates that the sample has a larger breathability'. Without this breathability, the build-up of condensation within the material will reduce its hygroscopic ability. Especially in residential properties, this is particularly problematic because as the water vapour diffuses through the individual wall components, building envelope and temperatures drop to reach the dew point and form interstitial condensation. The associated problems of this condensation are found in section 2.2. By reducing the performance of the building fabric and particularly the insulation could result in a reduced thermal resistance and especially in UK residential properties, exacerbate condensation issues. It could therefore be associated that the lower the water vapour permeability value, the more likely the aforementioned issues are to arise and in turn reduce the durability of the material (as highlighted in Claisse (2014)).

From Table 7.2 it is shown that SMR has the greatest value of WVP ($2.5 \times 10^{-11} \text{ kg.m}^{-1}.\text{s}^{-1}.\text{Pa}^{-1}$). This result is concurrent with the MBV of this material having the largest value ($1.26 \text{ g}/(\text{m}^2 \text{ \%RH})$). PL also had the lowest value ($1.6 \times 10^{-11} \text{ kg.m}^{-1}.\text{s}^{-1}.\text{Pa}^{-1}$) as this composite has no bio-fibres, the microstructural shape would be more homogeneous. By comparison to the bio-fibre composites it is proposed that the breathability is increased not only on the external surface but due to the tortuosity of pores interacting and combining with the bio-fibres themselves (Anatoly et al., 2020). The value of μ demonstrates how reluctant the diffusion of water vapour is into the sample. This is shown in Table 7.2 as PL has the lowest value of μ and therefore has the most resistance for water vapour entering the sample and is the least porous and permeable in accordance within Figure 5.16.

By comparison to Cagnon et al. (2014) and Faria, Santos and Aubert (2016) the values presented in Table 7.2 are generally slightly lower than expected values than in the literature, which could be accounted to the differing thickness of the samples. Another potential explanation could be due to testing of these samples after only 28 days. As the lime has not yet fully carbonated, this could be affecting the microstructure of the pores. As this measurement is calculated after only 28 days of curing, after a longer term of exposure the affect the deterioration of the bio-fibres would be interesting to understand how this affects WVP. The degradation to building materials under cyclical drying and wetting can considerably affect the thermal performance (Barreira, Delgado and Freitas, 2014). Particularly with wool, uneven and continual wetting and drying deteriorates the fibre. Further to this as the fibre cures with the mortar matrix, air voids are created. This effect on the overall material properties would be noteworthy to understand the long term service life performance of the composites as outlined by Zirkelbach, Holm and Künzel (2005). Further analysis of the WVP could include a better understanding on not only WVP as an empirical value but understanding

the quantity and the quality of the wetting the vapour gives across the surface of the composite; for example understanding the uniformity of this across the material.

7.4.2. Sorption Isotherms

By understanding the adsorption behaviour of the composites this will enhance the understanding and interpretation of hygrothermal behaviour. Investigations into other bio-fibre mortars such as hemp was explored in Collet et al. (2008) but the utilisation of a locally sourced earth is not as well researched. Within the literature that sorption is greatly affected by temperature it was imperative that the isothermal temperature was kept constant (Poyet and Charles, 2009). The curve for how adsorption is affected over a wide range of relative humidities can be found in Figure 7.4.

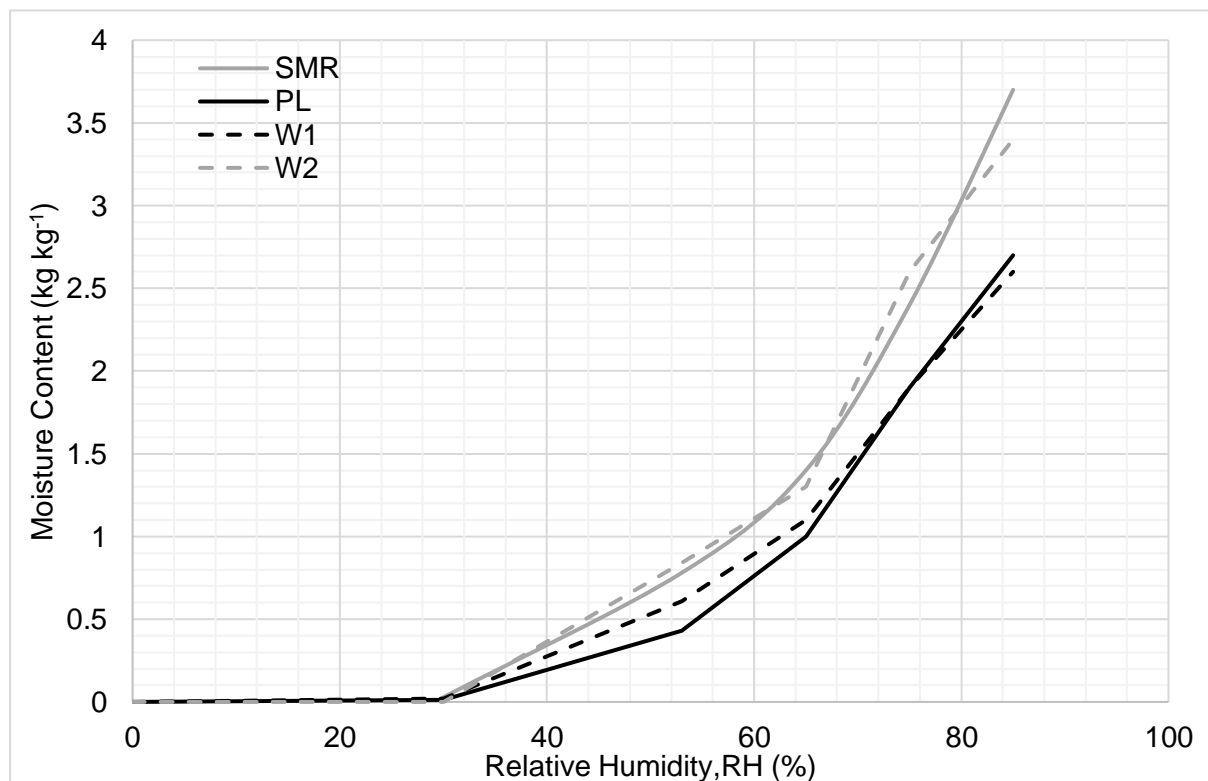


Figure 7.4. Adsorption curves for bio-earth mortar composites.

Over the course of the experiment it can be demonstrated that the incorporation of fibres increases the rate in which the mortars adsorb water molecules. This is particularly highlighted as above 30% RH sample begin to increase in moisture content with this rapidly increasing from approximately 65% RH. This is inline with the behaviour demonstrated within 2.5.3.

Within Figure 7.4., it is illustrated that the largest adsorption during isothermal moisture content over all the composites is SMR and the lowest is PL. W2 has similar adsorption across the range of RH but not as great as SMR. Over the service range of RH it is important to understand that Figure 7.4 also demonstrates the availability of materials to be able to accept

water molecules over this range. Due to the polarised nature of water molecules, van der Waal forces ensure the water molecules are adsorbed into the composite. To have more adsorption within the sample it could be suggested that to continually adsorb over such a large range of RH, SMR and W2 have a larger quantity of van der Waal sites due to both the bio-fibre and earth mortar matrix.

Further works should be done in order to understand the effect desorption has on the quantity of hysteresis in addition to true a classification of the hysteresis loop as per IUPAC classification loops (IUPAC, (1986) and Thommes et al. (2015)). This would further aid the understanding of the pore structure within the composite. Many different theories contribute to the understanding of what sorption hysteresis is. As explored in (Hill, Norton and Newman, 2009a), the isothermal sorption/desorption characteristics of natural fibres and identified that the extent of hysteresis relies upon the specific fibre type examined. Jiang et al. (2019) outlined that there is limited research on the mechanisms behind moisture sorption in specifically plant based bio-materials. It was explored in (Karoglou et al., 2005) the sorption isotherms of common building materials were examined and it was identified that all building materials even those non bio-based experience hysteresis phenomena.

Research by Skaar (1984) outlined that within cellulose based materials capillary suction starts at higher RH because of nanopores within the cell wall, yet the quantity, arrangement and the mechanisms for adsorbing water is yet to be fully understood. Jiang et al. (2019) states that during adsorption after the first and subsequent cycles, hysteresis has been examined within the sample. However, when considering these materials when combined into an earth mortar matrix it is evident that this is also true. The research conducted by Jiang et al (2019) also demonstrated the top layer of these cellulose based materials that the binding force with initial layer of water was stronger but weaker for subsequent layers.

Figures 3.10a to 3.10u demonstrates when samples have a higher relative humidity their storage capacity alters as water moves through the different pores within the composite. At these different relative humidities it has also been explored that this alters the materials thermal conductivity and other thermal properties. When relative humidity increases, pores that were previously occupied by air is replaced by water where water has a higher thermal conductivity. This filling of the pores and particularly the interconnected pores is problematic as the mechanisms within earth based construction in section 2.5.4.1. will create 'blocking' within the pore structure and facilitate hysteresis (Rouquerol, 2014).

7.4.3. Latent heat of sorption

By casting the thermocouples to within the mortar matrix and on the surface within this experimentation (due to the hygrothermal nature of these materials), any potential latent heat can be attributed to the changing state of water molecules (Hens, 2017). Figures 7.5. to 7.8. demonstrates the temperature that has been recorded for the first 24 hour cycle at the surface and 15mm below the surface of samples. From these Figures the adsorption and the further evaporation of water molecules, from varying hygrothermal environments has resulted in a latent heat exchange. This will also have a significant effect on the balance of heat within the sample as identified in Kraniotis et al. (2016).

Due to the relationship between moisture and heat transfer in hygroscopic materials, as the accumulation of condensation of moisture increases as does indoor temperature and vice versa for evaporation of moisture. As outlined in Hameury (2005) water condenses from vapour to liquid phase, heat is released at 2501kJ/kg vapour condensing at 0°C (Latent heat of vapourisation). However, within standard room temperatures varying from 10-25°C reduces the latent heat of vapourisation to approximately 2477.7 – 2441.7 kJ/kg. Understanding the role of latent heat within these hygroscopic materials is imperative for their full utilisation. The factors which affect the latent heat of moisture within a samples depends on the addition of latent heat of vapourisation and differential heat of condensation – which has been explored in the literature for building materials (Mavrigiannaki and Ampatzi, 2016).

Figures 7.5. and 7.6. demonstrate the differences in temperature for M1 PL, W1, SMR and W2 where all mortars demonstrated dynamic temperature change. For all Figures, there are three distinguished regions where latent heat varies. The first occurs during the first hour probably due to mass sample stabilisation, the second during the first 8 hours and then the desorption during the next 16 hours. These samples were tested under the same dynamic hygrothermal conditions of 8 hours at 75% RH and 16 hours at 53% RH which is reflected within the temperature changes in the figures – similar to that of James et al. (2010) PL and W1 exhibit the centre of the sample demonstrating a greater temperature than that of the surface. This is shown throughout the first 24 hours of the experiment, where there is constant heat flow release from the sample. Conversely, within Figures 7.7. and 7.8. SMR and W2 demonstrate that the surface temperature is higher than in the centre of the sample showing heat flow absorption into the sample.

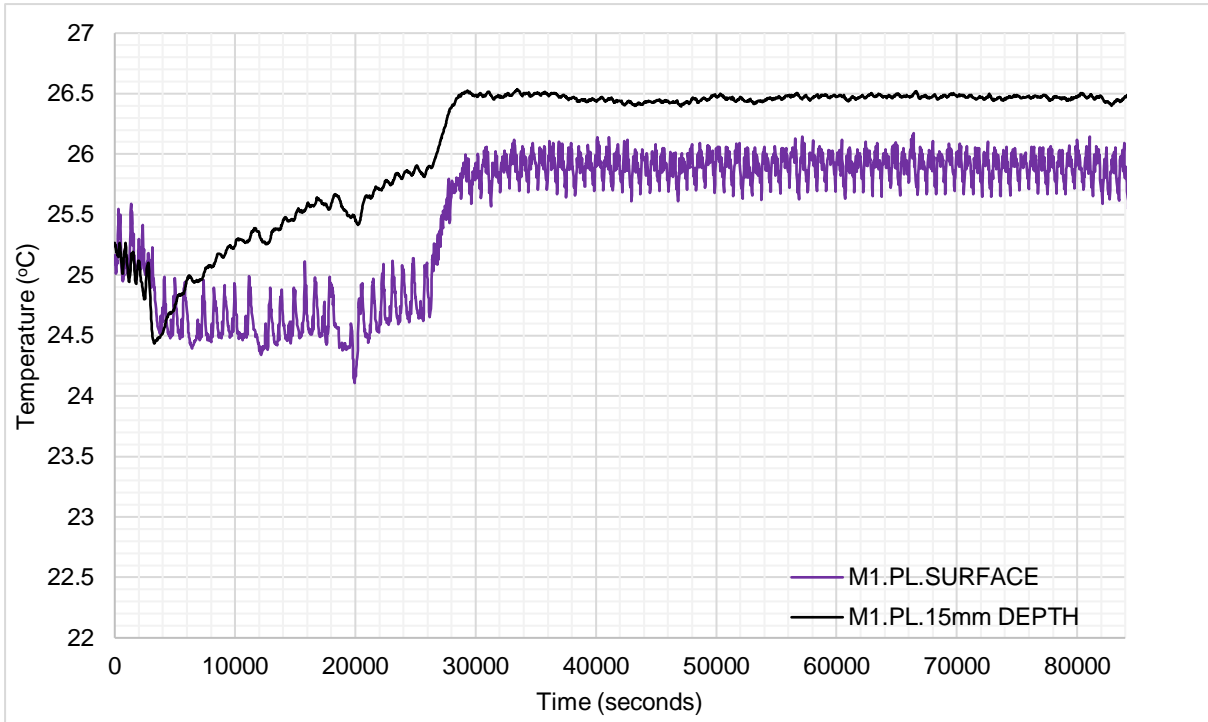


Figure 7.5. Dynamic temperature variation of M1 PL for cycle 1.

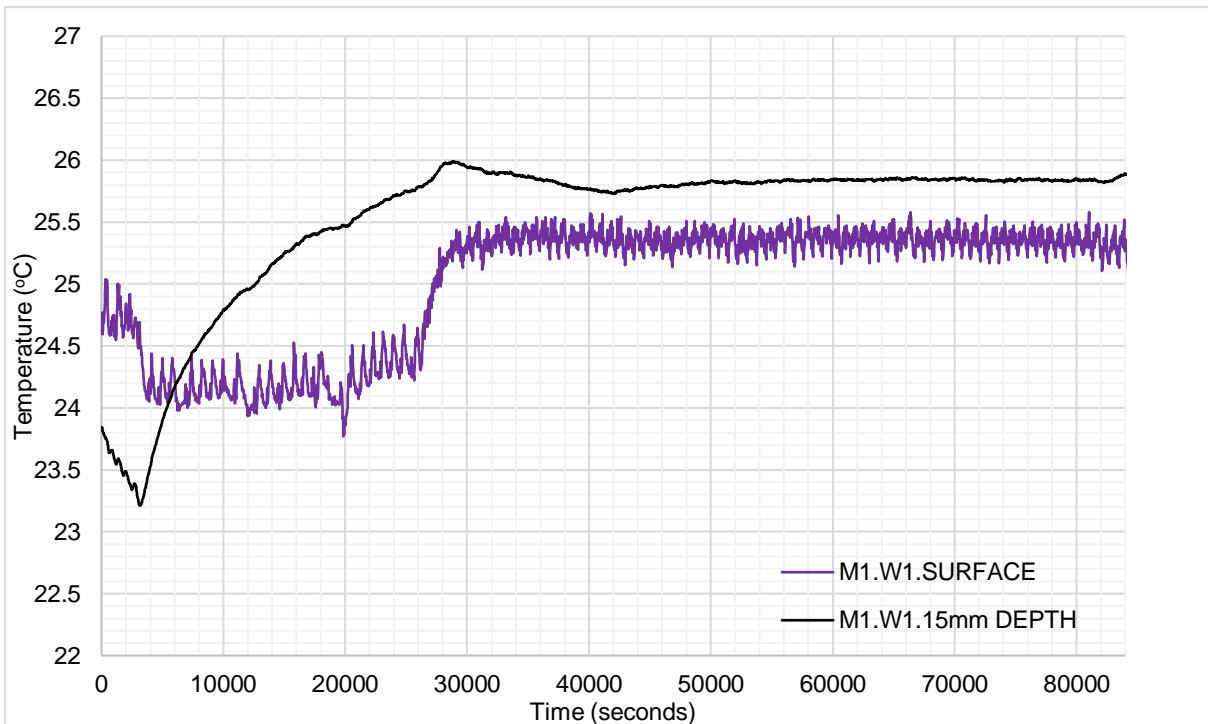


Figure 7.6. Dynamic temperature variation of M1 W1 for cycle 1.

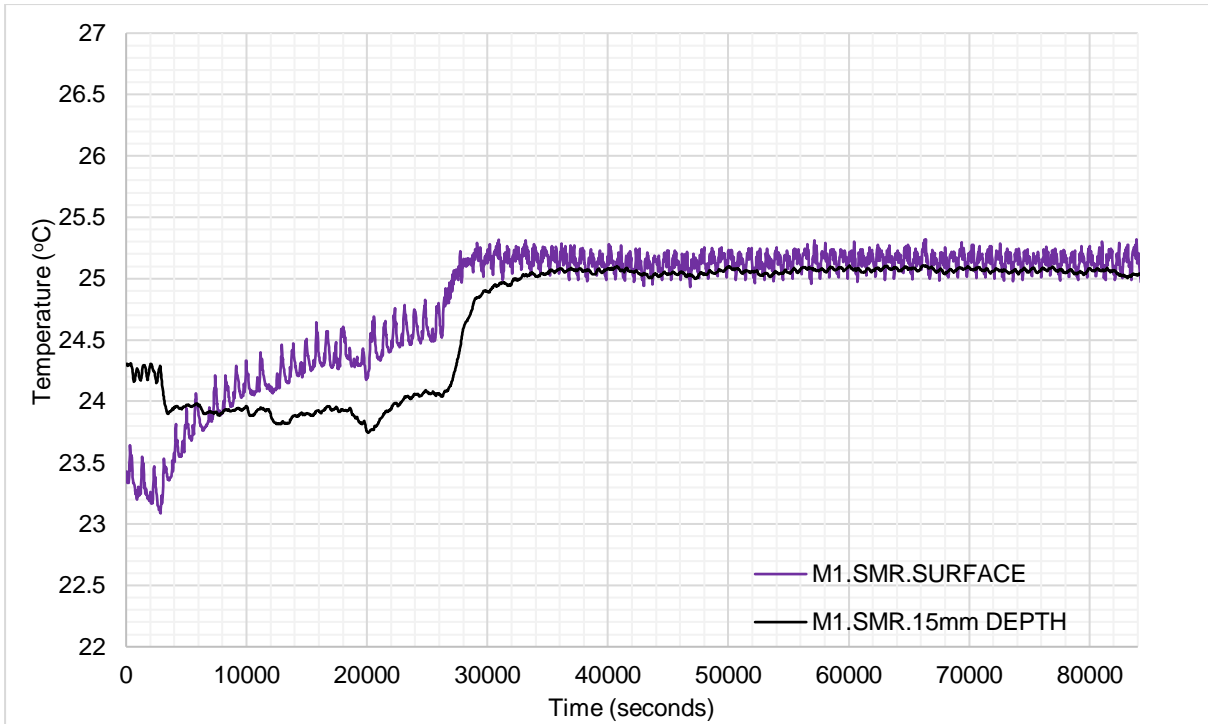


Figure 7.7. Dynamic temperature variation of M1 SMR for cycle 1.

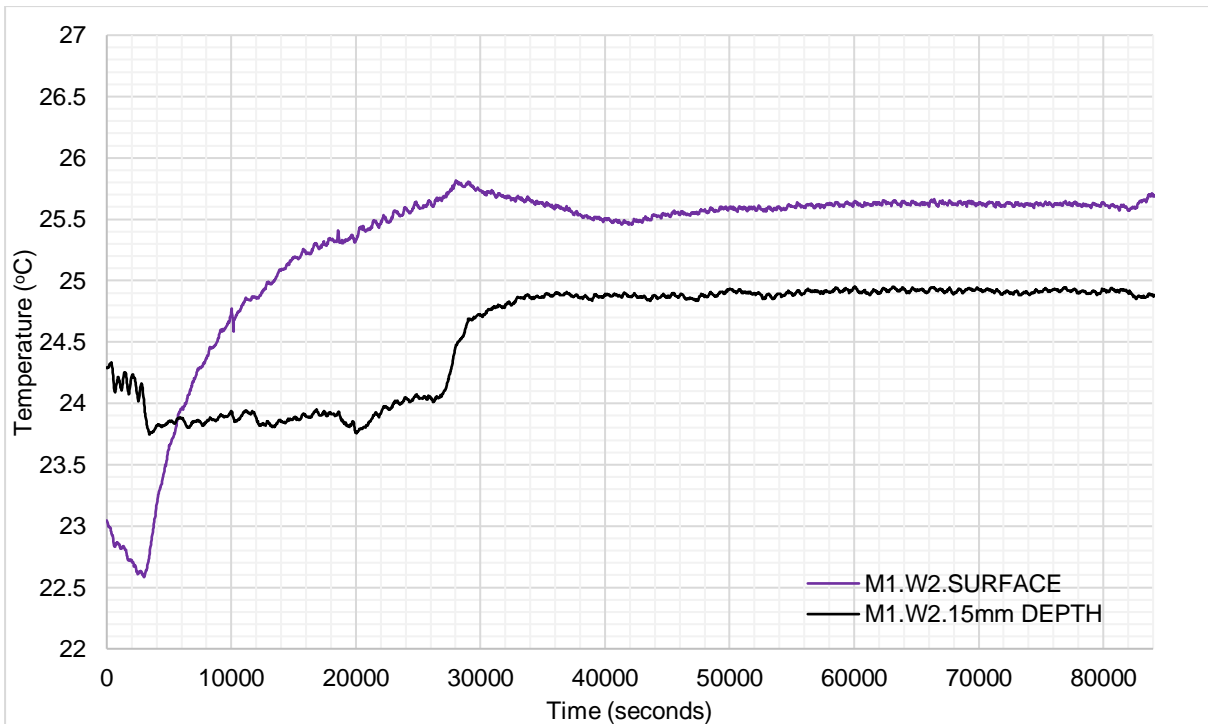


Figure 7.8. Dynamic temperature variation of M1 W2 for cycle 1.

Further Figures 7.9. to 7.12. represent the dynamic temperature change in the samples after 21 cycles of 24 hours.

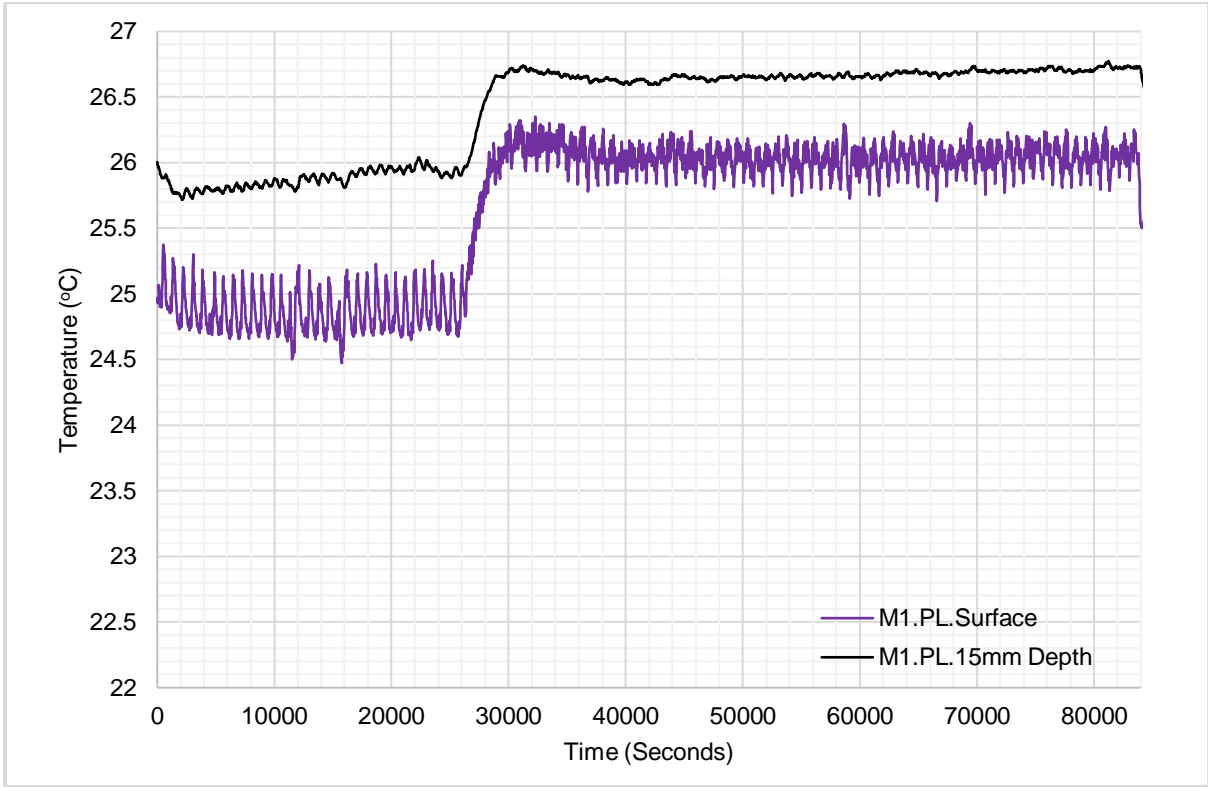


Figure 7.9. Dynamic temperature variation of M1 PL for cycle 21.

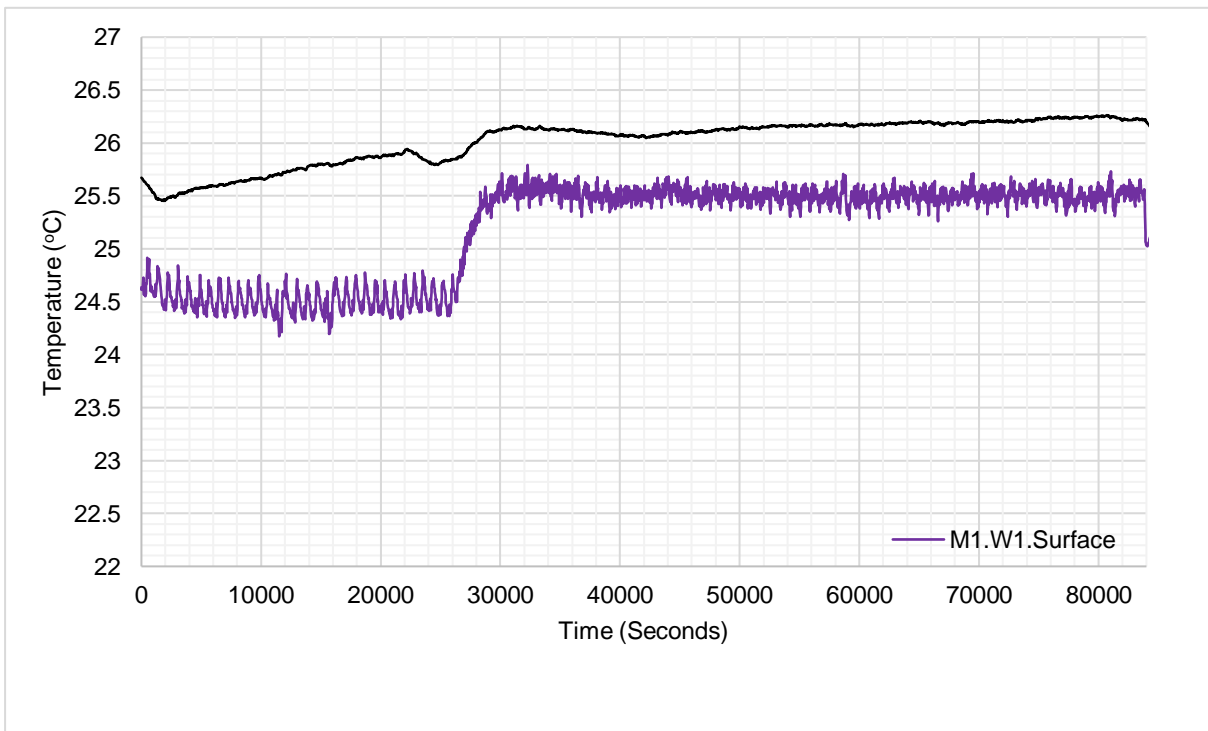


Figure 7.10. Dynamic temperature variation of M1 W1 for cycle 21

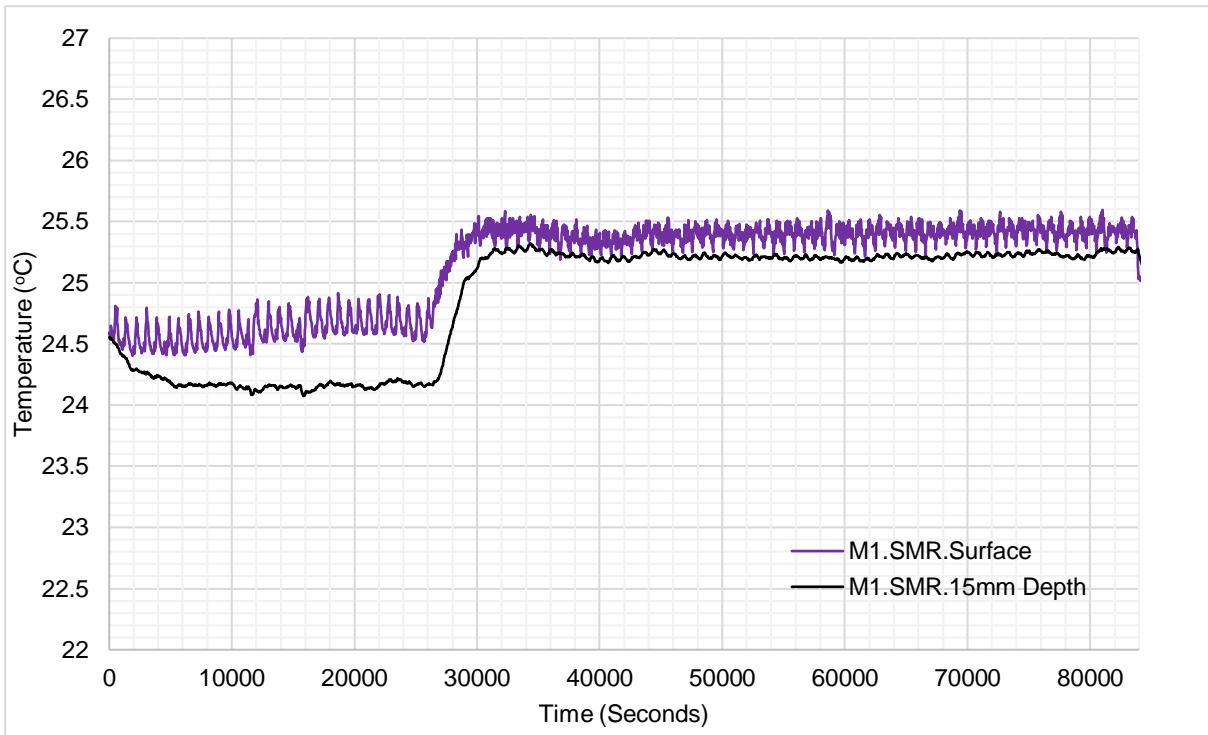


Figure 7.11. Dynamic temperature variation of M1 SMR for cycle 21.

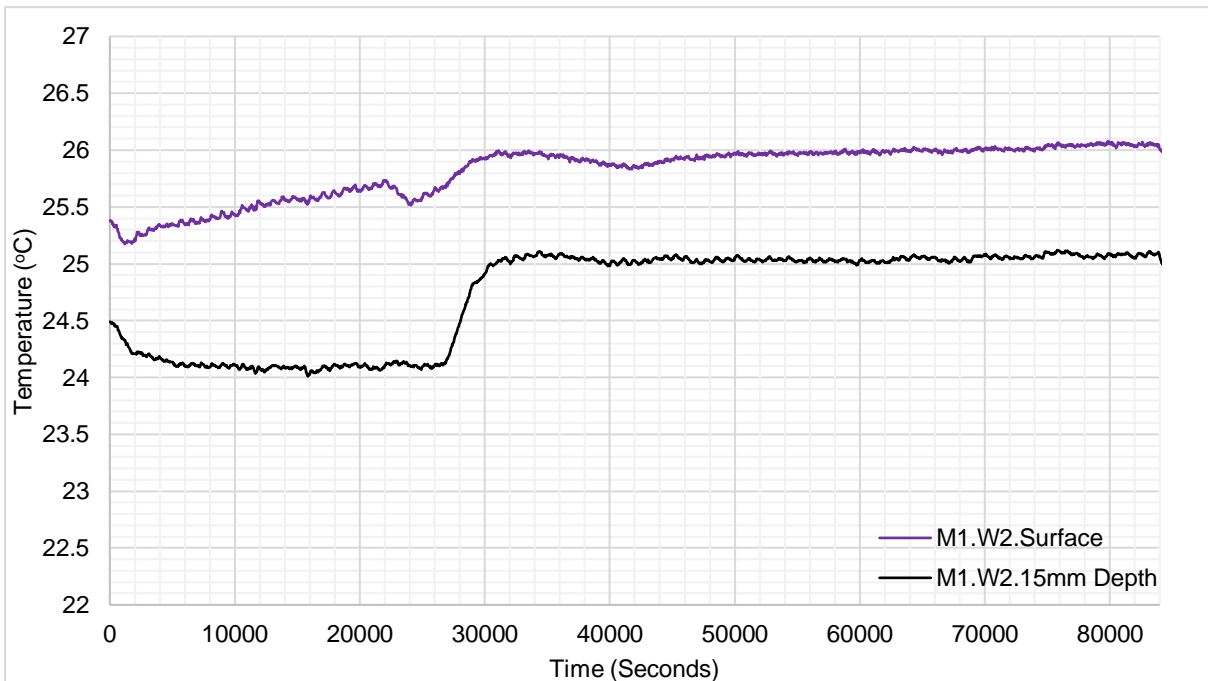


Figure 7.12. Dynamic temperature variation of M1 W2 for cycle 21.

From the initial cycle (Figure 7.5. to 7.8.) the adsorption period and a consistent increase in temperature is demonstrated. However, when considering the shape of the adsorption temperature after 21 cycles it is clear that the temperature evolution is more defined between the two phases. For the first cycle in the adsorption phase the temperature seemed to rise linearly throughout the experiment but after 21 cycles the difference between two RHs is more of a clear step change in temperature difference.

To understand the relationship between the two thermocouples within the earth based composite throughout the full 21 cycles, the surface minus the centre of the sample was plotted in Figure 7.13. There is a sustained difference in temperature of all the samples throughout the duration of the experiment and no external heat source – this temperature differential can be attributed to latent heat. Particularly obvious within samples after 21 cycles, the quantity of latent heat is larger of the adsorption period rather than desorption. The absorption period is 50% shorter than the desorption period at 8 hours compared to 16.

SMR (Figure 7.11) also has the lowest quantity of latent heat even by comparison to the plain sample as there is a sustained difference of approximately only 0.5°C between samples. This establishes that throughout the experiment SMR requires less heat energy in order for the water to change to and from vapour and liquid state. As outlined in Chapter 6 (section 6.4.2.1), it could be suggested that some composites have an innate ability to readily accept water molecules more than others due to the quantity of available hydroxyl groups.

For all samples within Figure 7.13, all adsorption phases are mirrored by a desorption phase and whilst these phases may have different temperatures, the relationship stays the same. It is clear that all adsorption and desorption phases PL and W1 demonstrate the opposite behaviour of SMR and W2. For W2 until cycle 9 and SMR until cycle 8, the surface temperature was greater than the centre of the sample. After cycle 8 the temperature at the centre of the surface is larger than the centre for two cycles and then returns to the surface temperature being greater. Conversely, PL and W1 have the same behaviour and very similar average desorption temperatures until cycle 7. However, after cycle 8 the temperature change for adsorption of PL is negligible and compared to the other composites with bio-fibres, the heat flow through the sample (even if its vapourisation or condensation) latent heat is consistently produced.

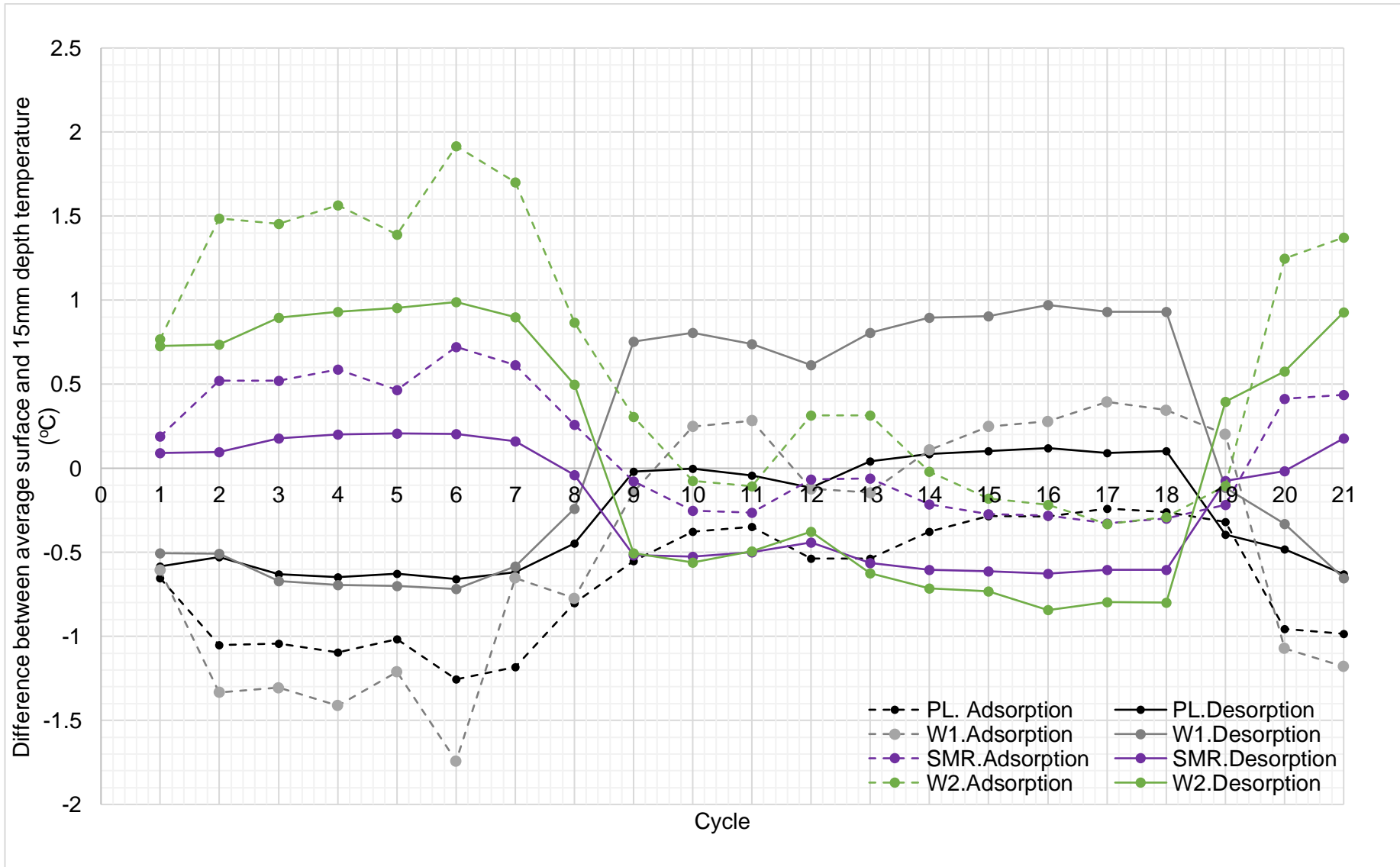


Figure 7.13. Difference between average surface and 15mm depth temperature over 21 cycles

Limitations of this study are the effect that the air velocity produced by the fans within the climatic chamber has on the surface temperature of the composites. It is also important to note that the thermocouples represent only one point in the centre of the material and whilst it gives a good indication of the properties, is not truly presentative for the whole surface.

7.5. Conclusion

Understanding the movement of water within the bio-fibre composites gives an assessment of their hygrothermal characteristics. Similar to the MBV performance, SMR has the largest WVP whereas PL has the largest water vapour diffusion resistance factor. The adsorption isotherm demonstrated that SMR has the largest moisture content over a wide range of RH, this ability to adsorb water molecules could be associated to the quantity of sites available for van der Waal forces to incorporate the vapour into liquid water. This chapter has also demonstrated the effective utilisation of using K type thermocouples to measure latent heat in an earth mortar composite from both the surface and at 50% depth. The measurement of latent heat is displayed from cycle 1 all the way through to cycle 21 at the end of the experiment.

Chapter 8 – Overall Conclusion

8.1. Main Findings

Understanding the typology of the housing stock within the UK demonstrates there is an urgent need for a retrofitting tool as a solution to reducing fuel demand and improving indoor moisture conditions. The mandate to reduce carbon emissions has given rise to the use of bio-based materials as structural and non-structural components in construction. As a solution, bio-based materials have established themselves as a superior to conventional construction materials due to their relative simplicity, abundance and ability to mimic (and if not better) the equivalent fossil fuel based materials (such as concrete or brick).

Through a literature review, it has shown that bio-based materials have good humidity buffering properties that reduce buildings energy use through both direct and indirect effects on heating load due to latent heat. In addition, the literature establishes that the fundamental differences between cellulose based and keratin-based materials are not fully realised and methodology for investigation is not understood or realised. The biochemical differences between hygric materials and their performance is not established as the literature loosely associates towards the latent heat and hydroxyl groups of the materials.

Ten samples of natural bio-based insulation materials and one thermoplastic polymer were analysed with and without the combination of earth-based mortars. Four different types of (Sheep and recycled) Wool insulation, Hemp, Wood Wool Board (WWB), Saw Mill Residue (SMR), Wood Fibre (WF), Straw, Insulated Cork Board (ICB) and Polyethylene terephthalate (PET) were analysed. Chapter 3 demonstrated using NORDTEST and ISO 21453 for Moisture Buffering Value (MBV) to create dynamic hygrothermal test conditions representative of a residential dwelling. Where MBV was used to act as a classification tool for materials performance, where the difference between values was negligible was not deemed to be enough to determine if a sample has better hygrothermal characteristics. Therefore, these materials were classified into one of three different groups; where Group 1 has the most efficient exchange of water molecules and Group 3 is the least. When considering the thermal conductivity of the materials within a dynamic environment, it was demonstrated that the bio-fibres can be classified into two different groups: those that exhibited identical and non-identical thermal conductivity values before and after hygrothermal cycling. Within the best performing 6 bio-based materials latent heat was observed.

Within Chapter 4, the thermal analysis of bio-fibres when stabilised at 53% and 75% RH demonstrates the effectiveness of this techniques for understanding how the hydroxyl groups within these materials affects hygrothermal performance. Further to this, the stabilisation period fosters an environment where the chemical stability can be analysed through each different physicochemical test. Differential Scanning Calorimetry (DSC) demonstrated only negligible differences between the two keratin based samples, whereas the cellulose based materials results varied. When utilising Fourier-transform infrared spectroscopy (FTIR) for the raw bio-based samples, the cellulose based samples had a greater overall crystallinity index and therefore was the most thermally stable. This thermal analysis of the microstructure of the fibres demonstrated their variation whilst visual analysis via SEM (Scanning Electron Microscopy) showed no clear and obvious differences between the conditioned samples.

Out of an initial 7 different mix designs, the best performing mix (Mix design 1) was selected. Within Chapter 5, the addition of fibres to mix 1 with SMR reduced the thermal conductivity of the mix design by 12.5% (from 0.2025 W/(m.K) to 0.1786 W/(m.K)). The analysis of these mixes also took into consideration the adsorption of water via capillary action comparing both the initial capillary coefficient but also the stabilised saturation absorption of each composite. Further to just analysing implicit MBV, the shape of the adsorption curves were observed to gain a better understanding of the dynamic way in which these hygroscopic material utilises the water exchange within its microstructure. This ability to exhibit hygrothermal characteristics is also linked to the network of pores within the composite. Properties of these materials such as dry bulk density, thermal conductivity and compressive strength all correlate a relationship for all samples.

The physicochemical analysis of earth mortar composites in Chapter 6 are fundamentally imperative to understanding their thermal performance. It is evident from the literature in Chapter 2 that there has been inadequate attention to understand the influence of earth and bio-fibres and their thermal properties. Traditionally, thermal method of analysis (using Thermogravimetric Analysis (TGA), Derivative Thermogravimetry (DTG) and DSC) has been for heritage and forensic investigation of the constituent elements of the material rather than a comparison with regards to their hygrothermal performance. Chapter 6 explored the calculation of Specific Heat Capacity (C_p) was also conducted to understand how the composites would be affected by a range of temperatures (5-50°C). This will give a better understanding of what is experienced by the composite over its service life, rather than within just a laboratory environment. For each temperature and stabilisation RH, C_p was calculated and the results it could be hypothesised that this is due to the materials ability to readily accept water molecules. Thus, the same material could have more 'free water' within the capillary pores of the material and upon heating is easier to release these water molecules. By

comparison, composites such as PL and SMR when stabilised at a higher RH present a larger Cp. Indicating that this material can not only initially adsorb water molecules but also bind to the samples chemical structure. Understanding the material properties via DSC has many benefits over other hygrothermal methods such as MBV not only for the speed of the test but also the multifaceted results per thermogram. When utilising FTIR (much like in Chapter 4 with the raw bio-fibres) demonstrates a change in the hydroxyl group peak for the composites.

Chapter 7 outlined that in addition to the works in Chapter 3, latent heat was apparent for all bio-fibre composites over 21, 24 hour cycles. It could therefore be suggested that to understand how latent heat affects a mortar composite, the use of K type thermo couples is an effect method to use. The adsorption isotherm demonstrated that SMR has the largest moisture content over a wide range of RH, this ability to adsorb water molecules could be associated to the quantity of sites available for van der Waal forces to incorporate the vapour into liquid water. By understanding how materials behaviour over a wide range of temperatures but also how they adsorb water vapour in a range of RH gives a better understanding of the 'real-life performance' of these composites.

Overall, this thesis has achieved the aims set out in section 1.2 and highlighted that utilising analytical chemistry and thermal methods of analysis for samples conditioned at different RH, gives a greater understanding of a building materials hygrothermal properties. The impact that this will carry within the industry is that the utilisation of analytical chemistry can help to identify and optimise hygrothermal behaviour of building materials. Particularly, this thesis will enable a better 'prescriptive' application of building materials for their service life temperature and RH.

8.2. Further Works

8.2.1 Laboratory Work

Other laboratory tests that could compliment the expansion of is work is an investigation into how pH values compare between the bio-fibre in earth and natural hydraulic lime matrixes. This experiment could contribute to the understanding of how overall compatibility affects the mix design. There also could be some potential that certain bio-based materials could be prescribed to different mix designs to boost their hygrothermal properties.

As stated throughout this thesis, the use of natural hydraulic lime within the mix design and samples were tested after 28 days where lime is acting as a filler rather than carbonating to its full-strength capacity. Therefore, it could be potential work stream to investigate how moisture movement throughout samples is affected by long-term carbonation of the

composite. This would be a long-standing experiment testing samples over a period of at least 6, 12, 18 and 24 months examining both microstructural and physical properties. It would be particularly interesting to understand how the pore networks develop.

Another potential aspect of investigation which the author has not found in the literature is a comparison of performance of either raw materials or bio-based composites comparing the orientation when in the climatic chamber. All samples within the literature in Chapter 2 put samples in horizontally but as the panel will be *in situ* vertically, it would be noteworthy to see the effects of this. Further to this, as a moisture buffering panel further investigation should be placed on the dimensionality of the panel (in terms of both overall surface area and thickness) and how this would affect its hygrothermal and physical properties. Further to the different sizes of the panel, the fungal and mould growth over the long term life span would be important for its impact on occupant health and IAQ.

In terms of having a greater understanding of how relative humidity and the movement of water affects the microstructure of each composite more investigation can be done utilising the DSC. This thesis has understood how Cp affects composites over a range of temperatures and at two different RH, however, it will be interesting to quantify the affect that the specific heat capacity of free and bound water has on the bio-earth mortar composites. The investigation that was carried out within this thesis demonstrated that there was a different in Cp due to the difference in RH. However, by investigating if this difference is free or bound water, it will help to examine how the sample interacts with the surrounding humid environment. Additionally, understanding the Cp of fossil fuel intensive building materials over varying service life conditions could boost the applicability of these materials, as if their performance was comparably superior it would give more evidence for their implementation.

8.2.2. Modelling

For this panel to be utilised within residential properties, the next step would be to understand how effective it would be in different construction typologies. This could be completed by *in situ* testing within the BRE exemplar houses on the LJMU campus. By utilising these houses it would give a better understanding as to how the panel would function within houses building within the conformity of building standards from 1920s, 1970s and 2010s. Another alternative is to use hygrothermal modelling software such as IES or WUFI to re-create these housing typologies but also where houses have been retrofitted and how this would have an effect on the panels performance. A comparison of performance from the laboratory to 'real life' homes and models would be intrinsically important. British weather is notoriously unpredictable so how this would affect the indoor thermal comfort and environment would be of experimental

interest. Another use of modelling would be to understand how the size of the panel affects its performance – complimented by laboratory and orientation tests this can be used to understand how the dimensional properties affect the samples characteristics.

References

(CCC), C.C.C. (2017) *UK Climate Change Risk Assessment 2017: Evidence Report* [online] Available at: <https://www.theccc.org.uk/uk-climate-change-risk-assessment-2017/> [Accessed: 02/10/2018]

(IUPAC), I.U.o.P.a.A.C. (1986) *Reporting Physisorption Data for Gas/Solid Systems with Special Reference to the Determination of Surface Area and Porosity* [online] Available at: <https://onlinelibrary.wiley.com/doi/abs/10.1002/9783527610044.hetcat0065> [Accessed: 10/07/2019]

Abdel-Kareem, O. and Elnagar, K. (2005) Non-Destructive Methods to Investigate the Deterioration Extent of Coptic Egyptian Textiles. *Journal of Textile and Apparel, Technology and Management*, 4 (1).

Achenza, M. and Fenu, L. (2006) On Earth Stabilization with Natural Polymers for Earth Masonry Construction. *Materials and Structures*, 39 (1), 21-27.

Achour, A., Ghomari, F. and Belayachi, N. (2017) Properties of cementitious mortars reinforced with natural fibers. *Journal of Adhesion Science and Technology*, 31 (17), 1938-1962.

Adl-Zarrabi, B. (2004) Determination of Thermal Properties of Wood and Wood Based Products by Using Transient Plane Source. *8th World Conference on Timber Engineering*, Lahti, Finland of Conference.

Aitkenhead. N., Barclay. W.J., Brandon. A., Chadwick. R.A., Chisholm. J.I., Cooper. A.H., Johnson. E.W., Chapman. G.R., Cheney. C.S., Colman. T.B., Highley. D.E., Lott. G.K., Pharaoh. T.C., Riley. N.J., Waters. C.N. and G., W. (2002) *Pennines and adjacent areas*. British Geological Survey.

Al-Horr, Y., Arif, M., Katafygiotou, M., Mazroei, A., Kaushik, A. and Elsarrag, E. (2016) Impact of indoor environmental quality on occupant well-being and comfort: A review of the literature. *International Journal of Sustainable Built Environment*, 5 (1), 1-11.

Al-Saadi, S.N. and Zhai, Z. (2013) Modeling phase change materials embedded in building enclosure: A review. *Renewable and Sustainable Energy Reviews*, 21, 659-673.

Alabdulkarem, A., Ali, M., Iannace, G., Sadek, S. and Almuzaiqer, R. (2018) Thermal analysis, microstructure and acoustic characteristics of some hybrid natural insulating materials. *Construction and Building Materials*, 187, 185-196.

Alén, R., Kuoppala, E. and Oesch, P. (1996) Formation of the main degradation compound groups from wood and its components during pyrolysis. *Journal of Analytical and Applied Pyrolysis*, 36 (2), 137-148.

Ali, M.E. and Alabdulkarem, A. (2017) On thermal characteristics and microstructure of a new insulation material extracted from date palm trees surface fibers. *Construction and Building Materials*, 138, 276-284.

Alvarez, V.A. and Vázquez, A. (2006) Influence of fiber chemical modification procedure on the mechanical properties and water absorption of MaterBi-Y/sisal fiber composites. *Composites Part A: Applied Science and Manufacturing*, 37 (10), 1672-1680.

Ammari, A., Bouassria, K., Zakham, N., Cherraj, M., Bouabid, H. and D'ouazzane, S. (2018) Durability of the earth mortar: Physico-chemical and mineralogical characterization for the reduction of the capillary rise. *MATEC Web of Conferences*, 149, 01024.

Amziane, S. and Sonebi, M. (2016) Overview on Biobased Building Material made with Plant Aggregate. *RILEM Technical Letters*, 1, 31-38.

Anatoly, C., Pavel, Z., Tatiana, C., Alexei, R. and Svetlana, Z. (2020) Water Vapor Permeability through Porous Polymeric Membranes with Various Hydrophilicity as Synthetic and Natural Barriers. *Polymers*, 12 (2).

Anggraini, V., Asadi, A., Huat, B.B.K. and Nahazanan, H. (2015) Effects of coir fibers on tensile and compressive strength of lime treated soft soil. *Measurement*, 59, 372-381.

Arnaud, L. (2009) Comparative Study of Hygrothermal Performances of Building Materials. *NOCMAT*,

Asdrubali, F., D'Alessandro, F. and Schiavoni, S. (2015) A review of unconventional sustainable building insulation materials. *Sustainable Materials and Technologies*, 4, 1-17.

Atkins, ICE and ITRC (2016) *National Needs Assessment. A Vision for the UK Infrastructure* [online] Available at: [https://www.ice.org.uk/getattachment/news-and-insight/policy/national-needs-assessment-a-vision-for-uk-infrastr/National-Needs-Assessment-PDF-\(1\).pdf.aspx#_ga=2.127230661.934501961.1595334399-1207784445.1579513083](https://www.ice.org.uk/getattachment/news-and-insight/policy/national-needs-assessment-a-vision-for-uk-infrastr/National-Needs-Assessment-PDF-(1).pdf.aspx#_ga=2.127230661.934501961.1595334399-1207784445.1579513083) [Accessed: 23/06/2018]

Aubert, J.E., Marcom, A., Oliva, P. and Segui, P. (2015) Chequered earth construction in south-western France. *Journal of Cultural Heritage*, 16 (3), 293-298.

B. Armel, L., Etienne, S., Marielle, A., Philippe, P., Leklou, N. and K.C.Dominique, S. (2017) Physicochemical and mechanical characterization of Benin's Kenaf fibers and its effect on the building compressed Earth Blocks (CEB) mechanical properties. *Research Journal of Chemical Sciences*, 7, 6-15.

Baetens, R., Jelle, B.P. and Gustavsen, A. (2010) Phase change materials for building applications: A state-of-the-art review. *Energy and Buildings*, 42 (9), 1361-1368.

Bakolas, A., Biscontin, G., Moropoulou, A. and Zendri, E. (1998) Characterization of structural Byzantine mortars by thermogravimetric analysis. *Thermochimica Acta*, 321, 151-160.

Balaras, C.A., Droutsas, K., Dascalaki, E. and Kontoyiannidis, S. (2005) Heating energy consumption and resulting environmental impact of European apartment buildings. *Energy & Buildings*, 37 (5), 429-442.

Ball, R., C. McIntosh, A. and Brindley, J. (1999) The role of char-forming processes in the thermal decomposition of cellulose. *Physical Chemistry Chemical Physics*, 1 (21), 5035-5043.

Barreca, F., Gabarron, A., Yepes, J. and Pastor, J. (2018) Innovative use of giant reed and cork residues for panels of buildings in Mediterranean area. *Resources Conservation and Recycling*, 140, 259-266.

Barreira, E., Delgado, J. and Freitas, V. (2014) Wetting and Drying Kinetics of Building Materials. In: (ed.). pp. 51-69.

Beall, F.C. (1971) Differential calometric analysis of wood and wood components. *Wood Science and Technology*, 5 (3), 159-175.

Belaadi, A., Bezazi, A., Bourchak, M., Scarpa, F. and Zhu, C. (2014) Thermochemical and statistical mechanical properties of natural sisal fibres. *Composites Part B*, 67, 481-489.

Benmansour, N., Agoudjil, B., Gherabli, A., Abdelhak, K. and Boudenne, A. (2014) Thermal and mechanical performance of natural mortar reinforced with date palm fibers for use as insulating materials in building. *Energy and Buildings*, 81, 98-104.

Bernal, S., Juenger, M., Ke, X., Matthes, W., Lothenbach, B., De Belie, N. and Provis, J. (2017) Characterization of supplementary cementitious materials by thermal analysis. *Materials and Structures*, 50 (1), 1-13.

Binici, H., Aksogan, O. and Demirhan, C. (2016) Mechanical, thermal and acoustical characterizations of an insulation composite made of bio-based materials. *Sustainable Cities and Society*, 20 (Supplement C), 17-26.

Bouguerra, A., Ledhem, A., de Barquin, F., Dheilily, R.M. and Quéneudec, M. (1998) Effect of microstructure on the mechanical and thermal properties of lightweight concrete prepared from clay, cement, and wood aggregates. *Cement and Concrete Research*, 28 (8), 1179-1190.

Bouhicha, M., Aouissi, F. and Kenai, S. (2005) Performance of composite soil reinforced with barley straw. *Cement and Concrete Composites*, 27 (5), 617-621.

Brás, A. and Gomes, V. (2015) LCA implementation in the selection of thermal enhanced mortars for energetic rehabilitation of school buildings. *Energy and Buildings*, 92 (Supplement C), 1-9.

Brás, A., Gonçalves, F. and Faustino, P. (2014) Economic evaluation of the energy consumption and thermal passive performance of Portuguese dwellings. *Energy and Buildings*, 76, 304-315.

Brás, A., Leal, M. and Faria, P. (2013) Cement-cork mortars for thermal bridges correction. Comparison with cement-EPS mortars performance. *Construction and Building Materials*, 49, 315-327.

BREEAM (2008) *Scheme Document - SD 5051* [online] Available at: https://tools.breeam.com/filelibrary/Technical%20Manuals/SD5051_4_1_BREEAM_Education_2008.pdf [Accessed: 21/10/2017]

Brígida, A.I.S., Calado, V.M.A., Gonçalves, L.R.B. and Coelho, M.A.Z. (2010) Effect of chemical treatments on properties of green coconut fiber. *Carbohydrate Polymers*, 79 (4), 832-838.

Brown, M. (1997) *Differential scanning calorimetry — An introduction for practitioners: G. Höhne, W. Hemminger and H.-J. Flammersheim, Springer — Verlag, Berlin, 1996 (ISBN: 3-340-59012-9). 222 pages, 136 figures and 13 tables. Price: DM 178,000 (hardback). 303: 117-117.*

BSI (1999a) *BS EN 1015-1:1999 - Methods of test for mortar for masonry. Determination of particle size distribution (by sieve analysis).*

BSI (1999b) *BS EN 1015-3:1999 - Methods of test for mortar for masonry. Determination of consistence of fresh mortar (by flow table).*

BSI (1999c) *BS EN 1015-10:1999 - Methods of test for mortar for masonry. Determination of dry bulk density of hardened mortar.*

BSI (1999d) *BS EN 1015-19:1999 - Methods of test for mortar for masonry. Determination of water vapour permeability of hardened rendering and plastering mortars.*

BSI (2010) *BS EN 15803:2009 - Conservation of cultural property. Test methods. Determination of water vapour permeability (δp).*

BSI (2017) *BS EN ISO 11272:2017 - Soil quality. Determination of dry bulk density.* British Standards Institute.

Bui, Q.-B., Morel, J.-C., Hans, S. and Meunier, N. (2009) Compression behaviour of non-industrial materials in civil engineering by three scale experiments: the case of rammed earth. *Materials and Structures*, 42 (8), 1101-1116.

Burke, M.J. and Stephens, J.C. (2018) Political power and renewable energy futures: A critical review. *Energy Research & Social Science*, 35, 78-93.

Cagnon, H., Aubert, J.E., Coutand, M. and Magniont, C. (2014) Hygrothermal properties of earth bricks. *Energy & Buildings*, 80, 208-217.

Cai, Y., Ke, H., Zhang, T., Qiao, H., Wang, H., Xu, Z., Wei, Q., Zhao, Y. and Fong, H. (2011) Preparation, Morphology and Properties of Electrospun Lauric Acid/PET Form-Stable Phase Change Ultrafine Composite Fibres. *Polymers and Polymer Composites*, 19, 773-780.

Callen, H.B. (1985) *Thermodynamics and an Introduction to Thermostatistics, 2nd Edition*. New York: Wiley.

Callum, A., Hill, C., Norton, A. and Newman, G. (2009) *NATURAL FIBRE INSULATION MATERIALS – THE IMPORTANCE OF HYGROSCOPICITY IN PROVIDING INDOOR CLIMATE CONTROL*. Conference: Proceedings of the 11th International Conference on Non-conventional Materials and Technologies (NOCMAT 2009) 6-9 September 2009, Bath, UK

Cancellieri, V., Cancellieri, D. and Leoni, E. (2009) Relation between forest fuels composition and energy emitted during their thermal degradation. *Journal of Thermal Analysis and Calorimetry*, 96, 293-300.

Cao, J. (1997) DSC Studies of the Melting Behavior of α -Form Crystallites in Wool Keratin. *Textile Research Journal*, v. 67 (no. 2), pp. 117-123-v.167 no.112.

Cao, J. (1999) Melting study of the α -form crystallites in human hair keratin by DSC1 Presented at the 9th Chinese Conference on Chemical Thermodynamics and Thermal Analysis (CTTA), Beijing, China, August 1998.1. *Thermochimica Acta*, 335 (1), 5-9.

Cao, J. and Bhojro, A. (2001) Structural Characterization of Wool by Thermal Mechanical Analysis of Yarns. *Textile Research Journal*, 71, 63-66.

Cardoso, C., Eires, R. and Camões, A. (2013) *Natural Fibre Reinforced Earth and Lime Based Mortars*.

Carter, H.G. and Kibler, K.G. (1978) Langmuir-Type Model for Anomalous Moisture Diffusion In Composite Resins. *Journal of Composite Materials*, 12 (2), 118-131.

CAT (2018) *Climate Action Tracker: Scaling up climate action - Key opportunities for transitioning to a zero emissions society* [online] Available at: https://climateactiontracker.org/documents/505/CAT_2018-12-06_ScalingUp_EU_FullReport.pdf [Accessed: 14/01/2019]

CCC (2019) *UK housing: Fit for the future?* [online] Available at: <https://www.theccc.org.uk/publication/uk-housing-fit-for-the-future/> [Accessed: 21/01/2020]

Céline, A., Fréour, S., Jacquemin, F. and Casari, P. (2013) Characterization and modeling of the moisture diffusion behavior of natural fibers. *Journal of Applied Polymer Science*, 130 (1), 297-306.

Céline, A., Gonçalves, O., Jacquemin, F. and Fréour, S. (2014) Qualitative and quantitative assessment of water sorption in natural fibres using ATR-FTIR spectroscopy. *Carbohydrate Polymers*, 101, 163-170.

CEN (1999a) *BS EN 1015-2:1999 - Methods of test for mortar for masonry. Bulk sampling of mortars and preparation of test mortars.*

CEN (1999b) *BS EN 1015-11:1999 - Methods of test for mortar for masonry. Determination of flexural and compressive strength of hardened mortar.*

CEN (2002) *BS EN 1015-18:2002 - Methods of test for mortar for masonry. Determination of water absorption coefficient due to capillary action of hardened mortar.*

CEN (2007) *BS EN 1936:2006 - Natural stone test methods. Determination of real density and apparent density, and of total and open porosity.*

CEN (2014) *BS EN 16575:2014 Bio-based products. Vocabulary* [online], Available at: <https://bsol.bsigroup.com/Bibliographic/BibliographicInfoData/00000000030277802> [Accessed: 17/09/2018]

CEN (2015) *BS EN 459-1:2015 - Building lime. Definitions, specifications and conformity criteria.*

CEN (2016) *BS EN ISO 12572:2016 - Hygrothermal performance of building materials and products. Determination of water vapour transmission properties. Cup method.*

Cerolini, S., D'Orazio, M., Di Perna, C. and Stazi, A. (2009) Moisture buffering capacity of highly absorbing materials. *Energy and Buildings*, 41 (2), 164-168.

Cetiner, I. and Shea, A.D. (2018) Wood waste as an alternative thermal insulation for buildings. *Energy and Buildings*, 168, 374-384.

Chabriac, P.-A., Morel, J.-C., Fabbri, A., J, B.-G. and Hans, S. (2013) *A case study of the hygrothermal behaviour of rammed earth building.*

Chao, H.J., Schwartz, J., Milton, D.K. and Burge, H.A. (2003) The work environment and workers' health in four large office buildings. *Environmental Health Perspectives*, 111 (9), 1242-1248.

Chen, Z. and Qin, M. (2016) Preparation and hygrothermal properties of composite phase change humidity control materials. *Applied Thermal Engineering*, 98, 1150-1157.

Church, J.S., Corino, G.L. and Woodhead, A.L. (1997) The analysis of Merino wool cuticle and cortical cells by Fourier transform Raman spectroscopy. *Biopolymers*, 42 (1), 7-17.

Claisse, P.A. (2014) *Transport properties of concrete : measurement and applications.* Waltham, Massachusetts : Woodhead Publishing.

Collet, F., Bart, M., Serres, L. and Miriel, J. (2008) Porous structure and water vapour sorption of hemp-based materials. *Construction and Building Materials*, 22, 1271-1280.

Collet, F. and Pretot, S. (2012) Experimental investigation of moisture buffering capacity of sprayed hemp concrete. *Construction and Building Materials*, 36, 58–65.

Commission, E. (2011) *A Roadmap for moving to a competitive low carbon economy in 2050* [online] Available at: <http://www.cbss.org/wp-content/uploads/2012/12/EU-Low-Carbon-Road-Map-2050.pdf> [Accessed: 19/10/2017]

Commission, E. (2017) *Review of the 2012 European Bioeconomy Strategy* [online] Available at: https://ec.europa.eu/research/bioeconomy/pdf/review_of_2012_eu_bes.pdf [Accessed: 10/19/2018]

Coppola, L., Bellezze, T., Belli, A., Bignozzi, M.C., Bolzoni, F., Brenna, A., Cabrini, M., Candamano, S., Cappai, M., Caputo, D., Carsana, M., Casnedi, L., Cioffi, R., Cocco, O., Coffetti, D., Colangelo, F., Coppola, B., Corinaldesi, V., Crea, F., Crotti, E., Daniele, V., De Gisi, S., Delogu, F., Diamanti, M.V., Di Maio, L., Di Mundo, R., Di Palma, L., Donnini, J., Farina, I., Ferone, C., Frontera, P., Gastaldi, M., Giosuè, C., Incarnato, L., Liguori, B., Lollini, F., Lorenzi, S., Manzi, S., Marino, O., Marroccoli, M., Mascolo, M.C., Mavilia, L., Mazzoli, A., Medici, F., Meloni, P., Merlonetti, G., Mobili, A., Notarnicola, M., Ormellese, M., Pastore, T., Pedefferri, M.P., Petrella, A., Pia, G., Redaelli, E., Roviello, G., Scarfato, P., Scoccia, G., Taglieri, G., Telesca, A., Tittarelli, F., Todaro, F., Vilardi, G. and Yang, F. (2018) Binders alternative to Portland cement and waste management for sustainable construction—part 1. *Journal of Applied Biomaterials & Functional Materials*, 16 (3), 186-202.

Corgié, S.C., Smith, H.M. and Walker, L.P. (2011) Enzymatic transformations of cellulose assessed by quantitative high-throughput fourier transform infrared spectroscopy (QHT-FTIR). *Biotechnology and Bioengineering*, 108 (7), 1509-1520.

Corti, C., Rampazzi, L., Bugini, R., Sansonetti, A., Biraghi, M., Castelletti, L., Nobile, I. and Orsenigo, C. (2013) Thermal analysis and archaeological chronology: The ancient mortars of the site of Baradello (Como, Italy). *Thermochimica Acta*, 572 (C), 71-84.

Costa, C., Rocha, F. and Velosa, A. (2016) Sustainability in earthen heritage conservation. *Geological Society Special Publications*, 416, 91.

Crawley, D. and Aho, I. (1999) Building environmental assessment methods: applications and development trends. *Building Research & Information*, 27 (4-5), 300-308.

Cui, Y., Xie, J., Liu, J. and Pan, S. (2015) Review of Phase Change Materials Integrated in Building Walls for Energy Saving. *Procedia Engineering*, 121, 763-770.

D'Alessandro, F., Baldinelli, G., Bianchi, F., Sambuco, S. and Rufini, A. (2018) Experimental assessment of the water content influence on thermo-acoustic performance of building insulation materials. *Construction and Building Materials*, 158, 264-274.

Dai, D. and Fan, M. (2010) Characteristic and Performance of Elementary Hemp Fibre. *Materials Sciences and Applications*, 01, 336-342.

Darling, E.K., Cros, C.J., Wargocki, P., Kolarik, J., Morrison, G.C. and Corsi, R.L. (2012) Impacts of a clay plaster on indoor air quality assessed using chemical and sensory measurements. *Building and Environment*, 57, 370-376.

Delgado, J.M.P.Q., Ramos, N.M.M. and De Freitas, V.P. (2006) Can Moisture Buffer Performance be Estimated from Sorption Kinetics? *Journal of Building Physics*, 29 (4), 281-299.

Deliski, N. (2011) Transient Heat Conduction in Capillary Porous Bodies In: (ed.) *Convection and Conduction Heat Transfer*. InTech.

Di Bella, G., Fiore, V., Galtieri, G., Borsellino, C. and Valenza, A. (2014) Effects of natural fibres reinforcement in lime plasters (kenaf and sisal vs. Polypropylene). *Construction and Building Materials*, 58, 159-165.

Di Foggia, G. (2018) Energy efficiency measures in buildings for achieving sustainable development goals. *Heliyon*, 4 (11), e00953.

DIN (2013) *DIN 18947:2013- 08: Earth plasters – terms and definitions, requirements, test methods* [online], Available at: <https://www.beuth.de/en/standard/din-18947/188145543>

[Accessed: 16/02/2019]

Dove, C.A., Bradley, F.F. and Patwardhan, S.V. (2016) Seaweed biopolymers as additives for unfired clay bricks. *Materials and Structures*, 49 (11), 4463-4482.

Eid, J. (2018) New construction material based on raw earth: cracking mechanisms, corrosion phenomena and physico-chemical interactions. *European Journal of Environmental and Civil Engineering*, 22 (12), 1522-1537.

El-Amoudy, E.S. and Osman, E.M. (2012) Thermal stability and fastness properties of wool fabric dyed with an ecofriendly natural dye "sambucus nigra" under the effect of different mordants. *Applied Chemistry*, 44C, 7080-7085.

El Hajam, M., Idrissi Kandri, N., Harrach, A., El khomsi, A. and Zerouale, A. (2019) Physicochemical characterization of softwood waste "Cedar" and hardwood waste "Mahogany": comparative study. *Materials Today: Proceedings*, 13, 803-811.

Ellis, P.R. (2000) Analysis of mortars (to include historic mortars) by differential thermal analysis. *Historic Mortars, Characteristics and Tests, Proceedings, RILEM Publications*.

Elsen, J. (2006) Microscopy of historic mortars—a review. *Cement and Concrete Research*, 36, 1416-1424.

Emirođlu, M., Yalama, A. and Erdođdu, Y. (2015) Performance of ready-mixed clay plasters produced with different clay/sand ratios. *Applied Clay Science*, 115, 221-229.

Engelund, E.T., Thygesen, L.G., Svensson, S. and Hill, C.A.S. (2013) A critical discussion of the physics of wood–water interactions. *Wood Science and Technology*, 47 (1), 141-161.

Fabbri, A. and Morel, J.-C. (2016) Earthen Materials and Constructions. In: Sharma, K. H. B. (ed.) *Nonconventional and Vernacular Construction Materials: Characterisation, Properties and Applications*. Woodhead Publishing.

Fabbri, A., Morel, J.-C. and Gallipoli, D. (2018) Assessing the performance of earth building materials: a review of recent developments. *RILEM Technical Letters*, 3, 46-58.

Fadele, O., Oguocha, I.N.A., Odeshi, A.G., Soleimani, M. and Tabil, L.G. (2019) Effect of chemical treatments on properties of raffia palm (*Raphia farinifera*) fibers. *Cellulose*, 26 (18), 9463-9482.

Fairbridge, C. and Ross, R.A. (1978) A kinetic and surface study of the thermal decomposition of cellulose powder in inert and oxidizing atmospheres. *Journal of Applied Polymer Science*, 22 (2), 497-510.

Fan, M., Dai, D. and Huang, B. (2012) 3 Fourier Transform Infrared Spectroscopy for Natural Fibres. *Fourier Transform-Materials Analysis*.

Faria, P., Dias, I., Jamú, N. and Silva, V. (2015) Air lime–earth blended mortars - Assessment on fresh state and workability. *Earthen Architecture: Past, Present and Future - Proceedings of the International Conference on Vernacular Heritage, Sustainability and Earthen Architecture.*, pp. 133-138

Faria, P., Santos, T. and Aubert, J.-E. (2016) Experimental Characterization of an Earth Eco-Efficient Plastering Mortar. *Journal of Materials in Civil Engineering*, 28 (1).

Fatma, N., Allègue, L., Salem, M., Zitoune, R. and Zidi, M. (2019) The effect of doum palm fibers on the mechanical and thermal properties of gypsum mortar. *Journal of Composite Materials*, 53 (19), 2641-2659.

Feng, C., Meng, Q., Feng, Y. and Janssen, H. (2015) Influence of Pre-conditioning Methods on the Cup Test Results. *Energy Procedia*, 78, 1383-1388.

Fengel, D. (1989) *Wood chemistry, ultrastructure, reactions*. Berlin New York: Berlin New York : Walter de Gruyter.

Ferraro, J.R. and Basile, L.J. (1978) *Fourier transform infrared spectroscopy applications to chemical systems. Volume 1*. New York: New York : Academic Press.

Forouharshad, M., Montazer, M., Moghadam, M.B. and Saligheh, O. (2011) Flame retardant wool using zirconium oxychloride in various acidic media optimized by RSM. *Thermochimica Acta*, 516 (1-2), 29-34.

Frankeová, D. and Slížková, Z. (2016) Determination of the pozzolanic activity of mortar's components by thermal analysis. *An International Forum for Thermal Studies*, 125 (3), 1115-1123.

Fratini, F., Pecchioni, E., Rovero, L. and Tonietti, U. (2011) The earth in the architecture of the historical centre of Lamezia Terme (Italy): Characterization for restoration. *Applied Clay Science*, 53 (3), 509-516.

Frost, R.L. and Vassallo, A.M. (1996) The Dehydroxylation of the Kaolinite Clay Minerals using Infrared Emission Spectroscopy. *Clays and Clay Minerals*, 44 (5), 635-651.

Galán-Marín, C., Rivera-Gómez, C. and Petric, J. (2010) Clay-based composite stabilized with natural polymer and fibre. *Construction and Building Materials*, 24 (8), 1462-1468.

Gallagher, W. (2005) FTIR Analysis of Protein Structure, Chem 455, Biochemistry Lab II - Synthesis and Characterisation of Amyloid Fibril - Forming Peptides - Manuals. *Polymer International of Conference*.

Garside, P. and Wyeth, P. (2003) Identification of Cellulosic Fibres by FTIR Spectroscopy I: Thread and Single Fibre Analysis by Attenuated Total Reflectance. *Studies in Conservation*, 48.

Gašparovič, L., Koreňová, Z. and Jelemenský, Ľ. (2010) Kinetic study of wood chips decomposition by TGA. *Chemical Papers*, 64 (2), 174-181.

Ge, H., Yang, X., Fazio, P. and Rao, J. (2014) Influence of moisture load profiles on moisture buffering potential and moisture residuals of three groups of hygroscopic materials. *Building and Environment*, 81 (Supplement C), 162-171.

Ghavami, K., Toledo Filho, R.D. and Barbosa, N.P. (1999) Behaviour of composite soil reinforced with natural fibres. *Cement and Concrete Composites*, 21 (1), 39-48.

Gibson, P.W. (2011) Effect of Wool Components in Pile Fabrics on Water Vapor Sorption, Heat Release and Humidity Buffering. *Journal of Engineered Fibers and Fabrics*, 6 (1), 155892501100600102.

Giesekam, J. and Pomponi, F. (2017) Embodied carbon dioxide assessment in buildings: guidance and gaps. *Engineering Sustainability*.

Giesekam, J., Tingley, D.D. and Cotton, I. (2018) Aligning carbon targets for construction with (inter)national climate change mitigation commitments. *Energy and Buildings*, 165, 106-117.

Gomes, M.G., Flores-Colen, I., Manga, L.M., Soares, A. and de Brito, J. (2017) The influence of moisture content on the thermal conductivity of external thermal mortars. *Construction and Building Materials*, 135, 279-286.

Gomes, M.I., Faria, P. and Gonçalves, T.D. (2018) Earth-based mortars for repair and protection of rammed earth walls. Stabilization with mineral binders and fibers. *Journal of Cleaner Production*, 172, 2401-2414.

González-Díaz, E. and Alonso-López, J.-M. (2017) Characterization by thermogravimetric analysis of the wood used in Canary architectural heritage. *Journal of Cultural Heritage*, 23, 111-118.

Gourlay, E., Glé, P., Marceau, S., Foy, C. and Moscardelli, S. (2017) Effect of water content on the acoustical and thermal properties of hemp concretes. *Construction and Building Materials*, 139, 513-523.

Government, H.M. (2019) *English Energy Housing Survey 2017-18* [online] Available at: <https://www.gov.uk/government/statistics/english-housing-survey-2018-energy-report> [Accessed: 01/02/2020]

Government, H. (2019a) *English Housing Survey 2017-18* [online] Available at: <https://www.gov.uk/government/collections/english-housing-survey#2017-to-2018> [Accessed: 19/02/2020]

Government, H.M. (2008) *The Climate Change Act 2008* [online] Available at: <https://www.legislation.gov.uk/ukpga/2008/27/contents> [Accessed: 27/09/2017]

Government, H.M. (2013a) *Construction 2025* [online] Available at: <https://www.gov.uk/government/publications/construction-2025-strategy> [Accessed: 11/10/2017]

Government, H.M. (2013b) *Infrastructure Carbon Review* [online] Available at: <https://www.gov.uk/government/publications/infrastructure-carbon-review> [Accessed: 26/09/2017]

Government, H.M. (2016) *Government Construction Strategy 2016-2020* [online] Available at: <https://www.gov.uk/government/publications/government-construction-strategy-2016-2020> [Accessed: 12/10/2017]

Government, H.M. (2019b) *Energy Performance of Buildings Certificates Statistical Release Q4 2018: England and Wales* [online] Available at: https://assets.publishing.service.gov.uk/government/uploads/system/uploads/attachment_data/file/756229/EPB_Cert_Statistics_Release_Qtr_3_2018_rev2.pdf [Accessed: 22/08/2019]

Grilo, J., Faria, P., Veiga, R., Santos Silva, A., Silva, V. and Velosa, A. (2014) New natural hydraulic lime mortars – Physical and microstructural properties in different curing conditions. *Construction and Building Materials*, 54 (C), 378-384.

Guo, A., Aamiri, O.B., Satyavolu, J. and Sun, Z. (2019) Impact of thermally modified wood on mechanical properties of mortar. *Construction and Building Materials*, 208, 413-420.

Gur'ev, V. and Khainer, S. (1999) Correlation of structure and thermal conductivity of highly disperse porous-fiber materials under variations of temperature and moisture. *Glass and Ceramics*, 56 (11-12), 364-368.

Hackitt, J. (2018) *Independent Review of Building Regulations and Fire Safety: Final Report* [online] Available at: https://assets.publishing.service.gov.uk/government/uploads/system/uploads/attachment_data/file/707785/Building_a_Safer_Future_-_web.pdf [Accessed: 29/11/2019]

Haines, P., Laye, P.G., Warrington, S.B., Thermal Methods, G., Heal, G.R., Price, D.M. and Wilson, R. (2002) *Principles of Thermal Analysis and Calorimetry*. Cambridge, UNITED KINGDOM: Royal Society of Chemistry.

Haiping, Y., Yan, R., Chen, H., Lee, D. and Zheng, C. (2007) Characteristics of Hemicellulose, Cellulose and Lignin Pyrolysis. *Fuel*, 86, 1781-1788.

Hall, M. and Allinson, D. (2009a) Analysis of the hygrothermal functional properties of stabilised rammed earth materials. *Building & Environment*, 44 (9), 1935-1943.

Hall, M. and Allinson, D. (2009b) Assessing the effects of soil grading on the moisture content-dependent thermal conductivity of stabilised rammed earth materials. *Applied Thermal Engineering*, 29 (4), 740-747.

Hall, M.R., Casey, S.P., Loveday, D.L. and Gillott, M. (2013) Analysis of UK domestic building retrofit scenarios based on the E.ON Retrofit Research House using energetic hygrothermics simulation – Energy efficiency, indoor air quality, occupant comfort, and mould growth potential. *Building and Environment*, 70, 48-59.

Haly, A.R., Abu-Isa, I. and Dole, M. (1965) Specific heat of wool in the temperature range –50 to 100°C. *Journal of Applied Polymer Science*, 9 (3), 893-902.

Hamard, E., Cazacliu, B., Razakamanantsoa, A. and Morel, J.-C. (2016) Cob, a vernacular earth construction process in the context of modern sustainable building. 106.

Hameury, S. (2005) Moisture buffering capacity of heavy timber structures directly exposed to an indoor climate: a numerical study. *Building & Environment*, 40 (10), 1400-1413.

Hawes, D.W., Feldman, D. and Banu, D. (1993) Latent heat storage in building materials. *Energy and Buildings*, 20 (1), 77-86.

He, C., Osbaeck, B. and Makovicky, E. (1995) Pozzolanic Reactions of six Principal Clay Minerals: Activation, Reactivity Assessments and Technological Effects. *Cement and Concrete Research - CEM CONCR RES*, 25, 1691-1702.

Hens, H.S.L.C. (2017) *Building physics : heat, air and moisture : fundamentals and engineering methods with examples and exercises*. Third edition. ed. Berlin, Germany : Ernst & Sohn, a Wiley brand.

Hill, C., Norton, A. and Newman, G. (2009a) The Water Vapor Sorption Behavior of Natural Fibers. *Journal of Applied Polymer Science*, 112, 1524-1537.

Hill, C.A.S., Norton, A. and Newman, G. (2009b) The water vapor sorption behavior of natural fibers. *Journal of Applied Polymer Science*, 112 (3), 1524-1537.

Hill, C.A.S., Ramsay, J., Keating, B., Laine, K., Rautkari, L., Hughes, M. and Constant, B. (2012) The water vapour sorption properties of thermally modified and densified wood. *Journal of Materials Science*, 47 (7), 3191-3197.

Hinterstoisser, B. and Salmén, L. (1999) Two-dimensional step-scan FTIR: a tool to unravel the OH-valency-range of the spectrum of Cellulose I. *Cellulose*, 6 (3), 251-263.

Holcroft, N. (2016) *Natural Fibre Insulation Materials for Retrofit Application*thesis.

Holcroft, N. and Shea, A. (2013) *Moisture buffering and latent heat effects in natural fibre insulation materials*.

Holcroft, N. and Shea, A. (2015) *Effect of compaction on moisture buffering of hemp-lime insulation*.

Hori, R. and Sugiyama, J. (2003) A combined FT-IR microscopy and principal component analysis on softwood cell walls. *Carbohydrate Polymers*, 52 (4), 449-453.

Housing Europe (2018) Decarbonisation of the building stock: a two-front battle. *Energy*.

Hsieh, S.-H., Huang, Z.K., Huang, Z.Z. and Tseng, Z.S. (2004) Antimicrobial and physical properties of woolen fabrics cured with citric acid and chitosan. *Journal of Applied Polymer Science*, 94 (5), 1999-2007.

Huang, P., Zeidler, A., Chang, W.-s., Ansell, M.P., Chew, Y.M.J. and Shea, A. (2016) Specific heat capacity measurement of *Phyllostachys edulis* (Moso bamboo) by differential scanning calorimetry. *Construction and Building Materials*, 125, 821-831.

Huijbregts, Z., Schellen, H., van Schijndel, J. and Ankersmit, B. (2015) Modelling of heat and moisture induced strain to assess the impact of present and historical indoor climate conditions on mechanical degradation of a wooden cabinet. *Journal of Cultural Heritage*, 16 (4), 419-427.

Huson, M., Church, J. and Heintze, G. (2001) Spectroscopy, microscopy and thermal analysis of the bi-modal melting of Merino wool. *Wool Technology and Sheep Breeding*, 50, 64-75.

Hussain, A., Calabria-Holley, J., Lawrence, M., Ansell, M.P., Jiang, Y., Schorr, D. and Blanchet, P. (2019) Development of novel building composites based on hemp and multi-functional silica matrix. *Composites Part B: Engineering*, 156, 266-273.

ISO, I.O.f.S. (2000) *BS EN ISO 12570:2000 Hygrothermal performance of building materials and products. Determination of moisture content by drying at elevated temperature* [online], Available at: <https://bsol.bsigroup.com/Bibliographic/BibliographicInfoData/000000000030350192> [Accessed: 15/04/2020]

ISO, I.O.f.S. (2008) *Hygrothermal performance of building materials and products - Determination of moisture adsorption/desorption properties in response to humidity* [online], Available at: <https://www.iso.org/standard/42167.html> [Accessed: 21/06/2019]

ISO, I.O.f.S. (2013) *BS EN ISO 12571:2013 Hygrothermal performance of building materials and products. Determination of hygroscopic sorption properties* [online], Available at: <https://bsol.bsigroup.com/Bibliographic/BibliographicInfoData/000000000030259581> [Accessed: 19/08/2019]

ISO, I.O.f.S. (2014) *BS EN ISO 113757-4 Plastics - Differential scanning calorimetry (DSC) Part 4: Determination of specific heat capacity* [online], Available at: <https://bsol.bsigroup.com/Bibliographic/BibliographicInfoData/000000000030291940> [Accessed: 24/04/2018]

ISO, I.O.f.S. (2016) *12572:2016 Hygrothermal performance of building materials and products — Determination of water vapour transmission properties* [online], Available at: <https://www.iso.org/standard/64988.html> [Accessed: 24/04/2018]

Iucolano, F., Liguori, B. and Colella, C. (2013) Fibre-reinforced lime-based mortars: A possible resource for ancient masonry restoration. *Construction and Building Materials*, 38, 785-789.

Jabbar, A., Militky, J., Wiener, J., Javaid, M. and Rwawiire, S. (2016) Tensile, surface and thermal characterization of jute fibres after novel treatments. *Indian J. Fibre Text. Tes.*, 41 (3), 249-254.

James, C., Simonson, C.J., Talukdar, P. and Roels, S. (2010) Numerical and experimental data set for benchmarking hygroscopic buffering models. *International Journal of Heat and Mass Transfer*, 53 (19), 3638-3654.

Janssen, H. and Roels, S. (2009) Qualitative and quantitative assessment of interior moisture buffering by enclosures. *Energy & Buildings*, 41 (4), 382-394.

Jerman, M. and Černý, R. (2012) Effect of moisture content on heat and moisture transport and storage properties of thermal insulation materials. *Energy and Buildings*, 53, 39-46.

Jiang, Y., Lawrence, M., Hussain, A., Ansell, M. and Walker, P. (2019) Comparative moisture and heat sorption properties of fibre and shiv derived from hemp and flax. *Cellulose*, 26 (2), 823-843.

JIS (2002) A1470: Test method of adsorption/desorption efficiency for building materials to regulate an indoor humidity – part 1: response method of humidity [online], Available at: https://infostore.saiglobal.com/en-us/standards/jis-a-1470-1-2002-625121_SAIG_JSA_JSA_1462327/ [Accessed: 15/08/2019]

John, M. and D. Anandjiwala, R. (2008) *Recent developments in chemical modification and characterization of natural fiber-reinforced composites*.

Johnson, N.A.G., Wood, E.J., Ingham, P.E., McNeil, S.J. and McFarlane, I.D. (2003) Wool as a Technical Fibre. *The Journal of The Textile Institute*, 94 (3-4), 26-41.

Jones, D. and Brischke, C. (2017) *Performance of Bio-based Building Materials*. Elsevier Science.

Jorgensen, W.L. and Madura, J.D. (1985) Temperature and size dependence for Monte Carlo simulations of TIP4P water. *Molecular Physics*, 56 (6), 1381-1392.

Joshi, S.V., Drzal, L.T., Mohanty, A.K. and Arora, S. (2004) Are natural fiber composites environmentally superior to glass fiber reinforced composites? *Composites Part A: Applied Science and Manufacturing*, 35 (3), 371-376.

Karamanos, A., Hاديarakou, S. and Papadopoulos, A.M. (2008) The impact of temperature and moisture on the thermal performance of stone wool. *Energy and Buildings*, 40 (8), 1402-1411.

Karatasios, I., Amenta, M., Tziotziou, M. and Kilikoglou, V. (2012) The Effect of Relative Humidity on the Performance of Lime-Pozzolan Mortars. In: (ed.). pp. 309-318.

Karoglou, M., Moropoulou, A., Maroulis, Z.B. and Krokida, M.K. (2005) Water Sorption Isotherms of Some Building Materials. *Drying Technology*, 23 (1-2), 289-303.

Kelly, M.J. (2009) Retrofitting the existing UK building stock. *Building Research & Information*, 37 (2), 196-200.

Koch, P. (1969) Specific heat of oven-dry spruce pine wood and bark. , . *Wood Science*, 4, 203-214.

KONDO, T. (1997) The assignment of IR absorption bands due to free hydroxyl groups in cellulose. *Cellulose*, 4 (4), 281.

Korjenic, A., Petránek, V., Zach, J. and Peterková, J. (2011) Development and performance evaluation of natural thermal-insulation materials composed of renewable resources. *Energy and Buildings*, 43, 2518-2523.

Kraniotis, D., Nore, K., Brückner, C. and Nyrud, A. (2016) Thermography measurements and latent heat documentation of Norwegian spruce (*Picea abies*) exposed to dynamic indoor climate. *Official Journal of the Japan Wood Research Society*, 62 (2), 203-209.

Krausmann, F., Wiedenhofer, D., Lauk, C., Haas, W., Tanikawa, H., Fishman, T., Miatto, A., Schandl, H. and Haberl, H. (2017) Global socioeconomic material stocks rise 23-fold over the 20th century and require half of annual resource use. *Proceedings of the National Academy of Sciences*, 114 (8), 1880-1885.

Kunkel, S., Kontonasiou, E., Arcipowska, A., Mariottini, F. and Atanasiu, B. (2015) *Indoor air quality, thermal comfort and daylight. Analysis of residential buildings regulations in eight EU member states.*

Labat, M. (2016) From the experimental characterization of the hygrothermal properties of straw-clay mixtures to the numerical assessment of their buffering potential. *Building & Environment*, 97, 69-82.

Laborel-Préneron, A., Aubert, J.E., Magniont, C., Tribout, C. and Bertron, A. (2016) Plant aggregates and fibers in earth construction materials: A review. *Construction and Building Materials*, 111 (Supplement C), 719-734.

Lanas, J., Sirera, R. and Alvarez, J.I. (2006) Study of the mechanical behavior of masonry repair lime-based mortars cured and exposed under different conditions. *Cement and Concrete Research*, 36 (5), 961-970.

Langley, K.D. and Kennedy, T.A. (1981) The Identification of Specialty Fibers. *Textile Research Journal*, 51 (11), 703-709.

Latif, E., Lawrence, R.M.H., Shea, A.D. and Walker, P. (2018) An experimental investigation into the comparative hygrothermal performance of wall panels incorporating wood fibre, mineral wool and hemp-lime. *Energy and Buildings*, 165, 76-91.

Latif, E., Tucker, S., Ciupala, M.A., Wijeyesekera, D.C., Newport, D.J. and Pruteanu, M. (2016) Quasi steady state and dynamic hygrothermal performance of fibrous Hemp and Stone Wool insulations: Two innovative laboratory based investigations. *Building and Environment*, 95 (Supplement C), 391-404.

Lawrence, M., Shea, A., Walker, P. and de Wilde, P. (2013) Hygrothermal performance of bio-based insulation materials. *Proceedings of Institution of Civil Engineers: Construction Materials*, 166 (4), 257-263.

Lawrence, R.M., Mays, T.J., Rigby, S.P., Walker, P. and D'Ayala, D. (2007) Effects of carbonation on the pore structure of non-hydraulic lime mortars. *Cement and Concrete Research*, 37 (7), 1059-1069.

Ledhem, A., Dheilly, R.M., Benmalek, M.L. and Quéneudec, M. (2000) Properties of wood-based composites formulated with aggregate industry waste. *Construction and Building Materials*, 14 (6), 341-350.

Lelievre, D., Colinart, T. and Glouannec, P. (2014) Hygrothermal behavior of bio-based building materials including hysteresis effects: Experimental and numerical analyses. *Energy and Buildings*, 84 (Supplement C), 617-627.

Lengsfeld, K., Holm, A. and Krus, M. (2007) MOISTURE-BUFFERING EFFECT-EXPERIMENTAL INVESTIGATIONS AND VALIDATION.

Lewin, M. (2006) *Handbook of Fiber Chemistry*. Boca Raton: CRC Press.

Li, Q., Hurren, C. and Wang, X. (2019) CHANGES IN WOOL PROTEIN STRUCTURE AND FABRIC PROPERTIES WITH ULTRASONIC TREATMENT.

Lima, J., Faria, P. and Santos Silva, A. (2016) Earthen plasters based on illitic soils from Barrocal region of Algarve: contributions for building performance and sustainability.

Liu, L., Li, H., Lazzaretto, A., Manente, G., Tong, C., Liu, Q. and Li, N. (2017) The development history and prospects of biomass-based insulation materials for buildings. *Renewable and Sustainable Energy Reviews*, 69, 912-932.

Liu, X., Ma, X. and Zhang, B. (2016) Analytical Investigations of Traditional Masonry Mortars from Ancient City Walls Built during Ming and Qing Dynasties in China. *International Journal of Architectural Heritage*, 10 (5), 663-673.

Liu X., Ma N., Wen G. and X., W. (2008) FTIR Spectrum and Dye Absorption of Cashmere and Native Fine Sheep Wool,. *Proc. 4th Int. Cashmere Determination Techniques Symposium*,

Liu, Z., Jiang, Z., Fei, B. and Liu, X. (2013) Thermal Decomposition Characteristics of Chinese Fir. *BioResources*, 8 (4), 5014-5024.

Ma, X. (2018) Deterioration of Earthen Building Materials. In: (ed.) *The Encyclopedia of Archaeological Sciences*. Wiley.

Man, X., Haque, M.A. and Chen, B. (2019) Engineering properties and microstructure analysis of magnesium phosphate cement mortar containing bentonite clay. *Construction and Building Materials*, 227, 116656.

Maréchal, Y. and Chanzy, H. (2000) The hydrogen bond network in I β cellulose as observed by infrared spectrometry. *Journal of Molecular Structure*, 523 (1), 183-196.

Martí, M., Ramírez, R., Manich, A., Coderch, L. and L. Parra, J. (2007) Thermal analysis of merino wool fibres without internal lipids. *Journal of Applied Polymer Science*, 104, 545-551.

Marti, M., Ramirez, R., Manich, A., Coderch, L. and Parra, J. (2007) Thermal analysis of merino wool fibres without internal lipids. *Journal of Applied Polymer Science*, 104 (1), 545-551.

Martin, A., Martins, M., R.R.F. da Silva, O. and H.C. Mattoso, L. (2010) Studies on the thermal properties of sisal fiber and its constituents. *Thermochimica Acta*, 506, 14–19.

Maskell, D., Da Silva, C., Mower, K., Rana, C., Dengel, A., Ball, R., P Ansell, M., Walker, P. and Shea, A. (2015) PROPERTIES OF BIO-BASED INSULATION MATERIALS AND THEIR POTENTIAL IMPACT ON INDOOR AIR QUALITY. *First International Conference on Bio-based Building Materials*,

Maskell, D., Ferreira Pinto Da Silva, C., Mower, K., Cheta, R., Dengel, A., Ball, R., Ansell, M., Thomson, A., Peter, U. and Walker, P. (2017) Bio-based plaster for improved indoor air quality.

Mataalkah, F., Soroushian, P., Weerasiri, R. and Peyvandi, A. (2017) Development of indigenous binders as construction materials. *Construction Materials*, 172.

Mathis, D., Blanchet, P., Landry, V. and Lagièrre, P. (2019) Thermal characterization of bio-based phase changing materials in decorative wood-based panels for thermal energy storage. *Green Energy & Environment*, 4 (1), 56-65.

Mavrigiannaki, A. and Ampatzi, E. (2016) Latent heat storage in building elements: A systematic review on properties and contextual performance factors. *Renewable and Sustainable Energy Reviews*, 60, 852-866.

Mazhoud, B., Collet, F., Pretot, S. and Lanos, C. (2017) Development and hygric and thermal characterization of hemp-clay composite. *European Journal of Environmental and Civil Engineering*, 1-11.

McAlinden, B. (2015) *Embodied Energy and carbon* [online] Available at: <https://www.ice.org.uk/knowledge-and-resources/briefing-sheet/embodied-energy-and-carbon> [Accessed: 14/08/17]

McDonough, W. (2002) *Cradle to cradle : remaking the way we make things*. New York: New York : North Point Press.

McGregor, B.A., Liu, X. and Wang, X.G. (2018) Comparisons of the Fourier Transform Infrared Spectra of cashmere, guard hair, wool and other animal fibres. *The Journal of The Textile Institute*, 109 (6), 813-822.

McGregor, F., Fabbri, A., Ferreira, J., Simões, T., Faria, P. and Morel, J.-C. (2017) Procedure to determine the impact of the surface film resistance on the hygric properties of composite clay/fibre plasters. *Materials and Structures*, 50 (4), 193.

McGregor, F., Heath, A., Fodde, E. and Shea, A. (2014) Conditions affecting the moisture buffering measurement performed on compressed earth blocks. *Building and Environment*, 75 (Supplement C), 11-18.

McGregor, F., Heath, A., Maskell, D., Fabbri, A. and Morel, J.-C. (2016) A review on the buffering capacity of earth building materials. *Proceedings of Institution of Civil Engineers: Construction Materials*, 169 (5), 241-251.

Melià, P., Ruggieri, G., Sabbadini, S. and Dotelli, G. (2014) Environmental impacts of natural and conventional building materials: a case study on earth plasters. *Journal of Cleaner Production*, 80, 179-186.

Menasria, F., Perrot, A. and Rangeard, D. (2017) *MECHANICAL ENHANCEMENT OF CASTED AND COMPACTED EARTH-BASED MATERIALS BY SAND, FLAX FIBER AND WOVEN FABRIC OF FLAX*.

Merzoud, M., Fertikh, S. and Habita, M. (2011) Influence of absorption by immersion and capillary on the physico-mechanical properties of composites made from local natural fibers. *Rabat, INVACO2of Conference*.

Mesbah, M.A., Morel, J.-C., Walker, P. and Ghavami, K. (2004) Development of a Direct Tensile Test for Compacted Earth Blocks Reinforced with Natural Fibers. *Journal of Materials in Civil Engineering*, 16.

Micheal, M.N. and El-Zaher, N.A. (2003) Efficiency of ultraviolet/ozone treatments in the improvement of the dyeability and light fastness of wool. *Journal of Applied Polymer Science*, 90 (13), 3668-3675.

Middendorf, B., Hughes, J.J., Callebaut, K., Baronio, G. and Papayianni, I. (2005) Investigative methods for the characterisation of historic mortars—Part 1: Mineralogical characterisation. *Materials and Structures*, 38 (8), 761.

Millogo, Y., Hajjaji, M. and Ouedraogo, R. (2008) Microstructure and physical properties of lime-clayey adobe bricks. *Construction and Building Materials*, 22 (12), 2386-2392.

Millogo, Y. and Morel, J.-C. (2012) Microstructural characterization and mechanical properties of cement stabilised adobes. *Materials and Structures*, 45 (9), 1311-1318.

Millogo, Y., Morel, J.-C., Aubert, J.-E. and Ghavami, K. (2014) Experimental analysis of Pressed Adobe Blocks reinforced with Hibiscus cannabinus fibers. *Construction and Building Materials*, 52, 71-78.

Millogo, Y., Traoré, K., Ouedraogo, R., Kaboré, K., Blanchart, P. and Thomassin, J.H. (2008) Geotechnical, mechanical, chemical and mineralogical characterization of a lateritic gravels of Sapouy (Burkina Faso) used in road construction. *Construction and Building Materials*, 22 (2), 70-76.

Minke, G. (2006) *Building with earth : design and technology of a sustainable architecture*. Basel ; Boston: Basel ; Boston : Birkhauser-Publishers for Architecture.

Minke, G. (2013) *Building with earth : design and technology of a sustainable architecture*. 3rd ed. ed. Basel, Switzerland : Birkhäuser.

Moropoulou, A., Bakolas, A. and Anagnostopoulou, S. (2005) Composite materials in ancient structures. *Cement and Concrete Composites*, 27 (2), 295-300.

Moropoulou, A., Bakolas, A. and Bisbikou, K. (1995) Characterization of ancient, Byzantine and later historic mortars by thermal and X-ray diffraction techniques. *Thermochimica Acta*, 269, 779-795.

Morshed, M.M., Alam, M.M. and Daniels, S.M. (2010) Plasma treatment of natural jute fibre by rie 80 plus plasma tool. *Plasma Science and Technology*, 12 (3), 325-329.

Mukherjee, A. and Achal, V. (2015) *A BIOLOGICAL ROUTE FOR PRODUCING LOW ENERGY BINDERS*.

Müller, U., Miccoli, L. and Fontana, P. (2016) Development of a lime based grout for cracks repair in earthen constructions. *Construction and Building Materials*, 110, 323-332.

Naaman, A.E. and Najm, H. (1991) Bond-Slip Mechanisms of Steel Fibers in Concrete. *ACI Materials Journal*, 88 (2).

Naktode, P., Chaudhari, S.R. and Waghe, U.P. (2014) Evaluation of Lime for Use in Mortar. *International Journal of Engineering Research and Applications*, 4 (2), 70-75.

Navarro, L., de Gracia, A., Niall, D., Castell, A., Browne, M., McCormack, S.J., Griffiths, P. and Cabeza, L.F. (2016) Thermal energy storage in building integrated thermal systems: A review. Part 2. Integration as passive system. *Renewable Energy*, 85 (C), 1334-1356.

Neithalath, N. (2006) Analysis of moisture transport in mortars and concrete using sorption-diffusion approach. *ACI Materials Journal*, 103 (3), 209-217.

Nelson, M.L. and O'Connor, R.T. (1964) Relation of certain infrared bands to cellulose crystallinity and crystal latticed type. Part I. Spectra of lattice types I, II, III and of amorphous cellulose. *Journal of Applied Polymer Science*, 8 (3), 1311-1324.

Oates, J.A.H. (2007) Lime and Limestone: Chemistry and Technology, Production and Uses. In: (ed.). pp. 258-298.

Osanyintola, O.F. and Simonson, C.J. (2006) Moisture buffering capacity of hygroscopic building materials: Experimental facilities and energy impact. *Energy & Buildings*, 38 (10), 1270-1282.

Osman, E. and Abd El-Zaher, N. (2011) *Effect of Mordant Type on Thermal Stability and Fastness Properties of Silk Fabric Dyed with Natural Dye "Sambucus Nigra"*.

Owen, N.L. and Thomas, D.W. (1989) Infrared Studies of "Hard" and "Soft" Woods. *Applied Spectroscopy*, 43 (3), 451-455.

P.H.E. (2014) *Local action on health inequalities: Fuel poverty and cold home-related health problems Health Equity* [online]

Available at:
https://assets.publishing.service.gov.uk/government/uploads/system/uploads/attachment_data/file/357409/Review7_Fuel_poverty_health_inequalities.pdf

[Accessed: 03/08/2019]

Paama, L., Pitkanen, I., Ronkkomaki, H. and Peramaki, P. (1998) Thermal and infrared spectroscopic characterization of historical mortars. *Thermochim. Acta*, 320 (1-2), 127-133.

Pacheco-Torgal, F. and Jalali, S. (2012) Earth construction: Lessons from the past for future eco-efficient construction. *Construction and Building Materials*, 29, 512-519.

Padfield, T. (1998) The Role of Absorbent Building Materials in Moderating Changes of Relative Humidity.

Padfield, T. (1999) *The role of absorbent building materials in moderating changes of relative humidity*. Dep. of Struct. Eng and Materials, DTU, Rep. R54.

Palumbo, M. (2015) *Contribution to the development of new bio-based thermal insulation materials made from vegetal pith and natural binders: hygrothermal performance, fire reaction and mould growth resistancethesis*.

Palumbo, M., Lacasta, A.M., Giraldo, M.P., Haurie, L. and Correal, E. (2018) Bio-based insulation materials and their hygrothermal performance in a building envelope system (ETICS). *Energy and Buildings*, 174, 147-155.

Palumbo, M., Lacasta, A.M., Holcroft, N., Shea, A. and Walker, P. (2016) Determination of hygrothermal parameters of experimental and commercial bio-based insulation materials. *Construction and Building Materials*, 124 (Supplement C), 269-275.

Parsa, A.R. and Farshchi, M. (1996) Environmental regulations and the real estate industry. *Property Management*, 14 (1), 6-23.

Passer, A., Lasvaux, S., Allacker, K., Lathauwer, D., Spirinckx, C., Wittstock, B., Kellenberger, D., Gschösser, F., Wall, J. and Wallbaum, H. (2015) *Environmental product declarations entering the building sector: critical reflections based on 5 to 10 years experience in different European countries*.

Pavlik, Z., Žumár, J., Medved, I. and Černý, R. (2011) *Water Vapor Adsorption in Porous Building Materials: Experimental Measurement and Theoretical Analysis*.

Pelton, J.T. and McLean, L.R. (2000) Spectroscopic methods for analysis of protein secondary structure. *Anal Biochem*, 277 (2), 167-176.

Pérez-Lombard, L., Ortiz, J. and Pout, C. (2008) A review on buildings energy consumption information. *Energy and Buildings*, 40 (3), 394-398.

Perrot, A., Rangeard, D., Menasria, F. and Guihéneuf, S. (2018) Strategies for optimizing the mechanical strengths of raw earth-based mortars. *Construction and Building Materials*, 167, 496-504.

Pizzi, A. and Mittal, K.L. (2011) *Wood Adhesives*. London: CRC Press.

Poletto, M., Pistor, V., Santana, R. and Zattera, A. (2012) Materials Produced From Plant Biomass. Part II: Evaluation of Crystallinity and Degradation Kinetics of Cellulose. *Materials Research*, 15, 421-427.

Pooley, L.I., Abu-Bakar, A.S., Cran, M.J., Wadhvani, R. and Moinuddin, K.A.M. (2019) Measurements of specific heat capacity of common building materials at elevated temperatures: a comparison of DSC and HDA. *Journal of Thermal Analysis and Calorimetry*.

Popescu, C.M., Popescu, M.C., Singurel, G., Vasile, C., Argyropoulos, D.S. and Willfor, S. (2007) Spectral characterization of eucalyptus wood. *Appl Spectrosc*, 61 (11), 1168-1177.

Poyet, S. and Charles, S. (2009) Temperature dependence of the sorption isotherms of cement-based materials: Heat of sorption and Clausius–Clapeyron formula. *Cement and Concrete Research*, 39 (11), 1060-1067.

Price, D. and Horrocks, A.R. (2013) 1 - Combustion processes of textile fibres. In: Kilinc, F. S. (ed.) *Handbook of Fire Resistant Textiles*. Woodhead Publishing. pp. 3-25.

Prime, R.B., Bair, H.E., Vyazovkin, S., Gallagher, P.K. and Riga, A. (2008) Thermogravimetric Analysis (TGA). In: (ed.) *Thermal Analysis of Polymers*. pp. 241-317.

Qin, M., Belarbi, R., Ait-Mokhtar, A. and Nilsson, L.-O. (2009) Coupled heat and moisture transfer in multi-layer building materials. *Construction and Building Materials*, 23 (2), 967-975.

Qin, M., Walton, G., Belarbi, R. and Allard, F. (2011) Simulation of whole building coupled hygrothermal-airflow transfer in different climates. *Energy Conversion and Management*, 52 (2), 1470-1478.

Radmanović, K., Đukić, I. and Pervan, S. (2014) Specific Heat Capacity of Wood. *Drvna industrija*, 65, 151-157.

Rahman, M., Hamdan, S. and Hui, J. (2017) Differential Scanning Calorimetry (DSC) and Thermogravimetric Analysis (TGA) of Wood polymer nanocomposites. *MATEC Web of Conferences*, 87, 03013.

Raj, S., Mohammad, S., Das, R. and Saha, S. (2017) Coconut fibre-reinforced cement-stabilized rammed earth blocks. *World Journal of Engineering*, 14, 208-216.

Ramacciotti, M., Rubio, S., Gallelo, G., Lezzerini, M., Columbu, S., Hernandez, E., Morales-Rubio, A., Pastor, A. and de la Guardia, M. (2018) - Chronological Classification of Ancient Mortars Employing Spectroscopy and Spectrometry Techniques: Sagunto (Valencia, Spain) Case.

Ramamurthi, D. and Sophia, M. (2016) A Review on Modified Lime based Mortars - an Alternative to Cement Mortar. *International Journal for Innovative Research in Science & Technology*, 2 (12), 350-356.

Rampazzi, L., Colombini, M.P., Conti, C., Corti, C., Lluveras-Tenorio, A., Sansonetti, A. and Zanaboni, M. (2016) Technology of Medieval Mortars: An Investigation into the Use of Organic Additives. *Archaeometry*, 58 (1), 115-130.

Rana, R., Langenfeld-Heyser, R., Finkeldey, R. and Polle, A. (2010) FTIR spectroscopy, chemical and histochemical characterisation of wood and lignin of five tropical timber wood species of the family of Dipterocarpaceae. *Wood Science and Technology*, 44 (2), 225-242.

Rawat, S.P.S. and Khali, D.P. (1999) Studies on adsorption behaviour of water vapour in lignin using the Brunauer-Emmett-Teller theory. *Holz als Roh- und Werkstoff*, 57 (3), 203-204.

Rawlins, B.G., McGrath, S.P., Scheib, A.J., Breward, N., Cave, M., Lister, T.R., Ingham, M., Gowing, C. and Carter, S. (2012) *The advanced soil geochemical atlas of England and Wales*. Keyword: British Geological Survey.

Rees, O.J. (2010) *Fourier transform infrared spectroscopy developments, techniques and applications*. New York: New York : Nova Science Publishers.

Reh, U., Kraepelin, G. and Lamprecht, I. (1986) Use of Differential Scanning Calorimetry for Structural Analysis of Fungally Degraded Wood. *Applied and Environmental Microbiology*, 52 (5), 1101.

Rode, C., Peuhkuri, R., Svennberg, K., Ojanen, T., Mukhopadhyaya, P., Kumaran, M. and W. Dean, S. (2007) *Moisture Buffer Value of Building Materials*.

Rode, C., Peuhkuri, R.H., Hansen, K.K., Time, B., Svennberg, K., Arfvidsson, J. and Ojanen, T. (2005) *NORDTEST Project on Moisture Buffer Value of Materials*. 47-52.

Roels, S. and Janssen, H. (2006) *A Comparison of the Nordtest and Japanese Test Methods for the Moisture Buffering Performance of Building Materials*.

Romano, A., Bras, A., Grammatikos, S., Shaw, A. and Riley, M. (2019a) Dynamic behaviour of bio-based and recycled materials for indoor environmental comfort. *Construction and Building Materials*, 211, 730-743.

Romano, A., Brás, A., Grammatikos, S., Shaw, A. and Riley, M. (2019b) BIO-BASED AND RECYCLED MATERIALS: CHARACTERISATION AND HYGROTHERMAL ASSESSMENT FOR PASSIVE RELATIVE HUMIDITY MANAGEMENT. *International Conference of Bio-based Building Materials (ICBBM)*, Belfast, UK, June 26th – 28th 2019 of Conference.

Romano, A., Brás, A., Grammatikos, S., Wylie, S., Kot, P. and Shaw, A. (2018) On the development of self-controlled bio-based panels for building's thermal management. *European Conference on Composite Materials*

Rosa, M.E. and Fortes, M.A. (1993) Water Absorption by Cork. *Wood and Fiber Science*, 25 (4), 339-348.

Rouquerol, F. (2014) *Adsorption by powders and porous solids : principles, methodology and applications*. 2nd ed. ed. Kidlington, Oxford : Academic Press.

Růžička, J. and Diviš, J. (2019) *The Influence of Building Materials on Relative Humidity of Internal Microclimate*. 290: 012029.

Sabbioni, C., Bonazza, A. and Zappia, G. (2002) Damage on hydraulic mortars: The Venice Arsenal. *J. Cult. Herit.*, 3 (1), 83-88.

Santarelli, M., Sbardella, F., Zuena, M., Tirillo, J. and Sarasini, F. (2014) Basalt fiber reinforced natural hydraulic lime mortars: A potential bio-based material for restoration. *Materials and Design*, 63 (C), 398-406.

Scarlat, N., Dallemand, J.-F., Monforti-Ferrario, F. and Nita, V. (2015) The role of biomass and bioenergy in a future bioeconomy: Policies and facts. *Environmental Development*, 15 (Supplement C), 3-34.

Schwanninger, M., Rodrigues, J., Pereira, H. and Hinterstoisser, B. (2004) Schwanninger M , Rodriguez JC , Pereira H , Hinterstoisser B . Effects of short-time vibratory ball milling on the shape of FT-IR spectra of wood and cellulose. *Vibr. Spec. Vibrational Spectroscopy*, 36, 23-40.

Segetin, M., Jayaraman, K. and Xu, X. (2007) Harakeke reinforcement of soil–cement building materials: Manufacturability and properties. *Building and Environment*, 42 (8), 3066-3079.

Ševčík, R., Šašek, P., Pérez-Estébanez, M. and Viani, A. (2015) Chemical Analysis of Historic Lime Mortars: Role of Sample Preparation. *Advanced Materials Research*, 1100, 17-20.

Shafizadeh, F. and Bradbury, G.W. (1979) A kinetic model for pyrolysis of cellulose. *Journal of Applied Polymer Science*, 23 (11), 3271-3280.

Shea, A., Wall, K. and Walker, P. (2013) *Evaluation of the thermal performance of an innovative prefabricated natural plant fibre building system.*

Simonson, C.J., Salonvaara, M. and Ojanen, T. (2004) Heat and Mass Transfer between Indoor Air and a Permeable and Hygroscopic Building Envelope: Part I – Field Measurements. *Journal of Thermal Envelope and Building Science*, 28 (1), 63-101.

Simonson, C.J., Salonvaara, M., Ojanen, T., Walker, I. and Levin, H. (2002) *Moderating indoor conditions with hygroscopic building materials and outdoor ventilation.* 110: 804-819.

Simpson, W. and TenWolde, A. (2009) Physical Properties and Moisture Relations of Wood. *Wood Handbook.*

Skaar, C. (1984) Wood-Water Relationships. In: (ed.) *The Chemistry of Solid Wood.* American Chemical Society. pp. 127-172.

Soudani, L., Fabbri, A., Chabriac, P.-A., Morel, J.-C., Woloszyn, M. and Grillet, A.-C. (2015) On the relevance of neglecting the mass vapor variation for modelling the hygrothermal behavior of rammed earth. *1st International Conference on Rammed Earth Construction*, Perth; Australia, 10-13 February 2015 of Conference.

Srinivasa Murthy, N. (2014) Stabilized Mud Mortar. Volume: 03, 2321-7308.

Straube, J.F. (2006) Moisture and materials. *Building Science Digest*, 138, 1-7.

Swan, A.J., Rteil, A. and Lovegrove, G. (2011) Sustainable Earthen and Straw Bale Construction in North American Buildings: Codes and Practice. *Journal of Materials in Civil Engineering*, 23 (6), 866-872.

Swift, J.A. and Smith, J.R. (2001) Microscopical investigations on the epicuticle of mammalian keratin fibres. *Journal of Microscopy*, 204 (3), 203-211.

Tarrío-Saavedra, J., Naya, S., Francisco-Fernández, M., López-Beceiro, J. and Artiaga, R. (2011) Functional nonparametric classification of wood species from thermal data. *Journal of Thermal Analysis and Calorimetry*, 104 (1), 87-100.

Temiz, A., Gezer, E.D., Yildiz, U.C. and Yildiz, S. (2008) Combustion properties of alder (*Alnus glutinosa* L.) Gaertn. subsp. *barbata* (C.A. Mey) Yalt.) and southern pine (*Pinus sylvestris* L.) wood treated with boron compounds. *Construction and Building Materials*, 22 (11), 2165-2169.

Thieblisson, L.M., Collet, F., Prétot, S., Lanos, C., Kouakou, H. and Boffoue, O. (2017) Elaboration and Characterization Of Eco-Materials Made From Recycled Or Bio-Based Raw Materials. *Energy Procedia*, 139, 468-474.

Thommes, M., Kaneko, K., Neimark, A., Olivier, J., Rodriguez-Reinoso, F., Rouquerol, J. and Sing, K. (2015) Physisorption of gases, with special reference to the evaluation of surface area and pore size distribution (IUPAC Technical Report). *Pure and Applied Chemistry*, 87.

Tingley, D.D. and Davison, B. (2011) *Design for deconstruction and material reuse*. 164: 195-204.

Tomassetti, M., Marini, F., Campanella, L., Positano, M. and Marinucci, F. (2015) Suitable classification of mortars from ancient Roman and Renaissance frescoes using thermal analysis and chemometrics. *Chemistry Central Journal*, 9 (1), 1-7.

Troppová, E., Švehlík, M., Tippner, J. and Wimmer, R. (2015) Influence of temperature and moisture content on the thermal conductivity of wood-based fibreboards. *Materials and Structures*, 48 (12), 4077-4083.

Tsujiyama, S. and Miyamori, A. (2000) Assignment of DSC thermograms of wood and its components. *Thermochim. Acta*, 351 (1-2), 177-181.

U.N. (2008) *Kyoto Protocol Reference Manual* [online] Available at: https://unfccc.int/resource/docs/publications/08_unfccc_kp_ref_manual.pdf [Accessed: 16/10/2017]

Üreyen, M., Torsun, M., Yilmaz, Ü.Y. and Koparal, A. (2018) Effect of polyamide ratio on the flammability of wool/PA blended aircraft seat fabrics. *IOP Conference Series: Materials Science and Engineering*, 460, 012033.

Vasconcelos, A., Freddi, G. and Cavaco-Paulo, A. (2009) Biodegradable Materials Based on Silk Fibroin and Keratin. *Biomacromolecules*, 10, 1019.

Verbeke, S. and Audenaert, A. (2018) Thermal inertia in buildings: A review of impacts across climate and building use. *Renewable and Sustainable Energy Reviews*, 82, 2300-2318.

Vert, M., Doi, Y., Hess, M., Hodge, P., Kubisa, P., Rinaudo, M. and Schué, F. (2012) Terminology for biorelated polymers and applications (IUPAC Recommendations 2012). *Pure and Applied Chemistry. Chimie Pure et Appliquee*, 84 (2), 377-410.

Viel, M., Collet, F. and Lanos, C. (2017) *Thermal insulation materials from renewable resources: Thermal and hygric performances*.

Vololonirina, O. and Perrin, B. (2016) Inquiries into the measurement of vapour permeability of permeable materials. *Construction and Building Materials*, 102, 338-348.

Wargocki, P., Wyon, D.P., Sundell, J., Clausen, G. and Fanger, P.O. (2000) The Effects of Outdoor Air Supply Rate in an Office on Perceived Air Quality, Sick Building Syndrome (SBS) Symptoms and Productivity. *Indoor Air*, 10 (4), 222-236.

Wl, X. (2003) Thermal analysis of ultrafine wool powder. 87, 2372.

Wojciechowska, E., Włochowicz, A. and Weselucha-Birczyńska, A. (1999) Application of Fourier-transform infrared and Raman spectroscopy to study degradation of the wool fiber keratin. *Journal of Molecular Structure*, 511-512, 307-318.

World Health, O. (2009) *WHO guidelines for indoor air quality dampness and mould*. Copenhagen: Copenhagen : WHO.

Xia, Z., Yao, C.e., Zhou, J., Ye, W. and Xu, W. (2016) Comparative study of cotton, ramie and wool fiber bundles' thermal and dynamic mechanical thermal properties. *Textile Research Journal*, 86 (8), 856-867.

Xu, W., Wang, X., li, W., Peng, X., Liu, X. and Wang, X. (2007) Characterization of Superfine Wool Powder/Poly(propylene) Blend Film. *Macromolecular Materials and Engineering*, 292, 674-680.

Yang, L. (2019) Relationship between sorptivity and capillary coefficient for water absorption of cement-based materials: theory analysis and experiment. *Royal Society open science*, 6 (6), 190112.

Yang, X., Fazio, P., Ge, H. and Rao, J. (2012) Evaluation of moisture buffering capacity of interior surface materials and furniture in a full-scale experimental investigation. *Building and Environment*, 47 (Supplement C), 188-196.

Yang, Y., Zhang, Y., Lang, Y. and Yu, M. (2017) Structural ATR-IR analysis of cellulose fibers prepared from a NaOH complex aqueous solution. *IOP Conference Series: Materials Science and Engineering*, 213, 012039.

Yao, P., Liu, Y., Suoting, Y. and Jianzhong, L. (2008) Characterization of Secondary Structure Transformation of Stretched and Slenderized Wool Fibers with FTIR Spectra. *Journal of Engineered Fibers and Fabrics*, 3.

Yorulmaz, S.Y. and Atimtay, A.T. (2009) Investigation of combustion kinetics of treated and untreated waste wood samples with thermogravimetric analysis. *Fuel Processing Technology*, 90 (7), 939-946.

Yu, C. and Crump, D. (1998) A review of the emission of VOCs from polymeric materials used in buildings. *Building and Environment*, 33 (6), 357-374.

Zach, J., Korjenic, A., Petránek, V., Hroudová, J. and Bednar, T. (2012) Performance evaluation and research of alternative thermal insulations based on sheep wool. *Energy and Buildings*, 49, 246-253.

Zargarkazemi, A., Sadeghi-Kiakhani, M., Arami, M. and Bahrami, H. (2014) Modification of wool fabric using prepared chitosan-cyanuric chloride hybrid. *The Journal of The Textile Institute*, 106.

Zhang, H., Yoshino, H. and Hasegawa, K. (2012) Assessing the moisture buffering performance of hygroscopic material by using experimental method. *Building and Environment*, 48 (Supplement C), 27-34.

Zhang, H., Yoshino, H., Hasegawa, K., Liu, J., Zhang, W. and Xuan, H. (2017) Practical moisture buffering effect of three hygroscopic materials in real-world conditions. *Energy and Buildings*, 139, 214-223.

Zhang, Z., Thiery, M. and Baroghel-Bouny, V. (2016) Investigation of moisture transport properties of cementitious materials. *Cement and Concrete Research*, 89 (C), 257-268.

Zhao, H., Xiao, Q., Huang, D. and Zhang, S. (2014) - Influence of Pore Structure on Compressive Strength of Cement Mortar. - 2014.

Zirkelbach, D., Holm, A. and Künzle, H.M. (2005) Influence of temperature and relative humidity on the durability of mineral wool in ETICS. *10DBMC International Conference On Durability of Building Materials and Components*, Lyon, France, 17-20 April 2005 of Conference.

